

MFZ. This aftershock zone appears to cut off the southeasternmost corner of the Gorda plate just north of the abrupt eastward termination of intense seismicity along the MFZ, at a point that might be taken as the Mendocino triple junction from the viewpoint of seismicity.

Relative horizontal extension at seismogenic depths is suggested by events 2 and 8. Event 2 (Nov. 10, 1980; 7 km deep) was the largest in a detached cluster of shallow aftershocks 20 km east of the 1980 main shock, and event 8 (Apr. 9, 1987; 26 km deep) occurred about 100 km east of the 1980 main shock in the zone of seismicity associated with the subducting Gorda plate.

DISCUSSION

The Pacific plate moved northwestward with respect to the North American plate by 300 to 400 mm during the 7-yr interval 1980–86. Earthquakes occurring along the San Andreas fault system during the same interval, however, accommodated only a small fraction of this relative plate motion. Only four earthquakes of $M > 5$ occurred along branches of the San Andreas fault system during 1980–86: the pair of $M = 5.9$ – 5.3 Livermore earthquakes (events 29, 30, fig. 5.10A) on the Greenville fault (Jan. 24–27, 1980), the $M = 6.2$ Morgan Hill earthquake (event 33) on the Calaveras fault (Apr. 24, 1984), and the $M = 5.6$ North Palm Springs earthquake (event 80) on the Banning segment of the San Andreas fault (July 8, 1986). Each of these moderate San Andreas earthquakes ruptured fault segments limited to 20 to 30 km in length, with average displacements over the respective rupture surfaces of 100 to 200 mm (see Hartzell and Heaton, 1986). As is typical of earthquakes along the San Andreas fault system, each of these events involved nearly pure right-lateral strike-slip displacement coincident with the local strike of the fault. As is also typical of San Andreas earthquakes, slip on the first three events occurred on near-vertical fault planes with a northwestward to north-northwestward strike. The North Palm Springs earthquake, which ruptured a section of the east-west-striking Banning fault in the structurally complex San Geronio bend in the fault system at the southern margin of the Transverse Ranges, represents an important deviation from typical San Andreas earthquakes. Although its displacement was dominantly right-lateral strike slip, it occurred along a plane that dips 45° N. (Jones and others, 1986) and included a small but significant component of reverse slip (Mendoza and Hartzell, 1988). With the arguable exception of the North Palm Springs earthquake (arguable because of the complex section of the fault system in which it occurred), however, none of these $M > 5$ earthquakes ruptured the main trace of the San Andreas fault. Indeed, the two most recent $M > 5$ earth-

quakes to clearly do so were the $M = 6$ Parkfield earthquake of 1966 (Bakun and McEvilly, 1984) and the $M = 7.1$ Loma Prieta earthquake of 1989 (see chap. 6).

Thus, aside from the displacement accommodated by steady aseismic slip at a rate of 32 to 37 mm/yr along the creeping section of the fault in central California, most relative plate motion across the San Andreas transform boundary during this 7-yr interval accumulated as elastic shear strain. Accordingly, the earthquakes plotted in figures 5.3 through 5.9 are symptomatic of accumulating strain along the San Andreas fault system rather than of effective strain release. The latter requires rupture with a major earthquake along one of the locked stretches of the San Andreas fault.

SEISMICITY PATTERNS AND THE EARTHQUAKE CYCLE

What changes in spatial-temporal patterns of earthquake occurrence might we expect to see as the next great earthquake on the San Andreas fault approaches? Both historical and instrumental seismicity records indicate that the spatial distribution of earthquakes in California changes only slowly over periods of decades to centuries, although the intensity of activity within this distribution fluctuates year to year (Ellsworth and others, 1981; Hill and others, in press; Hutton and others, in press). Temporal fluctuations in activity during the interval 1980–86, for example, were dominated by a short-lived aftershock sequence following the 1980 Eureka $M = 7.2$ earthquake and by the long-lived aftershock sequence following the 1983 Coalinga $M = 6.7$ earthquake. The overall spatial distribution of earthquakes in California, however, remained nearly stationary throughout this 7-yr interval. Furthermore, the spatial pattern defined by 1980–86 seismicity is much the same as that outlined by the record of $M \geq 5$ earthquakes that extends back nearly 200 yr (see chap. 6).

Variations in the historical rate of moderate to large ($M > 5$) earthquakes in central California before and after the 1906 San Francisco earthquake appear to mimic those described by Fedotov (1965) and Mogi (1968) for the earthquake cycle associated with great, subduction-zone earthquakes in Japan, Kamchatka, and the Kurile Islands (see chap. 6; Ellsworth and others, 1981). The history of instrumentally recorded $M < 5$ earthquakes in California is too short, however, to indicate whether we might expect to see distinctive changes in the seismicity pattern a short time (months to years) before the next great earthquake on the San Andreas fault. We have yet to see, for example, whether the quiescent (locked) segments of the San Andreas fault remain aseismic except for the rupture of a great earthquake, or whether these segments become active with small to moderate earthquakes as foreshock activity to great earthquakes.

DISTRIBUTED SEISMICITY AND DEFORMATION OF THE PLATE MARGINS

The two largest earthquakes in California during the interval 1980-86 occurred off the faults of the San Andreas system, and their occurrence emphasizes the importance of deformation within the plate margins along the San Andreas transform boundary. The $M=7.2$ Eureka event (Nov. 8, 1980), for example, involved deformation internal to the Gorda plate; and the $M=6.7$ Coalinga event (May 2, 1983) involved crustal shortening with reverse slip perpendicular to the San Andreas fault. These two earthquakes and the many smaller, "off fault" events (fig. 5.4A) reflect local deviations from the simple rigid-plate approximation of plate tectonics.

DEFORMATION OF THE GORDA PLATE

As the small, youthful Gorda plate is subducted obliquely northeastward beneath the North American plate, it is being subjected to north-south compression in response to a component of convergence between the larger, older Juan de Fuca plate to the north and the Pacific plate to the south (Jachens and Griscom, 1983; Wilson, 1986). Distorted marine magnetic anomalies within the Gorda plate indicate that it has undergone progressive internal deformation over the past 5 Ma in response to this compression (Silver, 1971), and current seismicity within the plate (fig. 5.4) indicates that this deformation continues to the present.

The 1980 Eureka $M=7.2$ earthquake emphasizes that part of this deformation occurs with left-lateral slip on northeast-striking faults within the plate. The seismicity map and cross sections (fig. 5.4) demonstrate that deformation associated with the Gorda plate terminates abruptly against the Pacific plate in a steeply north-dipping zone of interaction along the MFZ, which can be followed on shore beneath the North American plate as a gently east-dipping, subhorizontal zone of widely scattered small to moderate earthquakes. Thus, convergence between the Gorda and Pacific plates across the MFZ apparently occurs by crushing and thickening of the southern margin of the Gorda plate as it is jammed against the anvil-like mass formed by the thicker and colder Pacific plate. Diminished east-west stress in the Gorda plate resulting from the subducting limb of the plate farther east serves to increase the difference between the maximum (north-south) and minimum (east-west) compressive stresses within the plate, leading to left-lateral strike-slip displacements along northeast-striking faults, as in the $M=7.2$ Eureka earthquake. This process accommodates the convergent component of Gorda-Pacific plate motion along the east end of the MFZ

at the expense of fragmentation and eastward expansion of the Gorda plate north of the MFZ.

THE SAN ANDREAS DISCREPANCY

Much of the seismicity adjacent to the San Andreas fault system is attributable to differences between the long-term slip rate and direction (slip vector) along the San Andreas fault system and that predicted for relative motion between the Pacific and North American plates along the San Andreas transform boundary on the basis of global models of plate motion. Minster and Jordan (1978, 1987) predicted that the direction of dextral slip between the Pacific and North American plates along the San Andreas transform boundary in central California is N. 35° W. The main trace of the San Andreas system, however, strikes N. 41° W. through central and northern California and N. 65° - 70° W. through the Transverse Ranges in southern California. DeMets and others (1987) concluded that the marine magnetic anomalies at the mouth of the Gulf of California constrain the slip rate to an average of 49 mm/yr over the past 3 to 4 Ma. Both long-term geologic offset data and geodetic data measured over the past several decades, however, indicate that the average slip rate along the San Andreas fault system is only about 35 mm/yr. The contribution to deformation of the western margin of the North American plate from spreading across the Basin and Range province is about 10 mm/yr in a N. 56° W. direction (Minster and Jordan, 1987). Ellsworth (see chap. 6) suggests that most of the San Andreas discrepancy can be explained if the component of dextral slip associated with historical Basin and Range earthquakes reflects a long-term trend superimposed on the N. 56° W. spreading direction. If so, then the residual component of Basin and Range extension perpendicular to the San Andreas fault system is approximately balanced by convergence across the Coast Ranges and continental margin.

CONVERGENCE NORMAL TO THE SAN ANDREAS FAULT SYSTEM

Focal mechanisms of earthquakes occurring off the San Andreas fault system suggest that the component of the San Andreas discrepancy normal to the fault system may, indeed, be accommodated by distributed brittle deformation on either side of the fault system. These mechanisms range from dextral strike slip on planes subparallel to the San Andreas fault, through oblique-reverse slip, to nearly pure reverse slip with a slip direction perpendicular to the San Andreas fault.

The Coalinga-North Kettleman Hills earthquake sequence provides clear evidence for crustal convergence perpendicular to the San Andreas fault system in the

Coast Ranges. The several smaller events with similar mechanisms to the north along both the eastern and western (coastal) margins of the Coast Ranges (fig. 5.11) suggest that the convergence responsible for the Coalinga earthquake may be active the length of the Coast Ranges (Wong and others, 1988; Eaton and Rymer,

1990). The subparallelism of fold axes within the Coast Ranges with the San Andreas fault indicates that fault-normal convergence has been important for the past 3 Ma in central California (fig. 5.12; Page and Engebretson, 1984). Namson and Davis (1988) proposed that the entire system of Coast Range folds may be genetically related to

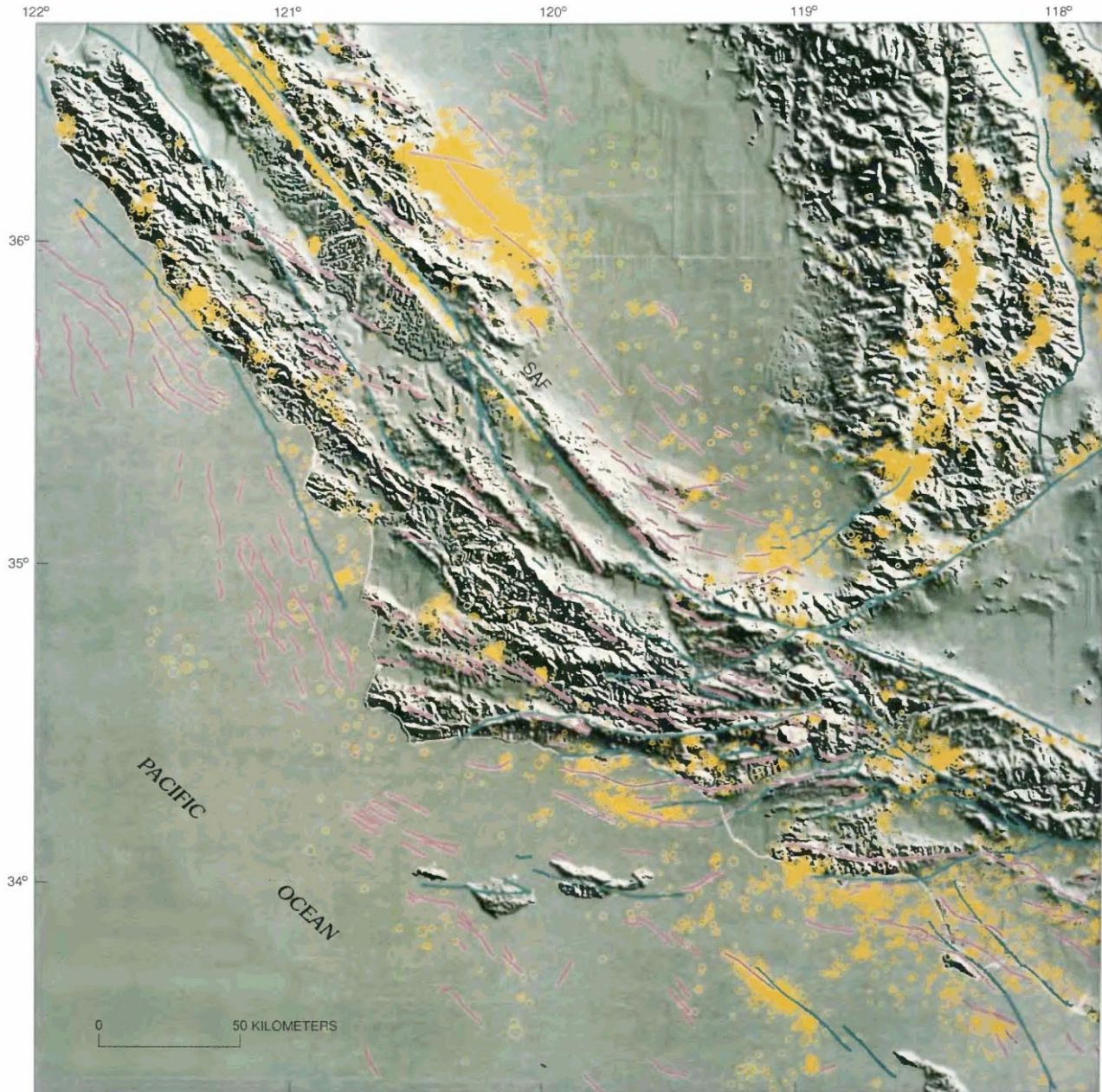


FIGURE 5.12.—Seismicity from 1980 to 1986 superimposed on digital shaded-relief image of central California, showing faults (blue) and fold axes (red). Size of symbol for epicenters (yellow) increases with magnitude from 1 to 6. Shaded relief by Raymond Batson, U.S. Geological Survey (illumination from north at 30°); overlays from Ross Stein (unpub. data, 1989). SAF, San Andreas fault.

Coalinga-like earthquake sequences and low-angle (blind) thrust faults that are rooted in a decollement near the base of the seismogenic crust. The reverse focal mechanisms for earthquakes associated with offshore faults along the western margin of the Coast Ranges suggest that, here, convergence involves westward thrusting of the Coast Ranges over oceanic crust of the Pacific plate.

The pronounced discrepancy in the strike of the San Andreas fault through the Transverse Ranges with respect to the Pacific-North American plate slip direction provides an obvious source of local crustal convergence (Hill and Dibblee, 1953; Atwater, 1970), and the associated structural complexities serve to distribute brittle deformation (seismicity) much more widely about the San Andreas fault system in southern California than about the relatively straight sections of the fault system in central and northern California. The largest earthquake in California since the great 1906 San Francisco earthquake occurred near the northern margin of this convergent regime; this $M=7.7$ Kern County earthquake ruptured some 35 km of the southeast-dipping White Wolf fault with left-oblique reverse slip on July 21, 1952.

The focal mechanisms of larger Transverse Range earthquakes, together with the mapped attitudes of major faults with Holocene offsets, show that much of this convergence occurs with slip on north-dipping thrust faults within and along the southern margin of the central Transverse Ranges (fig. 5.11A). For earthquakes in the western Transverse Ranges, the direction of reverse slip is more southwestward, consistent with thrusting of the western Transverse Ranges over the Pacific plate similar to that in the Coast Ranges to the north.

EXTENSIONAL DEFORMATION AND THE SOUTHERN SECTION OF THE SAN ANDREAS FAULT SYSTEM

The fault-normal convergence that dominates deformation adjacent to the San Andreas fault system through both the Coast Ranges and Transverse Ranges gives way rather abruptly to the extensional regime of the Salton Trough near the southern margin of the intensely active San Geronio bend in the fault. Focal mechanisms of earthquakes occurring on secondary structures adjacent to the seismically quiescent Indio segment of the San Andreas fault, for example, show a mix of strike- and dip-slip mechanisms. As is the case farther north, however, P -axes for these earthquakes tend to be oriented at a high angle (60° - 65°) to the fault, suggesting that the Indio segment of the fault may also be relatively weak (Jones, 1988).

One particularly noteworthy aspect of seismicity south of the Transverse Ranges is the tendency for earthquakes to occur along conjugate strike-slip structures. Recall that the Sierra Nevada-Great Basin boundary

zone also shows this tendency and that both regions are subject to extensional deformation, earthquake swarms, and late Quaternary volcanism. Earthquake sequences within the southern section of the San Andreas fault system commonly produce epicenter lineations that intersect at nearly a 90° angle with the northwest-striking right-slip plane and the northeast-striking left-slip plane. Earthquake-swarm sequences in the Brawley seismic zone, for example, typically occur along northeast-striking lineations normal to the trace of the adjacent Imperial fault (Johnson, 1979), and the $M=5.7$ Westmorland earthquake of 1981 involved left-lateral slip along several subparallel, northeast-striking planes (Johnson and Hutton, 1982). The diffuse lineations of epicenters spanning the area of the Peninsular Ranges between the San Jacinto and Elsinore faults also tend to be orthogonal to these two branches of the San Andreas fault system (fig. 5.10A). An impressive recent example of this orthogonal conjugate pattern is the $M=6.2$ and 6.6 Superstition Hills earthquakes of November 24, 1987 (Magistrale and others, 1988).

The kinematics of these conjugate structures remains a matter of conjecture. Dextral slip along throughgoing faults of the San Andreas system must certainly dominate deformation, and the shorter, northeast-striking structures must play only a secondary role. Nicholson and others (1986) proposed that the northeast-striking lineations represent the boundaries between blocks rotating clockwise much like roller bearings, between subparallel pairs of dextral strike-slip faults. Hill (1977) and Weaver and Hill (1978/79) suggested that within local spreading centers, such as the Brawley seismic zone, conjugate strike-slip structures form miniature triple junctions with a dike or normal fault that subtends the acute angle between the conjugate strike-slip faults.

MAXIMUM FOCAL DEPTHS AND THICKNESS OF THE SEISMOGENIC CRUST

Maximum focal depths of earthquakes beneath the San Andreas transform boundary range from less than 5 km beneath the Geysers geothermal field in the northern Coast Ranges to more than 20 km beneath the Transverse Ranges, the eastern margin of the Coast Ranges, and the San Jacinto and Elsinore faults in southernmost California. Beneath relatively straight segments of the San Andreas fault system through central California, maximum focal depths range from 12 to 15 km (figs. 5.7, 5.8). Sibson (1983) pointed out that these variations in maximum focal depth along the San Andreas fault system are inversely correlated with surficial heat flow, and he argued that the maximum depth of earthquakes coincides with the temperature-dependent transition from brittle failure in the upper crust to aseismic, quasi-plastic flow in

the lower crust and upper mantle. For quartz-bearing rocks typical of the upper crust and deformation rates typical of the San Andreas fault system (1×10^{-14} to $1 \times 10^{-13} \text{ s}^{-1}$), this brittle/ductile transition occurs at about 300 °C (Sibson, 1983). By this interpretation, the thin seismogenic crust beneath both the Geysers and Brawley geothermal fields in northern and southern California, respectively, reflects elevated temperatures in the shallow crust, whereas the relatively thick seismogenic crust beneath the Transverse Ranges and the eastern margin of the Coast Ranges reflects depressed temperatures in the midcrust associated with crustal convergence. Although temperature may dominantly influence the thickness of the seismogenic crust, local variations in rock composition (particularly the presence or absence of modal quartz and structural water) and in strain rate can also be important. These variations, for example, may help explain isolated clusters of deep earthquakes, such as the 20- to 24-km-deep events north of San Pablo Bay in central California (see cross secs. *F-F'*, *G-G'*, fig. 5.8*B*).

In any case, the thickness of the seismogenic crust beneath the San Andreas transform boundary seems to be much more strongly related to temperatures in the crust than to the structural thickness of crust defined by the depth to the Moho (see chap. 8). This relation is strikingly illustrated by the twofold increase in thickness of the seismogenic crust beneath the rootless Transverse Ranges.

DECOLLEMENT AT THE BASE OF THE SEISMOGENIC CRUST?

A theme common to models of crustal convergence along the San Andreas fault system involves low-angle reverse slip on decollement surfaces near the base of the seismogenic crust (Wentworth and others, 1983; Webb and Kanamori, 1985; Namson and Davis, 1988; Eaton and Rymer, 1990). A natural extension of this theme leads to a view of the seismogenic crust as a conglomeration of relatively rigid blocks interacting by frictional slip along weak preexisting faults (block boundaries) in response to regional stresses transmitted through both the brittle crust and quasi-plastic deformation in the underlying lithosphere (Hill, 1982). However, the nature of a decollement surface at the base of the brittle crust and the relation of the seismogenic San Andreas fault system to the aseismic transform boundary in the underlying lithosphere remain speculative. It is not yet clear, for example, whether the San Andreas fault continues below the seismogenic crust as a narrow, near-vertical boundary (possibly offset a substantial distance from the seismogenic fault by slip on the horizontal decollement surface) that slips by quasi-plastic, mylonitic deformation

or whether it broadens rapidly with depth into a wide shear zone spanning, say, the entire width of the Coast Ranges (see chap. 7; Sibson, 1983).

CONCLUSIONS

The spatial-temporal pattern of earthquake occurrence within the seismogenic crust along the San Andreas fault system is the brittle manifestation of distributed deformation of the lithosphere between the Pacific and North American plates along the San Andreas transform boundary. As we develop a more complete model of the long-term behavior of the seismogenic crust, including relations between great, plate-boundary earthquakes that periodically rupture the principal strand of the San Andreas fault system and the persistent background of small to moderate earthquakes on adjacent structures, our image of the deeper deformation will improve. Together will come a more complete understanding of the processes controlling deformation along the transform boundary and of the earthquake cycle.

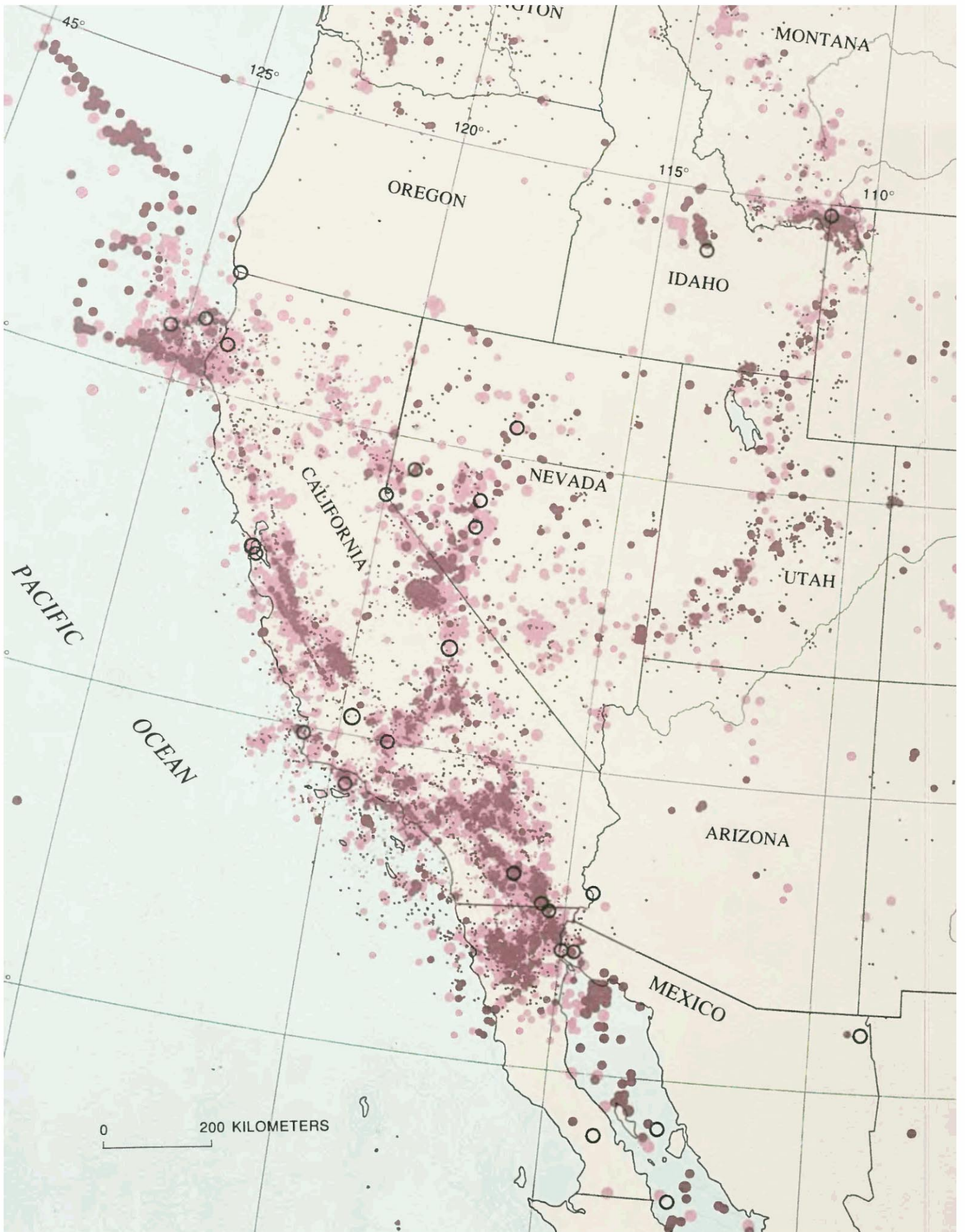
REFERENCES CITED

- Allen, C.R., 1968, The tectonic environments of seismically active and inactive areas along the San Andreas fault system, in Dickinson, W.R., and Grantz, Arthur, eds., Proceedings of conference on geologic problems of San Andreas fault system: Stanford, Calif., Stanford University Publications in the Geological Sciences, v. 11, p. 70-82.
- 1981, The modern San Andreas fault, in Ernst, W.G., ed., The geotectonic development of California (Ruby volume 1): Englewood Cliffs, N.J., Prentice-Hall, p. 511-534.
- Astiz, Luciana, and Allen, C.R., 1983, Seismicity of the Garlock fault, California: Seismological Society of America Bulletin, v. 73, no. 6, pt. A, p. 1721-1734.
- Atwater, Tanya, 1970, Implications of plate tectonics for the Cenozoic evolution of western North America: Geological Society of America Bulletin, v. 81, no. 12, p. 3513-3535.
- Bakun, W.H., Clark, M.M., Cockerham, R.S., Ellsworth, W.L., Lindh, A.G., Prescott, W.H., Shakal, A.F., and Spudich, Paul, 1984, The 1984 Morgan Hill, California, earthquake: Science, v. 225, no. 4659, p. 288-291.
- Bakun, W.H., and Lindh, A.G., 1985, The Parkfield, California, earthquake prediction experiment: Science, v. 229, no. 4714, p. 619-623.
- Bakun, W.H., and McEvilly, T.V., 1984, Recurrence models and Parkfield, California earthquakes: Journal of Geophysical Research, v. 89, no. B5, p. 3051-3058.
- Bolt, B.A., McEvilly, T.V., and Uhrhammer, R.A., 1981, The Livermore Valley, California, sequence of January 1980: Seismological Society of America Bulletin, v. 71, no. 2, p. 451-463.
- Bolt, B.A., and Miller, R.D., 1975, Catalogue of earthquakes in northern California and adjoining areas 1 January 1910-31 December 1972: Berkeley, University of California, Seismographic Station, 567 p.
- Boore, D.M., 1977, Strong-motion recordings of the California earthquake of April 18, 1906: Seismological Society of America Bulletin, v. 67, no. 3, p. 561-577.

- Cockerham, R.S., 1984, Evidence for a 180-km-long subducted slab beneath northern California: *Seismological Society of America Bulletin*, v. 74, no. 2, p. 569-576.
- Cockerham, R.S., and Corbett, E.J., 1987, The 1986 Chalfant Valley, California, earthquake sequence: Preliminary results: *Seismological Society of America Bulletin*, v. 77, no. 1, p. 280-289.
- Dehlinger, Peter, and Bolt, B.A., 1984, Seismic parameters along the Bartlett Springs fault zone in the Coast Ranges of northern California: *Seismological Society of America Bulletin*, v. 74, no. 5, p. 1785-1798.
- DeMets, Charles, Gordon, R.G., Stein, Seth, and Argus, D.F., 1987, A revised estimate of the Pacific-North America motion and implications for western North America plate boundary zone tectonics: *Geophysical Research Letters*, v. 14, no. 9, p. 911-914.
- Dickinson, W.R., 1981, Plate tectonics and the continental margin of California, in Ernst, G.W. ed., *The geotectonic development of California* (Ruby volume 1): Englewood Cliffs, N.J., Prentice-Hall, p. 2-28.
- Donnelly-Nolan, J.M., Hearn, B.C., Jr., Curtis, G.H., and Drake, R.E., 1981, Geochronology and evolution of the Clear Lake Volcanics, in McLaughlin, R.J., and Donnelly-Nolan, J.M., eds., *Research in the Geysers-Clear Lake geothermal area, northern California*: U.S. Geological Survey Professional Paper 1141, p. 47-60.
- Eaton, J.P., 1989, Dense microearthquake network study of northern California earthquakes, chap. 13 of Litehiser, J.J., ed., *Observatory seismology, a centennial symposium for the Berkeley Seismographic Stations*: Berkeley, University of California Press, p. 199-224.
- 1990, The earthquake and its aftershocks from May 2 through September 30, 1983, chap. 8 of Rymer, M.J., and Ellsworth, W.E., eds., *The Coalinga, California, earthquake of May 2, 1983*: U.S. Geological Survey Professional Paper 1487, p. 113-170.
- Eaton, J.P., Lee, W.H.K., and Pakiser, L.C., 1970a, Use of micro-earthquakes in the study of the mechanics of earthquake generation along the San Andreas fault in central California: *Tectonophysics*, v. 9, no. 2-3, p. 259-282.
- Eaton, J.P., O'Neill, M.E., and Murdock, J.N., 1970b, Aftershocks of the 1966 Parkfield-Cholame, California, earthquake: A detailed study: *Seismological Society of America Bulletin*, v. 60, no. 4, p. 1151-1197.
- Eaton, J.P., and Rymer, M.J., 1990, Regional seismotectonic model for the southern Coast Ranges, chap. 7, of *The Coalinga, California, earthquake of May 2, 1983*: U.S. Geological Survey Professional Paper 1487, p. 97-111.
- Eberhart-Phillips, Donna, and Oppenheimer, D.H., 1984, Induced seismicity in the Geysers geothermal area, California: *Journal of Geophysical Research*, v. 89, no. B2, p. 1191-1207.
- Ellsworth, W.L., 1975, Bear Valley, California, earthquake sequence of February-March 1972: *Seismological Society of America Bulletin*, v. 65, no. 2, p. 483-506.
- Ellsworth, W.L., Lindh, A.G., Prescott, W.H., and Herd, D.G., 1981, The 1906 San Francisco earthquake and the seismic cycle, in Simpson, D.W., and Richards, P.G., eds., *Earthquake prediction: An international review* (Maurice Ewing Series 4): Washington, American Geophysical Union, p. 126-140.
- Ellsworth, W.L., Olson, J.A., Shijo, L.N., and Marks, S.M., 1982, Seismicity and active faults in the eastern San Francisco Bay region, in Hart, E.W., Hirschfeld, S.E., and Schulz, S.S., eds., *Conference on Earthquake Hazards in the Eastern San Francisco Bay Area, Hayward, Calif., 1982*, Proceedings: California Division of Mines and Geology Special Publication 62, p. 83-91.
- Fletcher, J.B., Haar, L.C., Hanks, T.C., Baker, L.M., Vernon, F.L., Berger, Jon, and Brune, J.N., 1987, The digital array at Anza California: Processing and initial interpretation of source parameters: *Journal of Geophysical Research*, v. 92, no. B1, p. 369-382.
- Fedotov, S.A., 1965, Regularities in the distribution of strong earthquakes in Kamchatka, the Kuril Islands and northeastern Japan: *Akademia Nauk SSSR, Institut Fiziki Zemli Trudy*, v. 36, p. 66-93.
- Hanks, T.C., Hileman, J.A., and Thatcher, Wayne, 1975, Seismic moments of the larger earthquakes of the southern California region: *Geological Society of America Bulletin*, v. 86, no. 8, p. 1131-1139.
- Hartzell, S.H., and Heaton, T.H., 1986, Rupture history of the 1984 Morgan Hill, California, earthquake from the inversion of strong motion records: *Seismological Society of America Bulletin*, v. 76, no. 3, p. 649-674.
- Heaton, T.H., 1982, The 1971 San Fernando, [California], earthquake: A double event?: *Seismological Society of America Bulletin*, v. 72, no. 6, p. 2037-2062.
- Hileman, J.A., Allen, C.R., and Nordquist, J.M., 1973, Seismicity of the southern California region 1 January 1932 to 31 December 1972: Pasadena, California Institute of Technology, Seismological Laboratory, 487 p.
- Hill, D.P., 1977, A model for earthquake swarms: *Journal of Geophysical Research*, v. 82, no. 8, p. 1347-1352.
- 1982, Contemporary block tectonics: California and Nevada: *Journal of Geophysical Research*, v. 87, no. B7, p. 5433-5450.
- Hill, D.P., Bailey, R.A., and Ryall, A.S., 1985a, Active tectonic and magmatic processes beneath Long Valley caldera, eastern California: An overview: *Journal of Geophysical Research*, v. 90, no. B13, p. 11111-11120.
- Hill, D.P., Eaton, J.E., Ellsworth, W.L., Cockerham, R.S., Lester, F.W., and Corbett, E.J., in press, The Seismotectonic fabric of central California, in Slemmons, D.B., Engdahl, E.R., Blackwell, D.D., Schwartz, D.P., and Zoback, M.D., eds., *Neotectonics of North America* (DNAG Associated Volume GSMV-1): Boulder Colo., Geological Society of America.
- Hill, D.P., Mowinkel, Penelope, and Peake, L.G., 1975, Earthquakes, active faults, and geothermal areas in the Imperial Valley, California: *Science*, v. 188, no. 4195, p. 1306-1308.
- Hill, D.P., Wallace, R.E., and Cockerham, R.S., 1985b, Review of evidence on the potential for major earthquakes and volcanism in the Long Valley-Mono Craters-White Mountains regions of eastern California: *Earthquake Prediction Research*, v. 3, no. 3-4, p. 571-594.
- Hill, M.L., and Dibblee, T.W., 1953, San Andreas, Garlock, and Big Pine faults—a study of the character, history, and tectonic significance of their displacements: *Geological Society of America Bulletin*, v. 64, no. 4, p. 435-438.
- Hutton, L.K., Jones, L.M., Hauksson, Egill, and Given, D.D., in press, Seismotectonics of southern California, in Slemmons, D.B., Engdahl, E.R., Blackwell, D.D., Schwartz, D.P., and Zoback, M.D., eds., *Neotectonics of North America* (DNAG Associated Volume GSMV-1): Boulder, Colo., Geological Society of America.
- Jachens, R.C., and Griscom, Andrew, 1983, Three-dimensional geometry of the Gorda plate beneath northern California: *Journal of Geophysical Research*, v. 88, no. B11, p. 9375-9392.
- Johnson, C.E., 1979, I, CEDAR—an approach to the computer automation of short-period local seismic networks; seismotectonics of the Imperial Valley of southern California: Pasadena, California Institute of Technology, Ph.D. thesis, 343 p.
- Johnson, C.E., and Hill, D.P., 1982, Seismicity of the Imperial Valley, in *The Imperial Valley, California, earthquake of October 15, 1979*: U.S. Geological Survey Professional Paper 1254, p. 59-76.
- Johnson, C.E., and Hutton, L.K., 1982, Aftershocks and pre-earthquake seismicity, in *The Imperial Valley, California, earthquake of October 15, 1979*: U.S. Geological Survey Professional Paper 1254, p. 15-24.

- Jones, L.M., 1988, Focal mechanisms and the state of stress on the San Andreas fault in southern California: *Journal of Geophysical Research*, v. 93, no. B8, p. 8869-8891.
- Jones, L.M., and Dollar, R.S., 1986, Evidence for basin-and-range extensional tectonics in the Sierra Nevada: The Durwood Meadows swarm, Tulare County, California (1983-1984): *Seismological Society of America Bulletin*, v. 76, no. 2, p. 439-462.
- Jones, L.M., Hutton, L.K., Given, D.D., and Allen, C.R., 1986, The North Palm Springs, California, earthquake sequence of July 1986: *Seismological Society of America Bulletin*, v. 76, no. 6, p. 1830-1837.
- LaForge, R., and Lee, W.H.K., 1982, Seismicity and tectonics of the Ortigalita fault and southeast Diablo Range, California, in Hart, E.W., Hirschfeld, S.E., and Schulz, S.S., eds., Conference on Earthquake Hazards in the Eastern San Francisco Bay Area, Hayward Calif., 1982, Proceedings: California Division of Mines and Geology Special Publication 62, p. 93-101.
- Lee, W.H.K., Eaton, M.S., and Brabb, E.E., 1971, The earthquake sequence near Danville, California, 1970: *Seismological Society of America Bulletin*, v. 61, no. 6, p. 1771-1794.
- Lee, W.H.K., and Stewart, S.W., 1981, Principles and applications of microearthquake networks: New York, Academic Press, 293 p.
- Lomnitz, Cinna, Mosser, Federico, Allen, C.R., Brune, J.N., and Thatcher, Wayne, 1970, Seismicity and tectonics of the northern Gulf of California region, Mexico. Preliminary results: *Geofisica Internacional*, v. 10, no. 2, p. 27-48.
- Louie, J.N., Allen, C.R., Johnson, D.C., Haase, P.C., and Cohn, S.N., 1985, Fault slip in southern California: *Seismological Society of America Bulletin*, v. 75, no. 3, p. 811-833.
- Magistrale, Harold, Jones, L.M., and Kanamori, Hiroo, 1988, The Superstition Hills, California, earthquakes of 24 November 1987: *Seismological Society of America Bulletin*, v. 79, no. 2, p. 239-251.
- Mayer-Rosa, Dieter, 1973, Travel-time anomalies and distribution of earthquakes along the Calaveras fault zone, California: *Seismological Society of America Bulletin*, v. 63, no. 2, p. 713-729.
- Mendoza, Carlos, and Hartzell, S.H., 1988, Inversion for slip distribution using teleseismic *P* waveforms: North Palm Springs, Borah Peak, and Michoacan earthquakes: *Seismological Society of America Bulletin*, v. 78, no. 3, p. 1092-1111.
- Minster, J.B., and Jordan, T.H., 1978, Present-day plate motions: *Journal of Geophysical Research*, v. 83, no. B11, p. 5331-5354.
- Minster, J.B., and Jordan, T.H., 1987, Vector constraints on western U.S. deformation from space geodesy, neotectonics, and plate motions: *Journal of Geophysical Research*, v. 92, no. B6, p. 4798-4804.
- Mogi, Kiyoo, 1968, Some features of recent seismic activity in and near Japan (1): University of Tokyo, Earthquake Research Institute Bulletin, v. 46, pt. 6, sec. A, p. 1225-1235.
- Morton, D.M., and Matti, J.C., 1987, The Cucamonga fault zone: geologic setting and Quaternary history, chap. 12 of *Recent reverse faulting in the Transverse Ranges, California*: U.S. Geological Survey Professional Paper 1339, p. 179-203.
- Namson, J.S., and Davis, T.L., 1988, Seismically active fold and thrust belt in the San Joaquin Valley, central California: *Geological Society of America Bulletin*, v. 100, no. 2, p. 257-273.
- Nicholson, Craig, Seeber, Leonardo, Williams, Patrick, and Sykes, L.R., 1986, Seismicity and fault kinematics through the eastern Transverse Ranges, California: Block rotation, strike-slip faulting and low-angle thrusts: *Journal of Geophysical Research*, v. 91, no. B5, p. 4891-4908.
- Norris, Robert, Jones, L.M., and Hutton, K.L., 1986, The Southern California Network Bulletin, July 01 through December 31, 1985: U.S. Geological Survey Open-File Report 86-337, 15 p.
- Oppenheimer, D.H., 1986, Extensional tectonics at The Geysers geothermal area, California: *Journal of Geophysical Research*, v. 91, no. B11, p. 11463-11476.
- Oppenheimer, D.H., Reasenberg, P.A., and Simpson, R.W., 1988, Fault-plane solutions for the 1984 Morgan Hill, California, earthquake sequence: Evidence for the state of stress on the Calaveras fault: *Journal of Geophysical Research*, v. 93, no. B8, p. 9007-9026.
- Page, B.M., and Engebretson, D.C., 1984, Correlation between the geologic record and computed plate motions for central California: *Tectonics*, v. 3, no. 2, p. 133-155.
- Pavoni, Nazario, 1973, A structural model for the San Andreas fault zone along the northeast side of the Gabilan Range, in Kovach, R.L., and Nur, Amos, eds., Proceedings of the conference on tectonic problems of the San Andreas fault system: Stanford, Calif., Stanford University Publications in the Geological Sciences, v. 13, p. 259-267.
- Poley, C.M., 1988, The San Ardo, California, earthquake of 24 November 1985: *Seismological Society of America Bulletin*, v. 78, no. 3, p. 1360-1366.
- Reasenberg, P.A., and Ellsworth, W.L., 1982, Aftershocks of the Coyote Lake, California, earthquake of August 6, 1979: A detailed study: *Journal of Geophysical Research*, v. 87, no. B13, p. 10637-10655.
- Richter, C.F., 1958, Elementary seismology: San Francisco, W.H. Freeman, 768 p.
- Rogers, A.M., Harmsen, S.C., Corbett, E.J., Priestley, K.F., and DePolo, D.M., in press, The seismicity of Nevada and some adjacent areas of the Great Basin, in Slemmons, D.B., Engdahl, E.R., Blackwell, D.D., Schwartz, D.P., and Zoback, M.D., eds., Neotectonics of North America (DNAG Associated Volume GSMV-1): Boulder, Colo., Geological Society of America.
- Sanders, C.O., and Kanamori, Hiroo, 1984, A seismotectonic analysis of the Anza seismic gap, San Jacinto fault zone, southern California: *Journal of Geophysical Research*, v. 89, no. B7, p. 5873-5890.
- Sauber, Jeanne, McNally, K.C., Pechmann, J.C., and Kanamori, Hiroo, 1983, Seismicity near Palmdale, California, and its relation to strain changes: *Journal of Geophysical Research*, v. 88, no. B3, p. 2213-2219.
- Savage, J.C., and Cockerham, R.S., 1987, Quasi-periodic occurrence of earthquakes in the 1978-1986 Bishop-Mammoth Lakes sequence, eastern California: *Seismological Society of America Bulletin*, v. 77, no. 4, p. 1347-1358.
- Schulz, S.S., Mavko, G.M., Burford, R.O., and Stuart, W.D., 1982, Long-term fault creep observations in central California: *Journal of Geophysical Research*, v. 87, no. B8, p. 6977-6982.
- Sibson, R.H., 1983, Continental fault structure and the shallow earthquake source: *Geological Society of London Journal*, v. 140, no. 5, p. 741-767.
- Sieh, K.E., 1978, Slip along the San Andreas fault associated with the great 1857 earthquake: *Seismological Society of America Bulletin*, v. 68, no. 5, p. 1421-1448.
- 1981, A review of geological evidence for recurrence times of large earthquakes, in Simpson, D.W., and Richards, P.G., eds., *Earthquake prediction: An international review (Maurice Ewing Series 4)*: Washington, American Geophysical Union, p. 181-207.
- 1986, Slip rate across the San Andreas fault and prehistoric earthquakes at Indio, California [abs.]: *Eos (American Geophysical Union Transactions)*, v. 67, no. 44, p. 1200.
- Sieh, K.E., and Jahns, R.H., 1984, Holocene activity of the San Andreas fault at Wallace Creek, California: *Geological Society of America Bulletin*, v. 95, no. 8, p. 883-896.
- Silver, E.A., 1971, Tectonics of the Mendocino triple junction: *Geological Society of America Bulletin*, v. 82, no. 11, p. 9265-2878.

- Smith, K.D., and Priestly K.F., 1988, The foreshock sequence of the 1986 Chalfant, California, earthquake: *Seismological Society of America Bulletin*, v. 78, no. 1, p. 172-187.
- Spieth, M.A., 1981, Two detailed seismic studies in central California. Part I: Earthquake clustering and crustal structure studies of the San Andreas fault near San Juan Bautista. Part II: Seismic velocity structure along the Sierra foothills near Oroville, California: Stanford, Calif., Stanford University, Ph.D. thesis, 174 p.
- Stein, R.S., and King, G.C.P., 1984, Seismic potential revealed by surface folding: 1983 Coalinga, California, earthquake: *Science*, v. 224, no. 4651, p. 869-871.
- Stein, R.S., and Thatcher, Wayne, 1981, Seismic and aseismic deformation associated with the 1952 Kern County, California, earthquake and relationship to the Quaternary history of the White Wolf fault: *Journal of Geophysical Research*, v. 86, no. B6, p. 4913-4928.
- Sykes, L.R., and Seeber, Leonardo, 1985, Great earthquakes and great asperities, San Andreas fault, southern California: *Geology*, v. 13, no. 12, p. 835-838.
- Thatcher, Wayne, Hileman, J.A., and Hanks, T.C., 1975, Seismic slip distribution along the San Jacinto fault zone, southern California, and its implications: *Geological Society of America Bulletin*, v. 86, no. 8, p. 1140-1146.
- Thatcher, Wayne, and Lisowski, Michael, 1987, Long-term seismic potential of the San Andreas fault southeast of San Francisco, California: *Journal of Geophysical Research*, v. 92, no. B6, p. 4771-4784.
- Van Wormer, J.D., and Ryall, A.S., 1980, Sierra Nevada-Great Basin boundary zone: Earthquake hazards related to structure, active tectonic processes, and anomalous patterns of earthquake occurrence: *Seismological Society of America Bulletin*, v. 70, no. 5, p. 1557-1572.
- Walter, S.R., 1986, Intermediate-focus earthquakes associated with Gorda plate subduction in northern California: *Seismological Society of America Bulletin*, v. 76, no. 2, p. 583-588.
- Ward, S.N., 1988, North America-Pacific plate boundary, an elastic-plastic megashear: evidence from very long baseline interferometry: *Journal of Geophysical Research*, v. 93, no. B7, p. 7716-7728.
- Weaver, C.S., and Hill, D.P., 1978/79, Earthquake swarms and local crustal spreading along major strike-slip faults in California: *Pure and Applied Geophysics*, v. 117, no. 1-2, p. 51-64.
- Webb, T.H., and Kanamori, Hiroo, 1985, Earthquake focal mechanisms in the eastern Transverse Ranges and San Emigdio Mountains, southern California and evidence for a regional decollement: *Seismological Society of America Bulletin*, v. 75, no. 3, p. 737-757.
- Wentworth, C.M., Walter, A.W., Bartow, J.A., and Zoback, M.D., 1983, Evidence on the tectonic setting of the 1983 Coalinga earthquakes from deep reflection and refraction profiles across the southeastern end of Kettleman Hills, *in* Bennett, J.H., and Sherburne, R.W., eds., *The 1983 Coalinga, California earthquakes*: California Division of Mines and Geology Special Publication 66, p. 113-126.
- Wesson, R.L., Burford, R.O., and Ellsworth, W.L., 1973, Relationship between seismicity, fault creep, and crustal loading along the central San Andreas fault, *in* Kovach, R.L., and Nur, Amos, eds., *Proceedings of the conference on tectonic problems of the San Andreas fault system*: Stanford, Calif., Stanford University Publications in the Geological Sciences, v. 13, p. 303-321.
- Whitcomb, J.H., 1971, Fault-plane solutions of the February 9, 1971, San Fernando earthquake and some aftershocks, *in* *The San Fernando, California, earthquake of February 9, 1971*: U.S. Geological Survey Professional Paper 733, p. 30-33.
- Wilson, D.S., 1986, A kinematic model for the Gorda deformation zone as a diffuse southern boundary of the Juan de Fuca plate: *Journal of Geophysical Research*, v. 91, no. B10, p. 10259-10269.
- Wong, I.G., Ely, R.W., and Kollmann, A.C., 1988, Contemporary seismicity and tectonics of the northern and central Coast Ranges-Sierran Block boundary zone, California: *Journal of Geophysical Research*, v. 93, no. B7, p. 7813-7833.
- Zoback, M.D., Zoback, M.L., Mount, V.S., Suppe, John, Eaton, J.P., Healy, J.H., Oppenheimer, D.H., Reasenber, P.A., Jones, L.M., Raleigh, C.B., Wong, I.G., Scotti, Oona, and Wentworth, C.M., 1987, New evidence on the state of stress of the San Andreas fault system: *Science*, v. 238, no. 4830, p. 1105-1111.



Motion between the North American and Pacific plates at the latitude of the San Andreas fault produces a broad zone of large-magnitude earthquake activity extending more than 500 km into the continental interior. The San Andreas fault system defines the western limits of plate interaction and dominates the overall pattern of seismic strain release. Few of the $M \geq 6$ earthquakes that have occurred in the past 2 centuries were located on the San Andreas fault proper, an observation emphasizing the importance of secondary faults for both seismic-hazard assessment and tectonic processes.

6. EARTHQUAKE HISTORY, 1769–1989

By WILLIAM L. ELLSWORTH

CONTENTS

	Page		Page
Introduction-----	154	Seismicity of the western Basin and Range province—Continued	
Earthquake history of the San Andreas fault system-----	155	Principal earthquakes—Continued	
Principal earthquakes-----	156	December 21, 1932 ($M=7.2$)-----	167
July 28, 1769 ($M=6$)-----	156	July 6, 1954 ($M=6.6$) and August 24, 1954 ($M=6.8$) ---	167
December 8, 1812 ($M=7$)-----	157	December 16, 1954 ($M=7.1$ and 6.8)-----	168
December 21, 1812 ($M=7$)-----	157	July 21, 1986 ($M=6.2$)-----	168
June 10, 1836 ($M=6\frac{3}{4}$)-----	158	Seismicity of the Mendocino triple junction and the Gorda plate -	169
June 1838 ($M=7$)-----	158	Principal earthquakes-----	169
January 9, 1857 ($M=8\frac{1}{4}$)-----	158	November 23, 1873 ($M=6\frac{3}{4}$)-----	169
October 21, 1868 ($M=7$)-----	159	April 16, 1899 ($M=7$)-----	169
February 24, 1892 ($M=7$)-----	159	January 31, 1922 ($M=7.3$)-----	169
April 19 and 21, 1892 ($M=6\frac{1}{2}$ and $6\frac{1}{4}$)-----	159	January 22, 1923 ($M=7.2$)-----	169
December 25, 1899 ($M=6.4$)-----	159	December 21, 1954 ($M=6.6$)-----	169
April 18, 1906 ($M=8\frac{1}{4}$)-----	159	November 8, 1980 ($M=7.2$)-----	169
November 21, 1915 ($M=7.1$)-----	161	Discussion-----	169
April 21, 1918 ($M=6.9$)-----	162	Rate of seismicity-----	171
November 4, 1927 ($M=7.3$)-----	162	Paradox of the missing plate motion-----	171
March 11, 1933 ($M=6.3$)-----	162	Earthquake recurrence and characteristic earthquakes-----	172
December 30 and 31, 1934 ($M= 6.5$ and 7.0)-----	162	The seismic cycle-----	173
May 19, 1940 ($M=7.1$)-----	163	Future uses of earthquake history-----	174
July 21, 1952 ($M=7.7$)-----	163	Catalog of major earthquakes, 1769–1989-----	175
February 9, 1956 ($M=6.8$)-----	164	Catalog compilation-----	175
April 9, 1968 ($M=6.5$)-----	164	Quantification of earthquakes and magnitude scales-----	176
February 9, 1971 ($M=6.5$)-----	164	The Richter scale (M_L)-----	177
October 15, 1979 ($M=6.5$)-----	164	Surface-wave magnitude (M_S) and body-wave	
May 2, 1983 ($M=6.5$)-----	164	magnitude (m_b)-----	177
November 24, 1987 ($M=6.6$)-----	164	Seismic intensity and earthquake magnitude (M_I)-----	177
October 18, 1989 ($M=7.1$)-----	165	Seismic moment (M_0), radiated energy, and moment	
Seismicity of the western Basin and Range province-----	166	magnitude (M)-----	178
Principal earthquakes-----	166	Summary magnitude (M)-----	178
March 26, 1872 ($M=7.6$)-----	166	References cited-----	178
October 3, 1915 ($M=7.3$)-----	167		

◀ FIGURE 6.1.—Seismicity highlights broad and complex zones of active tectonism in the western United States. Dots, earthquakes scaled by magnitude in unit-magnitude steps, smallest for $M < 4$; circles, earthquakes of $M > 7$; red dots, recent events, generally since 1975; pink symbols, historical events. From Engdahl and Rinehart (1988).

INTRODUCTION

Between Punta Gorda on the northern California coast and the head of the Gulf of California, 1,350 km to the southeast, lies the active transform boundary that forms the modern San Andreas fault system (fig. 6.1). Dextral motion between the North American and Pacific plates along this system is accommodated within an elongate zone, broadening from about 100 km at its north end to about 300 km in southern California. The San Andreas fault proper hugs the east side of this zone at its south terminus and gradually migrates across the zone, lying on the west edge of the zone at its north terminus. The

San Andreas fault system transmits about three-fourths of the relative motion across the plate boundary, as shown by various geologic and geodetic evidence. Much of this motion is stored elastically in the upper crust along the major faults in the system, ultimately to be released in large plate-boundary earthquakes. These large earthquakes and their implications for the mechanics of North American-Pacific plate interactions are the subject of this chapter.

Earthquake activity in California and Nevada at the latitude of the San Andreas fault extends well beyond the confines of the San Andreas system (fig. 6.2). In the past century alone, only about half of the $M \geq 6$ activity has

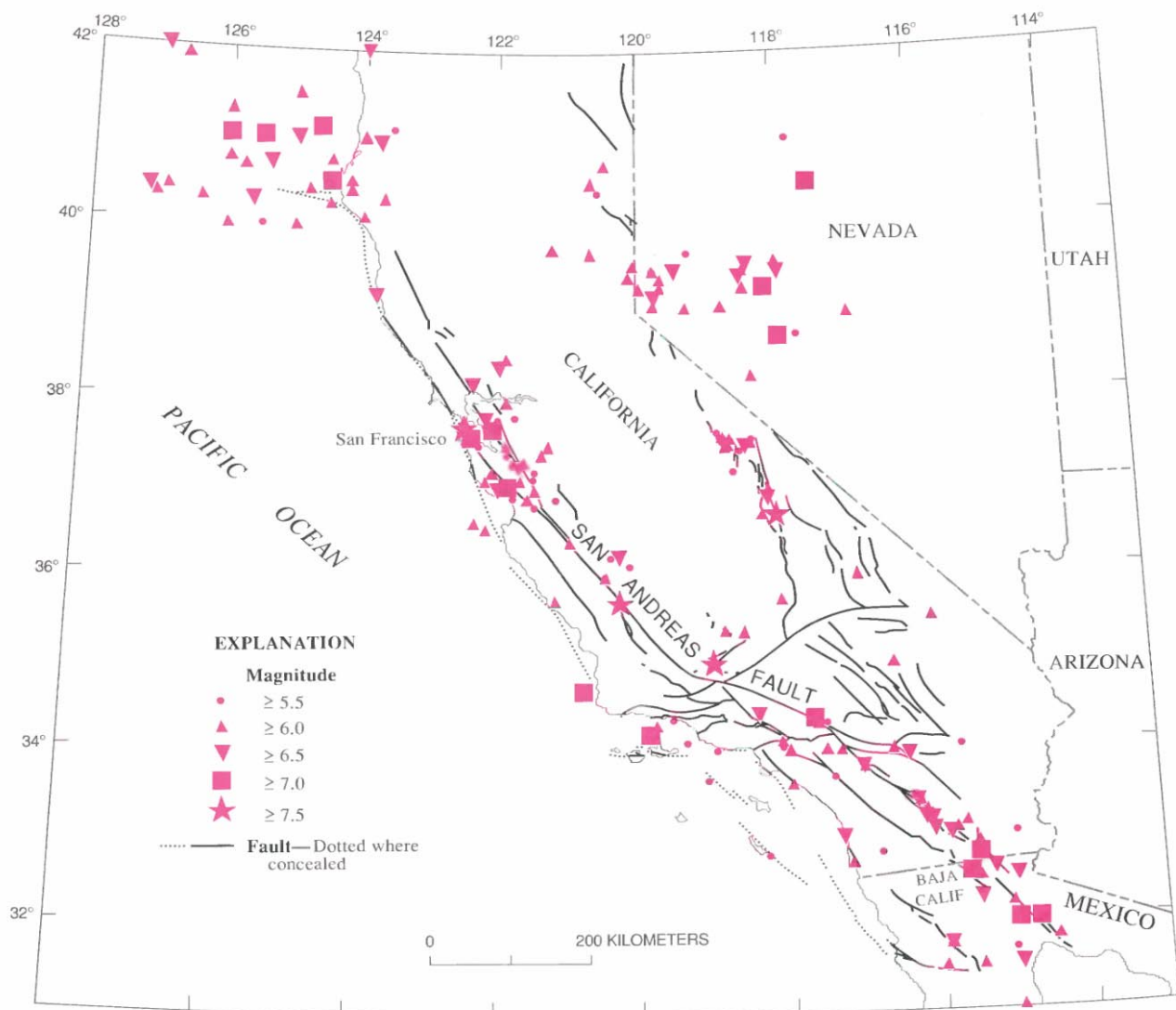


FIGURE 6.2.—Seismicity of California, Nevada, and northern Baja California, 1769–1989. Earthquakes are listed in table 6.1 and plotted by magnitude class.

fallen within the San Andreas system; of the rest, half is associated with the western Basin and Range province, and the other half with the Mendocino triple junction and the Gorda plate. Although activity in the latter region reflects the tectonics of the triple junction and the collision of the Gorda plate with the North American plate, seismicity east of the San Andreas system along the east flank of the Sierra Nevada and in the Basin and Range province reflects the incomplete accommodation of plate motion along the San Andreas fault system. A significant proportion of this "missing" motion occurs in the Basin and Range, the seismicity of which plays an integral role in the tectonics of the plate boundary.

EARTHQUAKE HISTORY OF THE SAN ANDREAS FAULT SYSTEM

The historical record of major earthquakes affecting California, western Nevada, and northernmost Baja California (table 6.1) includes basic seismologic data on 206 of the largest earthquakes occurring between 1769 and 1989. This catalog lists all known events of $M \geq 6$ and includes new and updated information on their locations.

The record of seismicity within the San Andreas fault system and surrounding regions is both geographically and temporally uneven and incomplete before the introduction of practical seismographic instrumentation around the turn of the 20th century. In general, the density and distribution of people who left written accounts of their experiences determines the reliability of the catalog during the preinstrumental period. From the establishment of the Franciscan missions beginning in 1769 until their secularization in the 1830's, detailed accounts of events that damaged the missions are available, and these accounts form the primary source material for earthquakes occurring during this period. Life in California was a constant struggle for survival at that time; posting to a mission evidently was considered a hardship assignment, and so essentially nothing was recorded about events that were only felt, even when they were destructive at nearby missions. After secularization and before the gold rush, the quality of the record degrades with the cessation of the annual reports of the missions. Other sources of records also are notably weak during the Mexican period, from the early 1830's until 1846.

The discovery of gold in 1848 transformed the written record of earthquakes with the advent of newspapers throughout the gold fields in the Sierran foothills and in the San Francisco Bay region. Printed accounts of earthquakes have been extensively used, notably by Topozada and others (1988), to quantify the seismicity of California from 1850 onward. They estimated that their historical catalog is probably complete for the San

Francisco Bay region and central Sierra Nevada from 1850 on for earthquakes of $M \approx 6$. The same level of completeness is not achieved, however, for the San Andreas fault system in southern California until the 1890's. Statewide, the catalog of earthquakes is substantially complete for earthquakes of $M \approx 7$ after about 1850 (see Agnew, 1985). The quality of the catalog for central Nevada, where much significant 20th century seismicity has occurred, is less complete. Questions remain today about purported events as late as 1903 in this region (Slemmons and others, 1959).

Reports of the local effects of earthquakes continue to play a major role in determining the locations and sizes of earthquakes well into the 20th century. The earliest seismographs capable of systematically detecting California and Nevada earthquakes were installed throughout the world by John Milne beginning in 1896. Seismograms from these instruments and their successors provide useful instrumental magnitudes from 1898 onward. However, not until the development of the Wood-Anderson seismograph and its deployment throughout California beginning in 1926 do instrumental measurements fully supplant noninstrumental magnitudes and epicentral locations.

The objective in assembling a single catalog from these many sources, spanning many different types and qualities of information, has been to achieve uniform spatial coverage without sacrificing any events of historical significance. $M=6$ was chosen as the threshold magnitude because probably all events of this magnitude are known from the instrumental period beginning in 1898, and the preinstrumental record is reasonably complete at this level in some areas for an additional half-century. All earthquakes with at least one reported magnitude of at least 6.0 have been included in the catalog. Because magnitude is an estimated quantity and has some inherent uncertainty, events with reported magnitudes within a few tenths of a unit of 6.0 are also included. In addition to those earthquakes with cataloged magnitudes, original documents for others with reported high intensities or of particular historical significance have been reexamined in an attempt to refine their locations and magnitudes.

A word of introduction should be added about earthquake locations and magnitude scales and their use in this chapter. Earthquakes are complex physical processes generated by sudden slip on faults, and as such they can only be grossly characterized by simple concepts. Two seismologic conventions are in common use for assigning a single geographic coordinate to an earthquake: One measures the center of energy release, frequently as estimated from the intensity distribution for preinstrumental events; the other measures the location of the initial point of rupture, or hypocenter, as determined from seismic traveltime measurements. Either point on

the Earth's surface above the hypocenter or the center of the intensity distribution is sometimes referred to as the epicenter, and each type of location appears in table 6.1, with preference given to instrumental epicenters. Fortunately, the geographic differences between these distinct physical measures become significant only for the largest events, $M \approx 7$, when viewed at the scale of the entire San Andreas fault system.

Magnitude, as commonly used to compare the sizes of different earthquakes, also represents an extreme simplification of the earthquake process and by itself cannot fully characterize the size of any event. Traditionally, seismologists have developed a suite of magnitude scales, each with its own purpose and range of validity to measure an earthquake. Because no single magnitude scale can be systematically applied to the entire historical record, a summary magnitude, M , is introduced here to facilitate comparisons between events. As described below in the subsection entitled "Quantification of Earthquakes and Magnitude Scales," M is taken as the surface-wave magnitude (M_S), when available, and as a modified intensity magnitude (M_I) during the preinstrumental era. Generally speaking, M provides a better relative measure of the static, geologic increment of fault slip in the earthquake than it does of the severity of shaking.

The earthquake history of California, western Nevada, and northern Baja California presented here has apparent limitations and can doubtlessly be improved through further research. Nevertheless, it provides a firm observational basis for assessing the tectonic implications of the 2-century-long seismic history, as well as of the prospects for future earthquake activity.

PRINCIPAL EARTHQUAKES

In this section, we briefly discuss some events of particular historical, social, or scientific significance. Although each of the 117 San Andreas fault system events in table 6.1 merits discussion, this task is far beyond the scope of this review, and so the reader is referred to the reports by Richter (1958), Coffman and others (1982), and Townley and Allen (1939) for an introduction to many of these events. Table 6.1 also omits several historically significant events with magnitudes well below the nominal threshold of $M=6$ adopted here, and so it something less than a complete reference on San Andreas seismicity.

My major effort in constructing this catalog has gone into identifying and validating all reported events of $M \geq 6$. Two conspicuous omissions from table 6.1, events that are commonly mentioned in the literature but that could not be substantiated upon further inspection, should be noted. The first is the 1852 earthquake alleged

to have ruptured the Big Pine fault (for example, Jennings, 1975). Topozada and others (1981) failed to find any evidence supporting the occurrence of a major earthquake at that time in the region. Geologic inspection of the surface trace of the fault by M.M. Clark (oral commun., 1988) similarly failed to provide evidence of any historical activity. The other deleted event appears on the seismicity map by Goter (1988) at lat 35° N., long 125° W., with an epicenter from the catalog of Abe and Noguchi (1983). Although a large ($M_S=6.8$) earthquake certainly took place on March 22, 1902, no evidence has been uncovered to support a location anywhere on shore in California or, for that matter, in the Western United States. The original location determined by Milne in 1903 placed the event well off the California-Oregon coast at lat 42° N., long 130° W.

JULY 28, 1769 ($M=6$)

The earthquake history of California serendipitously begins with the first overland expedition through the State in 1769. In response to the perceived threat posed by Russian expansion into the northern Pacific and growing British presence in the northwestern Pacific, Spain embarked on the colonization of present-day California through the establishment of a series of Franciscan missions, supported by military garrisons at San Diego and Monterey. In the summer of 1769, Gaspar de Portolá led the first expedition from San Diego to establish a land route to Monterey.

On July 28, while camped along the Santa Ana River, about 50 km southeast of Los Angeles, a sharp earthquake was felt that " * * * lasted about half as long as an Ave Maria" (fig. 6.3). From the diaries of three members of the expedition, we know that earthquakes were felt on nearly a daily basis through August 3, as the party traveled northwestward to near San Gabriel and then westward across Los Angeles to the Pacific. The diary of Fray Juan Crespi (Bolton, 1927) mentions no fewer than a dozen aftershocks, some described as violent. After August 4, no further earthquakes were mentioned as the expedition traveled into the San Fernando Valley and exited to the north.

These sketchy reports suggest that the explorers traveled near or through the epicentral area of a moderate earthquake (Richter, 1973; Topozada and others, 1981). Comparisons between the accounts of the aftershocks and more recent events suggest an event of similar size and location to the 1933 Long Beach, 1971 San Fernando, or 1987 Whittier Narrows earthquake. If significance is placed on the absence of aftershocks while crossing the source region of the 1971 San Fernando earthquake, the evidence would seem to favor a source in the Los Angeles Basin. An event on either the San

Andreas or San Jacinto faults, some 50 km to the northeast, could conceivably have been the source of the 1769 earthquake. The description of the duration of strong shaking, however, suggests a magnitude more of 5-6 than of 7-8.

A more distant source would make the long, felt aftershock sequence even more remarkable because it would be well removed from the expedition route.

DECEMBER 8, 1812 ($M=7$)

The first of two significant earthquakes to occur in southern California in 1812 occurred on December 8 and destroyed the church at Mission San Juan Capistrano, killing 40 neophytes (fig. 6.4); damage was also sustained

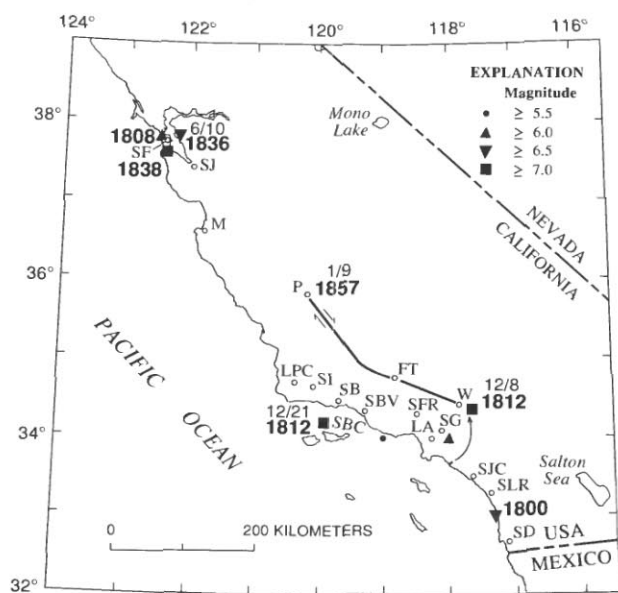


FIGURE 6.3.—Early accounts of significant earthquakes reflect the sparse settlement of California in a narrow coastal corridor before the population explosion accompanying the gold rush in 1849. Accounts of the few well-documented events (dates shown) principally derive from mission records at San Diego (SD), San Luis Rey (SLR), San Juan Capistrano (SJC), San Gabriel (SG), San Fernando Rey (SFR), San Buenaventura (SBV), Santa Barbara (SB), Santa Inez (SI), and La Purisima Concepción (LPC), and from the towns of Los Angeles (LA) and Fort Tejon (FT) in southern California. Accounts from the Spanish capital Monterey (M), San Francisco (SF), and San Jose (SJ), as well as mission sources, detail events in north half of the State. Uncertainties in the interpretation of every event before the great earthquake of 1857 (rupture shown; arrows indicate direction of relative movement) are well illustrated by newly uncovered evidence suggesting a San Andreas origin for the December 8, 1812, shock near Wrightwood (head of connecting arrow), well inland of traditional location along the coastal Newport-Inglewood fault (tail of arrow). Earthquake of December 21, 1812, locates in the Santa Barbara Channel (SBC). Foreshocks of the great earthquake of 1857 locate near Parkfield (P), suggesting unilateral rupture propagation to the southeast.

at San Gabriel. The accounts of this earthquake and the later one on December 21 cannot be readily disentangled at San Fernando Rey and at San Buenaventura, considerably complicating the interpretation of this event.

Analyses of these scanty data by Topozada and others (1981) and Evernden and Thompson (1985) place the epicenter along the south half of the Newport-Inglewood fault zone (fig. 6.3). This location is somewhat constrained by the interpretation of no damage at Buenaventura during the event. The Los Angeles Star of January 10, 1857, however, stated that the December 8 event severely damaged the church tower (Agnew and Sieh, 1978). The same story attributed the collapse of the stone arch roof of the church at San Juan Capistrano to poor construction, a possibility made credible by the death of the master mason before completion of the church (fig. 6.3; Duncan Agnew, oral commun., 1988).

Recently, Jacoby and others (1988) proposed that this event ruptured the San Andreas fault at Wrightwood (fig. 6.3), on the basis of dendrochronologic dating of distress to trees growing on the fault trace. Sieh and others (1989) argued that this rupture extended at least 25 km northwestward into the peat bog at Pallet Creek. The fault rupture in this event preserved at Pallet Creek is comparable in size to the rupture formed in the 1857 earthquake.

The preferred location of the December 8, 1812, earthquake on the San Andreas fault as proposed by Jacoby and others appears in table 6.1. A magnitude of about 7 is consistent with the inferred extent of damage. The lateral extent of rupture is unconstrained to the southeast and may well have extended into the San Bernardino Valley. However, the accounts of the earthquake from Indians living in the San Bernardino Valley that were thought to place some constraint on the rupture are now believed to be fictitious (Harley, 1988), leaving Mission San Gabriel, some 40 km from the rupture, as the nearest point of observation.

DECEMBER 21, 1812 ($M=7$)

The second major episode of earthquake activity in 1812 damaged the missions along the Santa Barbara Channel and western Transverse Ranges just 13 days later, on December 21 (fig. 6.3). All investigators place this event in the Santa Barbara Channel and assign a magnitude of about 7 (see Topozada and others, 1981, and Evernden and Thompson, 1985, for two recent analyses). This sequence appears to have involved two events of comparable magnitude separated in time by about 15 minutes. A vigorous aftershock sequence accompanied the earthquakes and lasted until the end of the year at Mission Santa Barbara and Mission La Purisima Concepción. Reports of a tsunami appear to be exagger-

ated, although some kind of wave activity probably accompanied the earthquake (Topozada and others, 1981; McCulloch, 1985).

JUNE 10, 1836 ($M=6\frac{3}{4}$)

Little is known about the strong earthquake of June 10, 1836, that struck the then lightly populated San Francisco Bay region. An account of the event, published in the aftermath of the 1868 earthquake, provides the principal rationale for associating this event with the Hayward fault. Louderback (1947) systematically compared the two events and concluded that the 1836 earthquake probably ruptured the Hayward fault. Lindh (1983) proposed that the 1836 event ruptured the north half of the fault, whereas the 1868 event is known to have ruptured the south half, thereby avoiding the paradox of two large events on the same segment separated by a scant 32 years.

JUNE 1838 ($M=7$)

The pioneering historical work of Louderback (1947) reveals that a major earthquake with probable rupture of the San Andreas fault occurred in June 1838. Documentation of the event is so poor that its date cannot be fixed more precisely than "late June." Louderback concluded that the shock was comparable in magnitude to the 1906 earthquake. Current opinion suggests a smaller event involving only the 60+-km-long segment of the fault on the San Francisco peninsula (Working Group on Earthquake Probabilities, 1988).

JANUARY 9, 1857 ($M=8\frac{1}{4}$)

The great Fort Tejon earthquake of January 9, 1857, ruptured 300 km of the San Andreas fault from near Parkfield to Wrightwood and offset the fault by as much as 9½ m on the Carrizo Plain. The fault rupture and the effects of the earthquake have been extensively studied, notably by Agnew and Sieh (1978) and Sieh (1978b). The epicenter of this event appears to have been at the extreme northwest end of the fault rupture, as determined by the intensity patterns of two $M=6$ foreshocks centered near Parkfield (Sieh, 1978a). Strong shaking lasted from 1 to 3 minutes, consistent with unilateral rupture propagation to the southeast (fig. 6.3).

The earthquake caused only two deaths in the sparsely settled southern California region. Damage was most severe along the fault zone; nearly every building sustained damage at Fort Tejon. In Los Angeles, then a city of about 4,000 people located approximately 60 km from the fault, some houses were cracked, but none were severely damaged (Agnew and Sieh, 1978). Modified Mercalli intensities (MMI's) of VII or more occurred in the San Fernando Valley, San Gabriel Valley, and Ventura region.

It is natural to compare the 1857 and 1906 earthquakes, the two greatest earthquakes of the San Andreas fault in historical time. The 1906 fault break was longer, whereas maximum and average surface offsets were larger in 1857. These differences approximately balance each other, and so the seismic moments of the two events are approximately equal. Moment magnitudes computed using comparable data are $M=7.8$ for the 1857 earthquake

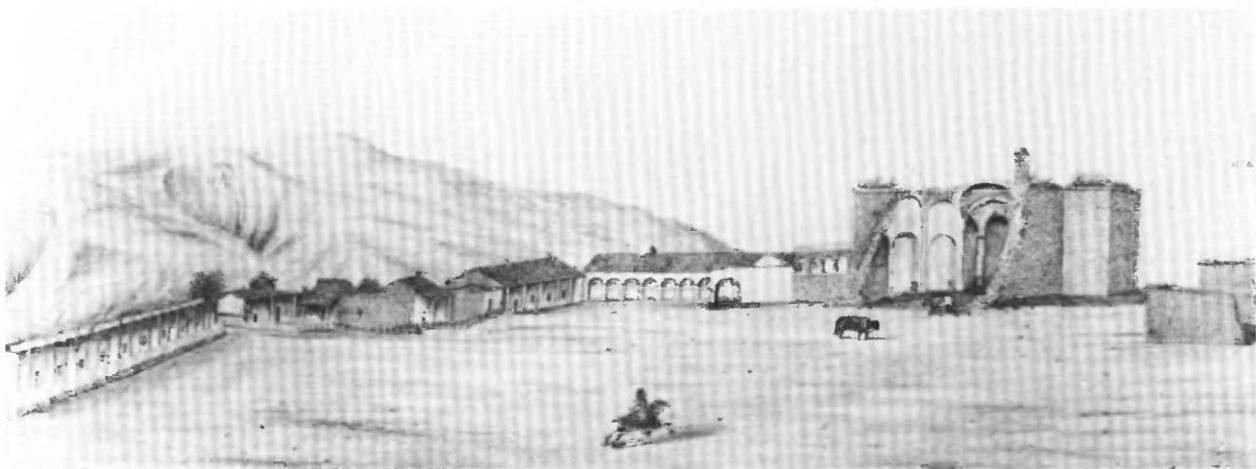


FIGURE 6.4.—Mission San Juan Capistrano as drawn by Henry Miller in 1856, 43 years after the December 8, 1812, earthquake. Vaulted stone church at right collapsed in that earthquake, killing 40 worshippers. Photograph courtesy of the Bancroft Library.

and $M=7.7$ for the 1906 event. A summary magnitude of $M=8\frac{1}{4}$ was assigned by analogy with the 1906 earthquake.

OCTOBER 21, 1868 ($M=7$)

Known as the "great San Francisco earthquake" until 1906, one of California's most destructive earthquakes occurred on October 12, 1868, resulting from slip on the Hayward fault. Heavy damage occurred in communities situated along the fault and in San Francisco and San Jose (fig. 6.5). Sadly, many of the engineering lessons learned from this earthquake and openly discussed at the time, such as the hazards of building on "made ground" reclaimed from the San Francisco Bay or the admonition to "build no more cornices," were long forgotten by the time of the 1906 earthquake.

FEBRUARY 24, 1892 ($M=7$)

The strong earthquake of February 24, 1892, located near the United States-Mexican border was assigned to the Agua Caliente fault north of the border by Topozada and others (1981) and to the Laguna Salada fault in Baja California by Strand (1980). The literature on earthquakes in Baja California contains numerous references to this earthquake as having originated near the Agua Blanca fault, about 100 km southwest of Strand's epicenter (for example, Richter, 1958). The two recent intensity maps clearly rule out this epicenter and place it on the southern section of the Elsinore fault system.

APRIL 19 AND 21, 1892 ($M=6\frac{1}{2}$ AND $6\frac{1}{4}$)

A pair of strong earthquakes rocked the west side of the Sacramento Valley on April 19 and 21, 1892, heavily damaging the towns of Vacaville, Dixon, and Winters. The first shock was stronger and caused heavy damage at Vacaville; the aftershock was more severe at Winters. The earthquakes are reminiscent of the 1983 Coalinga, Calif., earthquake, in that both sequences were positioned along the western margin of the Central Valley. Focal mechanisms of small earthquakes located along this boundary zone show numerous examples of low-angle-thrust focal-mechanism solutions of similar orientation to the Coalinga earthquake, in addition to strike-slip mechanisms (see chap. 5; Wong and others, 1988), suggesting the possibility of a similar mechanism for these 1892 earthquakes.

DECEMBER 25, 1899 ($M=6.4$)

Heavy damage occurred in the towns of San Jacinto and Hemet, located along the San Jacinto fault, from an

earthquake on Christmas Day 1899. Six fatalities were attributed to the earthquake.

APRIL 18, 1906 ($M=8\frac{1}{4}$)

The California earthquake of April 18, 1906, ranks as one of the most significant earthquakes of all time. Today, its importance comes more from the wealth of scientific knowledge derived from it than from its sheer size. Rupturing the northernmost 430 km of the San Andreas fault from northwest of San Juan Bautista to the triple junction at Cape Mendocino (fig. 6.6), the earthquake confounded contemporary geologists with its large, horizontal displacements and great rupture length. Indeed, the significance of the fault and recognition of its large cumulative offset would not be fully appreciated until the advent of plate tectonics more than half a century later. Analysis of the 1906 displacements and strain in the surrounding crust led Reid (1910) to formulate his elastic-rebound theory of the earthquake source, which remains today the principal model of the earthquake cycle.

As a basic reference about the earthquake and the damage it caused, geologic observations of the fault rupture and shaking effects, and other consequences of the earthquake, Lawson's (1908) report remains the authoritative work, as well as arguably the most important study of a single earthquake. In the public's mind, this earthquake is perhaps remembered most for the fire it spawned in San Francisco, giving it the somewhat misleading appellation of the "San Francisco earthquake" (fig. 6.7). Shaking damage, however, was equally severe in many other places along the fault rupture. The frequently quoted value of 700 deaths caused by the earthquake and fire is now believed to underestimate the total loss of life by a factor of 3 or 4. Most of the fatalities occurred in San Francisco, and 189 were reported elsewhere.

At almost precisely 5:12 a.m. local time, a foreshock occurred with sufficient force to be felt widely throughout the San Francisco Bay area. The great earthquake broke loose some 20 to 25 s later, with an epicenter near San Francisco (Bolt, 1968; Boore, 1977). Violent shocks punctuated the strong shaking, which lasted some 45 to 60 s. The earthquake was felt from southern Oregon to south of Los Angeles and inland as far as central Nevada (fig. 6.6). The highest MMI's of VII to IX paralleled the length of the rupture, extending as far as 80 km inland from the fault trace. One important characteristic of the shaking intensity noted in Lawson's (1908) report was the clear correlation of intensity with underlying geologic conditions. Areas situated in sediment-filled valleys sustained stronger shaking than nearby bedrock sites, and the strongest shaking occurred in areas where ground

reclaimed from San Francisco Bay failed in the earthquake. Modern seismic-zonation practice accounts for the differences in seismic hazard posed by varying geologic conditions (see Borchardt, 1975, and Ziony, 1985, for analyses of the San Francisco Bay and Los Angeles regions, respectively).

The characteristics and amount of surface fault slip in this earthquake varied to a remarkable degree along the length of the rupture. Peak displacements of 6 m were measured near Olema on the Point Reyes peninsula, where the surface trace of the rupture formed a sharp, well-defined break (fig. 6.8). In contrast, the fault break was extremely difficult to recognize along its southernmost 90 km, where the surface offset averaged only about 1½ m or less (see chap. 7).

The magnitude of 8.3 commonly quoted for the 1906 earthquake comes from Richter (1958) and, within the precision of reporting, is identical to the 8¼ listed by Gutenberg and Richter (1954). Table 6.1 also lists other magnitudes for this earthquake, derived from recent analyses of both the same data used by Gutenberg and Richter and new data. Strictly speaking, a "Richter magnitude" (M_L) for the earthquake cannot be determined because no appropriate seismographs were in

operation at the time. Jennings and Kanamori (1979) used related measurements extracted from simple pendulums at Yountville, Calif., and Carson City, Nev., to derive $M_L=6.9$, substantially smaller than the traditionally quoted value. M_L , which is based on the single largest peak on a seismogram at approximately 1-s period and takes into account neither the duration of the event nor longer period motions, is saturated for this event.

Geller and Kanamori (1977) used the unpublished worksheets of Gutenberg and Richter to compute a body-wave magnitude of $m_b=7.4$, using the procedure of Gutenberg and Richter (1956). Because long-period (14 s) P -waves were used in this calculation, it cannot be directly compared to the short-period m_b values routinely reported today.

Other workers since Gutenberg and Richter have studied the long-period surface waves of the 1906 earthquake and computed M_S values. Bolt (1968) confirmed an M_S of about 8¼, whereas Lienkaemper (1984) found $M_S=8.3$ from an analysis of all the records collected by Reid (1910). Lienkaemper's magnitude combined data from both damped and undamped instruments, correcting each for magnification at the appropriate period of motion. Abe (1988), who analyzed only the undamped Milne seismograms, obtained $M_S=7.8$, using slightly different procedures and a systematic set of station-magnitude corrections. Also, the four damped seismometers (all in Europe) give $M_S=8.1$. Longer period (50-100 s) surface waves analyzed by Thatcher (1975) indicate a seismic moment of 4×10^{27} dyne-cm, equivalent to $M=7.7$, in agreement with the seismic moment of 5×10^{27} dyne-cm obtained from geodetic data, thus giving $M=7.8$ (Thatcher and Lisowski, 1987). Finally, Topozada and Parke (1982) assigned an intensity magnitude (M_I) of 7.8 on the basis of the total area (48,000 km²) undergoing shaking of MMI VII or higher.

The "traditional" magnitude of 8¼ is retained here, except where seismic moment is used for quantitative purposes.

NOVEMBER 21, 1915 ($M=7.1$)

The major earthquake of November 21, 1915, triggered a spectacular steam eruption of a mud volcano, creating a 100+-m crater in Volcano Lake, Baja California, near the north terminus of the Cerro Prieto fault. Extensive cracking of the levee around the lake was noted at the time of the shock, but no tectonic ground displacements were found (Seismological Society of America Bulletin, 1916). This event may well be related to the November 29, 1852, earthquake ($M=6\frac{1}{2} \pm$), which also triggered a mud-volcano eruption at Volcano Lake that was observed at Fort Yuma, Ariz. Each of these events was probably associated with the Cerro Prieto fault.

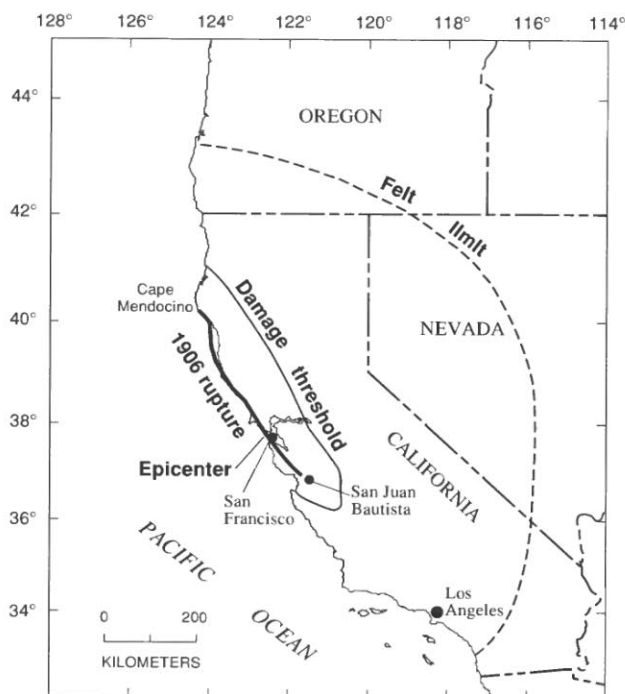


FIGURE 6.6.—California earthquake of 1906 showing extent of fault rupture along the San Andreas fault, location of epicenter near San Francisco, maximum extent of structural damage, and limits of perception of shock. Modified from Lawson (1908) and Topozada and Parke (1982).

APRIL 21, 1918 ($M=6.9$)

The communities of Hemet and San Jacinto were severely damaged for the second time in 19 years by the large earthquake of April 21, 1918, on the San Jacinto fault. Both the 1899 and 1918 earthquakes produced similar intensity patterns throughout the southern California region, and these two events have been compared to each other. However, surface waves on Milne seismograms at common stations (Victoria, British Columbia, and Toronto, Ontario, Canada; San Fernando, Spain) average 3 times larger for the 1918 earthquake, corresponding to a difference in M_S of $\frac{1}{2}$ unit. As with the 1836 and 1868 earthquakes on the Hayward fault, the relation between the rupture zones in these two events is unclear. Surprisingly, no surface rupture was found for an event of this size, despite a specific search for it.

NOVEMBER 4, 1927 ($M=7.3$)

The Lompoc earthquake of November 4, 1927, is the largest known event in the San Andreas system west of

the San Andreas fault proper. This event produced a tsunami with local runup heights of 1.5 to 1.8 m (McCulloch, 1985). The exact location of the earthquake and its association with any causative structure remain the subject of a spirited debate (Gawthrop, 1978, 1981; Hanks 1979, 1981).

MARCH 11, 1933 ($M=6.3$)

Rupture of the Newport-Inglewood fault on March 11, 1933, caused major damage and a loss of 115 lives in Long Beach and surrounding parts of the Los Angeles Basin. Structural damage to public schools was particularly serious, and had the event occurred when schools were in session, the calamity would have been far worse. The Field Act, mandating construction standards for schools in California, was enacted as a consequence of the earthquake.

DECEMBER 30 AND 31, 1934 ($M=6.5$ AND 7.0)

The major sequence that occurred along the Cerro Prieto fault on December 30 and 31, 1934, appears to



FIGURE 6.7.—San Francisco, Calif., on the morning of April 18, 1906. This famous photograph by Arnold Genthe shows Sacramento Street and approaching fire in the distance. Although some buildings sustained heavy damage in the earthquake, this and many other

photographs taken of the city before fire swept through show no visible evidence of damage in most structures. Photograph courtesy of the Fine Arts Museums of San Francisco, Achenbach Foundation for Graphic Arts.

have ruptured the surface trace of the fault near where it enters the Gulf of California. Aerial photographs of the fault crossing a tidal flat taken in 1935 show very fresh appearing fault morphology; subsequent photographs display a substantially subdued morphology (Kovach and others, 1962).



FIGURE 6.8.—Trace of 1906 earthquake rupture near point of maximum offset (6 m) near Olema on the Point Reyes peninsula north of San Francisco. Photograph by G.K. Gilbert. View northwestward.

MAY 19, 1940 ($M=7.1$)

The Imperial fault was discovered from its 60+-km-long rupture in the Imperial Valley earthquake of May 19, 1940. Faulting was predominantly right-lateral strike slip and attained a peak offset of more than 6 m at the United States-Mexican border (fig. 6.9). The first instrumental measurement of strong ground motion adjacent to a fault rupture was obtained from an accelerometer located about 7 km from the surface trace. This record, which provides clear evidence of irregular seismic-energy release during the course of the event (Trifunac and Brune, 1970), has played a major role in shaping building codes for earthquake-resistant design.

JULY 21, 1952 ($M=7.7$)

The Kern County or Arvin-Tehachapi earthquake of July 21, 1952, ruptured the White Wolf fault in the largest event to strike California since 1906. The earthquake led to 12 fatalities, and 2 more occurred during a large aftershock on August 22. Field studies of the earthquake (Oakeshott, 1955) describe the geologic, seismologic, and engineering aspects of the earthquake. From a tectonic standpoint, this event is notable for its conjugate relation to the San Andreas fault. Left-lateral slip with a significant reverse-slip component occurred on the northeast-striking, south-dipping fault plane.



FIGURE 6.9.—Surface faulting in 1940 Imperial Valley earthquake offset (6 m) regular rows of orange trees. Fault displacement along this section of the Imperial fault was confined to a narrow zone.

FEBRUARY 9, 1956 ($M=6.8$)

More than 19 km of the hitherto-unknown San Miguel fault in Baja California ruptured in the earthquake sequence of February 9, 1956. The fault offset was consistently right lateral and up to the northwest, and attained maximum horizontal and vertical separations of 78 and 91 cm, respectively (Shor and Roberts, 1958). The sequence contained numerous aftershocks, including three of $M \geq 6$. About 2 years earlier, a pair of $M=6$ events that occurred to the south and west of the San Miguel fault may have been associated with the Agua Blanca fault.

APRIL 9, 1968 ($M=6.5$)

The Borrego Mountain earthquake of April 9, 1968, produced the first documented rupture of the San Jacinto fault system when right-lateral displacements of nearly 0.4 m occurred along a 30-km-long segment of the Coyote Creek fault. The U.S. Geological Survey (1972) published a detailed description of the event.

FEBRUARY 9, 1971 ($M=6.5$)

The San Fernando earthquake of February 9, 1971, ranks as one of the most serious California earthquakes in historical time. The event claimed 58 lives and caused more than half a billion dollars in property damage, including the destruction of two hospitals, a freeway interchange, and the Van Norman Dam. The earthquake ruptured north-dipping, high-angle reverse faults beneath the southern margin of the San Gabriel Mountains and broke the surface along a discontinuous, 15-km-long zone. Surface displacements averaged about 1 m. Seismograms of the earthquake reveal a steeply dipping deep fault and a more shallowly dipping near-surface fault (Langston, 1978; Heaton, 1982). Numerous publications report on detailed investigations of this event, including the summary report published by the U.S. Geological Survey (1971).

OCTOBER 15, 1979 ($M=6.5$)

The Imperial fault ruptured for the second time in less than 40 years in a major surface-faulting earthquake on October 15, 1979 (U.S. Geological Survey, 1982). The event broke the north 30 km of the fault, or approximately half the length of the 1940 fault break. However, it was clearly much smaller than the earlier event; maximum surface offsets were well under 1 m, in contrast to 6 m observed in 1940, and the seismic moment was smaller by nearly an order of magnitude. Within the zone of overlapping surface rupture, the two events display nearly

identical displacement profiles (Sharp, 1982), suggesting that the 1979 earthquake represents a characteristic rupture of this segment of the fault. Strong-ground-motion records for the 1979 earthquake form an unparalleled suite of near-field recordings and have stimulated numerous investigations into the dynamics of the source.

MAY 2, 1983 ($M=6.5$)

Our understanding of the nature of the earthquake hazard posed by active faults in the San Andreas fault system was fundamentally altered by the occurrence of the Coalinga earthquake of May 2, 1983, on a low-angle thrust fault deep beneath the western margin of the San Joaquin Valley (Rymer and Ellsworth, 1990). Before this event, it had been thought that the major, seismically active faults in California could be recognized on the basis of their surface exposures and record of late Quaternary activity. However, no surface expression exists for the fault system responsible for either this event or the $M=5.9$ North Kettleman Hills earthquake of August 4, 1985, that adjoins it to the southeast. Instead of a surface fault, the buried deformation is expressed at the surface by active folds (the Coalinga anticline and the Kettleman Hills) that grew during the earthquakes (Stein and King, 1984).

The orientation of the fault and the style of movement on it present another major challenge to prevailing models of the San Andreas system, because this earthquake resulted from a release of compressive forces oriented nearly perpendicular to the trace of the San Andreas fault. Accumulating evidence on the orientation of the stress field astride the San Andreas fault suggests that only a small component of the total stress acts to accommodate the plate motion along the San Andreas fault itself (Mount and Suppe, 1987; Zoback and others, 1987).

NOVEMBER 24, 1987 ($M=6.6$)

The Superstition Hills fault ruptured in its entirety on November 24, 1987. The total amount of separation substantially increased by persistent afterslip in the months after the main shock; in fact, the rate of afterslip was so great on the south half of the surface break as to leave open the possibility that all of its displacement occurred as afterslip. The earthquake was preceded by a major foreshock ($M=6.2$), on a conjugate, northeast-trending, left-lateral strike-slip fault that intersected the Superstition Hills fault at the main-shock epicenter. The surface-faulting pattern of the entire sequence was particularly remarkable for the occurrence of numerous breaks on other conjugate faults in the north quadrant around the main break (see Hanks and Allen, 1989).

OCTOBER 18, 1989 ($M=7.1$)

In the late afternoon of October 17, 1989, the San Andreas fault ruptured in its first major earthquake since 1906 at 5:04 p.m. P.d.t. (0004 G.m.t. on Oct. 18). Centered along a remote segment of the fault in the southern Santa Cruz Mountains, the Loma Prieta earthquake reruptured the southernmost 40 km of the 1906 fault break, producing the Nation's most costly natural disaster. The earthquake claimed 62 lives and injured an additional 3,757 people. It destroyed 963 homes and damaged more than 18,000 others, displacing 12,000 people from their residences. The combined dollar loss to the private and public sectors exceeded \$6 billion (Plafker and Galloway, 1989).

Damage in the epicentral region was most severe where the earthquake shaking was compounded by local ground failures, commonly involving landslide movement but also including some fractures of probable tectonic origin; the shaking clearly reactivated some fissures observed in 1906. Primary fault displacement, however, did not reach the surface. In the hard-hit communities of Santa Cruz, Watsonville, and Los Gatos, unreinforced-masonry buildings bore the brunt to the damage, and ground conditions played a significant role in the damage patterns.

The earthquake also caused grave damage and claimed the greatest number of lives far to the north, in San Francisco and Oakland, about 100 km from the epicenter. There, the earthquake selectively destroyed structures known to be at risk or located on poor ground (Plafker and Galloway, 1989). The root cause of the devastation in the Marina District of San Francisco (fig. 6.10), as well as at most other sites along the margin of the San Francisco Bay, was liquefaction-induced ground failure. All of these localities sit on land reclaimed from the bay and are underlain by young, water-saturated sedimentary deposits. As we know from the clear lessons of history, provided by the earthquakes of 1865, 1868, and 1906 (Lawson, 1908), such materials perform poorly even under modest levels of earthquake shaking. The collapse of the double-decked section of California Interstate Highway 880 in Oakland (fig. 6.10), where 41 people died, resulted principally from design defects. The section of the viaduct that collapsed was founded on soft estuarine sedimentary deposits that amplified the strong ground motion; the adjoining section, founded on alluvium, rode through the earthquake.

The earthquake broke the San Andreas fault where it makes a conspicuous leftward bend, connecting straighter subparallel segments to the north and south. The fault plane dips 70° SW., and movement in the earthquake involved comparable amounts of right-lateral strike slip and reverse slip, a kinematic response driven by the need

to remove material from this compressional fault bend as the Pacific plate moves to the northwest around it. The rupture nucleated at the base of the seismic zone, at 18-km depth, and spread unilaterally upward and bilaterally along strike, filling a conspicuous void in the preevent seismicity. Geodetic data collected immediately after the event suggest an average strike-slip displacement of 1.6 m and an average reverse-slip displacement of 1.2 m, rising from the hypocenter at 18 km to within 6 km of the surface.

The Loma Prieta earthquake fulfilled a long-term forecast for the rupture of this specific segment of the San Andreas fault (Lindh, 1983; Sykes and Nishenko,



FIGURE 6.10.—Damage in October 18, 1989, Loma Prieta earthquake occurred at distances as far as 100 km from the epicenter in areas underlain by water-saturated, unconsolidated material. *A*, Liquefaction-induced ground failure in the Marina district of San Francisco (top) was restricted to land reclaimed from the San Francisco Bay. *B*, In Oakland, the second deck of Interstate Highway 880 collapsed onto the first deck. Here, poor design was the principal culprit, although failed section sits atop estuarine sedimentary deposits that amplified the shaking.

1984; Working Group on California Earthquake Probabilities, 1988). The high earthquake potential assigned to this segment stemmed from its behavior in the 1906 earthquake, when the fault displacement, as measured at the surface, averaged about 1.5 m, far less than the average for the entire rupture. Estimates of the long-term slip rate along this segment of the San Andreas fault suggested that the strain released in the 1906 earthquake would be renewed in 75 to 136 years, implying that another earthquake was possible in the coming decades. With its occurrence, the Loma Prieta earthquake became the second event in 2 years to fill a recognized seismic gap along the San Andreas; the first was the 1987 Superstition Hills earthquake. The Loma Prieta earthquake also represents the third historical rupture of this segment of the San Andreas fault; the first was the October 8, 1865, earthquake, nominally assigned $M=6\frac{1}{2}$, which also caused liquefaction-induced ground failure in San Francisco.

SEISMICITY OF THE WESTERN BASIN AND RANGE PROVINCE

The advent of plate tectonics and its application to western North America by Atwater (1970) provided a unifying framework for the contemporary tectonics of the western Basin and Range and its interaction with the San Andreas fault system to the west. Deformation within the province reflects soft coupling of the San Andreas fault system to the North American craton and distribution of the relative plate motion—by mechanisms yet unknown—well over 500 km into the continental interior. The ubiquity of normal-fault-bounded ranges throughout the province tends to belie the underlying nature of present-day deformation within the region. Within historical time, this region has undergone nearly equal proportions of extension on normal faults and dextral shear on strike-slip faults.

The earthquake history of the western Basin and Range province is poorly known before the instrumental period, owing to sparse settlement of this high-desert region. The deficiencies of this record are illustrated by the uncertainties associated with fresh-appearing fault scarps discovered in 1911 near the north end of what would become the rupture zone of the 1954 Fairview Peak earthquake. Upon reviewing the scant historical evidence, Slemmons and others (1959) concluded that these scarps formed about 1903. The absence of an event of sufficient size in the instrumental record, however, suggests that the scarp forming event is older (or substantially smaller than $M=6$). Current understanding of 19th-century seismicity includes an episode of activity along the California-Nevada State line, including a probable rupture of the Olinghouse fault on December 27,

1869 (Sanders and Slemmons, 1979), although this conclusion was questioned by Topozada and others (1981).

Surface faulting has accompanied numerous earthquakes in the region, the most significant of which are discussed below. Notable additional surface-faulting events include the $M=6.3$ Excelsior Mountain, Nev., earthquake of 1934 and the $M_L=5.6$ Fort Sage Mountain earthquake of December 14, 1950, located in northeastern California (Gianella, 1957). Ground rupture may have also accompanied the $M=6$ earthquake of January 24, 1875 (see Gianella, 1957). If so, this observation would move the epicenter listed in table 6.1 to lat $39\frac{3}{4}^\circ$ N., long $120\frac{1}{2}^\circ$ W.

PRINCIPAL EARTHQUAKES

MARCH 26, 1872 ($M=7.6$)

The town of Lone Pine, Calif., was virtually leveled when the entire 100 to 110-km length of the Owens Valley fault ruptured on March 26, 1872, in one of the largest earthquakes in U.S. history. This fault, which lies in the middle of Owens Valley, is distinct from the normal faults bounding the front of the Sierra Nevada to the west. Considerable confusion has existed in the literature regarding the style of faulting in the 1872 earthquake, including interpretations of right-lateral, left-lateral, and normal-fault movement. A recent study of the earthquake offsets by Beanland and Clark (in press) unambiguously demonstrates that fault movement was predominately right-lateral strike slip, with an average horizontal displacement of 6 m (fig. 6.10). The vertical offsets were clearly smaller and averaged about 1 m down to the east. Beanland and Clark estimate a moment magnitude of $M=7.5-7.7$. Faulting in 1872 largely reactivated earlier Holocene scarps, as recognized by G.K. Gilbert when he visited the area in 1883.

The event was felt throughout most of California and Nevada, and as far east as Salt Lake City, Utah. Adobe and brick buildings in Owens Valley sustained the brunt of the damage. Minor damage also occurred in the San Joaquin and Sacramento Valleys on the opposite side of the Sierra Nevada, at distances of as far as 400 km. In Yosemite Valley, John Muir witnessed a spectacular rockfall triggered by the earthquake. As severe as the ground shaking must have been, it was noted in the Inyo, Calif., *Independent* of April 6, 1982, “* * * that not a person would have been killed or hurt had their houses all been made of wood.” It is of some historical interest that the first long-term earthquake forecast, made by G.K. Gilbert in 1883 to the citizens of Salt Lake City, was based in part on his observations of the 1872 earthquake. In it, he noted that the rebuilding of Independence with wood-frame buildings was an extravagance, because this

great shock had relieved the accumulated strain, and so many generations would pass before conditions would permit another similar shock to occur (Gilbert, 1884):

The old maxim, "Lightning never strikes in the same spot twice" is unsound in theory and false in fact; but something similar might truly be said about earthquakes. The spot which is the focus of an earthquake (of the type here discussed [1872 Owens Valley]) is thereby exempted for a long time.

Many comparisons have been drawn between the Owens Valley earthquake and the great San Andreas earthquakes of 1857 and 1906. The size of the regions shaken in all three events are comparable, as are the maximum fault displacements. The two San Andreas events have significantly longer rupture lengths, and their seismic moments are larger by a factor of 2 to 3. Whether or not any or all of these earthquakes can be classified as "great" earthquakes becomes a question of semantics. All of them can be classified as great on the basis of their rupture lengths of 100 km or more (Kanamori, 1977), but they all have seismic moments more than 100 times smaller than the largest known earthquakes, such as the $M=9.2$ Alaska earthquake of 1964. Practically speaking, these events are among the largest known strike-slip events, and they must be close to the size of the largest possible strike-slip events along the San Andreas fault system.

OCTOBER 3, 1915 ($M=7.3$)

The 1915 Pleasant Valley, Nev., earthquake of October 15, 1915, created a series of spectacular normal-fault scarps in the central Nevada seismic zone of the Basin and Range province (figs. 6.11, 6.12). Four major scarps formed during the earthquake, with an aggregate length of 59 km, and reruptured Holocene scarps at the base of the mountain blocks (Wallace, 1984). Fault movement in the earthquake appears to have been purely dip slip and averaged about 2 m on the steeply dipping fault plane. The earthquake was felt from western Utah to the Pacific coast and from northeastern Oregon to the United States-Mexican border. Instrumental measures of the magnitude range from 7.3 to $7\frac{3}{4}$ and exceed the moment magnitude of 7.2 derived from field measurements ($M_0=6.1 \times 10^{27}$ dyne-cm).

The Pleasant Valley earthquake lies at the north end of a 500-km-long belt of historical surface-faulting earthquakes within the central Nevada seismic zone and Owens Valley fault system. The four major earthquake sequences in this zone since 1872 leave two conspicuous seismic gaps that have been discussed as the potential loci of future major earthquake activity (fig. 6.11; Wallace, 1984).

DECEMBER 21, 1932 ($M=7.2$)

The second historical surface-faulting event in the central Nevada seismic zone on December 21, 1932, produced a discontinuous zone of surface faulting and fissures in the valleys west and north of Cedar Mountain (Gianella and Callaghan, 1934). Within the 60-km-long, north-northwest-trending zone where faulting was observed, most breaks struck east of north and showed clear evidence of right-lateral displacements (fig. 6.11).

JULY 6, 1954 ($M=6.6$), AND AUGUST 24, 1954 ($M=6.8$)

The Rainbow Mountain earthquakes of July 6 and August 24, 1954, produced a zone of east-facing normal-fault scarps along the base of Rainbow Mountain, extend-

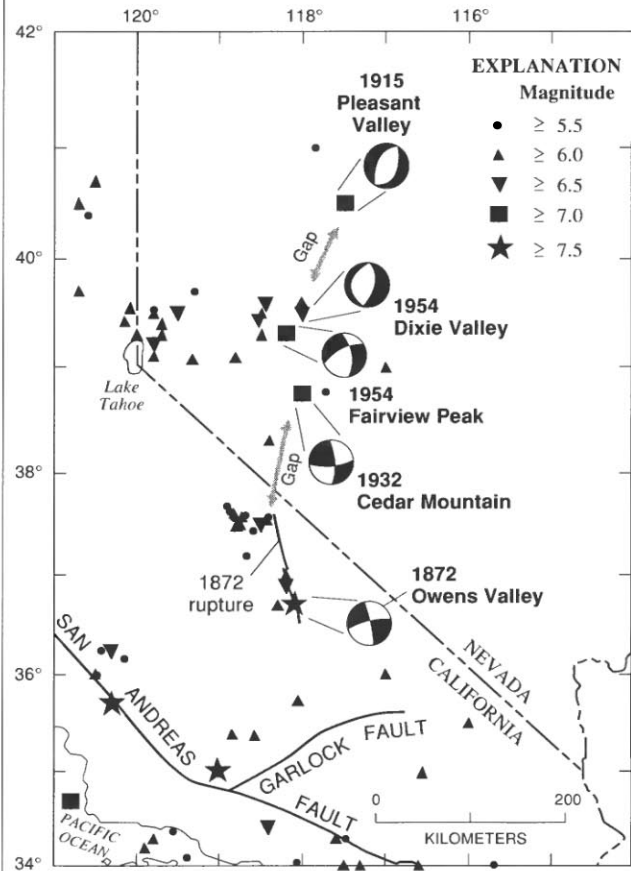


FIGURE 6.11.—California-Nevada region, showing locations of major historical earthquakes in the western Basin and Range province, 1857-1989. Focal mechanisms of five largest events in lower-hemisphere projection show compressional quadrant shaded and indicate significant shear as well as extensional strain in province. Seismic gaps (labeled) are potential loci of future major earthquake activity (Wallace, 1984).

ing northward into the Carson Sink. The July 6 event produced an 18-km-long surface rupture at the south end of this zone striking N. 15° E., with maximum displacements of about 30 cm. The August 24 shock extended the zone by 22 km in a N. 20° E. direction, with as much as 75 cm of normal-fault slip. Tocher (1956) noted that the displacement on the northern part of the July 6 break approximately doubled in amplitude between July 16 and September 9; the timing of the additional slip could not be determined.

DECEMBER 16, 1954 ($M=7.1$ AND 6.8)

The Dixie Valley-Fairview Peak earthquakes of December 16, 1954, produced a 90-km-long zone of right-lateral oblique and normal faulting in the central Nevada seismic zone (fig. 6.11; Slemmons, 1957). The first shock, which occurred east of Fairview Peak, produced lateral displacements of more than 4 m and vertical displacements of as much as 3 m. Faulting along this 50-km-long zone was predominantly down to the east opposite Fairview Peak and changed polarity to the north. The second shock, which occurred 4 minutes later, had an epicenter on the east side of Dixie Valley in a left-stepping echelon arrangement with the earlier event. Normal-fault scarps formed along a 40-km-long zone at the base of the Stillwater Range some 20 km west of the

Rainbow Mountain faulting. Vertical displacements exceeded 2 m, and consistent strike-slip displacements were absent.

JULY 21, 1986 ($M=6.2$)

The Chalfant Valley earthquake of July 21, 1986, is the largest event to date in a series of 33 earthquakes of $M_L \geq 5$ to occur since 1978 in the White Mountain seismic gap (Savage and Cockerham, 1987). Other principal events in this series include the May 25-27, 1980, Mammoth Lakes earthquakes ($M=6.1, 5.9, 5.8, 6.0$) and the November 23, 1984, Round Valley earthquake ($M=5.7$). The series of shocks is of interest not only because of its wide geographic distribution in the White Mountain seismic gap but also because of the contemporaneous uplift of Long Valley caldera (Hill and others, 1985). The Chalfant Valley earthquake created a 10+-km-long zone of fractures with as much as a few centimeters of dextral slip on the frontal-fault zone of the White Mountains (Lienkaemper and others, 1987). The earthquake focal mechanism and aftershock distribution show that the predominately dextral strike-slip displacement associated with this event occurred on a west-dipping fault plane that projects upward to meet the surface break.



FIGURE 6.12.—Fault trace of 1915 Pleasant Valley, Nev., earthquake remains clearly visible in this photograph by R.E. Wallace more than 60 years after event (Wallace, 1984).

SEISMICITY OF THE MENDOCINO TRIPLE JUNCTION AND THE GORDA PLATE

The San Andreas fault terminates at its north end in a transform/transform/trench triple junction just seaward of Punta Gorda. Major earthquake activity lies along the Mendocino Fracture Zone, where it is an active transform fault, and to the north within the Gorda plate, which is undergoing intense internal deformation. The Wadati-Benioff zone is well defined to a depth of 30 km and can be traced eastward to a depth of more than 80 km (see fig. 5.5; Walter, 1986). Strong earthquakes within the Gorda plate locate off shore and span the position of the megathrust; these events appear to lie entirely within the oceanic lithosphere. The 1980 Eureka earthquake, for example, ruptured the Gorda plate from the landward to the seaward side of the megathrust. Despite the high level of seismicity, underthrusting events are rare.

PRINCIPAL EARTHQUAKES

NOVEMBER 23, 1873 ($M=6\frac{3}{4}$)

The severe earthquake of November 23, 1873, was felt from San Francisco to Portland, Oreg.; it inflicted the heaviest damage to Crescent City, Calif., and surrounding communities in the Klamath Mountains. The macroseismic epicenter near the California-Oregon State line and probably inland of the coastline is unique within both the historical and instrumental records.

APRIL 16, 1899 ($M=7$)

Little is known about the large earthquake of April 16, 1899, with an epicenter seaward of Eureka, where it was described as "one of the severest shocks of earthquake ever experienced." Toppozada and others (1981) corrected the origin time of this event and assigned a nearshore epicenter and an M_I of 5.7. The earthquake was assigned an epicenter in the Gulf of Alaska by Milne (1901) on the basis of the traveltime of the maximum amplitude from the five reporting stations; however, a California location satisfies his data equally well. The absence of significant damage along the coast suggests an epicenter well out to sea. An instrumental magnitude (M_S) of 7.0 is derived from the surface-wave amplitudes reported by Milne (see Abe and Noguchi, 1983).

JANUARY 31, 1922 ($M=7.3$)

The intensity pattern of the large earthquake of January 31, 1922, is generally similar to that of the 1899 event. This event was well recorded throughout the world.

JANUARY 22, 1923 ($M=7.2$)

The earthquake of January 22, 1923, strongly shook the Cape Mendocino region and toppled many chimneys in the area. This earthquake was probably associated with the Mendocino Fracture Zone.

DECEMBER 21, 1954 ($M=6.6$)

The strong earthquake of December 21, 1954, apparently was located in the crust of the North American plate above the descending Gorda plate. The relocation of this event by Smith and Knapp (1980) suggests a possible association with the active Mad River fault zone. One fatality is attributed to the earthquake.

NOVEMBER 8, 1980 ($M=7.2$)

The Eureka earthquake of November 8, 1980, resulted from 100-km-long, left-lateral strike-slip rupture of the Gorda plate along a northeast-striking fault (see fig. 5.5). Aftershocks of the earthquake extended from within 30 km of the coastline southwestward to the Mendocino Fracture Zone. The focal mechanism of the earthquake is thus conjugate to the San Andreas, with its tension axis aligned in the downdip direction. This event argues for high rates of internal deformation within the subducting oceanic lithosphere and against the extension of San Andreas-style faulting northward of the triple junction.

DISCUSSION

The spatial distribution of large earthquakes during the past 2 centuries defines the San Andreas fault system as a 100- to 300-km-wide zone containing numerous active faults in addition to the San Andreas fault proper (fig. 6.1). Except for the two largest events, the great 1857 and 1906 earthquakes that together ruptured two-thirds of the total length of the San Andreas fault, large earthquakes are conspicuously absent along the master fault itself. Although these two great earthquakes account for half of the seismic-strain release since 1769, most of the rest occurs on other, smaller elements of the fault system. Major historical events on these secondary faults, such as the 1927 Lompoc and 1952 Kern County earthquakes, serve to define the boundaries of the San Andreas system. Their mechanisms differ significantly from right-lateral strike slip parallel to the plate-motion vector and illustrate the diversity and complexity of seismic-strain release within the plate-boundary zone.

Over the timespan of the historical catalog, the most enduring characteristic of the earthquake distribution may be the spatial clustering of activity at specific localities along the plate boundary. Notable hotspots

include the Cerro Prieto, Imperial, San Jacinto, and Calaveras faults, all of which are major branches of the San Andreas fault, and the Parkfield segment of the San Andreas fault in the transition zone between the 1857 rupture and the 150-km-long central, creeping segment of the fault. In each of these areas, the seismic activity coincides with these high-slip-rate faults (1–3.5 cm/yr), and in some places it clearly represents recurrent rupture of the same segment of the fault. At greater distances from the San Andreas fault, the historical events (or sequences) tend to represent isolated occurrences on slower moving faults. Thus, although the overall seismicity spans the broad plate-boundary zone, seismic-strain release over the past 2 centuries correlates with the local rate of fault movement.

In general, the locations of historical earthquakes resemble the overall distribution of microearthquake activity, despite more than six orders of magnitude difference in average seismic moment (fig. 6.13; see chap. 5). One important difference between the distribution of large and small earthquakes is the virtual absence of smaller events along the San Andreas fault segments that ruptured in 1857 and 1906. Similarly, seismic activity is distinctly absent on the potentially dangerous segment between the 1857 break and the Imperial Valley. Except for the central, creeping segment, where numerous small events occur, the San Andreas fault is almost completely aseismic during the long intervals between its rupture in major earthquakes (see figs. 5.6, 5.9).

This inverse correlation between the source regions of large earthquakes and the distribution of smaller events can also be observed for smaller main shocks. Recent studies of the rupture dynamics of $M=6$ events occurring within seismically active regions indicate that the rupture zones of these events are similarly aseismic, with smaller events occurring predominantly outside the slip surface, even during the aftershock sequence (Reasenber and Ellsworth, 1982; Hartzell and Heaton, 1986; Mendoza and Hartzell, 1988). Thus, the sites of future large earthquakes cannot be identified on the basis of minor seismicity alone.

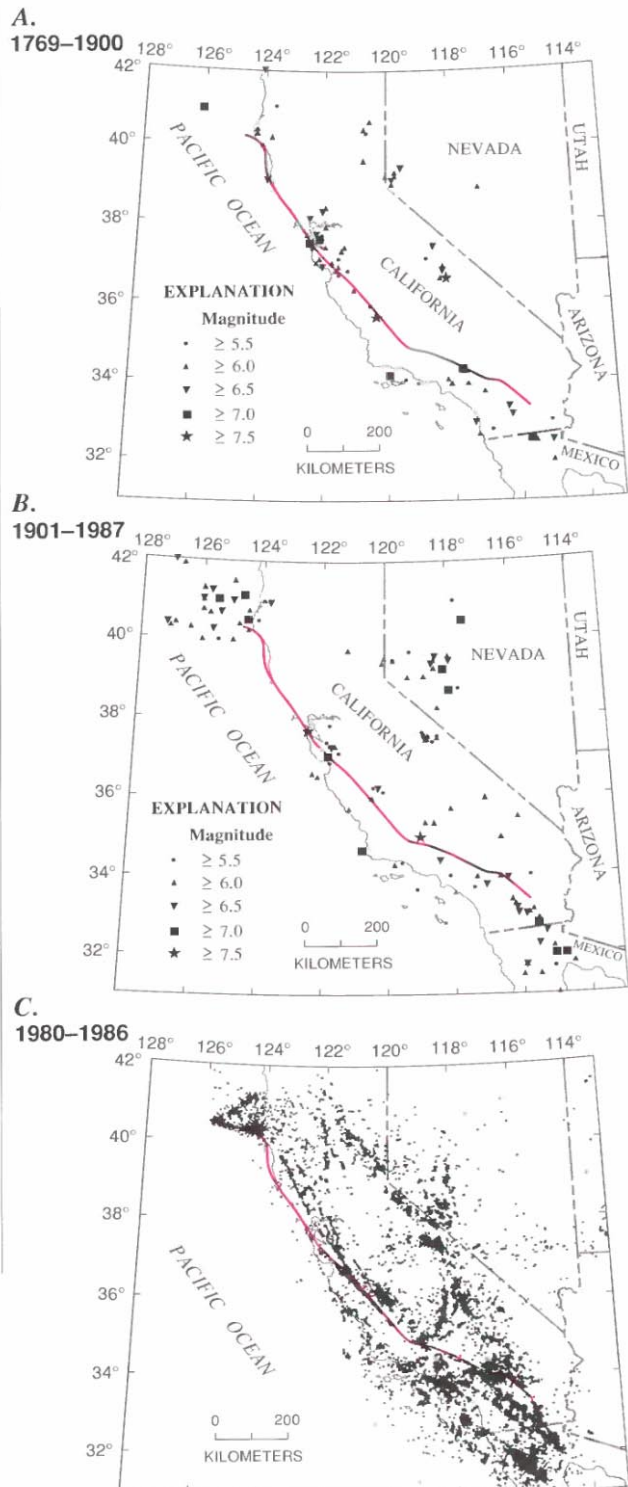


FIGURE 6.13.—Distribution of large and small earthquakes along the San Andreas fault system. In general, modern instrumental data (C; see chap. 5) portray same pattern of activity seen in large earthquakes from preinstrumental (A) and instrumental (B) eras. Some areas characterized by high levels of microearthquakes, such as well-defined faults east of northern section of the San Andreas fault (red line), have not produced significant earthquakes in historical time and so are considered probable sites of future activity.

RATE OF SEISMICITY

The average rate of earthquake activity within the San Andreas system can be estimated from the Gutenberg-Richter frequency-magnitude relation $\log N = a - bM$, where N is the cumulative number of events of magnitude equal to or greater than M during a given time period. For the 77 events along the fault system with summary magnitudes $M \geq 6$ since 1852, this relation well describes the population with $a = 5.74$ and $b = 1$ (fig. 6.14). Comparable results are obtained for subsets of $M = 6$ events, such as the instrumental period (1898-1989).

It is useful to compare these results from the historical record with the frequency-magnitude relation determined from systematic microearthquake observations. If the historical rate of activity applies today and the frequency-magnitude relation for microearthquakes ($M \geq 3$) is described by the same relation, then about 5,600 $M \geq 2$ events should be observed each year. This prediction exceeds the number of events observed during the interval 1980-87 by about a factor of 2 (see chap. 5) and suggests that a somewhat smaller value of $b = 0.93$ may be more appropriate for the extended magnitude range.

For the catalog as a whole, the rate of earthquake occurrence is well described by a Poisson process, in which the probability of finding one or more events in any

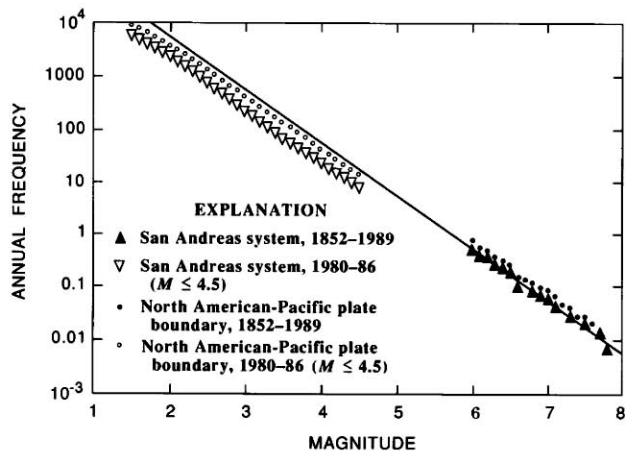


FIGURE 6.14.—Annual frequency of earthquakes of magnitude $\geq M$ as derived from historical and modern instrumental catalogs. Gutenberg-Richter frequency-magnitude relation, $\log N = a - bM$ with $a = 5.74/\text{yr}$ and $b = 1$, describes observed distribution of earthquakes of $M \geq 6$ within the San Andreas fault system during 138-yr interval from 1852 to 1989. Also shown are annual frequency of $M \geq 6$ events from the broader Pacific-North American plate boundary, including the San Andreas fault system and the western Basin and Range province, and of $M = 2-4.5$ events in both regions during 1980-86.

interval of t years is $P = 1 - e^{-\lambda t}$, where λ is the average rate of earthquake occurrence. It follows from the observed frequency-magnitude relation that the odds of having at least one $M \geq 6$ event per year are 0.43. There is also an even chance of at least one $M \geq 6$ event within any 15-month interval, one $M \geq 7$ within any 12½-year interval, or one $M \geq 8$ within any 125-year interval.

The rate of earthquake activity along the plate boundary can also be usefully compared with plate-motion estimates derived from plate-tectonic theory. Current estimates of the relative velocity across the North American-Pacific plate boundary, determined from the spreading rate in the Gulf of California of 5 cm/yr (DeMets and others, 1987), imply an annual seismic-moment rate of 2×10^{26} dyne-cm/yr for a 10-km-thick brittle crust, equivalent to a single $M = 6.8$ earthquake. Earthquakes of this size occur far less often, and the principal seismic contribution to the plate motion comes from infrequent large events. The erroneous notion that the smaller events substantially contribute to the total is demonstrably false, as shown by summing the contributions of all the earthquakes below some magnitude. The innumerable events of $M \leq 6$ occurring each year contribute less than 10 percent to the total seismic-strain release.

Within the San Andreas fault system, the total seismic-moment release since 1852 corresponds to 70 percent of the total North American-Pacific plate motion predicted by plate-tectonic models. This proportion is somewhat inflated because not all of the earthquakes act to transmit slip along the plate boundary; for example, the 1952 Kern County earthquake, the third largest in historic time, directly accommodated little plate-parallel motion. Although aseismic displacements account for some of the deficit, notably along the central, creeping section of the San Andreas fault, deformation occurring elsewhere, notably within the Basin and Range, contributes substantially to the relative motion between the North American and Pacific plates.

PARADOX OF THE MISSING PLATE MOTION

The discrepancy between plate-tectonic estimates of relative motion across the North American-Pacific plate boundary and seismic estimates also holds for geologic and geodetic estimates of motion along the San Andreas fault system. The explanation of this apparent paradox is thought to include deformation within the Basin and Range province in western Nevada and eastern California (Atwater, 1970), which has been the locus of major seismic activity in historical time, including the third

largest event, in 1872, and 3 of the 11 $M \approx 7$ events in the 20th century.

It has long been recognized that the Basin and Range province has undergone substantial extension during the Cenozoic and is presently opening in a N. 60° W. direction (Zoback and Zoback, 1980). Historical seismicity partly agrees with this geologically derived pattern; however, it also indicates a significant component of dextral shear in nearly every well-studied historical event (Shawe, 1965; Doser, 1986). Because the geologic expression of strike-slip displacement is much more difficult to recognize and quantify than vertical slip, a major question is raised about the significance of the historic seismicity for the total strain within the western Basin and Range.

Since the 1872 earthquake, the net seismic strain within the Basin and Range province can be estimated by summing the contributions of individual events. The net shear strain thus determined indicates nearly equal components of extensional strain in a N. 60° W. direction and dextral shear trending N. 10° W. The resulting average-motion vector nearly coincides with the orientation of the San Andreas fault, and the lateral slip largely balances the coastward expansion of the province that results from extension alone. If both the rate and style of historical faulting accurately portray the long-term deformation within the region, they diminish the discrepancy between the predicted and observed rates of motion across the North American-Pacific plate boundary.

EARTHQUAKE RECURRENCE AND CHARACTERISTIC EARTHQUAKES

Over geologic time, the net displacement across a fault accumulates through the action of countless individual slip events. Measured over many displacement cycles, the average interval between events must equal the average event displacement divided by the remote slip rate. First principles, however, provide little guidance as to the properties of the recurrence, which might range from a totally random distribution of events in both space and time to identical earthquakes repeating at fixed intervals. If recurrence is essentially random, then long-term seismic hazard is described by the Poisson rate of activity, as discussed above. Greater regularities and systematics in recurrence imply that useful time-dependent forecasts of future activity can be derived from knowledge of the past behavior of the fault system.

Results for San Andreas earthquakes have played a central role in establishing the existence of broad regularities in the recurrence process. At Parkfield, the San Andreas fault has ruptured six times since 1857 in $M \approx 6$ events with highly repeatable characteristics every 22 ± 6 years. The latest three events, in 1922, 1934, and 1966, for which instrumental records exist, are virtually iden-

tical (fig. 6.15; Bakun and McEvilly, 1984). Amplitude data from Milne seismographs uncovered in the preparation of table 6.1 show that the 1901 and 1922 events produced the same surface-wave amplitudes on common stations, strengthening earlier speculations that all the 20th-century events are similar. Intensity data for the 1881 event (Toppozada and others, 1981) and for foreshocks to the great 1857 earthquake (Sieh, 1978b) place them along the Parkfield segment as well. These regularities in the size, location, and timing of all known events at Parkfield led Bakun and Lindh (1985) to propose a specific recurrence model for Parkfield earthquakes. On the basis of this model, the next in the series of characteristic events is anticipated before 1993, and its forecast represents the first formally endorsed earthquake prediction in the United States.

Geodetic analysis of the strain released in the 1966 earthquake and its subsequent reaccumulation led Segall and Harris (1987; see Harris and Segall, 1987) to identify the zone where strain accumulates and is released, the

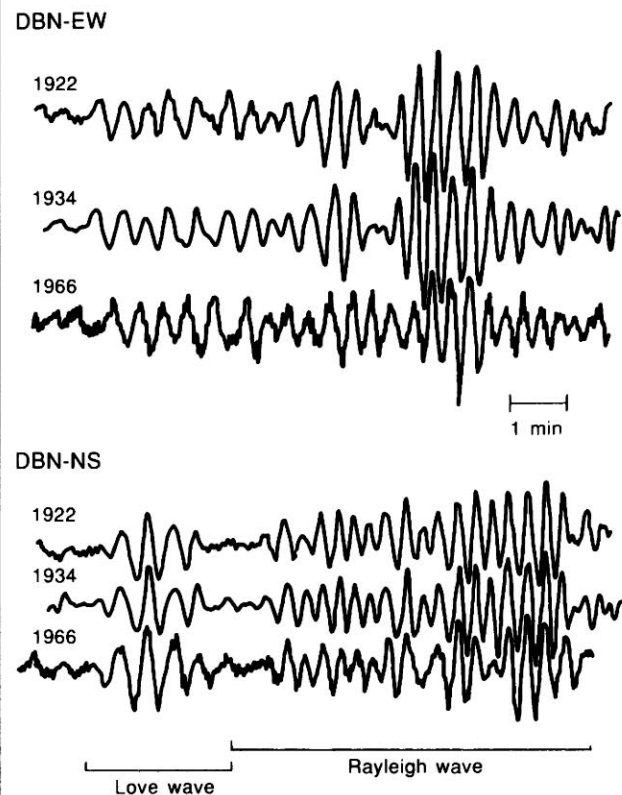


FIGURE 6.15.—Surface waves of 1922, 1934, and 1966 Parkfield, Calif., earthquakes as recorded on same seismograph in DeBilt, The Netherlands (DBN; EW, east-west; NS, north-south). These nearly identical waveforms and amplitudes led Bakun and McEvilly (1984) to propose recurrent rupture of same segment of the San Andreas fault as mechanism of Parkfield earthquakes.

"Parkfield asperity," as the center of the 1966 rupture zone. This zone of strain accumulation appears to be effectively locked during the interseismic period and corresponds to the center of the 1966 aftershock zone (Eaton and others, 1970) between about 4- and 10-km depth. The significantly fewer events in this part of the aftershock zone than in its periphery suggests that Parkfield earthquakes occur when this locked zone suddenly releases. Aftershocks appear to result from transfer of stress to the perimeter of the asperity.

This same pattern of concentrated coseismic slip occupying a quiet region within the overall aftershock distribution characterizes several recent, well-studied events (Mendoza and Hartzell, 1988), three of which, the Coyote Lake earthquake (Aug. 6, 1979), the Imperial Valley earthquake (Oct. 15, 1979), and the Morgan Hill earthquake (Apr. 24, 1984), all have probable antecedents within the historical record. Reasenber and Ellsworth (1982) identified the June 20, 1897, earthquake as a predecessor to the 1979 event and noted that the 82-year interval between events equaled the 1.2 m of coseismic slip determined by Liu and Helmberger (1983) divided by the long-term slip rate of 1.5 cm/yr for the Calaveras fault. Similarly, the 73-year interval between the July 11, 1911, event and the 1984 Morgan Hill earthquake (Bakun and others, 1984) well predicts the 0.8 to 1.0 m of maximum coseismic slip determined by Hartzell and Heaton (1986). The 1979 Imperial Valley earthquake is more complex because it reruptured only the northern 30 km of the May 19, 1940, fault break. Again, both the time interval between events and the fault-slip rate compare favorably with the fault slip at depth, as determined from seismograms (Hartzell and Heaton, 1983; Archuleta, 1984). Earlier ruptures of this or other segments of the Imperial fault may well be in the historical record, possibly including the April 19, 1906, event, which occurred the afternoon of the great 1906 earthquake in northern California.

Similar observations of recurrent faulting in events with characteristic magnitudes and locations from around the world (Nishenko and Buland, 1987) suggest a simple, first-order model for seismic potential. In this model, the future behavior of a specific segment of a fault can be forecast from knowledge of the size of past earthquakes, the timing and amount of slip in the latest event, and the long-term rate of fault movement (Lindh, 1983; Sykes and Nishenko, 1984). Accordingly, the probability of an event on a recently ruptured fault segment is low until the elastic strain rebuilds, which may be estimated from the geologic slip rate. As the strain rebuilds, the probability of another earthquake increases. Empirically, the time intervals between successive ruptures of a specific fault segment define a bell-shaped distribution that may be used to estimate the odds of the next event within

some future time interval, given that it has not yet occurred.

Probabilities for large earthquakes along the major branches of the San Andreas fault derived from this methodology differ markedly from Poisson estimates (Working Group on California Earthquake Probabilities, 1988). For example, the chance of a repetition of the great 1906 earthquake within the next 30 years (1988-2018) is less than 0.1. In contrast, the chance of an $M=7\frac{1}{2}$ -8 earthquake on the southern section of the San Andreas fault is 0.6. When the Working Group's report was written, the southernmost part of the 1906 fault break was assigned the highest chance of failure of any segment of the north half of the San Andreas fault. Now that it has ruptured in the October 18, 1989, Loma Prieta earthquake, the probability of another rupture will be small for several decades. A clearer understanding of past seismicity can only help to improve and refine estimates of future seismicity.

THE SEISMIC CYCLE

An important implication of the characteristic-earthquake model is the existence of a repetitive cycle of strain accumulation and release (Fedotov, 1968). Mogi (1981) suggested the existence of definite stages in the cycle, including a low level of seismicity in the first part of the cycle once aftershock of the latest event subside, a rise in regional activity as strain accumulates, and ultimately the occurrence of another earthquake with its attendant foreshocks and aftershocks, which initiates the next cycle.

The long-term seismicity within the San Andreas fault system displays these characteristics along the rupture zone of the great 1906 earthquake (figs. 6.16, 6.17; Ellsworth and others, 1981). Activity was relatively high during the 19th century, as becomes particularly apparent after 1850, when the record is virtually complete. After the great 1906 earthquake, the level of seismicity changed drastically, and moderate events essentially ceased for 50 years. Since the mid-1950's, the activity level has increased and begun to approach the 19th-century level (Tocher, 1959). This change in activity associated with the 1906 earthquake has been noted many times (for example, Gutenberg and Richter, 1954), and it is an open question whether it represents a premonitory increase (Topozada and others, 1988) or whether the long quiescent period since 1906 is the essential feature (Ellsworth and others, 1981).

Comparable variations in seismicity appear to be present in southern California, although the historical record there is less reliable until about 1890. Along the rupture zone of the great 1857 earthquake, the available data suggest a similar period of low activity for several

decades after the event (fig. 6.17). Farther south, along the section of the fault that has not ruptured in 3 centuries, the activity level since at least the 1880's is reminiscent of the activity in the San Francisco Bay region before the 1906 earthquake (fig. 6.18). As a potential long-term indicator of high seismic potential, the seismicity surrounding the dormant southern section

of the San Andreas fault agrees with independent estimates of long-term potential derived from paleoseismology.

FUTURE USES OF EARTHQUAKE HISTORY

At this stage in our understanding of the San Andreas fault system, seismicity is still best described as a random

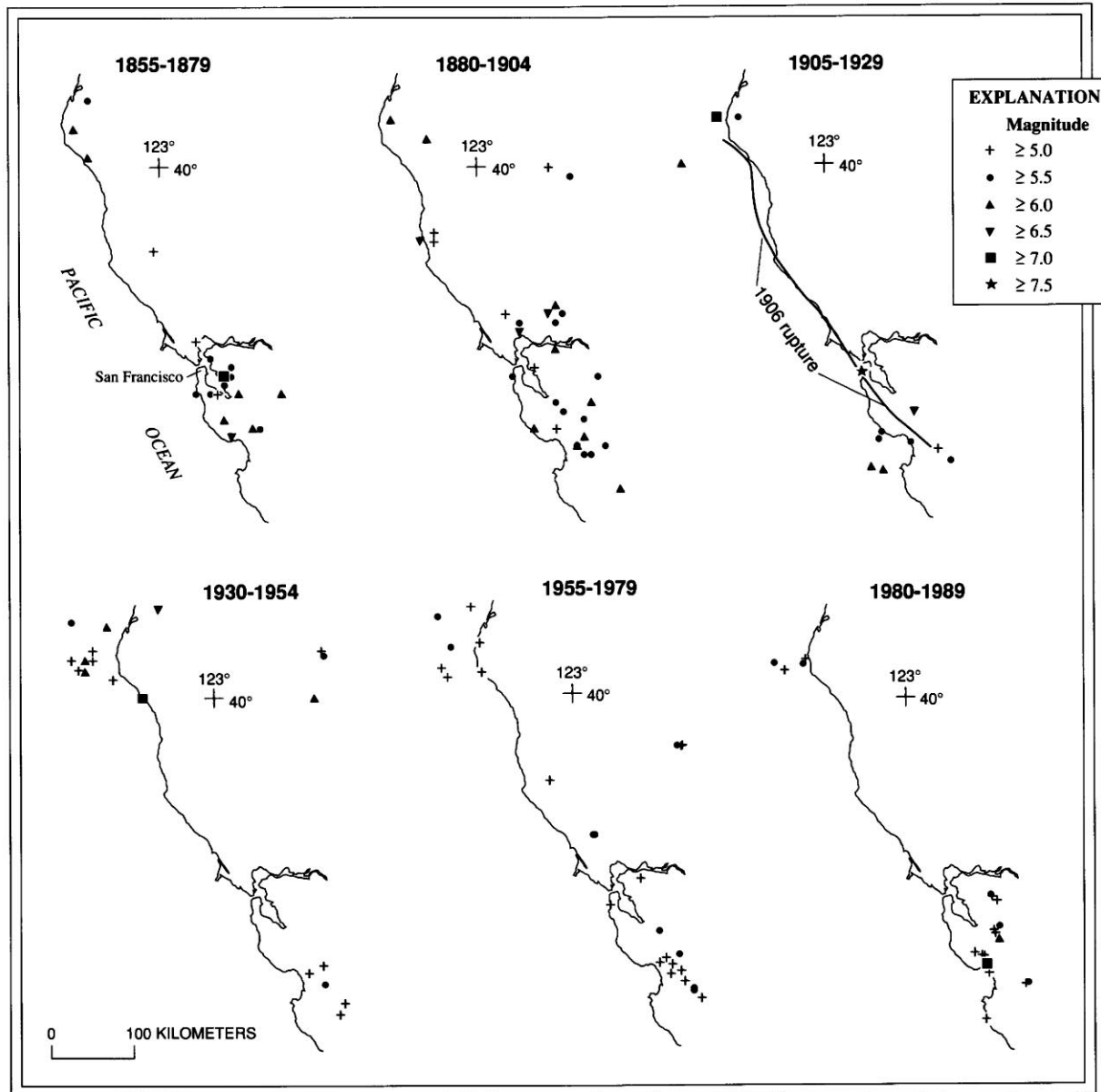


FIGURE 6.16.—Seismicity of the San Francisco Bay region in quarter-century epochs. Activity was high in the region during at least a half-century before 1906 earthquake and drastically declined afterward for the next half-century. Since the mid-1950's, activity has

begun to approach levels last seen in the 19th century. However, both geologic and geodetic evidence suggest that the next great earthquake will not occur for a century or more.

process over time, with a highly clustered spatial distribution. There are, however, tantalizing hints of underlying regularities, such as those in the characteristic earthquakes at Parkfield, or in the striking changes in seismicity associated with the 1906 earthquake. The next generation of refinements to this history will assuredly make comparable contributions by reducing the uncertainty in earthquake locations and magnitudes. Modern seismologic methods for extracting new information on the mechanisms of earthquakes have already proved practical for many events from the early instrumental period. Systematic treatment of the full instrumental catalog with these methods will provide a new basis for understanding the tectonics of the plate boundary and the mechanics of earthquakes.

CATALOG OF MAJOR EARTHQUAKES, 1769–1989

CATALOG COMPILATION

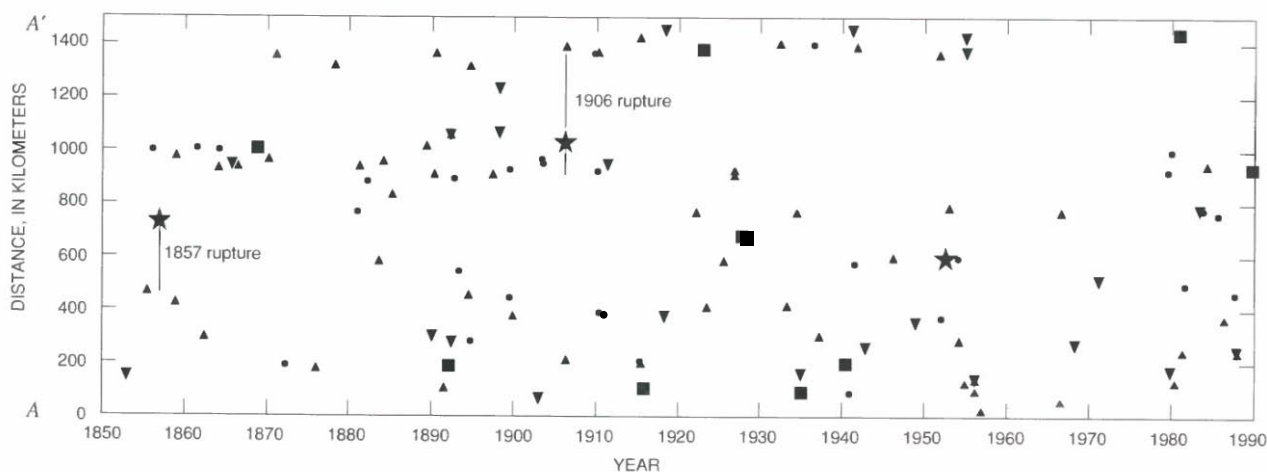
The publication of Edward S. Holden's catalog of Pacific coast earthquakes in 1898 represented the first systematic scientific inquiry into the seismic history of California and surrounding regions. This catalog, and its extension by McAdie (1907), formed the primary basis for the monumental catalog of Townley and Allen (1939) covering the years 1769–1928. These catalogs provide detailed descriptive accounts of virtually all the earth-

quakes that are now known from this period, and all subsequent analyses of seismicity up to the modern instrumental period build on these foundations.

Recent studies of preinstrumental seismicity have focused on quantification of the historical record. The catalog presented here relies heavily on the research of Tousson Topozada and his associates (Topozada and others, 1981; Topozada and Parke, 1982), who developed extensive new information on seismic intensities from newspaper accounts and other original sources, and determined locations and magnitudes from the resulting isoseismal maps. In addition, several special studies of important events by other workers have contributed to the catalog.

The development of practical seismographic instrumentation around the turn of the 20th century led to the rapid growth of seismologic data, particularly for those events large enough to register at teleseismic distances on the early instruments. The publication of the Circulars of the Seismological Committee of the British Association for the Advancement of Science (1899–1912) and their continuation as the International Seismological Summary from 1913 on indicate a detection threshold of about $M \approx 6$ for the Western United States as early as 1898. Data from these and other sources enabled Gutenberg and Richter (1954) to systematically catalog seismicity from 1904 onward.

Modern seismographic instrumentation first installed in California in 1910 ushered in the era of earthquake



EXPLANATION

Magnitude

- ≥ 5.5
- ▲ ≥ 6.0
- ▼ ≥ 6.5
- ≥ 7.0
- ★ ≥ 7.5

FIGURE 6.17.—Space-time diagram of seismicity since 1850 along the San Andreas fault system between head of the Gulf of California (A) and Punta Gorda (A'). Change in seismicity rate along northern section of the San Andreas fault associated with 1906 earthquake (fig. 6.13) may also be tentatively identified along 1857 earthquake rupture. Persistent activity characterizes south third of the plate boundary since 1890, spanning the entire interval of reliable earthquake reporting in this region.

observation at regional distances. The Bulletins of the Seismographic Stations of the University of California,

Berkeley, from 1910 to the present form the principal source for events in northern California and adjoining areas. Routine epicentral determinations and magnitude assignments for earthquakes in the southern California region date from 1932 and are taken from the catalog of the Seismological Laboratory of the California Institute of Technology, Pasadena. Additional instrumental results come from various other sources, chiefly the U.S. Geological Survey and the University of Nevada, Reno.

The resulting catalog of major earthquakes in California, western Nevada, and northernmost Baja California from 1769 to 1989 (table 6.1) contains 206 entries. This catalog omits several earthquakes listed in earlier catalogs where this or other recent studies have failed to corroborate previous interpretation as significant events or even, in some cases, their occurrence.

QUANTIFICATION OF EARTHQUAKES AND MAGNITUDE SCALES

Physical measures of the complex mechanical event producing the earthquake take many forms, including the dimensions of the faulted region, the amount of slip, and the strength of the radiated elastic waves. To relate the characteristics of one event to another, the observed quantities must generally be summarized through the use of either an empirical relation, such as magnitude, or a quantity derived from a physical model, such as seismic moment. Both procedures have their place, and the choice of one metric over another depends principally on the purposes of the comparison and the availability of common data.

Because no single procedure for determining magnitude can be applied to the entire historical record, the catalog must be quantified by using various magnitude scales. Each scale is briefly described below to define its origin and to clarify its relation to the other scales. I emphasize that each scale has a particular range of validity and that different magnitude scales will, in general, yield slightly different values for the same event. Such differences in magnitude seem to provide a never-ending source of interest and controversy for the news media, who commonly lump all scales together under the heading of "Richter scale." To the seismologist,

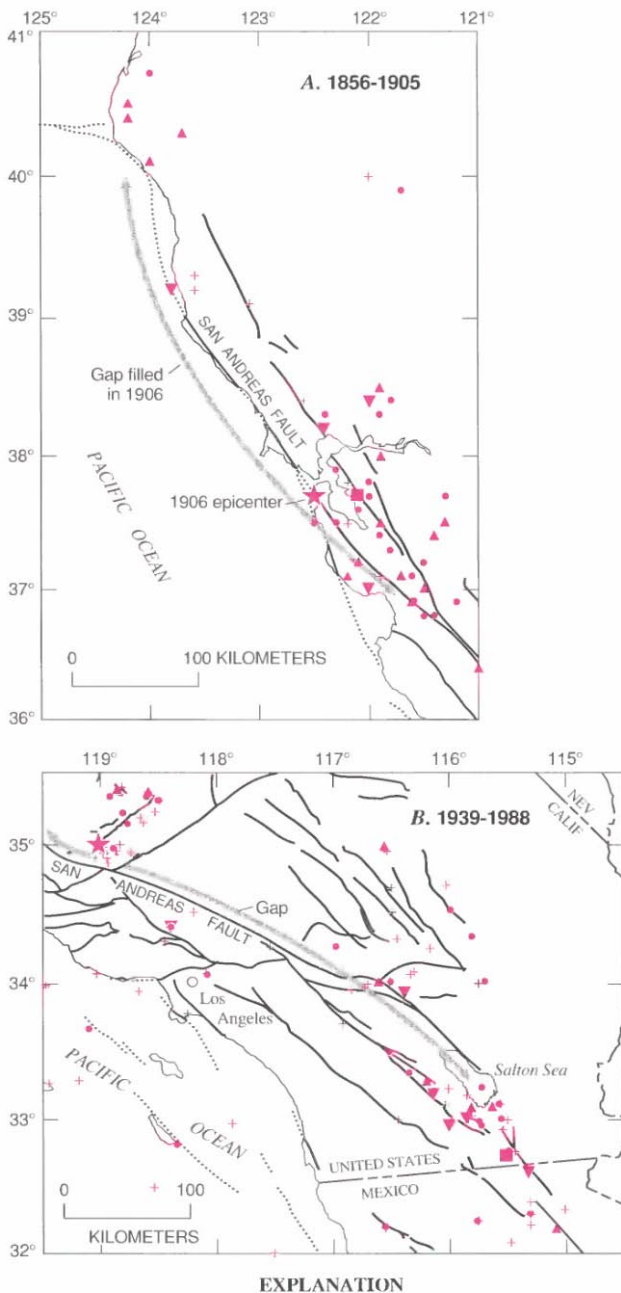


FIGURE 6.18.—Where will the next great earthquake strike along the San Andreas fault system? Numerous lines of evidence point to its long-dormant southernmost segment (B) as having the highest potential. Large earthquake activity in this region shares many similarities with activity in the San Francisco Bay region before 1906 earthquake (A). In both cases, absence of activity directly on the San Andreas fault is pronounced, and a high regional level of activity is concentrated along other major branches of the fault system.

such differences are neither surprising nor controversial and can, in fact, provide information on the underlying physical processes of the earthquake source.

I also emphasize that intensity scales characterize the effects of the earthquake at a particular location and are not magnitude scales. Strictly speaking, intensity values (or, for that matter, instrumentally measured values of ground-motion parameters) describe the vibratory motions that are the actual earthquake as observed at a particular location, whereas magnitude values describe the faulting event that generates the earthquake.

THE RICHTER SCALE (M_L)

The original magnitude scale of Richter (1935) was introduced for the purpose of providing an objective measure of the energy of each earthquake in the initial listing of earthquakes in the southern California region compiled by the Seismological Laboratory in Pasadena. Rather than attempting to measure the energy of the earthquake source directly, he chose to construct an empirical scale derived from a simple measure of the complex seismic waveform. Using only the maximum excursion of the seismogram as measured on a single type of instrument, the Wood-Anderson seismograph, he defined the local magnitude of an earthquake as

$$M_L = \log_{10} A - \log_{10} A_0(\Delta),$$

where the empirical function A_0 depends only on the epicentral distance of the station, Δ . The zero point was arbitrarily set by Richter to avoid negative magnitudes in the course of routine work. Use of common logarithms means that two earthquakes located at the same distance from a station and having peak amplitudes differing by a factor of 10 will differ by 1 magnitude unit. In practice, readings from all observing stations are averaged after adjustment with station-specific corrections to obtain the M_L value. Although Richter (1935) predicted that the local-magnitude scale "cannot hold to any high accuracy," history has proved it to be a powerful quantitative tool for ordering the relative sizes of earthquakes.

Several points about M_L should be emphasized. First, it is strictly defined only for the southern California region, although its applicability to coastal central and northern California has since been shown. Recent studies of the A_0 curve suggest that it will require revision and regionalization. Second, because M_L has no actual physical units associated with it, other empirical magnitude scales may be freely adjusted to coincide with it. The local-magnitude scale has, in fact, been used as the basis for establishing essentially all other magnitude scales. Finally, because M_L is derived from measurements taken from a single, band-limited seismograph, M_L values

saturate once an earthquake becomes large enough. Thus, the "correct" Richter magnitude $M_L=6.9$ for the great 1906 earthquake obtained by Jennings and Kanamori (1979) reflects the amplitude of seismic waves at periods near 1 s but not the total energy of this earthquake. Uniformly valid characterization of the "size" of an earthquake requires use of magnitude scales based on longer-period measures of the event.

SURFACE-WAVE MAGNITUDE (M_S) AND BODY-WAVE MAGNITUDE (m_b)

The successful development of the local-magnitude scale encouraged Gutenberg and Richter to develop magnitude scales based on teleseismic observations of earthquakes. Two scales were developed, one based on surface waves, M_S , and one on body waves, m_b .

Surface waves with a period near 20 s generally produce the largest amplitudes on a standard long-period seismograph, and so the amplitude of these waves is used to determine M_S , using an equation similar to that used for M_L .

The body-wave magnitude, m_b , which was developed specifically to treat deep-focus earthquakes, presents yet another alternative scale for magnitude determination. Although it presently is the most commonly reported teleseismic magnitude, current practice in its determination differs from that employed by Gutenberg, and so it is omitted from table 6.1. As a short-period magnitude, modern m_b values measure the same part of the earthquake energy spectrum as M_L .

The magnitudes listed by Gutenberg and Richter (1954) that appear in table 6.1 as M_{G-R} are essentially M_S according to Geller and Kanamori (1977); magnitudes attributed to Richter (1958) are based on M_L or M_S .

Useful estimates of M_S can be obtained from many different types of long-period seismographs, including the undamped instruments deployed by Milne beginning in 1897. Abe and Noguchi (1983) constructed estimates of M_S from Milne seismograms to resolve a longstanding controversy concerning an apparent peak in global seismicity between 1904 and 1912. Abe (1988) later used the Milne data to determine magnitudes for smaller earthquakes in California between 1898 and 1912. His procedures have been used to compute M_S for additional California events occurring between 1898 and 1934, which are listed in table 6.1.

SEISMIC INTENSITY AND EARTHQUAKE MAGNITUDE (M_I)

Before the development of seismographs in the late 19th century, descriptions of the effects of earthquakes provided the only means for assessing earthquake size in all but the rare cases where surface faulting was well

described. A robust method for relating the area undergoing shaking of a given intensity or greater to M_L was developed by Topozada (1975) for California and western Nevada. Using these relations, Topozada and others (1981, 1982) successfully assigned an intensity magnitude, M_I , to many earthquakes. The isoseismal maps developed in the course of their research also generally provide our best estimates of epicentral locations. New M_I values have been determined for several events, using the same procedures as part of this study.

SEISMIC MOMENT (M_0), RADIATED ENERGY, AND MOMENT MAGNITUDE (M)

Magnitude scales based on finite-bandwidth seismographs approach a maximum near which events of clearly different size or energy are indistinguishable. Saturation of M_L is apparent for both the 1906 and 1952 earthquakes listed in table 6.1. Recent work by Hutton and Boore (1987) suggests that the local-magnitude scale may begin to saturate at about $M_L=6$. Such saturation, which is understood to arise from the scaling law of the seismic spectrum (Aki, 1967), occurs when the peak of the energy spectrum lies below the frequency range of the Wood-Anderson seismograph.

By using the well-known properties of the seismic spectrum, magnitude scales can be constructed with uniform validity. One such scale, M_w , proposed by Kanamori (1977) is based on the seismic energy radiated in the form of elastic waves by the source. Another nearly equivalent magnitude scale, M , the moment magnitude, is based on the seismic moment, $M_0=\mu Au$ (Aki, 1966), where A is the area of the earthquake rupture surface, u is the average fault displacement, and μ is the shear modulus of the crustal volume containing the fault. Hanks and Kanamori (1979) took advantage of the nearly identical relations between M_0 and both M_L and M_S to define $M=2/3\log_{10} M_0-10.7$, where M_0 is measured in dyne-centimeters.

These two magnitude scales, though closely related, are not identical. Singh and Havskov (1980) showed that $M_w=2/3(\log_{10} M_0+\log_{10} \Delta\sigma/\mu-12.1)$, where $\Delta\sigma$ is the stress drop. Earthquake stress drops generally fall in a narrow range over the entire magnitude spectrum, and so with $\Delta\sigma/\mu\approx 10^{-4}$ (Kanamori, 1977), $M_w=M$. One advantage to M for the purpose at hand is its dependence on only the static fault offset and rupture area, which can be determined for the 1857 and 1872 earthquakes.

SUMMARY MAGNITUDE (M)

To construct a single, summary-magnitude scale, M , to characterize the relative size of all the events listed in table 6.1, I use each of the scales described above, being

careful to consider such factors as the historical period and event location, as well as the quality of individual determinations. Where choices between several magnitude estimates are possible, the summary magnitude, M , is weighted toward long-period estimates of magnitude. Specifically, M_S and M_{G-R} are selected when judged reliable (110 events). Many local magnitudes have thus been superseded by surface-wave magnitudes; this effect is most noticeable for the largest events, where saturation of M_L becomes important. M_L is the principal contributor to 20 summary magnitudes, half of which also have reported M values that agree well. For all but two events before 1898 (1857 and 1872) and for two 20th-century events, M is based on M_I . In effect, the summary magnitude is an intensity magnitude before 1898 and a teleseismic surface-wave magnitude thereafter.

If M is to be uniformly valid across the entire timespan of the catalog, M_I must be an unbiased estimator of M_S or M_{G-R} . To test this absence of bias, the correlation between M_I and the two surface-wave magnitudes has been examined for 23 events with reliable M_S or M_{G-R} estimates, and an M_I value determined from the isoseismal maps of Topozada and others (1981) and Topozada and Parke (1982). This comparison shows that although the two magnitude scales are well correlated, M_I systematically underestimates M_S and M_{G-R} by 0.3 ± 0.3 units. If the sample is restricted to $M_S\leq 6.5$ ($n=18$), the bias is 0.2 ± 0.3 units. To further investigate this apparent bias, M_L was compared with M_I for 10 common events, for which the bias was 0.25 ± 0.2 units. As a final check, the difference between M_S or M_{G-R} and M_I for the 12 events listed in table 6.1 also used by Topozada (1975) to develop M_I relations was found to be 0.10 ± 0.19 units.

On the basis of these results, the summary magnitudes from M_I values of Topozada and others (1981) have been adjusted upward by 0.15 units and then rounded to the nearest quarter magnitude unit. Thus, events of $M_I=5.7$ become $M=5\frac{3}{4}$, and those of $M_I=5.8$ become $M=6$. No magnitude adjustment exceeded a quarter unit. M_I values from other sources have simply been rounded to the nearest quarter unit, because they average 0.2 units higher than the values of Topozada and others (1981) and Topozada and Parke (1982), where comparisons can be made. Summary magnitudes for events before 1850 have not been adjusted upward, owing to the imprecision of the original estimates.

REFERENCES CITED

- Abe, Katsuyuki, 1988, Magnitudes and origin times from Milne seismograph data: Earthquakes in China and California, 1898-1912, in Lee, W.H.K., Meyers, Herbert, and Shimazaki, Kunihiko, eds., Historical seismograms and earthquakes of the

- world: San Diego, Calif., Academic Press, p. 37-50.
- Abe, Katsuyuki, and Noguchi, Shin'ichi, 1983, Revision of magnitudes of large shallow earthquakes, 1897-1912: *Physics of the Earth and Planetary Interiors*, v. 33, no. 1, p. 1-11.
- Agnew, D.C., 1985, Evidence on large Southern California earthquakes from historical records, in Shearer, C.F., *Minutes of the National Earthquake Prediction Evaluation Council*, March 29-30, 1985, Pasadena, California: U.S. Geological Survey Open-File Report 85-507, p. 77-90.
- Agnew, D.C., and Sieh, K.E., 1978, A documentary study of the felt effects of the great California earthquake of 1857: *Seismological Society of America Bulletin*, v. 68, no. 6, p. 1717-1729.
- Aki, Keiti, 1965, Maximum likelihood estimate of b in the formula $\log N = a - bM$ and its confidence limits: *University of Tokyo, Earthquake Research Institute Bulletin*, v. 43, pt. 2, p. 237-239.
- 1966, Generation and propagation of G waves from the Niigata earthquake of June 16, 1964. Part 2. Estimation of earthquake moment, release of energy, and stress-strain drop from G wave spectrum: *University of Tokyo, Earthquake Research Institute Bulletin*, v. 44, pt. 1, p. 73-88.
- 1967, Scaling law of seismic spectrum: *Journal of Geophysical Research*, v. 72, no. 4, p. 1217-1231.
- Archuleta, R.J., 1984, A faulting model for the 1979 Imperial Valley earthquake: *Journal of Geophysical Research*, v. 89, no. B6, p. 4559-4585.
- Atwater, Tanya, 1970, Implications of plate tectonics for the Cenozoic tectonic evolution of western North America: *Geological Society of America Bulletin*, v. 81, no. 12, p. 3513-3535.
- Bakun, W.H., and McEvilly, T.V., 1984, Recurrence models and Parkfield, California, earthquakes: *Journal of Geophysical Research*, v. 89, no. B5, p. 3051-3058.
- Bakun, W.H., Clark, M.M., Cockerham, R.S., Ellsworth, W.L., Lindh, A.G., Prescott, W.H., Shakal, A.F., and Spudich, Paul, 1984, The 1984 Morgan Hill, California, earthquake: *Science*, v. 225, no. 4659, p. 288-291.
- Bakun, W.H., and Lindh, A. G., 1985, The Parkfield, California, earthquake prediction experiment: *Science*, v. 229, no. 4714, p. 619-624.
- Beanland, Sarah, and Clark, M.M., in press, The Owens Valley fault zone, eastern California, and surface rupture associated with the 1872 earthquake: *U.S. Geological Survey Bulletin*.
- Bolt, B.A., 1968, The focus of the 1906 California earthquake: *Seismological Society of America Bulletin*, v. 58, no. 1, p. 457-471.
- Bolton, H.E., 1927, Fray Juan Crespi, missionary explorer on the Pacific coast, 1769-1774: Berkeley, University of California Press, 402 p.
- Boore, D.M., 1977, Strong-motion recordings of the California earthquake of April 18, 1906: *Seismological Society of America Bulletin*, v. 67, no. 3, p. 561-577.
- Borcherdt, R.D., ed., 1975, Studies for seismic zonation of the San Francisco Bay region: *U.S. Geological Survey Professional Paper 941-A*, p. A1-A102.
- Coffman, J.L., von Hake, C.A., and Stover, C.W., eds., 1982, *Earthquake history of the United States*: Boulder, Colo., U.S. Department of Commerce, National Oceanic and Atmospheric Administration Publication 41-1, 208 p.
- DeMets, Charles, Gordon, R.G., Stein, Seth, and Argus, D.F., 1987, A revised estimate of Pacific-North America motion and implications for western North America plate boundary zone tectonics: *Geophysical Research Letters*, v. 14, no. 9, p. 911-914.
- Doser, D.I., 1986, Earthquake processes in the Rainbow Mountain-Fairview Peak-Dixie Valley, Nevada, region 1954-1959: *Journal of Geophysical Research*, v. 91, no. B12, p. 12572-12586.
- Eaton, J.P., O'Neill, M.E., and Murdock, J.N., 1970, Aftershocks of the 1966 Parkfield-Cholame, California, earthquake: A detailed study: *Seismological Society of America Bulletin*, v. 60, no. 4, p. 1151-1197.
- Ellsworth, W.L., Lindh, A.G., Prescott, W.H., and Herd, D.G., 1981, The 1906 San Francisco earthquake and the seismic cycle, in Simpson, D.W., and Richards, P.G., eds., *Earthquake prediction: An international review* (Maurice Ewing Series 4): Washington, American Geophysical Union, p. 126-140.
- Engdahl, E.R., and Rinehart, W.A., 1988, *Seismicity map of North America*: Boulder, Geological Society of America.
- Evernden, J.F., and Thompson, J.M., 1985, Predicting seismic intensities, in Ziony, J.I., ed., *Evaluating earthquake hazards in the Los Angeles region—an earth-science perspective*: U.S. Geological Survey Professional Paper 1360, p. 151-202.
- Fedotov, S.A., 1968, The seismic cycle, quantitative seismic zoning, and long-term seismic forecasting, in Medvedev, S.V., ed., *Seismic zoning of the USSR: Jerusalem, Israel Program for Scientific Translations*, p. 133-164.
- Gawthrop, W.H., 1978, The 1927 Lompoc, California, earthquake: *Seismological Society of America Bulletin*, v. 68, no. 6, p. 1705-1716.
- 1981, Comments on "The Lompoc, California, earthquake (November 4, 1927, $M=7.3$) and its aftershocks," by Thomas C. Hanks: *Seismological Society of America Bulletin*, v. 71, no. 2, p. 557-560.
- Geller, R.J. and Kanamori, Hiroo, 1977, Magnitudes of great shallow earthquakes from 1904 to 1952: *Seismological Society of America Bulletin*, v. 67, no. 3, p. 587-598.
- Gianella, V.P., 1957, Earthquake and faulting, Fort Sage Mountains, California, December, 1950: *Seismological Society of America Bulletin*, v. 47, no. 3, p. 173-177.
- Gianella, V.P., and Callaghan, Eugene, 1984, The Cedar Mountain, Nevada, earthquake of December 20, 1932: *Seismological Society of America Bulletin*, v. 24, no. 4, p. 345-384.
- Gilbert, G.K., 1884, A theory of the earthquakes of the Great Basin, with a practical application: *American Journal of Science*, ser. 3, v. 27, no. 157, p. 49-53.
- Goter, S.K., compiler, 1988, *Seismicity map of California*: U.S. Geological Survey Open-File Report 88-286, scale 1:1,000,000.
- Gutenberg, Beno, and Richter, C.F., 1954, *Seismicity of the earth and associated phenomena* (2d ed.): Princeton, N.J., Princeton University Press, 310 p.
- 1956, Earthquake magnitude, intensity, energy and acceleration: *Seismological Society of America Bulletin*, v. 46, no. 2, p. 105-145.
- Hanks, T.C., 1979, The Lompoc, California, earthquake (November 4, 1927, $M=7.3$) and its aftershocks: *Seismological Society of America Bulletin*, v. 69, no. 2, p. 451-462.
- 1981, Reply to W. Gawthrop's comments on "The Lompoc, California, earthquake (November 4, 1927, $M=7.3$) and its aftershocks": *Seismological Society of America Bulletin*, v. 71, no. 2, p. 561-565.
- Hanks, T.C., and Kanamori, Hiroo, 1979, A moment magnitude scale: *Journal of Geophysical Research*, v. 84, no. B5, p. 2348-2350.
- Hanks, T.C., and Allen, C.R., 1989, The Elmore Ranch and Superstition Hills earthquakes of 24 November 1987: Introduction to the special issue: *Seismological Society of America Bulletin*, v. 79, no. 2, p. 231-238.
- Harley, R.B., 1988, Rev. Juan Caballeria: Historian or storyteller? Rethinking the 1810 Dumetz expedition: Redlands, Calif., San Bernardino County Museum Association Quarterly, v. 35, p. 42.
- Harris, R.A., and Segall, Paul, 1987, Detection of a locked zone at depth on the Parkfield, California, segment of the San Andreas fault: *Journal of Geophysical Research*, v. 92, no. B8, p. 7945-7962.
- Hartzell, S.H., and Heaton, T.H., 1983, Inversion of strong ground motion and teleseismic waveform data for the fault rupture history of the 1979 Imperial Valley, California, earthquake: *Seismological*

- Society of America Bulletin, v. 73, no. 6, pt. A, p. 1553-1583.
- 1986, Rupture history of the 1984 Morgan Hill, California earthquake from the inversion of strong motion records: *Seismological Society of America Bulletin*, v. 76, no. 3, p. 649-674.
- Heaton, T.H., 1982, The 1971 San Fernando earthquake: A double event?: *Seismological Society of America Bulletin*, v. 72, no. 6, p. 2037-2062.
- Hill, D.P., Wallace, R.E., and Cockerham, R.S., 1985, Review of evidence on the potential for major earthquakes and volcanism in the Long Valley-Mono Craters-White Mountains regions of eastern California: *Earthquake Prediction Research*, v. 3, no. 3-4, p. 571-594.
- Hutton, K.L., and Boore, D.M., 1987, The M_L scale in southern California: *Seismological Society of America Bulletin*, v. 77, no. 6, p. 2074-2094.
- Jacoby, G.C., Sheppard, P.R., and Sieh, K.E., 1988, Irregular recurrence of large earthquakes along the San Andreas fault: Evidence from trees: *Science*, v. 241, no. 4862, p. 196-199.
- Jennings, C.W., compiler, 1975, Fault map of California with locations of volcanoes, thermal springs, and thermal wells: California Division of Mines and Geology Geologic Data Map 1, scale 1:750,000.
- Jennings, P.C., and Kanamori, Hiroo, 1979, Determination of local magnitude M_L , from seismoscope records: *Seismological Society of America Bulletin*, v. 69, no. 4, p. 1267-1288.
- Kanamori, Hiroo, 1977, The energy release in great earthquakes: *Journal of Geophysical Research*, v. 82, no. 20, p. 2981-2987.
- Kovach, R.L., Allen, C.R., and Press, Frank, 1962, Geophysical investigations in the Colorado Delta region: *Journal of Geophysical Research*, v. 67, no. 7, p. 2845-2871.
- Langston, C.A., 1978, The February 9, 1971 San Fernando earthquake: A study of source finiteness in teleseismic body waves: *Seismological Society of America*, v. 68, no. 1, p. 1-29.
- Lawson, A.C., chairman, 1908, The California Earthquake of April 18, 1906: Report of the State Earthquake Investigation Commission: Carnegie Institution of Washington Publication 87, 2 v.
- Lienkaemper, J.J., 1984, Comparison of two surface-wave magnitude scales: M of Gutenberg and Richter (1954) and M_S of "Preliminary Determination of Epicenters": *Seismological Society of America Bulletin*, v. 74, no. 6, p. 2357-2378.
- Lienkaemper, J.J., Pezzopane, S.K., Clark, M.M., and Rymer, M.J., 1987, Fault fractures formed in association with the 1986 Chalfant Valley, California, earthquake sequence: Preliminary report: *Seismological Society of America Bulletin*, v. 77, no. 1, p. 297-305.
- Lindh, A.G., 1983, Preliminary assessment of long-term probabilities for large earthquakes along selected fault segments of the San Andreas fault system in California: U.S. Geological Survey Open-File Report 83-63, 14 p.
- Liu, H.-L., and Helmsberger, D.V., 1983, The near-source ground motion of the 6 August 1979 Coyote Lake, California, earthquake: *Seismological Society of America Bulletin*, v. 73, no. 1, p. 201-218.
- Louderback, G.D., 1947, Central California earthquakes of the 1830's: *Seismological Society of America Bulletin*, v. 37, no. 1, p. 33-74.
- McAdie, A.G., 1907, Catalogue of earthquakes on the Pacific coast, 1897-1906: Smithsonian Institution of Washington Miscellaneous Collections, v. 49, art. 5, 64 p.
- McCulloch, D.S., 1985, Evaluating tsunami potential, in Ziony, J.I., ed., *Evaluating earthquake hazards in the Los Angeles region—an earth-science perspective*: U.S. Geological Survey Professional Paper 1360, p. 375-413.
- Mendoza, Carlos, and Hartzell, S.H., 1988, Aftershock patterns and main shock faulting: *Seismological Society of America Bulletin*, v. 78, no. 4, p. 1438-1449.
- Milne, John, 1901, Analyses of large earthquakes recorded in 1899: British Association for the Advancement of Science Meeting, 70th, Dover, 1900, Report, p. 60-104.
- Mogi, Kiyoo, 1981, Seismicity in western Japan and long-term earthquake forecasting: in Simpson, D.W., and Richards, P.G., eds., *Earthquake prediction: An international review (Maurice Ewing Series 4)*: Washington, American Geophysical Union, p. 43-51.
- Mount, V.S., and Suppe, John, 1987, State of stress near the San Andreas fault: Implications for wrench tectonics: *Geology*, v. 15, no. 12, p. 1143-1146.
- Nishenko, S.P., and Buland, Ray, 1987, A generic recurrence interval distribution for earthquake forecasting: *Seismological Society of America Bulletin*, v. 77, no. 4, p. 1382-1399.
- Oakeshott, G.B., ed., 1955, Earthquakes in Kern County, California during 1952: California Division of Mines Bulletin 171, 283 p.
- Plafker, George, and Galloway, J.P. eds., 1989, Lessons learned from the Loma Prieta, California, earthquake of October 17, 1989: U.S. Geological Survey Circular 1045, 48 p.
- Reasenber, P.A., and Ellsworth, W.L., 1982, Aftershocks of the Coyote Lake, California earthquake of August 6, 1979: A detailed study: *Journal of Geophysical Research*, v. 87, no. B13, p. 10637-10655.
- Reid, H.F., 1910, The mechanics of the earthquake, v. 2 of *The California earthquake of April 18, 1906: Report of the State Earthquake Investigation Commission*: Carnegie Institution of Washington Publication 87, 192 p.
- Richter, C.F., 1935, An instrumental earthquake scale: *Seismological Society of America Bulletin*, v. 25, no. 1, p. 1-32.
- 1958, *Elementary seismology*: San Francisco, W.H. Freeman and Co., 768 p.
- 1973, Historical seismicity of San Fernando earthquake area, in Benfer, N.A., Coffman, J.L., and Bernick, J.R., eds., *San Fernando, California, earthquake of February 9, 1971*: Washington, U.S. Department of Commerce, National Oceanic and Atmospheric Administration, Environmental Research Laboratories, v. 3, p. 5-11.
- Rymer, M.J., and Ellsworth, W.L., eds., 1990, *The Coalinga, California, earthquake of May 2, 1983*: U.S. Geological Survey Professional Paper 1487, 417 p.
- Sanders, C.O., and Slemmons, D.B., 1979, Recent crustal movements in the central Sierra Nevada-Walker Lane region of California-Nevada: Part III, The Olinghouse fault zone: *Tectonophysics*, v. 52, no. 1-4, p. 585-597.
- Savage, J.C., and Cockerham, R.S., 1987, Quasi-periodic occurrence of earthquakes in the 1978-1986 Bishop-Mammoth Lakes sequence, eastern California: *Seismological Society of America Bulletin*, v. 77, no. 4, p. 1347-1358.
- Segall, Paul, and Harris, R.A., 1987, Earthquake deformation cycle on the San Andreas fault near Parkfield, California: *Journal of Geophysical Research*, v. 92, no. B10, p. 10511-10525.
- Seismological Society of America Bulletin*, 1916, The earthquake at Volcano Lake, Mexico, November 20, 1915: v. 6, no. 2-3, p. 181-184.
- Sharp, R.V., 1982, Comparison of 1979 surface faulting with earlier displacements in the Imperial Valley, in *The Imperial Valley, California earthquake of October 15, 1979*: U.S. Geological Survey Professional Paper 1254, p. 213-221.
- Shawe, D.R., 1965, Strike-slip control of Basin-Range structure indicated by historical faults in western Nevada: *Geological Society of America Bulletin*, v. 76, no. 12, p. 1361-1378.
- Shor, G.G., Jr., and Roberts, Ellis, 1958, San Miguel, Baja California Norte, earthquakes of February, 1956: A field report: *Seismological Society of America Bulletin*, v. 48, no. 2, p. 101-116.

- Sieh, K.E., 1978a, Central California foreshocks of the great 1857 earthquake: *Seismological Society of America Bulletin*, v. 68, no. 6, p. 1731-1749.
- 1978b, Slip along the San Andreas fault associated with the great 1857 earthquake: *Seismological Society of America Bulletin*, v. 68, no. 5, p. 1421-1448.
- Sieh, K.E., Stuiver, Minze, and Brillinger, David, 1989, A more precise chronology of earthquakes produced by the San Andreas fault in southern California: *Journal of Geophysical Research*, v. 94, no. B1, p. 603-623.
- Singh, S.K., and Havskov, Jens, 1980, On moment-magnitude scale: *Seismological Society of America Bulletin*, v. 70, no. 1, p. 379-383.
- Slemmons, D.B., Steinbrugge, K.V., Tocher, Don, Oakeshott, G.B., and Gianella, V.P., 1959, Wonder, Nevada, earthquake of 1903: *Seismological Society of America Bulletin*, v. 49, no. 3, p. 251-265.
- Smith, S.W., and Knapp, J.S., 1980, The northern termination of the San Andreas fault, *in* Streitz, Robert, and Sherburne, R.W., eds., *Studies of the San Andreas fault zone in northern California*: California Division of Mines and Geology Special Report 140, p. 153-164.
- Stein, R.S., and King, G.C.P., 1984, Seismic potential revealed by surface folding: 1983 Coalinga, California, earthquake: *Science*, v. 224, no. 4651, p. 869-871.
- Strand, C.L., 1980, Pre-1900 earthquakes of Baja California and San Diego County: San Diego, Calif., San Diego State University, 320 p.
- Sykes, L.R., and Nishenko, S.P., 1984, Probabilities of occurrence of large plate rupturing earthquakes for the San Andreas, San Jacinto, and Imperial faults, California, 1983-2003: *Journal of Geophysical Research*, v. 89, no. B7, p. 5905-5927.
- Thatcher, Wayne, 1975, Strain accumulation and release mechanism of the 1906 San Francisco earthquake: *Journal of Geophysical Research*, v. 80, no. 35, p. 4862-4872.
- Thatcher, Wayne, and Lisowski, Michael, 1987, 1906 earthquake slip on the San Andreas fault in offshore northwestern California [abs.]: *Eos (American Geophysical Union Transactions)*, v. 68, no. 44, p. 1507.
- Tocher, Don, 1956, Movement on the Rainbow Mountain fault: *Seismological Society of America Bulletin*, v. 46, no. 1, p. 10-14.
- 1959, Seismic history of the San Francisco region, in *San Francisco earthquakes of March 1957*: California Division of Mines Special Report 57, p. 39-48.
- Topozada, T.R., 1975, Earthquake magnitude as a function of intensity data in California and western Nevada: *Seismological Society of America Bulletin*, v. 65, no. 5, p. 1223-1238.
- Topozada, T.R., and Parke, D.L., 1982, Areas damaged by California earthquakes, 1900-1949: California Division of Mines and Geology Open-File Report 82-17 SAC, 65 p.
- Topozada, T.R., Real, C.R., and Parke, D.L., 1981, Preparation of isoseismal maps and summaries of reported effects for pre-1900 California earthquakes: California Division of Mines and Geology Open-File Report 81-11 SAC, 182 p.
- 1988, Earthquake history of California, *in* Lee, W.H.K., Meyers, Herbert, and Shimazaki, Kunihiko, eds., *Historical seismograms and earthquakes of the world*: San Diego, Calif., Academic Press, p. 267-275.
- Townley, S.D., and Allen, M.W., 1939, Descriptive catalog of earthquakes of the Pacific coast of the United States 1769 to 1928: *Seismological Society of America Bulletin*, v. 29, no. 1, p. 1-297.
- Trifunac, M.D., and Brune, J.N., 1970, Complexity of energy release during the Imperial Valley, California, earthquake of 1940: *Seismological Society of America Bulletin*, v. 60, no. 1, p. 137-160.
- U.S. Geological Survey, 1971, The San Fernando, California, earthquake of February 9, 1971: Professional Paper 733, 254 p.
- 1972, The Borrego Mountain earthquake of April 9, 1968: Professional Paper 787, 207 p.
- 1982, The Imperial Valley, California, earthquake of October 15, 1979: Professional Paper 1254, 451 p.
- Wallace, R.E., 1984, Fault scarps formed during the earthquakes of October 2, 1915, in Pleasant Valley, Nevada, and some tectonic implications: U.S. Geological Survey Professional Paper 1274-A, p. A1-A33.
- Walter, S.R., 1986, Intermediate-focus earthquakes associated with Gorda plate subduction in northern California: *Seismological Society of America Bulletin*, v. 76, no. 2, p. 583-588.
- Wong, I.G., Ely, R.W., and Kollmann, A.C., 1988, Contemporary seismicity and tectonics of the northern and central Coast Ranges-Sierran block boundary zone, California: *Journal of Geophysical Research*, v. 93, no. B7, p. 7813-7833.
- Working Group on California Earthquake Probabilities, 1988, Probabilities of large earthquakes occurring in California on the San Andreas fault: U. S. Geological Survey Open File Report 88-398, 62 p.
- Ziony, J.I., ed., 1985, Evaluating earthquake hazards in the Los Angeles region—an earth-science perspective: U.S. Geological Survey Professional Paper 1360, 505 p.
- Zoback, M.D., Zoback, M.L., Mount, V.S., Suppe, John, Eaton, J.P., Healy, J.H., Oppenheimer, D.H., Reasenber, P.A., Jones, L.M., Raleigh, C.B., Wong, I.G., Scotti, Oona, and Wentworth, C.M., 1987, New evidence on the state of stress of the San Andreas fault system: *Science*, v. 238, no. 4830, p. 1105-1111.
- Zoback, M.L., and Zoback, M.D., 1980, Faulting patterns in north-central Nevada and strength of the crust: *Journal of Geophysical Research*, v. 85, no. B1, p. 275-284.

TABLE 6.1

Earthquake origin times, magnitudes, and locations before 1990 principally derived from interpretations of felt reports by Topozada and others (1981); after 1900, data principally derived from Gutenberg and Richter (1954) and bulletins of the California Institute of Technology, University of California, Berkeley, University of Nevada, Reno, and U.S. Geological Survey. See text for discussion of summary magnitude M . Other magnitude scales are M_L , local-magnitude scale of Richter (1935); M_{G-R} , magnitudes from Gutenberg and Richter (1954), generally based on 20-s surface waves; M_S , 20-s surface-wave magnitude; M_I , magnitude estimated from felt area at various intensity levels; and M , moment magnitude, defined as $M = \frac{2}{3} \log_{10} M_0 - 10.7$, where M_0 is in dyne-centimeters—parentetical values based on seismogram envelope. M_S values before 1935 generally derived from undamped Milne seismographs, using the formula of Abe (1988)—parentetical values based on one or two amplitudes; M_S values since 1968 measured from vertical seismographs. Absence of reported amplitudes on Milne seismographs (*) suggests $M_S < 6$.

TABLE 6.1.—Major California and Nevada earthquakes, 1769–1989

Date and origin time (GMT)	<i>M</i>	Lat N. and Long W.	Locality	<i>M_L</i>	<i>M_{G-R}</i>	<i>M_S</i>	<i>M_I</i>	<i>M</i>
1769/07/28	6?	34° 118°	Los Angeles Basin-----	—	—	—	6	—
1800/11/22 21:30	6½?	33° 117°18'	San Diego region-----	—	—	—	≥6½	—
1808/06/21	6?	37°48' 122°30'	San Francisco region-----	—	—	—	6	—
1812/12/08 15:00	7	34°22' 117°39'	Wrightwood-----	—	—	—	6.9	—
1812/12/21 19:00	7	34°12' 119°54'	Santa Barbara Channel-----	—	—	—	7.1	—
1827/09/24 04:00	5½?	34° 119°	Los Angeles region-----	—	—	—	5½ to 6	—
1836/06/10 15:30	6¼	37°48' 122°12'	Hayward fault-----	—	—	—	6.8	—
1838/06/7 p.m.	7	37°36' 122°24'	San Francisco Peninsula-----	—	—	—	≥7.0	—
1852/11/29 20:00	6½	32°30' 115°	Volcano Lake, B.C.-----	—	—	—	6 to 7	—
1855/07/11 04:15	6?	34° 6' 118° 6'	Los Angeles region-----	—	—	—	6	—
1856/02/15 13:25	5¾	37°30' 122°18'	San Francisco Peninsula-----	—	—	—	5.5	—
1857/01/09 16:00	8¼	35°42' 120°18'	Great Fort Tejon earthquake-----	—	—	—	7.6	7.8
1857/09/03 03:05	6¼	39°18' 120°	Western Nevada or eastern Sierra Nevada-----	—	—	—	6.0	—
1858/11/26 08:35	6¼	37°30' 121°54'	San Jose region-----	—	—	—	6.1	—
1858/12/16 10:00	6	34° 117°30'	San Bernadino region-----	—	—	—	6	—
1860/03/15 19:00	6½	39°30' 119°30'	Carson City, Nev. region-----	—	—	—	6.3	—
1861/07/04 00:11	5¼	37°48' 122° 0'	San Ramon Valley-----	—	—	—	5.6	—
1862/05/27 20:00	6	32°42' 117°12'	San Diego region-----	—	—	—	5.9	—
1864/02/26 13:47	6	37° 6' 121°42'	Southern Santa Cruz Mountains-----	—	—	—	5.9	—
1864/03/05 16:49	5¾	37°42' 122°	East of San Francisco Bay-----	—	—	—	5.7	—
1865/10/08 20:46	6½	37° 0' 122° 0'	Southern Santa Cruz Mountains-----	—	—	—	6.3	—
1866/07/15 06:30	6	37°30' 121°18'	Western San Joaquin Valley-----	—	—	—	5.8	—
1868/05/30 05:10	6	39°18' 119°42'	Virginia City, Nev.-----	—	—	—	5.8, 6	—
1868/10/21 15:53	7	37°42' 122° 6'	Hayward fault-----	—	—	—	6.8	—
1869/12/27 01:55	6¼	39°24' 119°42'	Olinghouse fault, Nev. (?)-----	—	—	—	6.1	—
1869/12/27 10:00	6	39° 6' 119°48'	Carson City, Nev. region-----	—	—	—	5.9	—
1870/02/17 20:12	6	37°12' 122° 6'	Los Gatos-----	—	—	—	5.8	—
1871/03/02 21:05	6	40°24' 124°12'	Cape Mendocino-----	—	—	—	5.9	—
1872/03/26 10:30	7.6	36°42' 118° 6'	Owens Valley-----	—	—	—	7.3	7.6
1872/03/26 14:06	6¾	36°54' 118°12'	Owens Valley-----	—	—	—	6.5	—
1872/04/03 12:15	6¼	37° 118°12'	Owens Valley-----	—	—	—	6.1	—
1872/04/11 19:00	6¼	37°30' 118°30'	Owens Valley-----	—	—	—	6.6	—
1872/05/03 01:00	5¾	33° 115°	Imperial Valley (?)-----	—	—	—	≥5.5	—
1872/11/12 00:00	6	39°? 117°?	Austin, Nev. region (?)-----	—	—	—	6	—
1873/11/23 05:00	6¼	42° 124°	Crescent City-----	—	—	—	6.7	—
1875/01/24 12:00	6	40°12' 120°30'	Honey Lake-----	—	—	—	5.8	—
1875/11/15 22:30	6¼	32°30' 115°30'	Imperial Valley to Colorado River delta (?)-----	—	—	—	6.2	—
1878/05/09 04:25	6	40° 6' 124°	Punta Gorda region-----	—	—	—	5.8	—
1881/02/02 00:11	5¾	36° 0' 120°30'	Parkfield-----	—	—	—	5.6	—
1881/04/10 10:00	6	37°24' 121°24'	Western San Joaquin Valley-----	—	—	—	5.9	—
1882/03/06 21:45	5¾	36°54' 121°12'	Hollister-----	—	—	—	5.7	—
1883/09/05 12:30	6¼	34°12' 119°54'	Santa Barbara Channel-----	—	—	—	6.0	—
1884/01/28 07:30	5¾	41°6' 123°36'	Klamath Mountains-----	—	—	—	5.7	—
1884/03/26 00:40	6	37°6' 122°12'	Santa Cruz Mountains-----	—	—	—	5.9	—
1885/01/31 05:45	5¾	40°24' 120°36'	Susanville-----	—	—	—	5.7	—
1885/04/12 04:05	6¼	36°24' 121°	Southern Diablo Range-----	—	—	—	6.2	—
1887/06/03 10:48	6¼	39°12' 119°48'	Carson City, Nev. region-----	—	—	—	6.3	—
1888/04/29 04:48	6	39°42' 120°42'	Mohawk Valley-----	—	—	—	5.9	—
1889/05/19 11:10	6¼	38° 0' 121°54'	Antioch-----	—	—	—	6.0	—
1889/06/20 06:00	6	40°30' 120°42'	Susanville-----	—	—	—	5.9	—
1889/09/30 05:20	5¾	37°12' 118°42'	Bishop region-----	—	—	—	5.6	—
1890/02/09 12:06	6¼	33°24' 116°18'	San Jacinto or Elsinore fault region (?)-----	—	—	—	6.3	—
1890/04/24 11:36	6¼	36°54' 121°36'	Pajaro Gap-----	—	—	—	6.0	—
1890/07/26 09:40	6¼	40°30' 124°12'	Cape Mendocino-----	—	—	—	6.0	—
1891/07/30 14:10	6	32° 115°	Colorado River delta region-----	—	—	—	6.0	—

TABLE 6.1.—Major California and Nevada earthquakes, 1979-1989—Continued

Date and origin time (GMT)	M	Lat N. and Long W.	Locality	M_L	M_{G-R}	M_S	M_I	M
1892/02/24 07:20	7	32°33' 115°38'	Laguna Salada, B.C.	—	—	—	6.7, 7.2	—
1892/04/19 10:50	6½	38°24' 122° 0'	Vacaville	—	—	—	6.4	—
1892/04/21 17:43	6¼	38°30' 121°54'	Winters	—	—	—	6.2	—
1892/05/28 11:15	6½	33°12' 116°12'	San Jacinto or Elsinore fault region (?)	—	—	—	6.3	—
1892/11/13 12:45	5¾	36°48' 121°30'	Hollister	—	—	—	5.6	—
1893/05/19 00:35	5¾	34° 6' 119°24'	Pico Canyon	—	—	—	5.5, 5.9	—
1894/07/30 05:12	6	34°18' 117°36'	Lytle Creek region	—	—	—	5.9, 6.0	—
1894/09/30 17:36	6	40°18' 123°42'	Cape Mendocino region	—	—	—	5.8	—
1894/10/23 23:03	5¾	32°48' 116°48'	East of San Diego	—	—	—	5.7	—
1896/08/17 11:30	6	36°42' 118°18'	Southeastern Sierra Nevada	—	—	—	5.9	—
1897/06/20 20:14	6¼	37° 0' 121°30'	Gilroy	—	—	—	6.2	—
1898/03/31 07:43	6½	38°12' 122°24'	Mare Island	—	—	(6.5)	6.2	—
1898/04/15 07:07	6½	39°12' 123°48'	Mendocino	—	—	(6.7)	6.4	—
1899/04/16 13:40	7	41°? 126°?	West of Eureka	—	—	7.0	5.7	—
1899/07/06 20:10	5¾	37°12' 121°30'	Morgan Hill	—	—	(4.7)	5.8	—
1899/07/22 20:32	5¾	34°18' 117°30'	Lytle Creek region	—	—	(5.6)	6.5, 6.4	—
1899/12/25 12:25	6.4	33°48' 117° 0'	San Jacinto and Hemet	—	—	6.4	6.6, 6.7	—
1901/03/03 07:45	6.4	36° 0' 120°30'	Parkfield	—	—	6.4	5.8	—
1903/01/24 05:27	6.6	31°30' 115°	Colorado River delta region	—	7+	6.6	—	—
1903/06/11 13:12	5½	37°24' 121°54'	San Jose	—	—	(5.4)	5.8	—
1903/08/03 06:49	5½	37°18' 121°48'	San Jose	—	—	(5.3)	5.8	—
1906/04/18 13:12	8¼	37°42' 122°30'	Great 1906 earthquake	6.9	8¼, 8.3	7.8, 8.3	7.8	7.7
1906/04/19 00:30	6.2	32°54' 115°30'	Imperial Valley	—	6+	6.2	5.8	—
1906/04/23 09:10	6.4	41° 124°	Arcata	—	—	6.4	—	—
1907/09/20 01:54	5.3	34°12'? 117° 6'?	San Bernardino region	—	6	*	5.3	—
1908/11/04 08:37	6?	36°? 117°?	Death Valley region	—	6½	*	—	—
1909/10/29 06:45	5.8	40°30' 124°12'	Cape Mendocino	—	6+	5.8, (5.1)	6.4	—
1910/03/11 06:52	5.8	36°54' 121°48'	Watsonville	—	—	5.8	5.5	—
1910/03/19 00:11	6.0	40°? 125°?	West of Cape Mendocino	—	—	6.0	6.2	—
1910/05/15 15:47	5½	33°42' 117°24'	Glen Ivy Hot Springs	—	—	(5.5)	6.0, 5.3	—
1910/08/05 01:31	6.6	42° 127°	West of Crescent City	—	6.8	6.6	—	—
1911/07/01 22:00	6.5	37°15' 121°45'	Calaveras fault	—	6.6	6.5	6.2	—
1914/02/18 18:17	5½?	39°30' 119°48'	Truckee region	—	—	*	6	—
1914/04/24 08:34	6	39°30' 119°48'	Truckee region	—	—	(5.5), (5.6)	6.4	—
1915/05/06 12:09	6.2	40° 126°	West of Cape Mendocino	—	6¼	6.2, (6.0)	—	—
1915/06/23 03:59	6.0	32°48' 115°30'	Imperial Valley	—	6¼	6.0, (5.6)	5.6, 5.5	—
1915/06/23 04:56	5.9	32°48' 115°30'	Imperial Valley	—	6¼	5.9	5.6, 5.5	—
1915/10/03 06:52	7.3	40°30' 117°30'	Pleasant Valley, Nev.	—	7¾	7.6, 7.4, 7.3	—	7.2
1915/11/21 00:13	7.1	32° 115°	Volcano Lake, B.C.	—	7.1	7.1, 6.8	—	—
1915/12/31 12:20	6.5	41° 126°	West of Eureka	—	6½	6.5, (6.4)	—	—
1916/02/03 05:03	5.9	41° 117°48'	North of Pleasant Valley, Nev.	—	—	(5.1)	5.9	—
1916/10/23 02:44	5.3	34°54' 118°54'	Tejon Pass region	—	5½±	6	5.2, 5.3	(5.3)
1916/11/10 09:11	6.1	35°30' 116° 0'	South of Death Valley	—	6.1	(5.7, 5.9)	—	—
1918/04/21 22:32	6.9	33°48' 117° 0'	San Jacinto	—	6.8	7.2, 6.9	6.6	(6.8)
1918/07/15 00:23	6.5	41° 125°	West of Eureka	—	6½	6.5	5.9	—
1922/01/26 09:31	6.0	41° 126°	West of Eureka	—	6	(6.1)	—	—
1922/01/31 13:17	7.3	41° 125°30'	West of Eureka	—	7.3	7.4	—	—
1922/03/10 11:21	6.3	36° 0' 120°30'	Parkfield	—	6½	6.3	6.3	6.1
1923/01/22 09:04	7.2	40°30' 124°30'	Cape Mendocino	—	7.2	7.3	6.5, 6.8	—
1923/07/23 07:30	6.0	34° 0' 117°18'	San Bernardino region	—	6¼	—	6.0	6.0
1925/06/04 12:02	6	41°30' 125°	West of Eureka	—	6	(5.8)	—	—
1925/06/29 14:42	6.3	34°18' 119°48'	Santa Barbara	—	6¼	—	6.3	(6.9)
1926/10/22 12:35	6.1	36°37' 122°21'	Monterey Bay	—	6.1	—	6.1	—
1926/10/22 13:35	6.1	36°33' 122°11'	Monterey Bay	—	6.1	—	—	—
1926/12/10 08:38	6.0	40°45' 126°	West of Cape Mendocino	—	6.0	(6.2)	—	—

TABLE 6.1.—Major California and Nevada earthquakes, 1979–1989—Continued

Date and origin time (GMT)	<i>M</i>	Lat N. and Long W.	Locality	<i>M_L</i>	<i>M_{G-R}</i>	<i>M_S</i>	<i>M_I</i>	<i>M</i>
1927/09/18 02:07	6	37°30' 118°45'	Bishop region-----	—	6	—	5.5	—
1927/11/04 13:50	7.3	34°42' 120°48'	Southwest of Lompoc-----	—	7.3, 7.5	(7.2)	6.2	(7.3)
1932/06/06 08:44	6.4	40°45' 124°30'	Eureka-----	—	6.4	(6.4)	5.9	—
1932/12/21 06:10	7.2	38°45' 118°	Cedar Mountain, Nev.-----	—	7.2	(7.4)	—	—
1933/01/05 06:51	5.9	38°46' 117°44'	Cedar Mountain, Nev.-----	5.7	5.9	—	—	—
1933/03/11 01:54	6.3	33°37' 117°58'	Long Beach-----	6.3	6¼	(6.5)	6.2	6.2
1933/06/25 20:45	6.1	39° 4' 119°20'	Yerington, Nev.-----	—	6.1	—	—	—
1934/01/30 20:16	6.3	38°18' 118°24'	Excelsior Mountain, Nev.-----	—	6.3, 6.3	(6.4)	—	—
1934/06/08 04:47	6.0	36° 0' 120°30'	Parkfield-----	5.2, 6.0, 6.1	6.0	—	5.6	6.1
1934/07/06 22:48	6.5	41°15' 125°45'	West of Eureka-----	—	6.5	—	—	—
1934/12/30 13:52	6.5	32°15' 115°30'	Laguna Salada, B.C.-----	6.5	6.5	—	—	(6.4)
1934/12/31 18:45	7.0	32° 114°45'	Colorado River delta-----	7.1	7.0	—	—	(7.1)
1935/02/24 01:45	5.3	31°59' 115°12'	Colorado River delta-----	6.0	5¼	—	—	(≤5.3)
1936/06/03 09:15	5.9	40° 125°30'	West of Cape Mendocino-----	—	5.9	—	—	—
1937/03/25 16:49	6.0	33°28' 116°25'	Buck Ridge-----	6.0, 5.9	6.0	—	5.9	—
1940/02/08 08:05	6	39°45' 121°15'	Chico-----	5.7	6	—	—	—
1940/05/19 04:36	7.1	32°44' 115°30'	Imperial Valley-----	6.2	6.7, 7.1	7.2	6.4, 6.6	6.9, 7.1
1940/12/07 22:16	5½	31°40' 115° 5'	Colorado River delta-----	6.0	5¼	—	—	(≤5.3)
1941/02/09 09:44	6.6	40°42' 125°24'	West of Cape Mendocino-----	6.4	6.6	—	—	—
1941/04/09 17:08	5.3	31° 114°	Gulf of California-----	6.0	5¼	—	—	—
1941/05/13 16:01	6.0	40°18' 126°24'	West of Cape Mendocino-----	6.0	6	—	—	—
1941/07/01 07:50	5.9	34°22' 119°35'	Carpenteria-----	5.9	5.9	—	5.5, 6.0	(6.0)
1941/09/14 16:43	5.8	37°34' 118°44'	Tom's Place-----	5.8, 6.0	5.8	—	5.6	—
1941/09/14 18:39	6.0	37°34' 118°44'	Tom's Place-----	6.0	6.0	—	5.6	(5.5)
1941/10/03 16:13	6.4	40°24' 124°48'	West of Cape Mendocino-----	6.4	6.4	—	—	—
1942/10/21 16:22	6.5	33° 3' 116° 5'	Fish Creek Mountains-----	6.5	6½	—	6.0, 6.3	6.6
1942/12/03 09:44	5.9	39°42' 119°18'	North of Wadsworth, Nev.-----	5.5	5.9	—	—	—
1945/05/19 15:07	6.2	40°24' 126°54'	West of Cape Mendocino-----	6.0	6.2	—	—	—
1945/09/28 22:24	6.0	41°54' 126°42'	West of Crescent City-----	6.0	6.0	—	—	—
1946/03/15 13:49	6.3	35°44' 118° 3'	Walker Pass-----	6.3	6¼	—	6.1	6.0
1947/04/10 15:58	6.4	34°59' 116°33'	Manix-----	6.2	6.4	—	6.3, 6.4	6.6
1948/12/04 23:43	6.5	33°56' 116°23'	Desert Hot Springs-----	6.5	6.5±	—	6.2, 6.5	6.0
1948/12/29 12:53	6.0	39°33' 120° 5'	Verdi, Nev.-----	6.0	6.0	—	5.7	—
1949/03/24 20:56	6.2	41°18' 126°	West of Eureka-----	5.9	6.2	—	—	—
1949/05/02 11:25	5.9	34° 1' 115°41'	Pinto Mountain-----	5.9	5.9	—	—	—
1951/10/08 04:10	6	40°15' 124°30'	West of Cape Mendocino-----	5.8	6	—	—	—
1951/12/26 00:46	5.9	32°48' 118°18'	San Clemente Island-----	5.9	5.9	—	—	—
1952/07/21 11:52	7.7	35° 0' 119° 1'	Kern County earthquake-----	7.2	7.7	7.8	7.0	7.5, 7.3
1952/07/21 12:05	6.4	35° 0' 119° 0'	Kern County-----	6.4	—	—	—	—
1952/07/23 00:38	6.1	35°22' 118°35'	Kern County-----	6.1	—	—	—	5.7
1952/07/29 07:03	6.1	35°23' 118°51'	Bakersfield-----	6.1	—	—	—	6.3
1952/11/22 07:46	6.0	35°44' 121°12'	Bryson-----	6.0	6±	—	—	—
1954/01/12 23:33	5.9	35° 0' 119° 1'	West of Wheeler Ridge-----	5.9	—	—	—	5.7
1954/03/19 09:54	6.2	33°17' 116°11'	Arroyo Salada-----	6.2, 6.2	—	—	6.2	6.4
1954/07/06 11:13	6.6	39°25' 118°32'	Rainbow Mountain, Nev.-----	6.8	6.6	6.3	—	6.2
1954/07/06 22:07	6.4	39°18' 118°30'	Rainbow Mountain, Nev.-----	6.0	6.4	—	—	6.1
1954/08/24 05:51	6.8	39°35' 118°27'	Stillwater, Nev.-----	6.8	6.8	6.9	—	6.6
1954/08/31 22:20	6.3	39°30' 118°30'	Stillwater, Nev.-----	5.8	6.3	—	—	5.8
1954/10/24 09:44	6.0	31°30' 116°	East of Santo Tomas, B.C.-----	6.0	—	—	—	6.0
1954/11/12 12:26	6.3	31°30' 116°	East of Santo Tomas, B.C.-----	6.3	—	—	—	6.3
1954/11/25 11:16	6.5	40°16' 125°38'	West of Cape Mendocino-----	6.1	6.5	7.2	—	—
1954/12/16 11:07	7.1	39°19' 118°12'	Fairview Peak, Nev.-----	7.2	7.1	—	—	7.2
1954/12/16 11:11	6.8	39°30' 118° 0'	Dixie Valley, Nev.-----	7.1	6.8	—	—	7.0
1954/12/21 19:56	6.6	40°56' 123°47'	East of Arcata-----	6.5	6.6	—	—	—
1956/02/09 14:32	6.8	31°45' 115°55'	San Miguel, B.C.-----	6.8	—	—	6.3	6.5

TABLE 6.1.—Major California and Nevada earthquakes, 1979–1989—Continued

Date and origin time (GMT)	M	Lat N. and Long W.	Locality	M_L	M_{G-R}	M_S	M_I	M
1956/02/09 15:24	6.1	31°45′ 115°55′	San Miguel, B.C.-----	6.1	—	—	—	6.0
1956/02/14 18:33	6.3	31°30′ 115°30′	San Miguel, B.C.-----	6.3	—	—	—	6.2
1956/02/15 01:20	6.4	31°30′ 115°30′	San Miguel, B.C.-----	6.4	—	—	—	6.2
1956/10/11 16:48	6.0	40°40′ 125°46′	West of Cape Mendocino-----	6.0	—	—	—	—
1956/12/13 13:15	6.0	31° 115°	Western shore, Gulf of California-----	6.0	—	—	—	—
1959/03/23 07:10	6.3	39°36′ 118° 1′	Dixie Valley, Nev.-----	6.3	—	—	—	—
1959/06/23 14:35	6.1	39° 5′ 118°49′	Schurz, Nev.-----	6.1	—	—	—	—
1960/08/09 07:39	6.2	40°19′ 127° 4′	West of Cape Mendocino-----	6.2	—	—	—	—
1966/06/28 04:26	6.0	36° 0′ 120°30′	Parkfield-----	5.5, 5.6, 5.7	—	6.0	5.7	6.1
1966/08/07 17:36	6.3	31°48′ 114°30′	Gulf of California-----	6.3	—	—	—	6.3
1966/09/12 16:41	6.0	39°25′ 120° 9′	Truckee-----	6.0	—	—	—	5.9
1968/04/09 02:28	6.5	33°11′ 116° 8′	Borrego Mountain-----	6.4, 6.3, 6.8	—	6.8	6.3	6.5
1968/06/26 01:42	5.4	40°14′ 124°16′	Punta Gorda-----	5.9	—	5.4	—	—
1971/02/09 14:00	6.5	34°25′ 118°24′	San Fernando-----	6.4, 5.8	—	6.5, 6.5	6.5	6.7
1973/02/21 14:45	5.2	34° 4′ 119° 2′	Point Mugu-----	5.9, 5.6	—	5.2	—	5.3
1979/08/06 17:05	5.7	37° 7′ 121°31′	Coyote Lake-----	5.8	—	5.7	5.6	5.7
1979/10/15 23:16	6.5	32°36′ 115°18′	Imperial Valley-----	6.6, 6.5, 6.4	—	6.9, 6.7	6.0	6.4 to 6.6
1980/01/24 19:00	5.8	37°50′ 121°47′	Livermore-----	5.8	—	5.9	—	5.8
1980/05/25 16:33	6.1	37°36′ 118°50′	Mammoth Lakes-----	6.1, 6.4, 6.2	—	6.1	—	6.2
1980/05/25 16:49	5.9	37°39′ 118°54′	Mammoth Lakes-----	6.0, 5.9	—	—	—	—
1980/05/25 19:44	5.8	37°33′ 118°49′	Mammoth Lakes-----	6.1, 6.6, 6.4	—	5.8	—	5.9
1980/05/27 14:50	6.0	37°29′ 118°48′	Mammoth Lakes-----	6.2, 6.4, 5.8	—	6.0	—	5.9
1980/06/09 03:28	6.4	32°12′ 115° 5′	Victoria, B.C.-----	6.1, 6.1	—	6.4	—	6.4
1980/11/08 10:27	7.2	41° 7′ 124°40′	West of Eureka-----	6.9	—	7.2	—	7.4
1981/04/26 12:09	6.0	33° 8′ 115°39′	Westmorland-----	5.6	—	6.0	—	5.9
1981/09/04 15:50	5.9	33°40′ 119° 7′	North of Santa Barbara Island-----	5.3	—	5.9	—	5.9
1981/09/30 11:53	5.8	37°35′ 118°52′	Mammoth Lakes-----	5.9, 6.0, 5.9	—	5.8	—	5.7
1983/05/02 23:42	6.5	36°14′ 120°19′	Coalinga-----	6.7, 6.1, 6.1	—	6.5	—	6.4, 6.5
1983/07/22 02:39	5.7	36°14′ 120°25′	Coalinga-----	6.0, 5.6	—	5.7	—	5.7, 6.0
1984/04/24 21:15	6.1	37°19′ 121°39′	Morgan Hill-----	6.2	—	6.1	—	6.2, 6.5
1984/09/10 03:14	6.7	40°23′ 127° 9′	Mendocino Fracture Zone-----	6.6	—	6.7	—	6.7
1984/11/23 18:08	5.7	37°27′ 118°36′	Round Valley-----	6.1, 6.2	—	5.7	—	5.8
1985/08/04 12:01	5.9	36° 8′ 120°10′	North Kettleman Hills-----	5.6	—	5.9	—	6.1, 6.1
1986/07/08 09:20	6.0	34° 0′ 116°36′	North Palm Springs-----	5.9	—	6.0	—	6.2
1986/07/20 14:29	5.6	37°34′ 118°26′	Chalfant Valley-----	5.9, 5.9	—	5.6	—	5.8
1986/07/21 14:42	6.2	37°32′ 118°26′	Chalfant Valley-----	6.5, 6.0	—	6.2	—	6.3, 6.4
1986/07/31 07:22	5.2	37°28′ 118°22′	Chalfant Valley-----	5.8, 5.9	—	5.2	—	5.5
1987/10/01 14:42	5.8	34° 3′ 118° 5′	Whittier Narrows-----	5.9	—	5.8	—	6.1
1987/11/24 01:53	6.2	33° 4′ 115°47′	Elmore Ranch fault-----	5.8	—	6.2	—	5.9
1987/11/24 13:16	6.6	33° 1′ 115°51′	Superstition Hills-----	6.0	—	6.6	—	6.5
1989/10/18 00:04	7.1	37° 2′ 121°53′	Loma Prieta-----	7.0	—	7.1	—	7.0



earthquakes have been documented, some on the same fault strand, and the entire zone of plate-boundary deformation is exceptionally broad. Major changes in fault strike also play a role in redistributing plate-boundary deformation and diffusing it over a wider zone. Compressional bends introduce uplift, crustal thickening, and subsidiary reverse faulting, such as in the Transverse Ranges of southern California. Extensional bends are characterized by subsidence, basin filling, and, possibly, volcanism, as occurs in the Imperial Valley. Extensional and compressional features are more localized at the smaller-scale discontinuities and changes in fault strike that occur throughout the San Andreas system.

Crustal movements observed at the surface reflect deformation processes occurring at depth in the lithosphere. Both laboratory rock-mechanics experiments and studies of exhumed fault zones define the nature of these processes, which, in turn, constrain the classes of large-scale faulting models consistent with surface measurements. In the cool and brittle seismically active parts of the crust, elastic processes are dominant, the frictional strength of active faults increases linearly with depth, and faulting is controlled by Coulomb failure. The transition from brittle seismic behavior to ductile aseismic deformation occurs in the midcrust. Although it is generally agreed that this transition occurs as a result of increasing temperature, its precise mechanism is uncertain. If deformation in the midcrust is concentrated within a narrow vertical shear zone lying beneath the seismically active fault plane, then the brittle/ductile transition may reflect either the increasing importance of ductile or cataclastic flow at depth (Sibson, 1982) or a thermally controlled transition from unstable to stable frictional sliding (Brace and Byerlee, 1966; Tse and Rice, 1986). However, if ductile deformation is broadly distributed in the midcrust, then the cyclic buildup and relief of stresses in the brittle seismogenic crust is controlled by the stress transfer between the elastic lithosphere and ductile "asthenosphere" and the flow properties of the latter.

Both the steady, aseismic movements within the San Andreas plate-boundary zone and the coseismic strain release in large earthquakes are well within the range of detectability of repeated geodetic-survey measurements. The purpose of this chapter is to summarize the salient features of these observations, demonstrating the constraints they place on the amount of present-day plate motion occurring across the San Andreas plate-boundary zone and showing how measurements shed light on the mechanics of the cycle of strain accumulation and release. The emphasis is necessarily on movements close to the main strands of the San Andreas fault system, where observations are most numerous, although some networks extend as far as 100 km from the major faults. The

measurements include triangulation, repeated observations of the angular separation of permanent survey markers, for which useful data date back to about 1850, when gold was first discovered in California; trilateration, repeated line-length measurements made by laser ranging since about 1970; and local measurements of aseismic fault slip made periodically or recorded continuously over apertures of about 10 to 100 m since about 1960.

OBSERVATIONS OF CRUSTAL DEFORMATION

The focus here is on the spatial and temporal patterns of interearthquake horizontal crustal movements in California that owe their origins to relative motion between the Pacific and North American plates, movements that supply the strain energy which is stored in crustal rocks and ultimately released in large shallow-focus earthquakes. Observations of purely coseismic crustal deformation are not explicitly considered in this chapter; such movements are now well-understood consequences of slip on approximately the upper 10 to 15 km of vertical strike-slip faults. These models and their predicted deformation patterns are discussed within the context of the entire earthquake deformation cycle in the next section. Readers interested in the coseismic movements observed for specific San Andreas earthquakes are referred to the reports by Lawson (1908) and Thatcher (1975) (1906 San Francisco earthquake), Zhang and others (1988) (1940 El Centro earthquake), and Segall and Harris (1987) (1966 Parkfield earthquake).

Vertical crustal movements can locally be substantial, at least when averaged over recent geologic time (see Yeats, 1977; Lajoie, 1986). Deformation from reverse-faulting earthquakes has also been well documented in several events (for example, 1952 Kern County earthquake by Stein and Thatcher, 1981; 1971 San Fernando earthquake by Castle and others, 1975; 1983 Coalinga earthquake by Stein, 1983). Nonetheless, vertical movements are second-order features along most of the San Andreas fault system, and so they are not considered further in this chapter.

Furthermore, in this chapter there is no review of measurement techniques, methods of analyzing and reducing data, or the mathematical and computational tools used in modeling deformation processes. Interested readers are referred to the reports by Bomford (1980) and Savage and Prescott (1973) for descriptions of horizontal-deformation-surveying methods and their precision, to those by Prescott (1976, 1981), Thatcher (1979), and Segall and Harris (1987) for discussions of data-analysis methods, and to the references cited below in the section entitled "Mechanics of Deformation" for details of the mathematical techniques used in model formulation.

Contemporary crustal movements in California are concentrated within a plate-boundary deformation zone that is typically 50 to 200 km wide, centered approximately on the San Andreas fault. Observations of coseismic, postseismic, and interseismic movements define the earthquake deformation cycle and constrain models of strain accumulation and release for strike-slip plate boundaries.

7. PRESENT-DAY CRUSTAL MOVEMENTS AND THE MECHANICS OF CYCLIC DEFORMATION

By WAYNE THATCHER

CONTENTS

	Page
Introduction-----	189
Observations of crustal deformation-----	190
Shear strain on the San Andreas fault system-----	191
Aseismic slip, integrated displacement rates, and Pacific-North American plate motion-----	191
Detailed displacement-rate patterns-----	193
Mechanics of deformation-----	195
Thick- and thin-lithosphere models-----	195
Stress-slip-constitutive-law fault models-----	201
Summary-----	202
Future directions for research-----	203
References cited-----	203

INTRODUCTION

Crustal movements measured in California today sample deformation processes that have continued through at least the past 5 Ma of Pliocene, Pleistocene, and Holocene time. During this interval, several hundred kilometers of right-lateral offset has accumulated across the San Andreas fault system, and many thousands of great earthquakes similar to the historical events of 1857 and 1906 have undoubtedly occurred. The observed deformation results from relative right-lateral translation of the Pacific and North American plates far from the main

plate-boundary faults, which are either freely slipping and without major seismic activity, or are in locked frictional contact and slip episodically in repeated great earthquakes. Aseismic fault slip (creep), as occurs across the San Andreas fault in central California (fig. 7.1), causes no crustal deformation beyond a growing offset across the fault, although this offset may be distributed across a zone as broad as a few tens or hundreds of meters. Where the plate-boundary fault is alternately locked aseismically in its upper 10 km or so and abruptly slipping in great earthquakes, deformation extends several tens of kilometers into the plate interiors. Between large events, elastic strains build up in this zone and are episodically released every few hundred years. Subsequent postearthquake recovery processes redistribute the strains aseismically for years to decades after a major shock, and this deformation gradually merges into the steady accumulation of elastic-strain energy that persists until the frictional strength of the fault is again exceeded. This sequence of interearthquake strain accumulation, coseismic strain release, and postseismic readjustment is thus a recurring process, here referred to inclusively as the earthquake deformation cycle.

Several fault-zone features result in measurable deformation spread over an extremely broad plate-boundary zone. This deformation occurs where the San Andreas fault system comprises several subparallel splays, as in both the San Francisco Bay region and southern California. There, both aseismic slip and major strike-slip

◀ FIGURE 7.1.—A wall and sidewalk in Hollister, Calif., are bent and offset by creep on the Calaveras fault. A slip rate of 5 to 6 mm/yr characterizes much of the Calaveras fault. View eastward along north side of Sixth Street. Photograph by R.E. Wallace, U.S. Geological Survey.

Horizontal interearthquake deformation is summarized below in rates of both displacement and shear strain. For both of these parameters, the components parallel to major active faults are the most significant and best illustrate the dominant pattern of present-day tectonic movements, and so in this chapter these components are commonly shown exclusively. For example, although three independent tensor components are needed to completely characterize the horizontal-deformation field, in California the only significantly nonzero strain-rate component is commonly the shear strain parallel to the local trend of faults in the San Andreas system. Here, I consider only the component of maximum horizontal shear-strain rate, which, within observational uncertainty, almost invariably parallels the San Andreas fault or one of its major strands.

SHEAR STRAIN ON THE SAN ANDREAS FAULT SYSTEM

Rates of contemporary shear strain are displayed in several complementary ways in figures 7.2 through 7.4; details of each rate determination are summarized in table 7.1. Although only the magnitude of the maximum shear-strain rate is shown in each figure, the orientation of the maximum-horizontal-contraction axis is listed in table 7.1. Note that for each of the strain rates shown in figures 7.2 through 7.4, aseismic fault slip contributes only negligibly, if at all, to the measured deformation. Further details on each strain field determination can be found in the references cited in table 7.1.

Shear-strain rates peak at 0.4 to 0.6 $\mu\text{rad/yr}$ (fig. 7.2) across the currently locked northern and southern sections of the San Andreas fault. Significant but slightly lower strain rates of 0.3 to 0.4 $\mu\text{rad/yr}$ are observed across right-lateral strike-slip faults in the northern California Coast Ranges (north of lat 38° N.) east of the San Andreas fault, as well as across the San Jacinto fault in southern California. Shear-strain rates resolvable greater than zero are observed as far as about 80 km from the San Andreas fault itself.

In addition, significant deformation is occurring across active faults in east-central California. In the White Mountains, along the southern California-Nevada State line, small but resolvable strain rates ($0.06 \pm 0.02 \mu\text{rad/yr}$) have been measured, and the orientation of the strain field indicates crustal extension perpendicular to north-south-striking normal faults in the area. Somewhat higher deformation rates are observed farther south, where right-lateral strain is occurring parallel to the Owens Valley fault, site of the $M \approx 8$ earthquake of 1872 (see chap. 6).

Shear-strain rate is plotted as a function of perpendicular distance from the San Andreas fault in figure 7.3. Deformation rates peak at the fault and decrease to half

their maximums at a distance of about 30 km from the fault. Most of the deformation is encompassed within a zone about 100 km wide centered on the fault ("San Andreas boundary deformation zone"), as discussed below. However, the reader may confirm that this total lies in the range of about 30–40 mm/yr by drawing a smooth curve through the data plotted in figure 7.3 and integrating this curve (that is, measuring and summing the total area underneath the curve) from -60 to $+60$ km.

Maximum shear-strain rates at the San Andreas fault tend to be higher across the 1906 earthquake rupture in northern California (approx 0.6 $\mu\text{rad/yr}$) than in southern California (0.4 $\mu\text{rad/yr}$), although the Carrizo Plain data violate this generalization. Rather high deformation rates are also observed 20 to 60 km east of the San Andreas fault in the northern California Coast Ranges.

Shear-strain rates at various locations on the two currently locked sections of the San Andreas fault are plotted versus time since the most recent great earthquake at each locality in figure 7.4. Most of these data are derived from triangulation measurements, many of which were first made in the late 19th or early 20th century. Thus, these determinations are much less precise than those listed in table 7.1 and plotted in figures 7.2 and 7.3, most of which are from the post-1970 period. Nonetheless, it is clear from figure 7.4 that deformation rates on the fault are much higher in the years to tens of years immediately after a great earthquake than they are later. Although it may be questionable to lump values from northern and southern California together on a single plot, the temporal decline in shear-strain rate shown in figure 7.4 depends only on about the first 70 years of data plotted, all of which come from the 1906 rupture on the northern section of the San Andreas fault.

ASEISMIC SLIP, INTEGRATED DISPLACEMENT RATES, AND PACIFIC-NORTH AMERICAN PLATE MOTION

Rates of surface aseismic slip (fault creep) at representative points on the San Andreas fault system are listed in table 7.2 and plotted in figure 7.5. All fault segments displaying measurable aseismic slip are represented, but the detailed distribution along each segment is not shown; interested readers are referred to the references cited in table 7.2 for more details. Figure 7.5 also displays the rates of relative right-lateral displacement integrated across geodetic networks of 50- to 140-km aperture that span the San Andreas and related faults in seven areas of California, for several of which the detailed displacement-rate pattern is shown in figures 7.6 and 7.7.

With the notable exception of the central, creeping section of the San Andreas fault, aseismic slip at the surface represents only a very small proportion of the

total right-lateral displacement across the San Andreas fault system. On the 160-km-long central section of the San Andreas fault, maximum fault-creep rates average 30 mm/yr, close to the geodetically derived displacement rate of 33 ± 1 mm/yr obtained over a 60-km aperture that spans the fault and the California Coast Ranges to the southwest. These data are the strongest evidence that no significant strain is accumulating in the crustal blocks

adjacent to the fault in this region, and so all the relative plate motion taken up by the San Andreas system is here being accommodated by rigid-block translation across the fault. Just north of this segment, on the southern section of the Calaveras fault, a significant amount of right-lateral slip at a rate of about 13 mm/yr, occurs as fault creep. Elsewhere in California, however, measured aseismic-slip rates range from 2 to 6 mm/yr, and creep

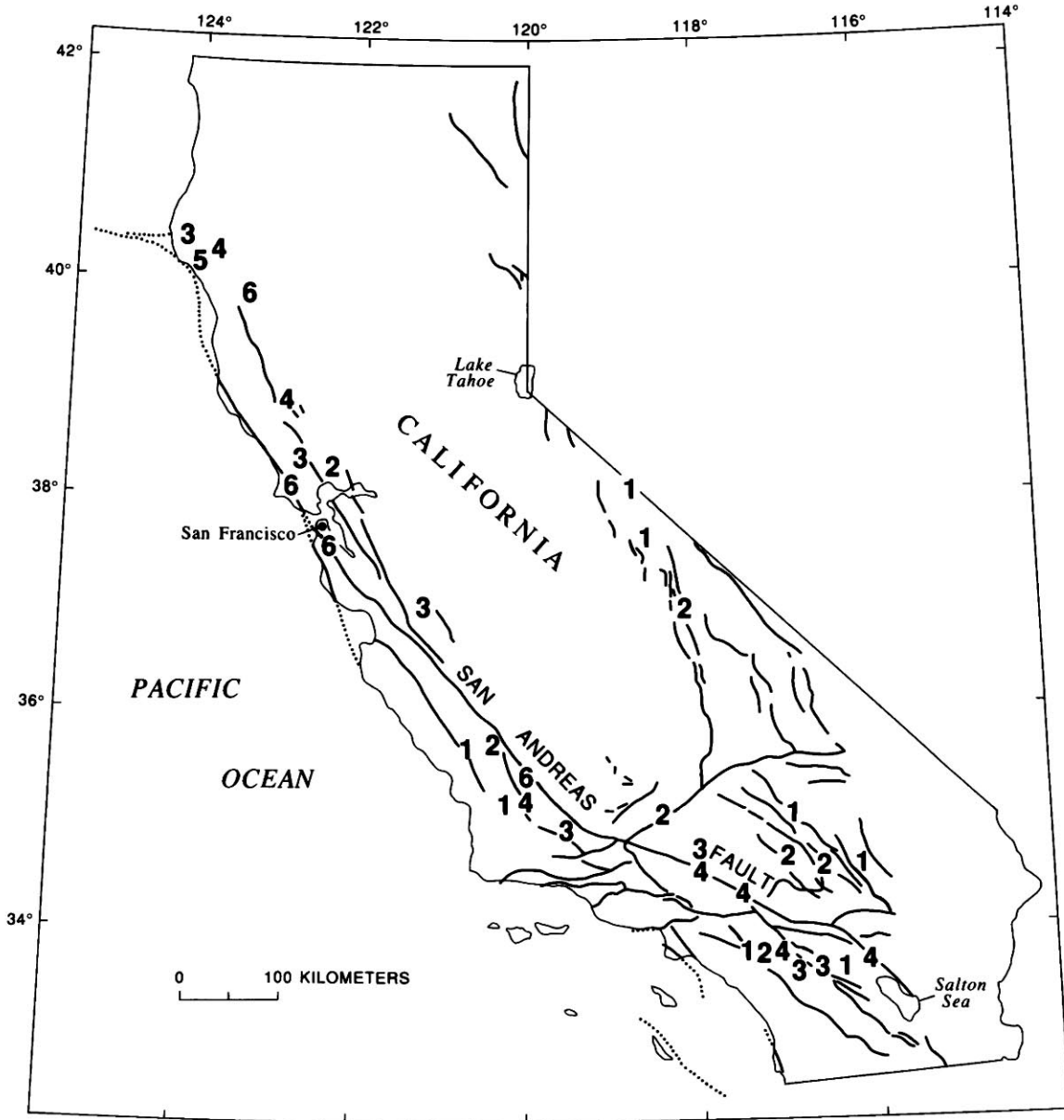


FIGURE 7.2.—Shear-strain rates (in 10^{-7} rad/yr) and major active Quaternary faults of California; faults dotted where concealed. See table 7.1 for details.

commonly occurs only on restricted segments of otherwise-locked faults (for example, the Garlock and San Jacinto faults).

The integrated right-lateral displacement rates shown in figure 7.5 firmly constrain the proportion of Pacific-North American relative plate motion accommodated across the San Andreas fault system in California. In northern, central, and southern California, maximum rates range from 33 to 37 mm/yr. Global reconstructions of the motions of the major tectonic plates over the past 3 Ma, as well as analyses of magnetic-anomaly lineations at the mouth of the Gulf of California, point to a relative Pacific-North American plate-motion rate of 49 ± 3 mm/yr (DeMets and others, 1987). The San Andreas fault system thus accounts for 70 to 80 percent of the relative plate motion, although the San Andreas fault itself does not everywhere take up all of this motion, and deformation is typically distributed across a boundary zone about 100 km wide.

Precisely how much additional relative plate motion is accommodated across other faults in California is uncertain, although the amount is probably very little. According to Minster and Jordan (1987), very long baseline interferometric (VLBI) surveying results indicate that oblique extension of the Basin and Range province, directly east of California, is occurring at a rate of 10 ± 2 mm/yr with an orientation of $N. 56^\circ \pm 10^\circ W$. Depending

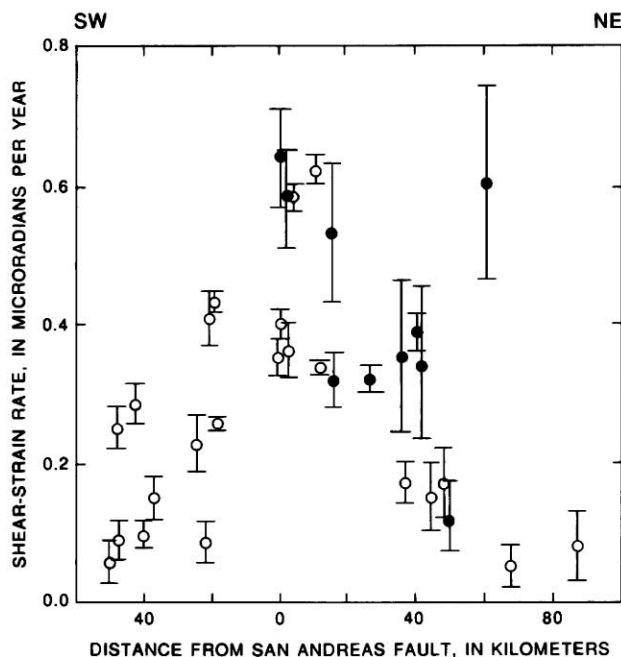


FIGURE 7.3.—Shear-strain rate versus perpendicular distance from the San Andreas fault. Dot, determination from northern California; circle, determination from southern California. $1-\sigma$ error bars shown for reference.

on the exact rate and orientation of this extension, as well as on the precise direction of relative Pacific-North American plate motion, the residual “missing” plate motion being accommodated in California on faults other than those of the San Andreas system ranges from negligibly small to possibly as much as 10 mm/yr. Thus, although the geodetic coverage in California is far from complete (see figs. 7.2, 7.5), all or most of the zone of significant plate-boundary deformation apparently has been encompassed.

DETAILED DISPLACEMENT-RATE PATTERNS

Considerable detail on the distribution of deformation in the San Andreas boundary zone is provided by the rather complete geodetic coverage available in the San Francisco Bay region and southern California. In the method used to reduce these data, geodetic-line-length changes are used to determine station-displacement rates relative to a point at the center of gravity of the network. Fault-normal displacements are permitted by this method, but their values are minimized in the inversion

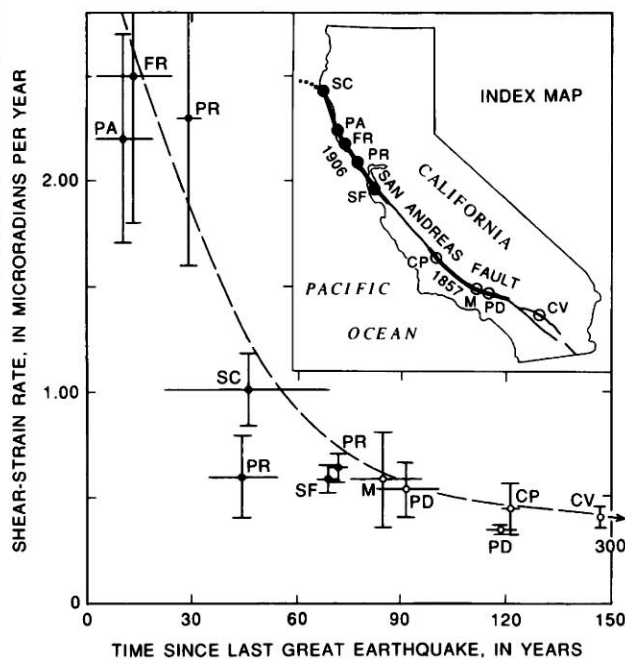


FIGURE 7.4.—Shear-strain rate versus time since last great earthquake (years 1906 and 1857 in inset; heavy line indicates extent of fault rupture) on the San Andreas fault. CP, Carrizo Plain; CV, Coachella Valley; FR, Fort Ross; M, Mojave; PA, Point Arena; PD, Palmdale; PR, Point Reyes; SC, Shelter Cove; SF, San Francisco. Locations of data points are keyed to index map. For each data point, vertical bar is 1σ , and horizontal line indicates time interval between surveys. Data points are plotted at middle of intervals. Dots, determinations from northern California; circles, determinations from southern California; dashed curve, approximate fit to data (Thatcher, 1983).

TABLE 7.1.—*Shear-strain rates in California*

[Maximum compression measured from north, with clockwise direction positive]

Area	Location		Rate (ppm/yr)	Maximum compression direction* (°)	Interval	Reference
	Lat N.	Long W.				
Mendocino	40.1°	124.0°	0.53±0.10	3±4	1981-84	Breen and others (1987).
	40.1°	123.7°	.35±0.11	11±6	--	
	40.2°	124.1°	.34±0.11	21±9	--	
Round Valley	39.9°	123.3°	.60±0.14	-11±5	1942-64	Prescott (1985).
Point Reyes	38.1°	122.8°	.64±0.07	2±2	1972-82	Prescott and Yu (1986).
Santa Rosa (Rodgers Creek fault).	38.4°	122.8°	.32±0.02	12±2	--	--
The Geysers (Maacama fault).	38.8°	122.9°	.39±0.03	11±3	--	--
Napa (West Napa fault)	38.8°	122.3°	.17±0.05	20±9	--	--
San Francisco peninsula	38.5°	122.4°	.58±0.07	-2±9	1970-80	Prescott and others (1981).
White Mountains	37.9°	118.6°	.06±0.02	-13±12	1972-79	Savage and Lisowski (1984).
	37.5°	118.5°	.06±0.02	-8±14	--	--
Owens Valley	36.9°	118.1°	.16±0.06	23±12	1974-79	Savage and Lisowski (1980).
Hollister (E. of Calaveras fault).	36.9°	121.3°	.32±0.04	-16±3	1971-78	Savage and others (1979).
San Luis network:						
Central	35.5°	120.4°	.23±0.04	-23±3	1977-83	N.E. King (unpub. data, 1988).
West	35.4°	120.7°	.09±0.03	-18±10	--	--
Carrizo network:						
A	35.4°	119.8°	.62±0.02	--	1977-83	N.E. King (unpub. data, 1983).
B	35.3°	119.8°	.58±0.02	--	--	--
C	35.1°	119.9°	.43±0.02	--	--	--
D	35.1°	120.2°	.10±0.02	--	--	--
Tehachapi network:						
Garlock fault	34.9°	118.5°	.17±.03	4±3	1973-83	King and Savage (1984).
San Andreas fault	34.6°	118.0°	.34±.01	-17±1	--	--
Cajon network	34.3°	117.5°	.36±.04	-16±2	1974-84	Savage and others (1986).
Los Padres network	34.8°	119.5°	.26±.01	-1±1	--	--
Barstow	35.0°	116.9°	.08±.05	24±17	1979-84	King (1985).
Palmdale	34.4°	118.2°	.35±.03	-19±4	1971-80	Savage and others (1981).
Mojave network:						
W1	34.6°	117.0°	.17±.05	4±11	1934-82	Sauber and others (1986).
W3	34.4°	116.6°	.15±.05	5±8	--	--
Eastern	34.5°	116.1°	.05±.03	--	--	--
Anza network:						
A	33.8°	117.4°	.06±.03	--	1973-81	King and Savage (1983).
B	33.8°	117.1°	.15±.03	30±13	--	--
C	33.8°	117.0°	.41±.04	21±5	--	--
D	33.5°	116.8°	.25±.03	30±8	--	--
E	33.5°	116.7°	.29±.03	1±5	--	--
F	33.6°	116.4°	.09±.03	--	--	--
G	33.7°	116.1°	.40±.02	8±2	--	--

process (see Prescott, 1981). Gross departures from this constraint would be revealed by notable disagreements between observed and predicted line-length changes, but no such discrepancies were found for the results presented here. Because the fault-normal displacement rates are small and show no consistent trends, they are not plotted on the profiles presented here.

Displacement rates in the San Francisco Bay region are plotted in figure 7.6. The distribution of deformation varies considerably across the San Andreas boundary zone from north to south of the San Francisco Bay. In the north bay, the integrated right-lateral-displacement rate across the network of 27 ± 3 mm/yr (fig. 7.6B) indicates

that not all of the boundary zone has been captured within its 110-km aperture. Within about 5 km of the San Andreas fault, rapid change in the gradient of deformation rate indicates that interearthquake strain is concentrated close to the fault. Outside this near-fault region, deformation southwest of the fault appears to be negligible. Northeast of the fault, however, the persistence of significant movements right to the edge of the profile suggests that the 5- to 10-mm/yr deficit in boundary-zone deformation across this profile is being accommodated to the east of the Green Valley fault. Across the central and south bay (fig. 7.6C), movements are more evenly distributed through the network, and the integrated

TABLE 7.2.—Representative aseismic-slip rates on faults of the San Andreas system

Fault	Site	Lat N.	Long W.	Rate (mm/yr)	Reference
Hayward.....	Hayward network.....	37.6°	122.1°	6	Prescott and Lisowski (1983).
Northern section of the Calaveras.	Camp Parks.....	37.7°	121.9°	3	Do.
Southern section of the Calaveras.	San Felipe.....	37.0°	121.5°	13	Lisowski and Prescott (1981).
San Andreas.....	Cienega Winery.....	36.7°	121.5°	13	Schulz and others (1982).
Do.....	Eade Ranch.....	36.4°	121.0°	30	Buford and Harsh (1980).
Do.....	Parkfield (Durham Ranch).....	35.9°	120.4°	13	Do.
Garlock.....	Cameron.....	35.1°	118.3°	4	Louie and others (1985).
San Andreas.....	Indio Hills.....	33.7°	116.2°	2	Do.
San Jacinto (Coyote Creek strand).	Bailey's Well.....	33.0°	116.0°	5	Do.
Imperial.....	Interstate Highway 80.....	32.8°	115.5°	5	Do.

displacement rate of 37 ± 3 mm/yr across the south bay suggests that the entire boundary zone has been spanned. Closer examination of the profile, however, reveals several zones of locally high deformation gradient, one across the San Andreas fault, where it resembles that observed near the fault in the north bay. In addition, rapid changes in the profile across the Hayward and Calaveras faults reflect aseismic slip at rates of 3 to 6 mm/yr on these faults (see fig. 7.5).

In southern California (fig. 7.7), deformation across the San Andreas boundary zone notably broadens from the Salton Sea, in the south, northwestward to the Big Bend region of the San Andreas fault north of Los Angeles (see fig. 7.5). At the south end of the Salton Sea, all of the boundary-zone deformation, 35 ± 1 mm/yr, occurs within an area about 50 km wide (profile S, fig. 7.7C) that rapidly broadens to more than 100 km wide north and west of the Salton Sea (profile N, fig. 7.7C) and, possibly, broader still by about 50 km farther northwest (fig. 7.7B). North and west of Los Angeles, networks of 100-km aperture capture only 18 ± 2 mm/yr of the total right-lateral-displacement rate (fig. 7.5). The profiles in figures 7.7B and 7.7C also show that in contrast with the northern section of the San Andreas fault, deformation gradients across the fault are smoother, and deformation is not so closely concentrated near the fault.

MECHANICS OF DEFORMATION

The observations described in the previous section point to a range of mechanical behavior for the faults comprised by the San Andreas system, from freely sliding with only minor accompanying seismicity, to completely locked from the surface to seismogenic depths except for abrupt slip during infrequent great earthquakes.

On the 160-km-long central section of the San Andreas fault, virtually all fault slip occurs aseismically. Slip rates measured at or near the fault are close to the average rate for the entire San Andreas boundary zone (fig. 7.5), no strain is detectable in the crustal blocks adjacent to the fault, and historical earthquakes of $M \geq 5\frac{1}{2}$ have not occurred. Abundant minor seismicity (see fig. 4.10) contributes only negligibly to the slip budget, and except for a few small patches of fault surface that are in frictional contact between these small earthquakes, the first-order steady-state model for this segment involves rigid translation of adjacent fault blocks across the freely sliding plane of the San Andreas.

A transitional behavior applies to those fault segments where steady-state fault creep is observed at the surface but historical or prehistoric earthquakes of $M \geq 6$ have been documented. Examples include the Parkfield and Coachella Valley segments of the San Andreas fault, the Hayward fault, and the Imperial fault. On these segments, during the interseismic phase of the earthquake cycle, the fault is inferred to be freely slipping in its upper few kilometers, in locked frictional contact at seismogenic depths (approx 3–10 km), and once again freely slipping at greater depths (fig. 7.8A). The result of this slip distribution is interseismic creep at the surface fault trace and elastic-strain accumulation in the adjacent blocks (figs. 7.8B, 7.8C).

THICK- AND THIN-LITHOSPHERE MODELS

The most extreme features of locked fault behavior are currently observed on the two San Andreas fault segments where great earthquakes have occurred in historical time, in 1857 and 1906 (see fig. 5.11 for locations and coseismic-slip distributions). On these segments, no aseismic slip is observed at the Earth's surface, the two faces of the fault are in locked frictional contact to depths

of 10 to 15 km, and interearthquake slip is either extremely small or absent. At greater depths, the mechanics of fault movement is uncertain, but two models bound the range of expected behavior (fig. 7.9). In the first, the thick-lithosphere model, the depth D of coseismic faulting is much less than the thickness H of elastically strong lithosphere. Interearthquake deforma-

tion then predominantly results from episodic or steady aseismic slip on the downward extension of the seismogenic fault zone, and any effects of the underlying weak asthenosphere can be safely neglected. In the second, the thin-lithosphere model (fig. 7.9), coseismic faulting depth is comparable to elastic-plate thickness. In this model, transient postseismic and steady interseismic flow in the

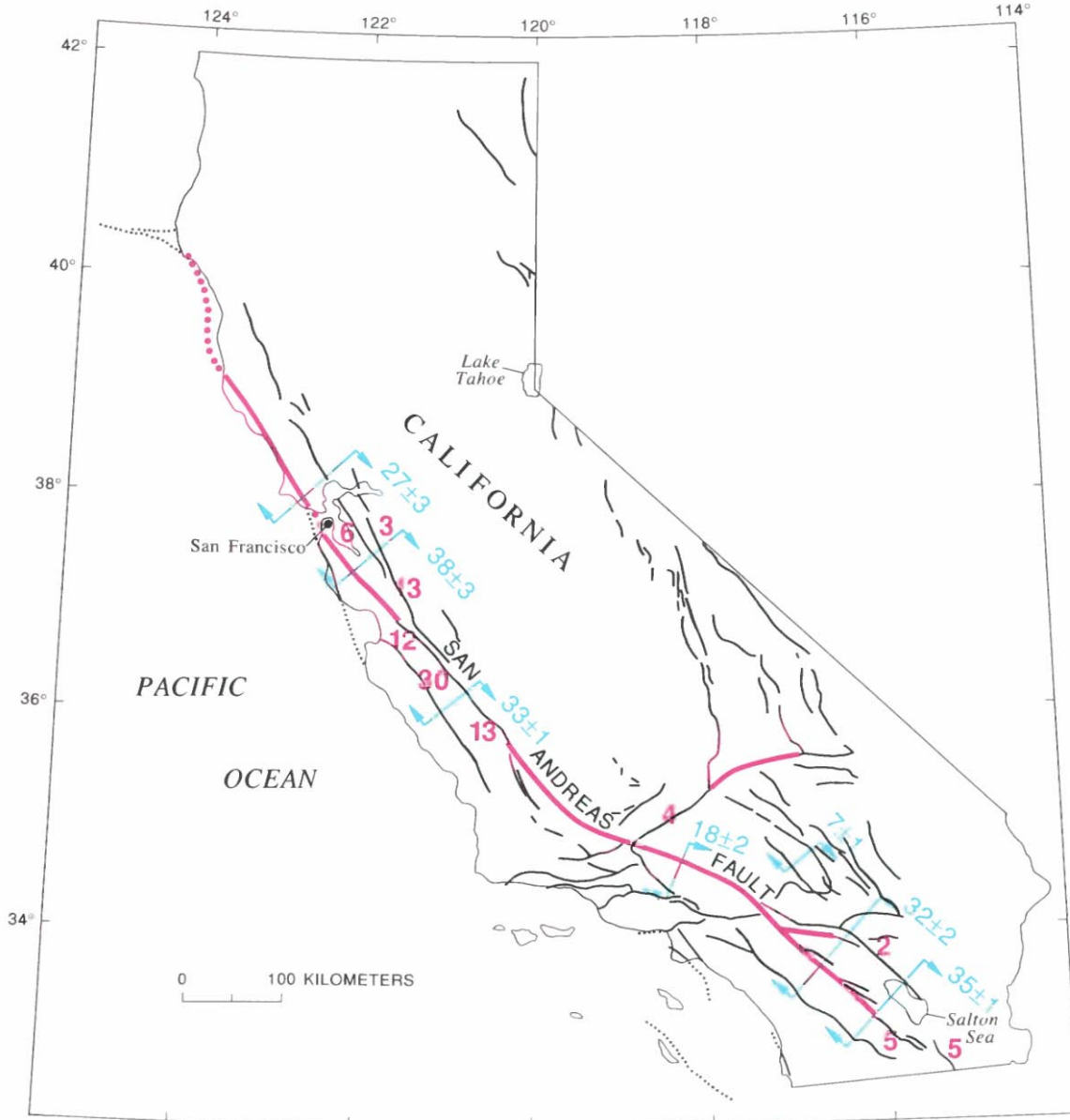


FIGURE 7.5.—Sketch map of California, showing rates (red numbers) of aseismic slip (fault creep) and relative right-lateral-displacement rates (blue numbers) near arrows, which indicate direction of relative movement along major active

strands of the San Andreas fault system. Values in millimeters per year. Locked (no surface slip) segment of major fault, red line; other Quaternary fault, black line; faults dotted where concealed. See table 7.2 for details.

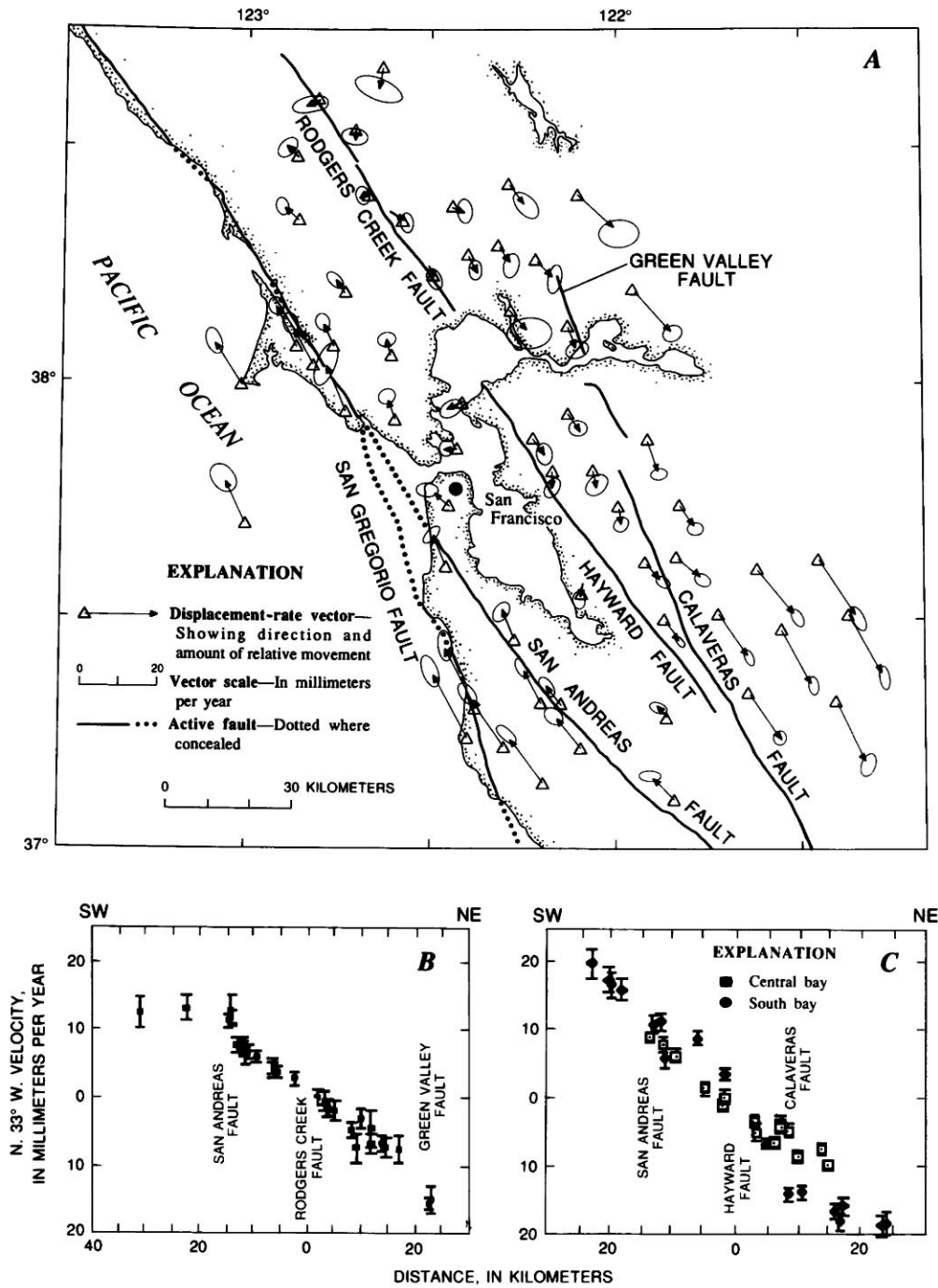


FIGURE 7.6. — Displacement rates across the San Francisco Bay region. A, Relative right-lateral displacement rates determined from repeated geodetic surveys made during 1971–87. Error ellipses show 95-percent-confidence limits for each determination (Prescott and others, 1987). B, Relative station velocities parallel to approximate trend of the San Andreas fault (N. 33° W.) plotted against distance perpendicular to this trend for north bay. 1- σ bars are indicated. Perpendicular velocity component is negligible and omitted here. C, Same as figure 7.6B for central and south bay.

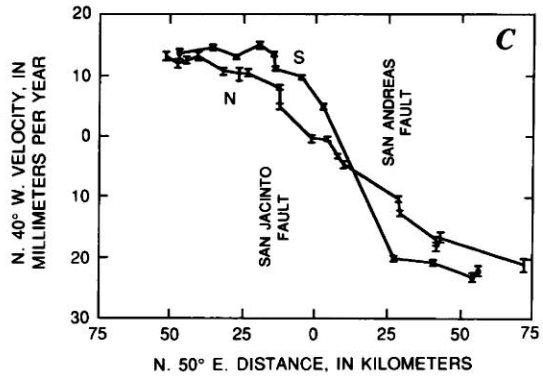
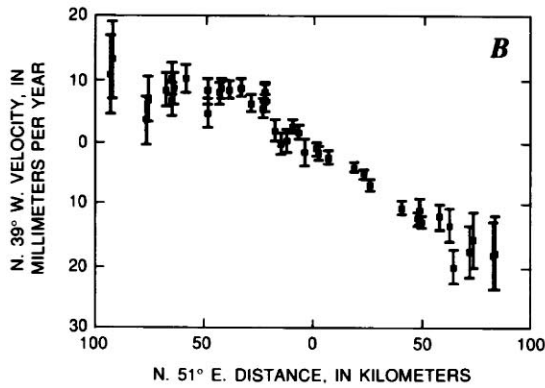
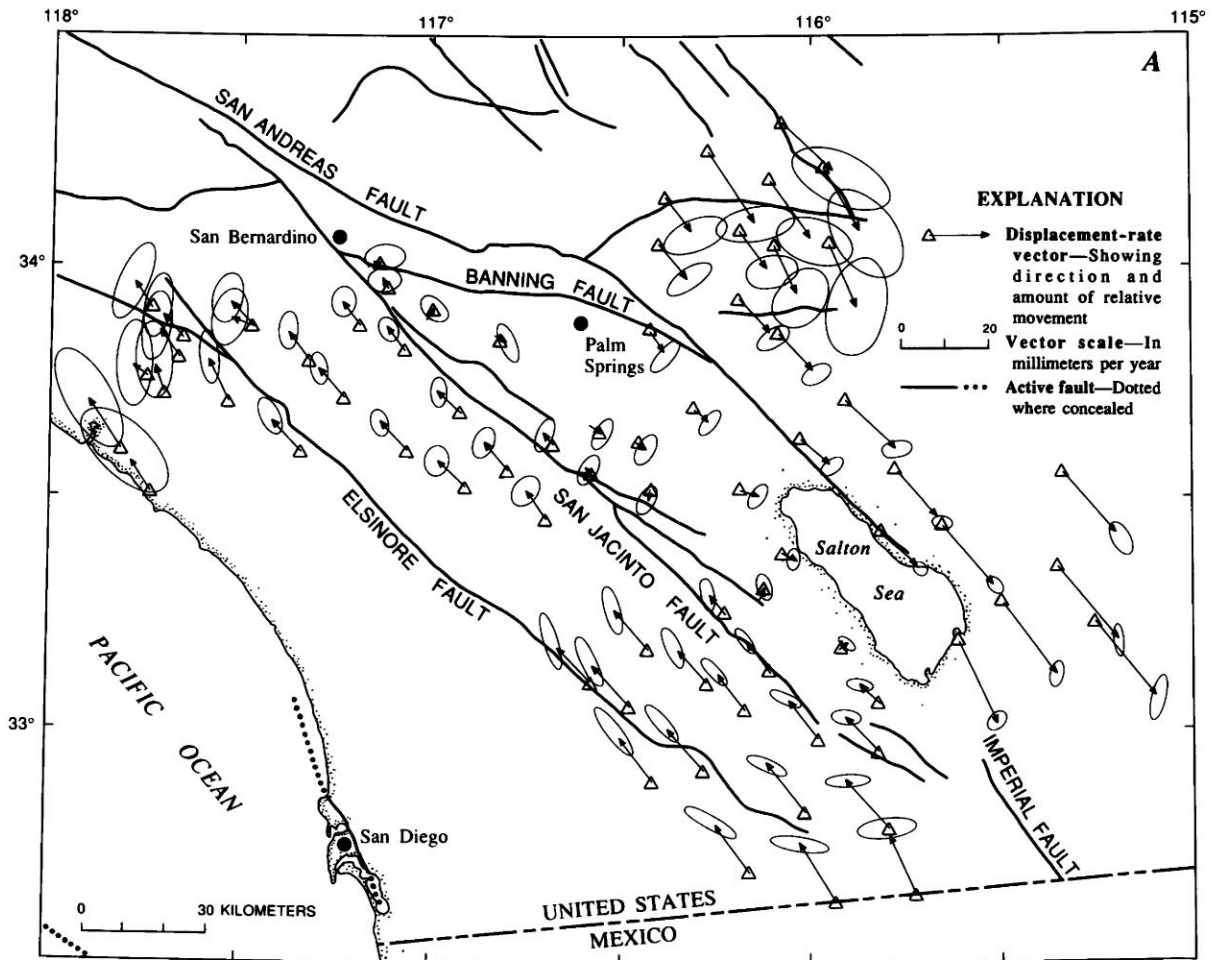


FIGURE 7.7.—Displacement rates in southern California. A, Relative right-lateral displacement rates determined from repeated geodetic-survey measurements during 1973–87. Error ellipses show 95-percent-confidence limits for each determination (Prescott and others, 1987). B, Relative station velocities parallel to approximate trend of the San Andreas fault (N. 39° W.) plotted

against distance perpendicular to this trend, for stations in northern part of map in figure 7.7A. 1- σ error bars are indicated. Perpendicular velocity component is negligible and is not plotted here. C, Same as figure 7.7B for stations largely to north (N) and south (S) of the Salton Sea.

asthenosphere provide the dominant mechanism for interearthquake strain accumulation.

Note that in the context of these two models, the terms "lithosphere" and "asthenosphere" are linked to mechanical properties of the Earth's crust and upper mantle: The lithosphere is the strong elastic layer near the Earth's surface, and the asthenosphere is the region of ductile flow that lies beneath. Their boundary may thus lie well above the thermal boundary layer that separates the moving plates from the convecting mantle. If so, then at least the upper part of the "asthenosphere" forms part of the tectonic plate and moves with it.

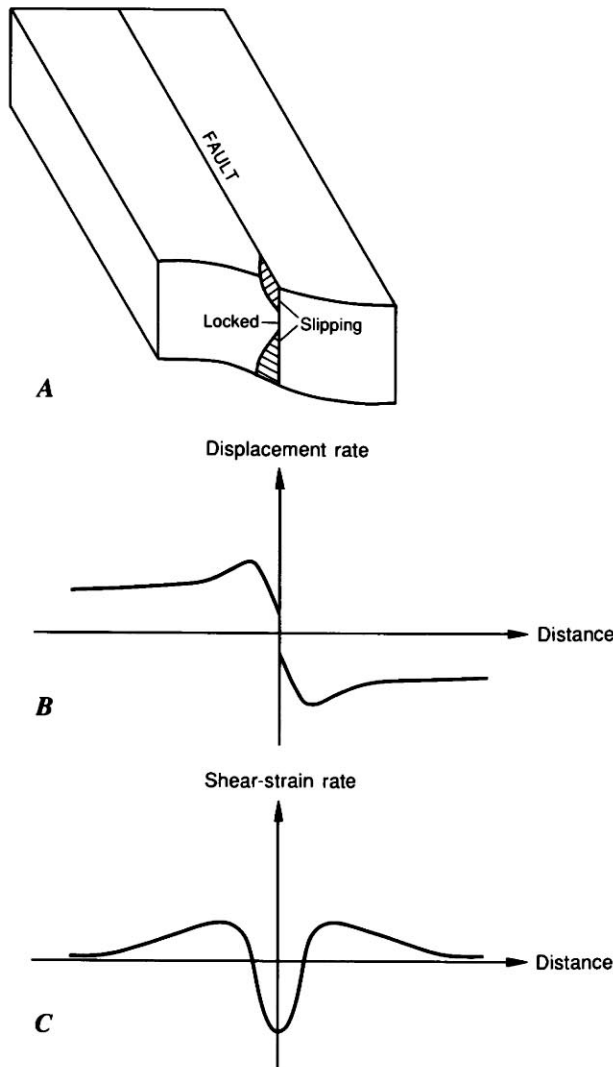


FIGURE 7.8.—Elastic-half-space model showing fault creep at surface, locked (nonslipping) fault at depth, and freely sliding zone at great depth (A). Displacement rate (B) and strain rate (C) are plotted against distance from fault.

Thus considered, the boundary between "lithosphere" and "asthenosphere" defines the zone of decoupling between surface tectonic processes and those that occur in the ductile region beneath. The location of this boundary is thus of central importance to the broad-scale tectonics of the San Andreas fault, the nature of the earthquake-generation process and its thermomechanical implications (see chap. 9), and the relation between shallow structural features and those inferred at depth (see chap. 8). I explore below the influence of this boundary location on cyclic earthquake-related deformation at the currently locked transform fault zones in the San Andreas, illustrating the contrasting mechanical behavior of the thick- and thin-lithosphere models.

All of the models considered here are two dimensional, and so neither slip nor mechanical properties vary along fault strike. Each model consists of only a single planar, vertical strike-slip fault. However, because the medium properties are linear elastic and (or) viscoelastic, the effects of multistranded fault zones can be obtained by simply superposing the deformation due to slip on individual fault segments. Furthermore, all of the two-dimensional models discussed here have also been considered in three dimensions, and so complexities arising from changes in fault strike, variations in slip along strike, and the finite extent of faulting can be incorporated straightforwardly as necessary. Similarly, except for the transition from elastic lithosphere to viscoelastic asthenosphere, depth variations in material properties are not considered, although, again, solutions have been obtained for faulting in plane-layered elastic

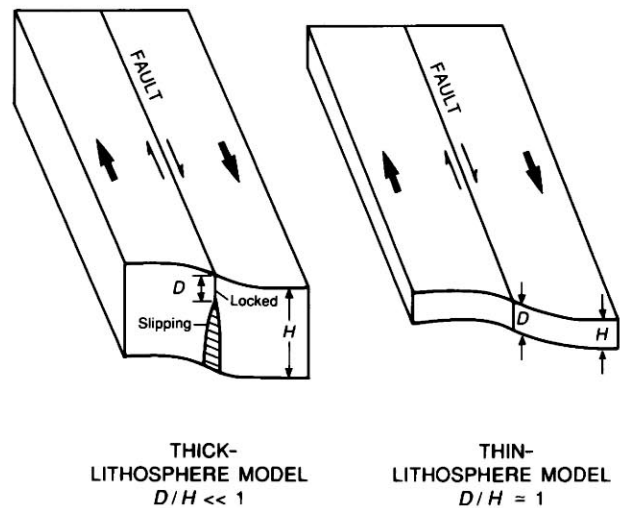


FIGURE 7.9.—Thick- and thin-lithosphere models. D , depth of coseismic faulting; H , thickness of elastically strong lithosphere. Small arrows along fault and larger arrows indicate direction of relative movement of fault and tectonic plates, respectively.

and viscoelastic media. Although fault end effects and changes in slip and geometry along fault strike can be locally important, these effects, as well as those due to depth-varying material properties, are generally second order relative to the deformation features described here. More important are the effects of the several subparallel strands that compose much of the San Andreas fault system along its two currently locked sections. In these sections, the interseismic deformation due to each major fault strand contributes significantly to the observed displacement pattern, and as a rule the effects of faults lying off the San Andreas proper cannot be safely ignored in matching models to data across the entire San Andreas boundary zone.

The simplest form of the thick lithosphere model, first proposed by Savage and Burford (1970), is illustrated in figure 7.10. In this idealized model, interearthquake strains accumulate uniformly throughout the deformation cycle and have precisely the same spatial pattern as coseismic strains, except that the sense of movement is reversed. The cycle consists of coseismic slip Δu extending from the surface to depth D and steady interearthquake aseismic slip at a constant rate \dot{u} ($=\Delta u/T$, where T is the earthquake recurrence interval) beginning at $z=D$ and extending to great depth. For this model of interearthquake deformation, simple expressions relate

surface-displacement rates $\dot{u}_x(y)$ and shear-strain rates $\dot{\epsilon}_{xy}(y)$ to the fault parameters \dot{u} and D and the distance y from the fault trace:

$$\frac{du_x(y)}{dt} = \dot{u}_x(y) = \frac{\dot{u}}{\pi} \tan^{-1} \left(\frac{y}{D} \right)$$

$$\text{and} \quad \dot{\epsilon}_{xy}(y) = \frac{d}{dy} [\dot{u}_x(y)] = \frac{\dot{u}}{\pi D} \left[\frac{1}{1 + \left(\frac{y}{D} \right)^2} \right]$$

A principal utility of this model is the ease with which approximate values of displacement and strain rate can be computed, commonly as a preliminary step to more detailed computations that employ complex models which nonetheless show many of the same general features. For example, using typical San Andreas values of $\Delta u=4$ m, $T=200$ yr, and $D=15$ km, then $\dot{u}=20$ mm/yr, and the engineering shear-strain rate (twice the tensor strain rate $\dot{\epsilon}_{xy}$) at the fault trace ($y=0$) is about $0.8 \mu\text{rad/yr}$, a value close to some of the peak strain rates plotted in figures 7.2 and 7.3. Furthermore, the bell-shaped distribution of secular strain across the model fault (middle right, fig. 7.10) generally accords with observations (fig. 7.3), and the width of the profile is a direct measure of the fault-locking depth D . (Note, however, that the observations summarized in figure 7.3 include strain rates determined from multistranded segments of the San Andreas fault system, and so they are not directly comparable to the model calculations for a single fault strand illustrated in fig. 7.10.) Recalling the observations discussed in the section above entitled "Observations of Crustal Deformation," the wider zone of secular strain across the southern section of the San Andreas can be rationalized if the depth of seismic slip and, thus, the locking depth of the fault are simply greater in southern than in northern California. As it stands, this model has no transient effects and so is too simple to explain the postearthquake strain changes plotted in figure 7.4. However, introducing a rather straightforward modification remedies this defect while accounting for the observed difference in strain-rate profiles between northern and southern California. Surprisingly, these same features are, for different reasons, natural consequences of the thin-lithosphere model.

The two models are illustrated in figure 7.11. In the thick-lithosphere model, postseismic effects are introduced by specifying transient postearthquake slip on a segment of the fault immediately beneath the coseismic rupture. Its time history is constrained by an exponentially decreasing slip rate (time constant α), and its magnitude by the requirement that the cumulative slip sum to the coseismic offset Δu by the end of the cycle. In the thin-lithosphere model, the transient deformation

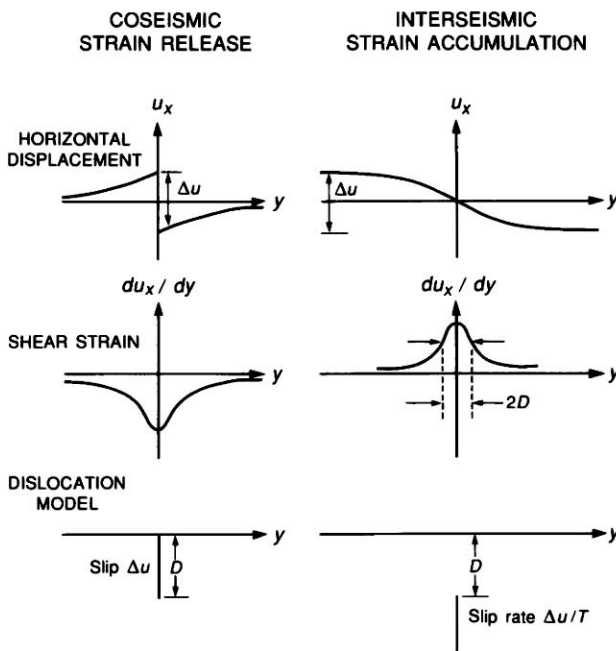


FIGURE 7.10.—Elastic-half-space model for earthquake cycle. Δu , coseismic slip; D , depth of coseismic slip; T , earthquake recurrence interval; u_x , horizontal displacement parallel to fault; du_x/dy , shear-strain component parallel to fault; y , distance from fault.

results from flow in the asthenosphere due to stress relaxation after seismic faulting in the lithosphere. Its time scale is controlled by the asthenosphere-relaxation time $\tau=2\eta/\mu$, when η is the effective viscosity of the asthenosphere and μ is the average shear modulus of lithosphere and asthenosphere, here taken to be equal. In both models, the transient motions are superimposed on a steady component of deformation that is due to relative plate motion.

Detailed computations show that the two models produce surface deformations that with suitable choices of model parameters are observationally indistinguishable (see Thatcher, 1983). Here, the discussion is restricted to qualitative features, as summarized in figure 7.12. Near the fault, shear-strain rates monotonically decrease over time and gradually approach a constant (fig. 7.12B), while the deformation profile broadens and strains diffuse into the interiors of the adjacent plates as the cycle progresses (fig. 7.12A). It is easy to match the observed temporal decline in strain rate with either model; the particular parameter combinations are themselves not unique, and a range of choices can provide equally good agreement. All satisfactory thin-lithosphere models, however, require an elastic plate only 10 to 15 km thick, the maximum depth of coseismic slip in the 1906 earthquake (Thatcher, 1975). Both models predict a broadening of the zone of deformation that depends on the time interval since the latest great earthquake, and so the greater width of the strain-rate profile in southern California can be accounted for. For example, data from the northern, locked section of the San Andreas fault may correspond to times t_1 to t_3 in figure 7.12, whereas those from the southern section may correspond to times t_4 and t_5 .

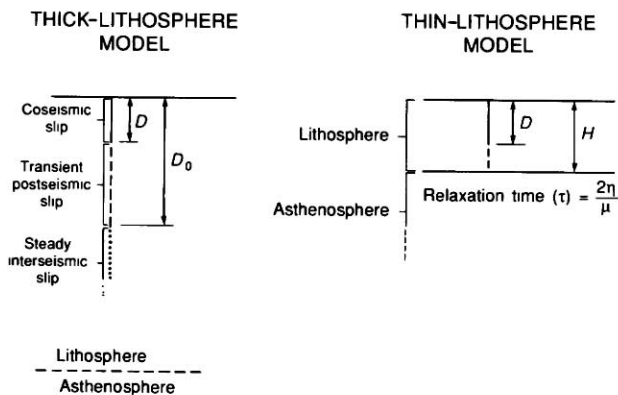


FIGURE 7.11.—Specific features of thick- and thin-lithosphere models. D , depth of coseismic slip; D_0 , depth to bottom of zone of transient postseismic slip; H , thickness of elastically strong lithosphere; η , effective viscosity of asthenosphere; μ , average shear modulus of lithosphere and asthenosphere.

More complex models that combine features of both the thick- and thin-lithosphere models are also consistent with available data (for example, Li and Rice, 1987). Furthermore, coseismic and interearthquake fault slip undoubtedly vary as a function of depth, rather than abruptly terminating at some specified fault depth. Although this gradationality of the slip distribution modifies the detailed patterns of surface strain and displacement from those illustrated in figure 7.10, for example, the same qualitative features are preserved, and it will be difficult to distinguish between differing slip-depth distributions on the basis of surface-deformation measurements alone.

In summary, at transform plate boundaries, available data are consistent with both thick- and thin-lithosphere models but do not strongly constrain either. The most geophysically interesting feature of both models is the predicted postearthquake diffusion-like spread of strain from the plate-bounding fault into the interiors of the adjacent plates. Postearthquake surveys, however, are sufficiently infrequent and areal coverage sufficiently limited that these effects, if they indeed occur, have not been directly observed. Details of the temporal decline in deformation rate near the fault are also absent.

STRESS-SLIP-CONSTITUTIVE-LAW FAULT MODELS

A completely different class of large-scale-faulting models are now being developed to more realistically incorporate the fault-failure process into the earthquake deformation cycle (for example, Stuart, 1979; Tse and Rice, 1986). Instead of specifying slip on the plate-bounding fault, these models extrapolate from laboratory

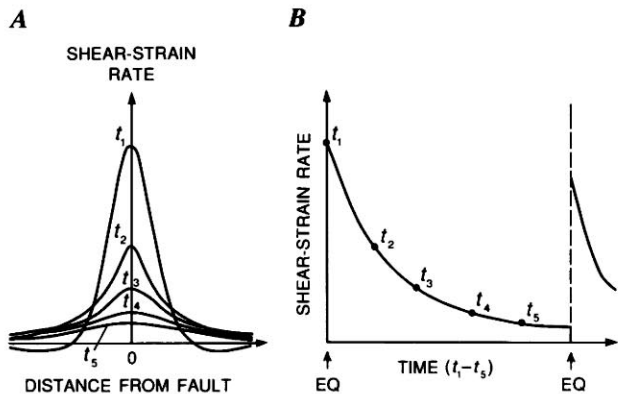


FIGURE 7.12.—Complete earthquake-cycle model predictions for thick- and thin-lithosphere models. A, Shear-strain rate versus distance from fault and its temporal evolution through deformation cycle. B, Shear-strain rate on fault versus time for one complete cycle. EQ, earthquake.

observations of the time-dependent frictional properties of rocks (for example, Dieterich, 1979; Tullis, 1988) to assign slip-stress-constitutive laws to the fault surface. As remotely applied stresses increase, each segment of the fault slips at a rate that depends on both the previous slip history and the current applied stress, and so the cycle of elastic-strain accumulation and release can be simulated. By specifying the depth dependence of fault frictional properties, a slip behavior nearly identical to that of the thick-lithosphere model (fig. 7.11A) follows naturally. A sample calculation of this type (Tse and Rice, 1986) illustrates the method and shows typical results (fig. 7.13). After a large coseismic slip event in approximately the upper 10 km of the model fault, transient postseismic slip occurs on both the coseismic fault plane and its downdip extension. As slip rates decline to near zero on the shallow segments of the fault, interseismic slip at greater depths approaches nearly steady-state values. Finally, near the end of the cycle, the constitutive model predicts an increase in slip rate on the shallow coseismic fault segment before the next large slip instability ("earthquake").

Although the appropriateness of this extrapolation of laboratory results to large-scale faulting is a matter of current debate and the scaling of laboratory parameters to the field is uncertain, Tse and Rice's calculations clearly demonstrate that the principal observed features

of the earthquake deformation cycle on the San Andreas fault can be reproduced by such models. Ongoing laboratory studies should refine and modify the stress-slip-constitutive laws, and geodetic and continuous strain-monitoring observations of preearthquake and postearthquake crustal deformation can test the applicability of these postulates to large-scale faulting processes.

SUMMARY

Contemporary crustal movements in California are concentrated within a plate-boundary-deformation zone that is typically 50 to 200 km wide, approximately centered on the San Andreas fault. Integrated right-lateral displacement rates across this zone range from 33 to 37 mm/yr, representing about 75 percent of the Pacific-North American relative plate motion. Most or all of the rest may be taken up east of the San Andreas fault system in the Basin and Range province. Although aseismic fault slip (creep) is a locally important component of this relative plate motion, most of the geodetically measured deformation represents elastic strain on the crustal blocks adjacent to faults of the San Andreas system. Rates of secular (interseismic) shear strain are a maximum on the two currently locked segments of the San Andreas fault, sites of the great 1857 and 1906

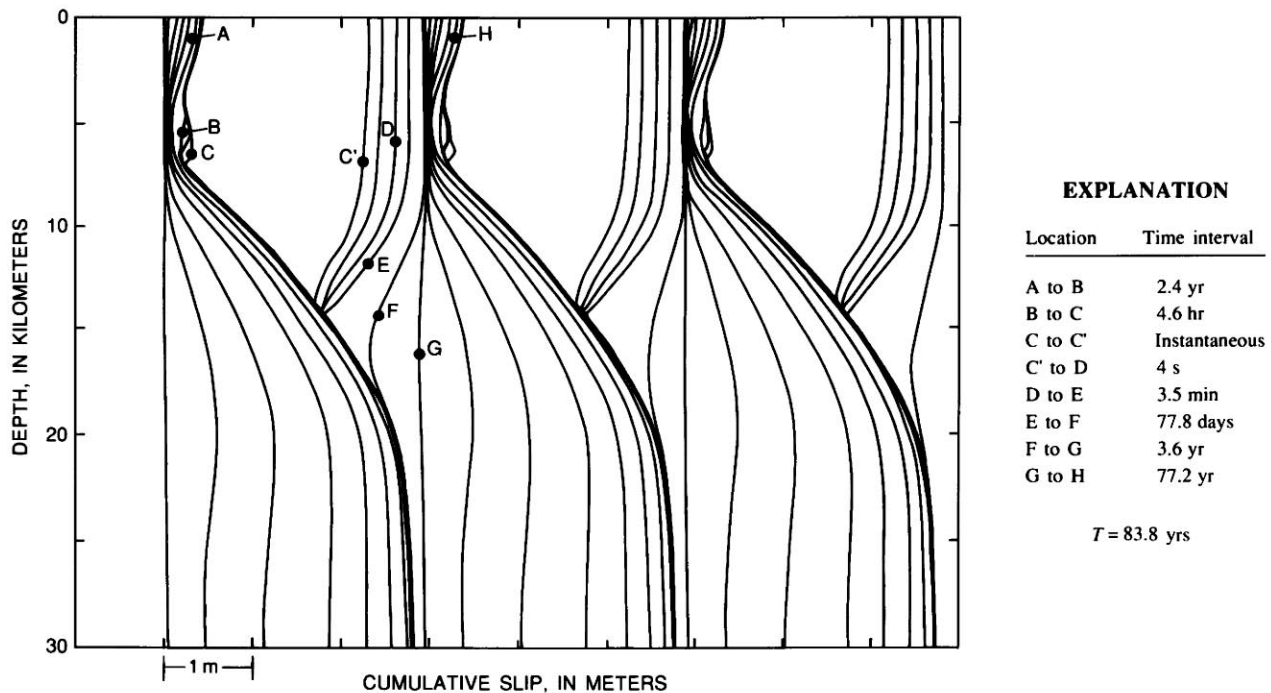


FIGURE 7.13.—Cumulative slip versus depth for selected time intervals through deformation cycle in quasi-static fault-instability model modified from Tse and Rice (1986). T , recurrence interval.

earthquakes. Values range from 0.4 to 0.6 parts per million per year (ppm/yr) at the fault to 0.1 ppm/yr 30 to 80 km from it. Deformation occurring at the times of large strike-slip earthquakes (coseismic strain) is concentrated within a few tens of kilometers of the surface fault rupture, indicating that earthquake fault slip is largely confined to the upper 10 to 15 km of the crust. After major events, postseismic shear strain occurs at transiently high rates (more than 2 ppm/yr) that decay to background interseismic rates over a time scale of years to tens of years.

Observations of coseismic, postseismic, and interseismic movements define the earthquake deformation cycle and constrain models of strain accumulation and release for strike-slip plate boundaries. Observations are fitted equally well by two contrasting models. In the first model, the depth of coseismic faulting is much less than the thickness of the elastically strong lithosphere, and postseismic and interseismic deformation result from transient and steady aseismic slip on the downward extension of the earthquake fault plane. At the other extreme, if earthquake slippage extends through most or all of the elastic lithosphere, interearthquake deformation is due to transient or steady flow in the underlying weak substrate ("asthenosphere").

FUTURE DIRECTIONS FOR RESEARCH

Although the broad outlines of current movement across the San Andreas boundary zone are now known and the main features of the cyclic deformation expected from great strike-slip earthquakes have been delineated, many issues still remain to be explored. Although all of the relative Pacific-North American plate motion occurring across California may have been measured geodetically, this determination is not yet definitive, and as much as 10 mm/yr of motion may be accommodated east or west of the approximately 100-km-wide zone defined by current measurements. Furthermore, the thickness of the elastically strong crust is uncertain by at least a factor of 3, and so major alternative models of the earthquake deformation cycle cannot be distinguished (fig. 7.9). Because surface-deformation observations cannot themselves resolve this ambiguity, other data, possibly gravity-field observations and lithospheric-deflection models (for example, McNutt, 1980), are needed.

Few details exist on the preseismic and postseismic movements related to large plate-boundary earthquakes. Whether detectably anomalous crustal movements precede large earthquakes is uncertain. Theoretical models and fragmentary observations suggest that precursory slip may occur on or beneath the eventual coseismic rupture plane. However, except for the observation that

premonitory deformations must be small relative to coseismic movements (for example, Johnston and others, 1987), precursory slip is otherwise unconstrained. Existing data are sufficient to demonstrate that postseismic movements, at least those from great earthquakes, are large—commonly, 10 to 30 percent of the coseismic deformation (Thatcher, 1984)—but the time scale and spatial distribution of these motions are not well determined at strike-slip plate boundaries. Laboratory experiments on lower-crustal rock types suggest that their ductile behavior is not approximated well by linear viscoelasticity, as assumed in the thin-lithosphere model, but postseismic observations are not yet sufficiently detailed to confirm this expectation.

Furthermore, vertical crustal movements in California are not well understood. Though not dominant in California's largely strike-slip-faulting environment, vertical movements can nonetheless be locally important in such regions as the Los Angeles and Ventura Basins, the Transverse Ranges of southern California, and the Cape Mendocino area of northern California. Current and future work that integrates geologic and geodetic information in these regions should begin to shed light on long-term, secular vertical-movement patterns and their origins.

Within complex, multistranded fault zones and, possibly, in simpler regions, permanent inelastic deformation of upper-crustal rocks may contribute significantly to the current movement pattern. For example, at subduction boundaries, geologic and geodetic observations indicate a substantial imbalance between cumulative interearthquake strain and coseismic strain release, commonly reflected in long-term uplift or subsidence of coastal and inland regions. However, at such predominantly transcurrent boundaries as the San Andreas, the observable effects of inelastic strain are more subtle. The thermal consequences of such deformation may be the most direct evidence for inelastic strain (see chap. 9). However, for California at least, the available data are either contradictory or ambiguous, and the extent to which measured interearthquake movements release elastically stored strain is currently unresolved.

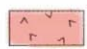
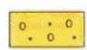





REFERENCES CITED

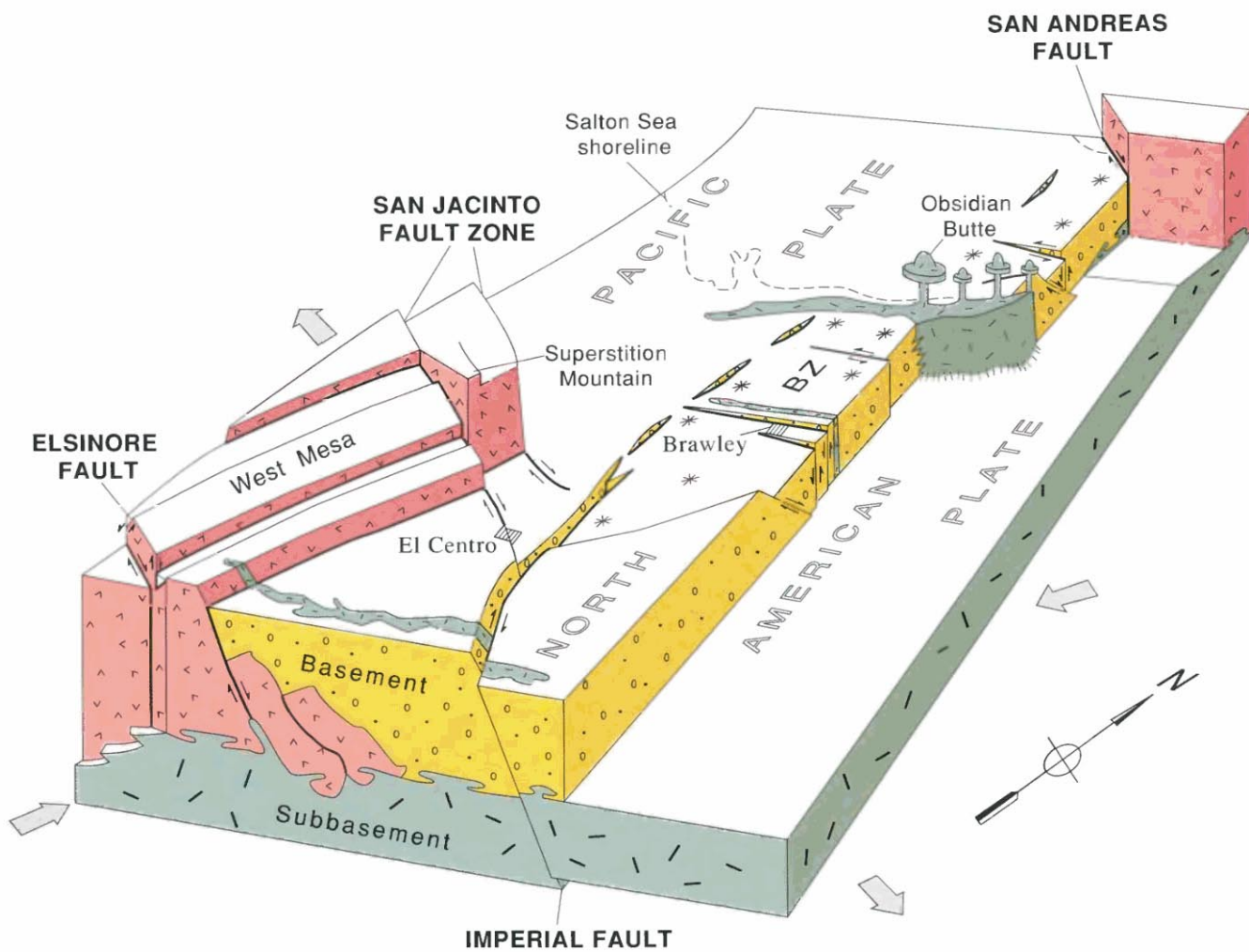
- Bornford, Guy, 1980, *Geodesy* (4th ed.): London, Oxford University Press, 731 p.
- Brace, W.F., and Byerlee, J.D., 1966, Stick-slip as a mechanism for earthquakes: *Science*, v. 153, no. 3739, p. 990-992.
- Breen, N.A., Lisowski, Michael, and Prescott, W.H., 1987, Spatially varying patterns of crustal strain near the Mendocino triple junction, California [abs.]: *Eos* (American Geophysical Union Transactions), v. 68, no. 44, p. 1240.
- Burford, R.O., and Harsh, P.W., 1980, Slip on the San Andreas fault in central California from alignment array surveys: *Seismological*

- Society of America Bulletin, v. 70, no. 4, p. 1223-1261.
- Castle, R.O., Church, J.P., Elliott, M.R., and Morrison, N.L., 1975, Vertical crustal movements preceding and accompanying the San Fernando earthquake of February 9, 1971: A summary: *Tectonophysics*, v. 29, p. 127-140.
- DeMets, Charles, Gordon, R.G., Stein, Seth, and Argus, D.F., 1987, A revised estimate of Pacific-North America motion and implications for western North America plate boundary zone tectonics: *Geophysical Research Letters*, v. 14, no. 9, p. 911-914.
- Dieterich, J.H., 1979, Modelling of rock friction, 1, Experimental results and constitutive equations: *Journal of Geophysical Research*, v. 84, no. B5, p. 2161-2168.
- Johnston, M.J.S., Linde, A.T., Gladwin, M.T., and Borcherdt, R.D., 1987, Fault failure with moderate earthquakes: *Tectonophysics*, v. 144, no. 1-3, p. 189-206.
- King, N.E., 1985, Horizontal deformation in the Mojave Desert near Barstow, California, 1979-1983: *Journal of Geophysical Research*, v. 90, no. B6, p. 4491-4494.
- King, N.E., and Savage, J.C., 1983, Strain-rate profile across the Elsinore, San Jacinto and the San Andreas faults near Palm Springs, California, 1973-81: *Geophysical Research Letters*, v. 10, no. 1, p. 55-57.
- 1984, Regional deformation near Palmdale, California, 1973-1983: *Journal of Geophysical Research*, v. 89, no. B4, p. 2471-2477.
- Lajoie, K.R., 1986, Coastal tectonics, in *Active tectonics*: Washington, National Academy Press, p. 95-124.
- Lawson, A.C., chairman, 1908, The California earthquake of April 18, 1906: Report of the State Earthquake Investigation Commission: Carnegie Institution of Washington Publication 87, 2 v.
- Li, V.C., and Rice, J.R., 1987, Crustal deformation in great California earthquake cycles: *Journal of Geophysical Research*, v. 92, no. B11, p. 11533-11551.
- Lisowski, Michael, and Prescott, W.H., 1981, Short-range distance measurements along the San Andreas fault system in central California, 1975 to 1979: *Seismological Society of America Bulletin*, v. 71, no. 5, p. 1607-1624.
- Louie, J.N., Allen, C.R., Johnson, D.C., Haase, P.C., and Cohn, S.N., 1985, Fault slip in southern California: *Seismological Society of America Bulletin*, v. 75, no. 3, p. 811-833.
- McNutt, Marcia, 1980, Implications of regional gravity for state of stress in the earth's crust and upper mantle: *Journal of Geophysical Research*, v. 85, no. B11, p. 6377-6396.
- Minster, J.B., and Jordan, T.H., 1987, Vector constraints on Western U.S. deformation from space geodesy, neotectonics, and plate motions: *Journal of Geophysical Research*, v. 92, no. B6, p. 4798-4804.
- Prescott, W.H., 1976, An extension of Frank's method for obtaining crustal shear strains from survey data: *Seismological Society of America Bulletin*, v. 66, no. 6, p. 1847-1853.
- 1981, The determination of displacement files from geodetic data along a strike slip fault: *Journal of Geophysical Research*, v. 86, no. B7, p. 6067-6072.
- 1985, An overview of the distribution of relative plate motion along the San Andreas fault system from Hollister, California, to the Mendocino triple junction, in Shearer, C.F., Minutes of the National Earthquake Prediction Evaluation Council, July 26-27, 1985, Menlo Park, California: U.S. Geological Survey Open-File Report 85-754, p. 232-246.
- Prescott, W.H., and Lisowski, Michael, 1983, Strain accumulation along the San Andreas fault system east of San Francisco Bay, California: *Tectonophysics*, v. 97, no. 1-4, p. 41-56.
- Prescott, W.H., Lisowski, Michael, and Savage, J.C., 1981, Geodetic measurement of crustal deformation on the San Andreas, Hayward, and Calaveras faults near San Francisco, California: *Journal of Geophysical Research*, v. 86, no. B11, p. 10853-10869.
- 1987, Velocity field along the San Andreas fault in southern California [abs.]: *Eos (American Geophysical Union Transactions)*, v. 68, no. 44, p. 1506.
- Prescott, W.H., and Yu, S.-B., 1986, Geodetic measurements of horizontal deformation in the northern San Francisco Bay region, California: *Journal of Geophysical Research*, v. 91, no. B7, p. 7475-7484.
- Sauber, Jeanne, Thatcher, Wayne, and Solomon, S.C., 1986, Geodetic measurement of deformation in the central Mojave Desert, California: *Journal of Geophysical Research*, v. 91, no. B12, p. 12683-12693.
- Savage, J.C., and Burford, R.O., 1970, Accumulation of tectonic strain in California: *Seismological Society of America Bulletin*, v. 60, no. 6, p. 1877-1896.
- Savage, J.C., and Lisowski, Michael, 1980, Deformation in Owens Valley, California: *Seismological Society of America Bulletin*, v. 70, no. 4, p. 1225-1232.
- 1984, Deformation in the White Mountain seismic gap, California-Nevada, 1972-1982: *Journal of Geophysical Research*, v. 89, no. B9, p. 7671-7687.
- Savage, J.C., and Prescott, W.H., 1973, Precision of geodolite distance measurements for determining fault movements: *Journal of Geophysical Research*, v. 78, p. 26, p. 6001-6008.
- Savage, J.C., Prescott, W.H., and Gu, Guohua, 1986, Strain accumulation in southern California 1973-1984: *Journal of Geophysical Research*, v. 91, no. B7, p. 7455-7473.
- Savage, J.C., Prescott, W.H., Lisowski, Michael, and King, N.E., 1979, Geodolite measurements of deformation near Hollister, California, 1971-1978: *Journal of Geophysical Research*, v. 84, no. B13, p. 7599-7615.
- 1981, Strain accumulation in southern California, 1973-1980: *Journal of Geophysical Research*, v. 86, no. B8, p. 6991-7001.
- Schulz, S.S., Mavko, G.M., Burford, R.O., and Stuart, W.D., 1982, Long-term fault creep observations in central California: *Journal of Geophysical Research*, v. 87, no. B8, p. 6977-6982.
- Segall, Paul, and Harris, R.A., 1987, Earthquake deformation cycle on the San Andreas fault near Parkfield, California: *Journal of Geophysical Research*, v. 92, no. B10, p. 10511-10525.
- Sibson, R.H., 1982, Fault zone models, heat flow, and the depth distribution of earthquakes in the continental crust of the United States: *Seismological Society of America Bulletin*, v. 72, no. 1, p. 151-163.
- Stein, R.S., 1983, Reverse slip on a buried fault during the 2 May 1983 Coalinga earthquake: Evidence from geodetic elevation changes, in Bennett, J.H., and Sherburne, R.W., eds., *The 1983 Coalinga, California earthquakes*: California Division of Mines and Geology Special Publication 66, p. 151-163.
- Stein, R.S., and Thatcher, Wayne, 1981, Seismic and aseismic deformation associated with the 1952 Kern County, California, earthquake and relationship to the Quaternary history of the White Wolf fault: *Journal of Geophysical Research*, v. 86, no. B6, p. 4913-4928.
- Stuart, W.D., 1979, Strain softening prior to two-dimensional strike slip earthquakes: *Journal of Geophysical Research*, v. 84, no. B3, p. 1063-1070.
- Thatcher, Wayne, 1975, Strain accumulation and release mechanism of the 1906 San Francisco earthquake: *Journal of Geophysical Research*, v. 80, no. 35, p. 4862-4872.
- 1979, Systematic inversion of geodetic data in central California: *Journal of Geophysical Research*, v. 84, no. B5, p. 2283-2295.
- 1983, Nonlinear strain buildup and the earthquake cycle on the San Andreas fault: *Journal of Geophysical Research*, v. 88, no. B7, p. 5893-5902.
- Tse, S.T., and Rice, J.R., 1986, Crustal earthquake instability in

- relation to the depth variation of frictional slip properties: *Journal of Geophysical Research*, v. 91, no. B9, p. 9452-9472.
- Tullis, T.E., 1988, Rock friction constitutive behavior from laboratory experiments and its implications for an earthquake prediction field monitoring program: *Pure and Applied Geophysics*, v. 126, no. 2-4, p. 555-588..
- Yeats, R.S., 1977, High rates of vertical crustal movement near Ventura, California: *Science*, v. 196, no. 4287, p. 295-298.
- Zhang, Y., Thatcher, Wayne, and Snay, R.A., 1988, Coseismic slip in the 1940 and 1979 Imperial Valley earthquakes and its implications [abs.]: *Eos (American Geophysical Union Transactions)*, v. 69, p. 1433.

EXPLANATION

-  Pre-late Miocene crystalline basement
-  Late Miocene and younger metasedimentary basement
-  Subbasement (basaltic intrusions)
-  Inferred intrusions or fractures underlying geothermal areas
-  Brawley seismic zone
-  Fault— Arrows indicate direction of relative movement
-  Principal stress direction



The crust of much of California was formed at an Andean-type continental margin during the Mesozoic and early Cenozoic, and was modified by large strike-slip offsets along the San Andreas fault system during the late Cenozoic. Decoupling within the crust, as implied by present upper-crustal tectonic wedging in central California, and decoupling between the crust and mantle, as implied by "subduction" of lithospheric mantle in southern California, indicates that the San Andreas fault system must change with depth in its location and (or) style of deformation.

8. LITHOSPHERIC STRUCTURE AND TECTONICS FROM SEISMIC-REFRACTION AND OTHER DATA

By GARY S. FUIS and WALTER D. MOONEY

CONTENTS

	Page		Page
Introduction-----	207	Southern California-----	222
Crustal-thickness map of California-----	208	Transect C3-----	223
Central California-----	212	Borderland-----	223
Transect C2-----	212	Peninsular Ranges-----	223
Offshore region-----	212	Salton Trough-----	226
Salinian block-----	212	Chocolate Mountains-----	228
Santa Clara Valley—San Andreas to Calaveras faults—	216	Tectonics—the three-dimensional picture-----	228
Diablo Range-----	217	Structure of the upper mantle-----	229
Great Valley and Sierran foothills-----	218	Summary-----	230
Discussion—tectonic wedging-----	220	Acknowledgments-----	231
Geologic history-----	220	References cited-----	231
Past and present tectonic regimes-----	221		

INTRODUCTION

Studies of the crustal and upper-mantle structure of California along the San Andreas fault system have been

underway for more than half a century, beginning with the early studies by Byerly and Wilson (1935) and Byerly (1946) in northern California and by Gutenberg (1943) in southern California. Crustal profiling along and

◀ **FIGURE 8.1.**—Schematic block diagram of Imperial Valley region of the Salton Trough, with unmetamorphosed sedimentary rocks removed and seismic basement cut away along line approximately parallel to the Brawley seismic zone (BZ; see fig. 8.7). Seismic basement consists of rocks with *P*-wave velocities of 5.5 to 6.5 km/s. In this region, there are two types of seismic basement: one type, on flanks of the Salton Trough, consists of pre-late Miocene igneous and metamorphic rocks; other type, in central part of trough, consists of late Miocene and younger metasedimentary rocks (similar in age and provenance to sedimentary rocks stripped off in this diagram). Pacific and North American plates are separating across the Brawley seismic zone,

an inferred onshore spreading center of the East Pacific Rise. North and south of the Brawley seismic zone, these two plates are separated from each other by transform faults, the San Andreas and Imperial faults, respectively. As the plates pull apart, subsidence occurs within the Brawley seismic zone, sediment is deposited to fill rift from above, and mafic intrusions (basalt, diabase, and gabbro) enter rift from below, metamorphosing sedimentary rocks below a certain depth (generally approx 5 km in central part of rift). This process is repeated until central part of rift consists entirely of young crust. Geographic locations projected downward onto seismic basement for reference.

near the San Andreas fault was first accomplished in the early 1960's by Eaton (1963), Healy (1963), and Roller and Healy (1963). Research accelerated after the 1966 $M=6.0$ Parkfield, Calif., earthquake to include both detailed crustal profiling and installation of dense seismic networks for the study of earthquakes (see chap. 5; Eaton and others, 1970). Since 1970, a wide variety of seismologic methods have been used to investigate crustal and upper-mantle structure in the vicinity of the San Andreas fault system. In this chapter, we summarize the main features of this structure and relate the structure to broad-scale tectonic processes.

Seismologic studies of crustal and upper-mantle structure in California make use of three primary data sources: (1) traveltimes of local earthquakes as measured by permanent and temporary seismic arrays, (2) seismic-refraction and reflection profiles, and (3) teleseismic delay times measured by seismic arrays. Traveltimes of local earthquakes, in addition to containing the information needed to locate earthquakes, contain a wealth of information regarding the seismic-velocity structure of the crust and upper mantle. Velocity structure can be determined from these traveltimes by iteratively adjusting an initial velocity model and associated hypocentral parameters, using inversion methods (for example, Crosson, 1976; Eberhart-Phillips and Oppenheimer, 1984). The resolution of velocity structure from local earthquake data is a function of the interstation spacing of the network and the abundance and distribution of seismicity.

Seismic refraction and reflection profiles together form a complementary set of seismic measurements. Seismic-refraction profiles provide the highest resolution of seismic P -wave velocities in the crust and upper mantle. The seismic-refraction method, however, generally does not provide the sharpest picture of lithologic interfaces, from which geologic structure is inferred; such a picture is better provided by seismic-reflection profiling.

Teleseismic delay-time studies offer the most effective means of determining the structure of the subcrustal lithosphere. The method is based on interpreting relative arrival times of compressional waves throughout a seismic array in terms of velocity variations at depth beneath the array. The Earth structure in the volume beneath the array generally is described by a series of blocks, and velocity deviations are derived for each block from the observed delay times (Aki and others, 1977; Thurber and Aki, 1987). The California seismic array is ideally suited for such investigations because of its large areal extent and the length of time it has been in operation (see chap. 5).

The primary product of the seismologic methods described above is a model of the seismic P -wave-velocity distribution in the crust and upper mantle. However, the

interpretation of seismic P -wave velocities in terms of rock type is highly nonunique because laboratory velocity data indicate that numerous rock types can have similar velocities (for example, Birch, 1960). This interpretation is further complicated by the fact that, in rocks at pressures of less than 2 kbars (depths above 8 km), seismic velocities are strongly affected by the presence of cracks (on all scales) and porosity. In addition, rock velocities are affected by temperature and the presence of water. Thus, the interpretation of P -wave velocities in terms of rock types must involve other data sets, including laboratory velocity measurements on rocks at different pressures, temperatures, and water saturations, surface geologic data, well data, and other geophysical data, including gravity and magnetic data. Fortunately, abundant laboratory velocity data (for example, Stewart and Peselnick, 1977; Lin and Wang, 1980), geologic data (see chaps. 1, 3), and geophysical data (see chap. 9) are available for California, making the lithosphere of this region one of the best studied in the world.

In this chapter, we summarize the lithospheric structure and tectonics along the San Andreas fault system of California (fig. 8.2) with maps of crustal thickness and upper-mantle seismic-velocity anomalies, and with crustal cross sections for central and southern California. Structure changes more rapidly parallel to the San Andreas fault in southern California than in central California, and so we supplement the cross section for southern California with a map showing crustal-block motions and a diagram illustrating the different motion of the lithospheric mantle below. Seismic and other data currently are still not dense enough to construct a cross section along the San Andreas fault system itself.

Construction of the crustal cross section for central California led us to a new interpretation of upper-crustal tectonic wedging, the mechanism whereby the Franciscan assemblage was emplaced in the Coast Ranges during the late Mesozoic(?) and Cenozoic. This interpretation extends that of Wentworth and others (1984) to include a two-part history whereby the observed structures atop the wedge, which include both extensional and compressional faults, were created. We further speculate that similar tectonic wedging occurred in southern California from the Mojave Desert to the Chocolate Mountains to emplace the Rand schist and the Pelona-Orocopia schist of Haxel and Dillon (1978) into rocks east of the San Andreas fault.

CRUSTAL-THICKNESS MAP OF CALIFORNIA

A contour map of crustal thicknesses in California (fig. 8.3A) provides an overview of the geophysical setting of the San Andreas fault system. The seismic and gravity

data used in compiling this map (fig. 8.3B) were discussed by Mooney and Weaver (1989).

Crustal thickness along the San Andreas fault increases from 16–24 km in northern California to 28–32 km in

southern California. Thus, the crust along the San Andreas fault system is everywhere thinner than the 36-km average for the conterminous United States (Braile and others, 1989), and in northern California it is

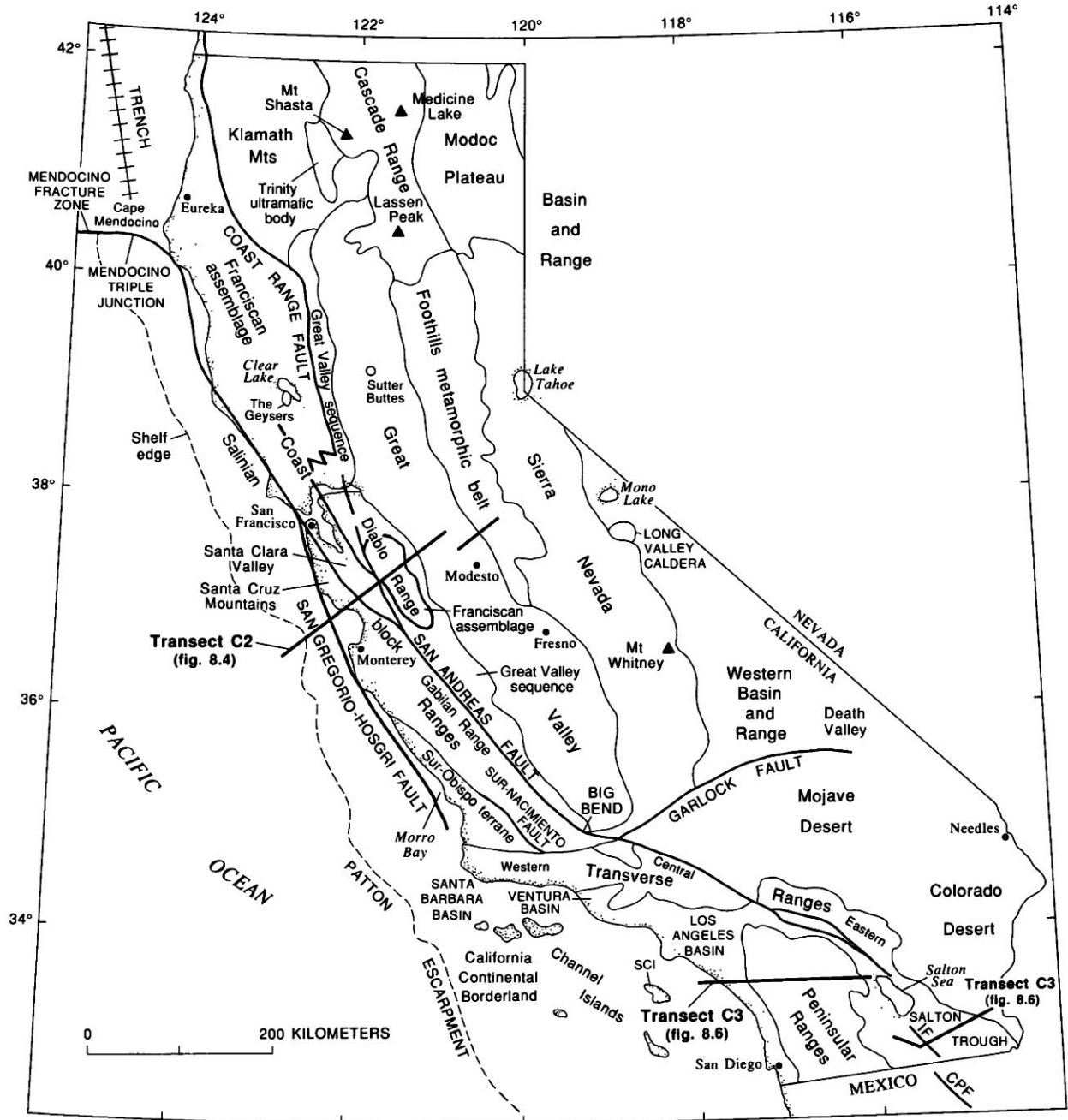


FIGURE 8.2.—California, showing place names, geologic provinces, selected geologic units, and locations of crustal transects shown in figures 8.4 and 8.6. The San Andreas fault extends from the Salton Trough to triple junction at Cape Mendocino. CPF, Cerro Prieto fault; IF, Imperial fault; SCI, Santa Catalina Island. Fault with crosslining is trench, offshore northern California.

substantially thinner than this average. To a first-order approximation, crustal thickness resembles the topography (see Jachens and Griscom, 1983, fig. 13).

Cape Mendocino in northern California marks the change from the strike-slip regime of the San Andreas fault to the subduction regime of the Cascade Range.

North of Cape Mendocino, the crust thickens eastward from about 16 km at the coast to about 38 km in the southern Cascade Range (fig. 8.3A). Near the coast, this thickness includes both the North American plate and the subducting Gorda plate. Estimates of crustal thickness in the northern Coast Ranges at Cape Mendocino lack

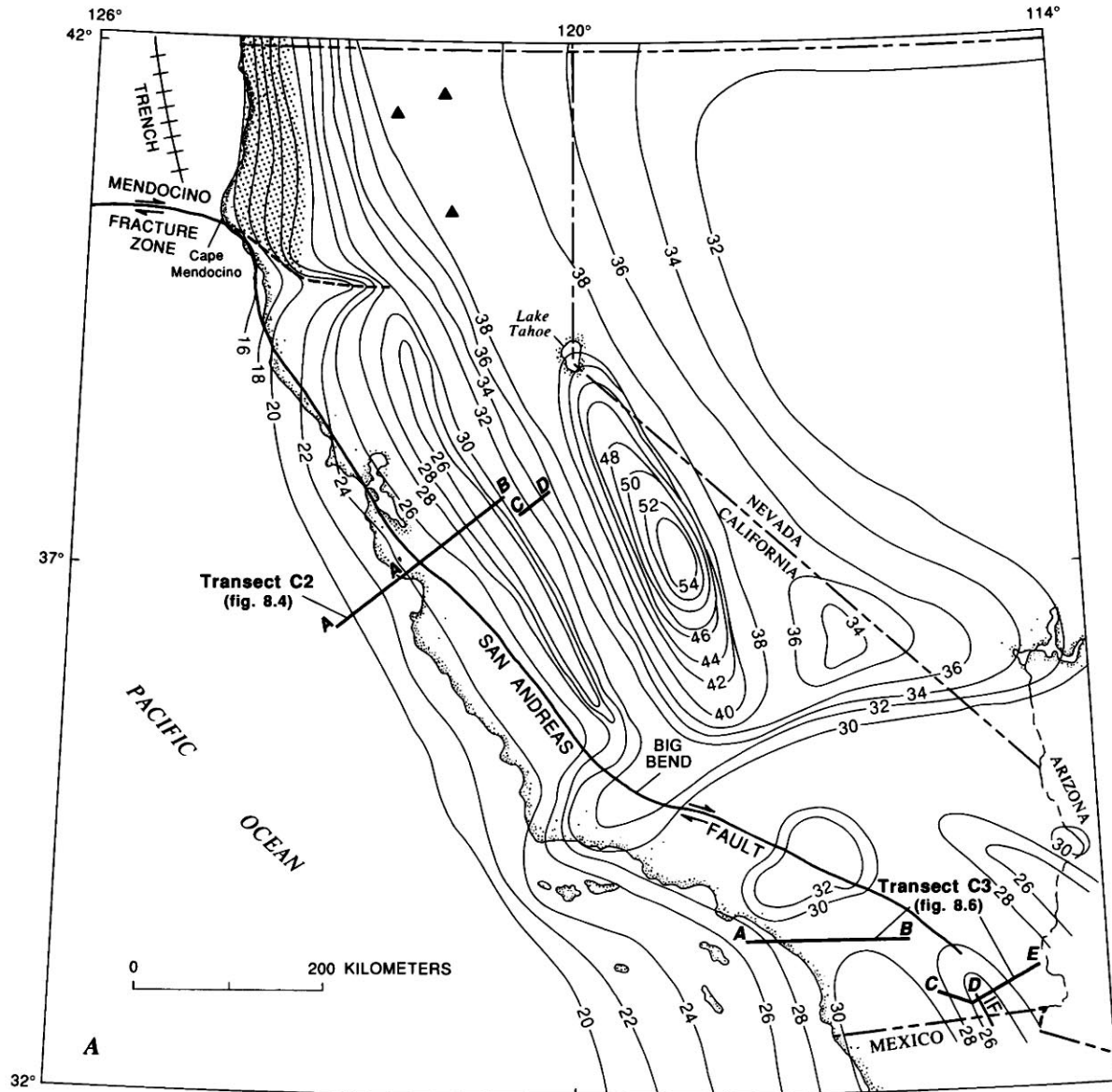


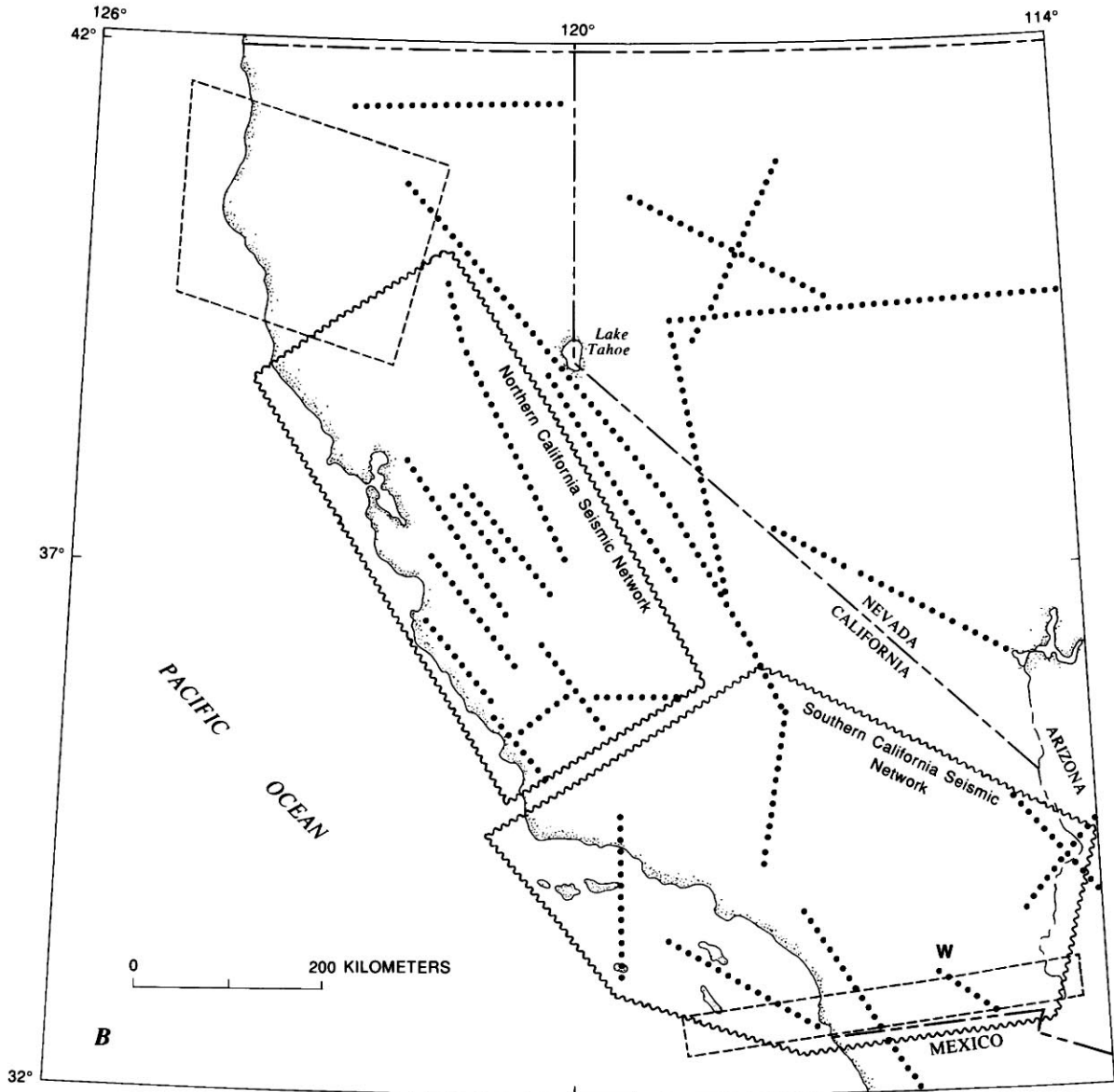
FIGURE 8.3.—Crustal thickness (A) for California and adjacent regions, modified from Mooney and Weaver (1989), with data sources (B). Contour interval, 2 km. Northeast of the San Andreas fault in central California, thin crust (within enclosed 28-km contour) corresponds to Mesozoic/early Cenozoic forearc basin (Great Valley; see fig. 8.2 for place names), and thick crust

(within enclosed 40-km contour) corresponds to magmatic arc of same age (Sierra Nevada). Southwest of the San Andreas fault in central California, this Andean-marginal sequence is repeated but shortened; crust is relatively thin there. In southern California, crustal thickness is relatively uniform (about 30 km), despite considerable tectonic activity throughout most of geologic time,

seismic refraction or reflection control, but detailed gravity models, heat-flow observations, and teleseismic data indicate an abrupt decrease in both crustal and lithospheric thickness southward of the landward projec-

tion of the Mendocino Fracture Zone (see chaps. 9, 10; Zandt and Furlong, 1982; Jachens and Griscorn, 1983).

In central California, the crust thickens eastward from about 25 km near the coast to as much as 55 km in the



including present subduction of lithospheric mantle (see below). Estimated error in figure 8.3A is 10 percent, or 1 to 1½ contour intervals. Heavy lines, faults—dashed where the Mendocino Fracture Zone extends onshore (and beneath North American plate); arrows indicate direction of relative movement; crosslined along trench, offshore northern California. Triangles, volcanoes of

Cascade Range continental arc. Dot pattern, area of contours on Gorda-plate Moho. IF, Imperial fault. Data sources in 8.3B include seismic-refraction profiles (dotted lines), earthquake networks (wavy outlines), and gravity (dashed outlines). "W" associated with seismic-refraction profile in the Salton Trough indicates that only wide-angle reflections are available to constrain Moho depth.

Sierra Nevada, but this general landward thickening is interrupted by thin crust (25 km) beneath the Great Valley (fig. 8.3A; compare Oppenheimer and Eaton, 1984). The crust of central California represents a Mesozoic and early Cenozoic Andean-type continental margin (see chap. 3; Hamilton, 1969) that has been modified by late Cenozoic strike-slip faulting along the San Andreas fault system and by uplift of the Sierra Nevada. Andean features include a subduction complex (eastern Coast Ranges), a forearc basin (Great Valley), and a magmatic arc (Sierra Nevada). Cenozoic strike-slip faulting along the San Andreas fault system has moved a shortened Andean-marginal sequence outboard of this sequence. Southwest of the San Andreas fault, the batholithic Salinian block (western Coast Ranges) is juxtaposed, across other right/oblique-slip faults of the San Andreas fault system, against an inactive accretionary prism, or subduction complex (western Coast Ranges and offshore California).

In southern California, the crust thickens eastward from about 20 km at the western margin of the California Continental Borderland to about 32 km in the eastern Transverse Ranges (fig. 8.3A). Over most of onshore southern California, crustal thickness is 30 ± 2 km. Considering the complex tectonic history of this region, including the present subduction of lithospheric mantle (see below), this uniformity in crustal thickness is remarkable.

CENTRAL CALIFORNIA

Crustal structure in central California is grossly two dimensional, as can be readily inferred from the crustal-thickness map (fig. 8.3A). There are five blocks or provinces with subparallel fault boundaries: an accretionary prism, which is partly off shore; the Salinian block, which underlies the western Coast Ranges, including the Santa Cruz Mountains and Gabilan Range; a complex block between the San Andreas and Calaveras faults, underlying the Santa Clara Valley; the Diablo block, beneath the Diablo Range; and the Great Valley/Sierran block (fig. 8.2). To illustrate the crustal structure of central California, we have modified and reinterpreted the part of Centennial Continent-Ocean Transect C2 (Saleeby, 1986) that extends from offshore California at Monterey Bay to the Sierran foothills near Modesto (figs. 8.2, 8.4). Seismic control, which is exceptionally good along this transect, has been augmented since Saleeby's (1986) study primarily by analysis of seismic-refraction profiles in the Great Valley (fig. 8.4A). The reader is referred to Hill (1978) for an earlier treatment of deep structure along approximately this same transect.

TRANSECT C2

OFFSHORE REGION

The offshore region of transect C2 is underlain by an inactive, early Tertiary accretionary prism overlapped by uppermost Oligocene to Holocene sedimentary rocks (see Saleeby, 1986). The San Simeon terrane, consisting of Late Cretaceous Franciscan rocks (disrupted marine sedimentary rocks; see chap. 3), is imbricated in this prism along with poorly known, lower Tertiary sedimentary rocks. The prism is underlain by oceanic crust with an inferred age of about 26 to 20 Ma (Atwater and Menard, 1970; Atwater, 1989). The accretionary prism is juxtaposed against granitic rocks of the Salinian block across the (inactive) Nacimiento fault, which is overlapped by upper Tertiary sedimentary rocks. This fault, in turn, is offset by the (active) right/oblique-slip San Gregorio-Hosgri fault. The Moho is 10 km below sea level near the west end of the transect (Shor and others, 1971) and deepens to 24- to 26-km depth beneath the Gabilan Range and Santa Cruz Mountains (Walter and Mooney, 1982).

We follow D.S. McCulloch (in Saleeby, 1986) in showing steep northeastward dips on both the Nacimiento and San Gregorio-Hosgri faults (fig. 8.4A) that are based on marine reflection data. Focal mechanisms for earthquakes on the San Gregorio-Hosgri fault at this latitude indicate nearly pure strike slip on vertical planes; however, farther south, they indicate chiefly reverse faulting on northeast- or southwest-dipping planes (see chap. 5).

SALINIAN BLOCK

The area between the Nacimiento and San Andreas faults is underlain by a batholithic terrane that has been transported northwestward by the San Andreas (and other?) fault(s) by amounts estimated to range from 550 km (see Ross, 1978) to 2,500 km (Champion and others, 1984). Plutonic rocks include tonalite, granodiorite, and quartz monzonite of mostly Late Cretaceous age (Ross, 1978; Mattinson, 1982). Metamorphic pendents and screens include mostly quartz-rich clastic rocks of amphibolite facies. Ross and McCulloch (1979) postulated that these upper-crustal plutonic and metamorphic rocks are not rooted to the lower crust but are in fault contact with a buried terrane, possibly consisting of Franciscan rocks.

The velocity structure derived by Walter and Mooney (1982) from Stewart's (1968) seismic-refraction measurements in the Gabilan Range and Santa Cruz Mountains can be subdivided into four separate crustal layers with velocities of 2.1–4.6 km/s (layer 1), 5.3–5.6 km/s (layer 2),

EXPLANATION FOR FIGURES 8.4A AND 8.6A

- 3.6/4.6 **P-wave velocity in kilometers per second at top/base of layer**—Velocities in parentheses are projected
- P-wave velocity boundary**—Heavy tick where profile perpendicular to page; light line where profile in plane of page; short dashed where change in gradient only; long dashed in figure 8.4A for model of Dean Whitman and others (unpub. data, 1985). Boundaries are determined by refraction profiling except for offshore central California (fig. 8.4A) where they are determined by reflection profiling
- ? **Reflector from reflection profiling**—Queried where uncertain
- **Density and magnetic boundary**
- ? **Inferred region in which midcrustal and Moho discontinuities may exist**—Queried where uncertain
- LVZ, **Possible low-velocity zone**
- **Fault**

EXPLANATION FOR FIGURES 8.4B AND 8.6B
LITHOLOGIC SYMBOLS FOR TECTONIC ENVIRONMENT

- Sedimentary rocks**
 - Oceanic Basin floor and trench turbidites**
 - Pelagic sedimentary rocks**
- Igneous and metamorphic rocks**
 - Seamounts**
 - Ophiolite, or top of ophiolite where undivided mafic crust is shown below**
 - Serpentine**
- Sedimentary rocks**
 - Magmatic arc**
 - Forearc rocks**
 - Intra-arc rocks**
- Volcanic rocks**
 - Rocks of mixed and (or) intermediate composition**
- Plutonic rocks**
 - Granite and quartz monzonite**
 - Granodiorite and tonalite**
 - Gabbro**

- Sedimentary rocks**
 - Continental and continental rift**
 - Nonmarine clastic rocks**—Circles, conglomerate; circles and dots, conglomerate and sandstone; darker color, metamorphosed
 - Marine clastic rocks**—Strike-and-dip symbol, carbonate bearing
- Volcanic rocks**
 - Rocks of mixed felsic to mafic composition**
- Metamorphic rocks**
 - Middle crust**—Inferred to be gneiss and schist developed at 10- to 20-km depth at greenschist to amphibolite facies
 - Lower crust**—Inferred to be gneiss developed below 20-km depth at amphibolite to granulite facies
- Mafic crust, undivided**—Denser pattern; higher velocity
- Mantle**—Closely spaced ticks, top of lithospheric mantle; widely spaced ticks, top of asthenospheric mantle or lithospheric mantle with partial melt

OTHER SYMBOLS

- Melange**—Symbols enclosed by zigzag lines indicate block type
- $\alpha \beta \gamma$ **Metamorphic facies**—Amphibolite, blueschist (\pm eclogite), greenschist
- Shear zone**
- Lithologic contact**
- Normal or strike-slip fault**—Sense of motion shown: arrows indicate direction of relative movement; A, away from observer; T, toward observer
- Mesozoic thrust fault**—Sawteeth on upper plate
- Mesozoic or Cenozoic thrust fault**—Teeth on upper plate; arrow indicates inferred motion of upper plate; dotted where inferred to have formerly existed
- Cenozoic thrust fault**—Teeth on upper plate; arrow indicates inferred motion of upper plate
- Mesozoic or Cenozoic detachment fault**—Ticks on upper plate
- Cenozoic detachment fault**—Ticks on upper plate
- In figure 8.6, Chocolate Mountains: Mesozoic or Cenozoic thrust or detachment fault ("Chocolate Mountains thrust fault"; see text)**

NOTE: Lithologic contacts and faults—Long dashed where not constrained by figures 8.4A and 8.6A or by earthquakes of chapter 5; short dashed where gradational (lithologic contact only) or projected above surface; queried where existence uncertain

? **Top of brittle-ductile transition zone inferred from earthquakes (see text)**—Queried where uncertain

W

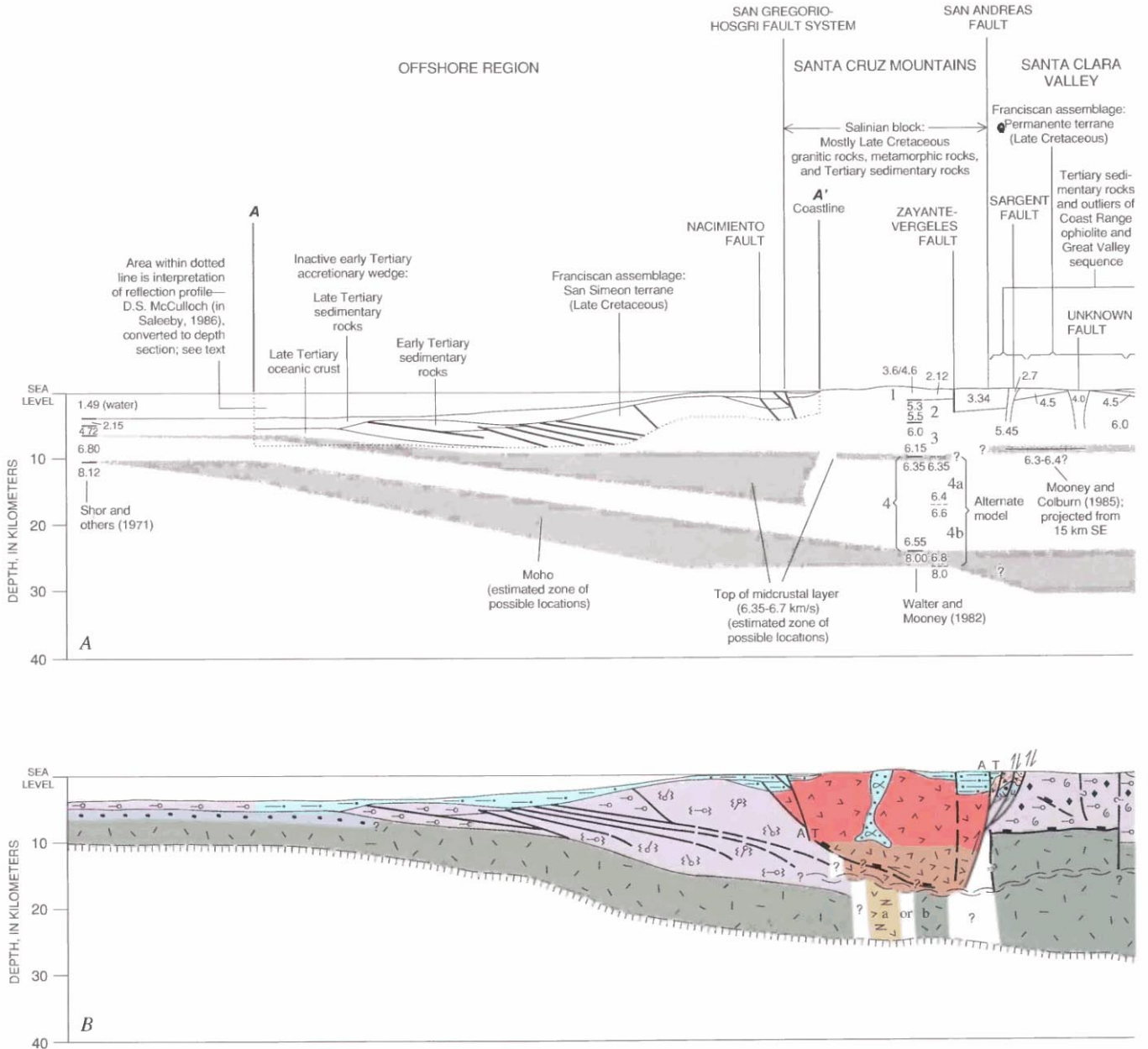
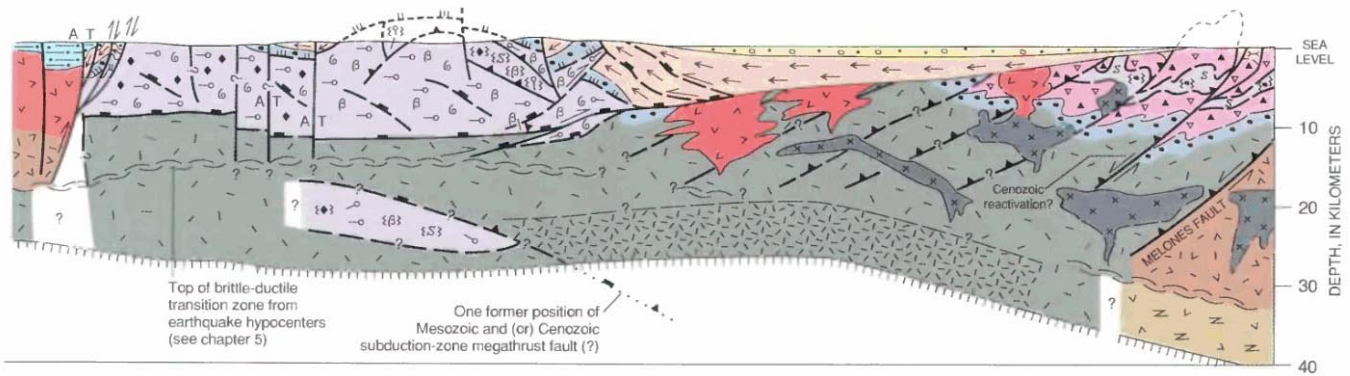
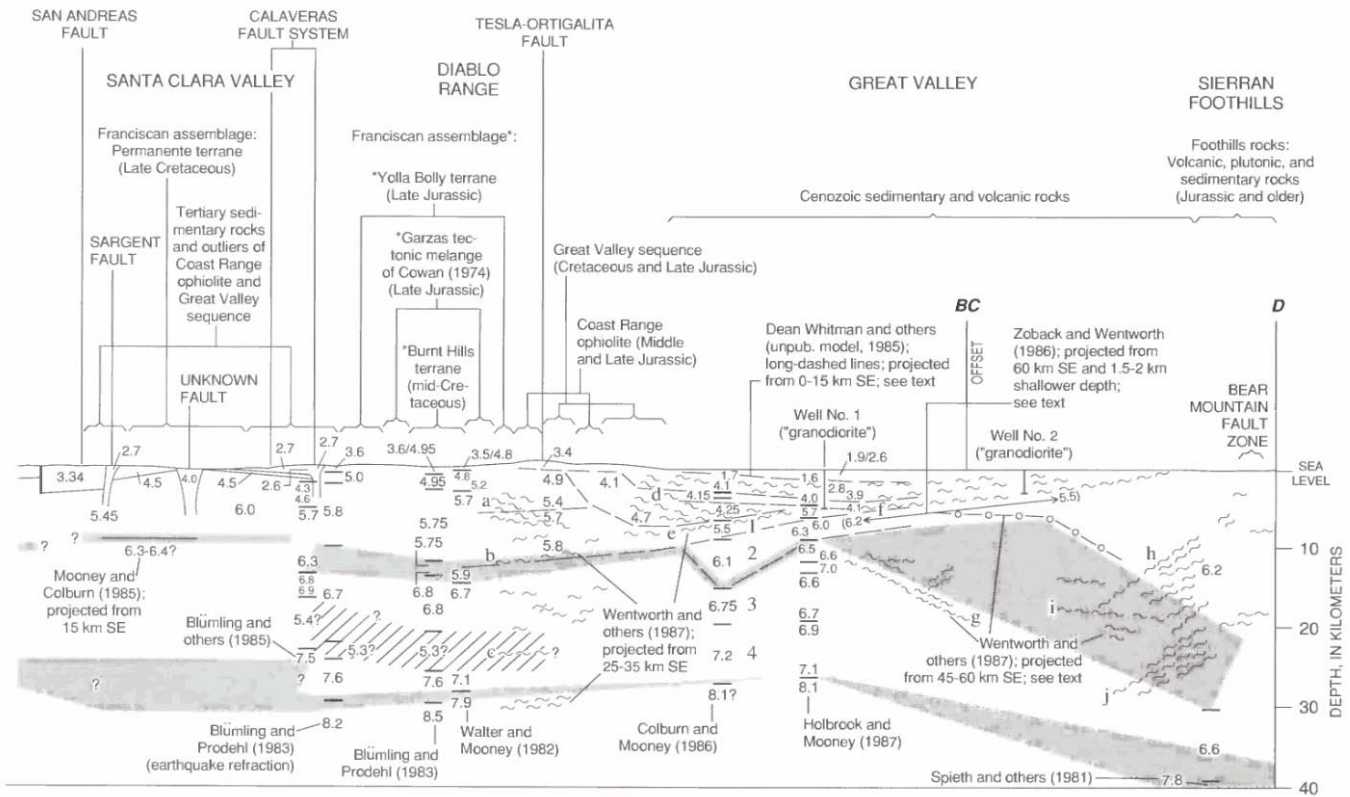


FIGURE 8.4.—Crustal structure of central California. *A*, Surface geology, depth-converted seismic-reflection data, and models of seismic-refraction, gravity, and magnetic data along western part of Centennial Continent-Ocean Transect C2 (see Saleeby, 1986). *B*, Reinterpretation of Transect C2. Major features in figure 8.4*B* include, from west to east, (1) offshore, inactive, early Tertiary accretionary wedge; (2) batholithic Salinian block of the Santa Cruz Mountains, positioned between the active oblique-slip San Gregorio-Hosgri and San Andreas faults; (3) Franciscan terranes of the Santa Clara Valley and Diablo Range, interpreted to compose a tectonic

wedge; (4) Mesozoic and Cenozoic sedimentary rocks of the Great Valley; and (5) rocks of the Sierran foothills, including Jurassic and older volcanic, plutonic, and related sedimentary rocks accumulated or emplaced in an island-arc setting and Cretaceous plutonic rocks. Tectonic wedge in feature 3 is interpreted to have moved during the late Mesozoic(?) and Cenozoic, possibly in several episodes, largely along contact between Mesozoic crystalline rocks and overlying Mesozoic sedimentary rocks. In the eastern Great Valley, these sedimentary rocks are still rooted to (or depositionally overlie) this basement. Movement of

E



wedge during present San Andreas transform-faulting regime may be along one or more thrust faults that merge with postulated decollement in brittle-ductile transition zone in the crust. This reinterpretation differs from Saleeby's (1986) in eliminating inferred east-dipping subduction zone or thrust fault beneath the western Great Valley. Off shore, interpretation of unmigrated reflection section by D.S. McCulloch (in Saleeby, 1986) has been converted to depth section, using assumed velocities for each inferred geologic unit. In the Santa Cruz Mountains, velocity model consisting of

layers 1 through 4 is shown (fig. 8.4A; see fig. 8.5A), along with alternative model in which layer 4 is subdivided into layers 4a and 4b. First model gives rise to interpretation a, and alternative model to interpretation b (fig. 8.4B). a-j, reflectors in the eastern Diablo Range, Great Valley, and Sierran foothills; 1-4, seismic-velocity layers in the Great Valley (fig. 8.4A) discussed in text. See figures 8.2 and 8.3 for location of Transect C2. No vertical exaggeration.

6.0–6.15 km/s (layer 3), and 6.35–6.55 km/s (layer 4). Layer 4, middle and lower crust, can alternatively be modeled as two layers of velocities 6.3 km/s (layer 4a) and 6.6–6.8 km/s (layer 4b). These layer velocities can be correlated to rock type using surface geologic data and laboratory velocity data. Layer 1 corresponds to outcrops of Cenozoic sedimentary rocks along the transect. Basement outcrops along or near the transect include abundant quartz monzonite (Ross, 1972). Lin and Wang (1980) studied the velocity behavior of a sample of quartz monzonite from this region as a function of pressure and temperature, and constructed a velocity-depth curve for this rock appropriate for the Coast Ranges. On their curve (fig. 8.5A), the rock is slightly faster than layers 2 and 3 and slower than layer 4. Walter and Mooney (1982) interpreted layers 2 and 3 as granitic rocks similar to this

quartz monzonite. The somewhat lower velocity of these two layers in comparison with the laboratory sample may be interpreted to result from (1) megascopic fractures in the Earth, not present in the laboratory sample; (2) a slightly lower content of mafic minerals (which have high seismic velocity) in the granitic rocks beneath the transect in comparison with the laboratory sample; or (3) both. Layer 4 is intermediate in velocity between the quartz monzonite sample and gabbro samples (hornblende gabbro and olivine gabbro) from the Coast Ranges. Walter and Mooney (1982) interpreted this layer to correspond to gneiss of intermediate composition, on the basis of a comparison of layer 4 with other laboratory data. In an alternative model, however, where middle and lower crust are separated as layers 4a and 4b, layer 4b may be reasonably interpreted as gabbro (fig. 8.5A).

Alternative interpretations of these several crustal layers are also possible, given the fact that different rock types may have similar velocities. Stewart and Peselnick (1977) and Lin and Wang (1980) studied the velocity behavior of Franciscan rocks, also common in the Coast Ranges (Jennings and Strand, 1958). Two lithologic components of the Franciscan assemblage, unmetamorphosed and metamorphosed graywacke, produce velocity-depth curves (fig. 8.5B) that bracket those for most other components of the Franciscan assemblage (including basalt). On the basis of velocity data alone, layers 2 and 3 might be interpreted as Franciscan rocks, but surface geologic data lead us to reject this interpretation. On the basis of velocity data alone, however, layer 4 is most likely not Franciscan rocks. Thus, if the middle and lower crust of the Salinian block represents a different terrane from the upper crust, as postulated by Ross and McCulloch (1979), that terrane is most likely not Franciscan assemblage.

In our cross section (fig. 8.4B), we show alternative interpretations of layer 4, given the alternative velocity models discussed above. In one interpretation (a, fig. 8.4B), layer 4 is entirely gneiss of intermediate composition. In a second interpretation (b, fig. 8.4B), layer 4a is intermediate gneiss, and layer 4b is gabbro. In interpretation a, no buried terranes are present; in interpretation b, the lower-crustal gabbro may be a buried terrane (oceanic crust) or magmatically underplated gabbro.

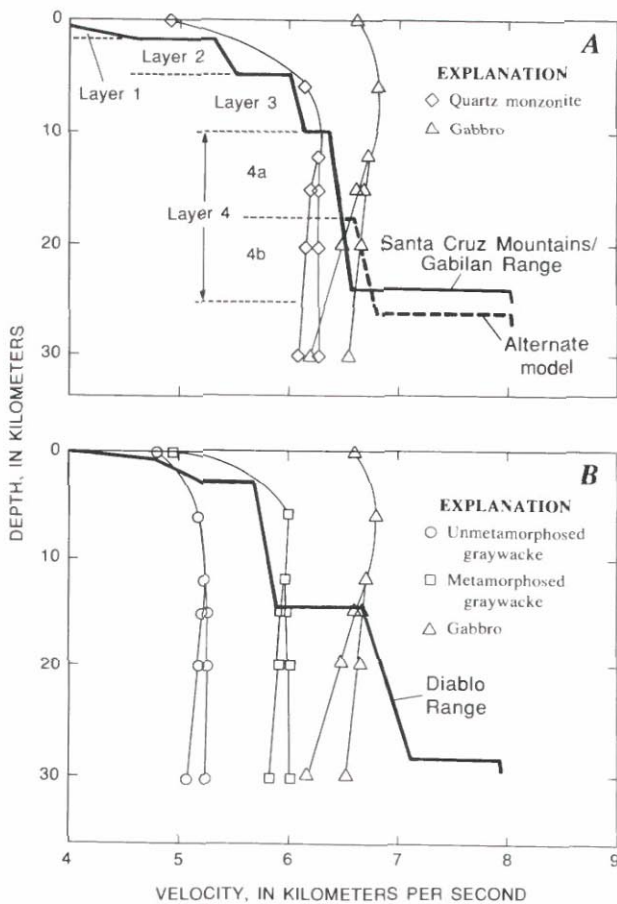


FIGURE 8.5.—Velocity-depth curves. A, Santa Cruz Mountains and Gabilan Range (Salinian block). B, Diablo Range. Heavy curves from seismic results (Walter and Mooney, 1982); light curves from laboratory velocity measurements and heat-flow modeling (two different geotherms assumed below about 10-km depth; Lin and Wang, 1980). See text for discussion of layers shown in figure 8.5A.

SANTA CLARA VALLEY—SAN ANDREAS
TO CALAVERAS FAULTS

In the Santa Clara Valley, between the San Andreas and Calaveras faults, Franciscan assemblage (Permanente terrane; Blake and others, 1982) is overlain by outliers of Late Jurassic Coast Range ophiolite and Upper Cretaceous Great Valley sequence (McLaughlin

and others, 1988a). The Franciscan assemblage includes melange, volcanogenic sandstone, pillow basalt, serpentine, chert, and limestone. The Franciscan sedimentary rocks were deposited in equatorial waters and presumably transported thousands(?) of kilometers northward before accretion to the North American Continent (Blake and others, 1982).

Along transect C2, the San Andreas fault juxtaposes a thick section of Tertiary marine sedimentary rocks on the southwest against slivers of Coast Range ophiolite, Great Valley sequence, and other Tertiary marine rocks on the northeast that have been imbricated along the southwest-dipping Sargent fault and related thrust faults (McLaughlin and others, 1988a). Presumably, the granitic rocks of the Salinian block and Franciscan assemblage are juxtaposed at depth. In contrast, similar rocks are juxtaposed on either side of the Calaveras fault, including Coast Range ophiolite, Great Valley sequence, and, at depth, presumably the Franciscan assemblage.

Aftershocks of the $M=7.1$ Loma Prieta earthquake of 1989 indicate a steep southwestward dip (approx 70°) on the San Andreas/Sargent fault zone, and the main shock produced subequal components of strike- and reverse-slip motion (Plafker and Galloway, 1989). Relatively low elevations in this region, however, indicated that the motion along this fault zone in the past has been chiefly strike slip, and seismicity before the Loma Prieta earthquake (Olsen and Lindh, 1985; Olsen, 1986) indicates a complex fault zone that may include both vertical and southwest-dipping fault strands (see fig. 8.4B).

Although a steep (80° – 85°) eastward dip on the Calaveras fault is indicated by earthquakes (see cross sec. $D-D'$, fig. 5.7B; Reasenber and Ellsworth, 1982; Oppenheimer and others, 1988), such an attitude is not resolvably different from a vertical dip (shown in fig. 8.4B), given errors in earthquake locations.

A seismic-refraction profile across the Santa Cruz Mountains and Santa Clara Valley reveals a heterogeneous upper crust (Mooney and Colburn, 1985). Layer offsets and velocity changes are visible in the model for this profile at the Zayante-Vergeles, Sargent, and Calaveras faults but, surprisingly, not at the San Andreas fault. An additional discontinuity is visible at an inferred buried fault in the central Santa Clara Valley (fig. 8.4A). Vertical zones of low velocity, 1 to 2 km wide, extending to a depth of as much as 3 to 5 km, are visible at a few of these faults (Mayer-Rosa, 1973; Blümling and others, 1985; Mooney and Colburn, 1985). The surficial layer (2.1–4.5 km/s) corresponds to different rocks in different places (fig. 8.4B). The “basement” layer has a velocity (5.4–6.0 km/s) appropriate for either granitic or Franciscan rocks at shallow crustal levels (Mooney and Colburn, 1985; see discussion above and fig. 8.5); presumably, it represents Franciscan rocks except west of

the San Andreas fault. The higher-velocity basement (6.0 km/s) in the eastern Santa Clara Valley may represent metamorphosed Franciscan rocks. A strong reflector is visible at 8- to 9-km depth beneath the Santa Clara Valley, but the seismic velocity below it is unknown. By analogy with the strong midcrustal reflector in the Diablo Range (see below), we infer this reflector to be the top of accreted island-arc and (or) oceanic crust.

Moho depth beneath the Santa Clara Valley is not known accurately enough to resolve whether the Moho steps downward to the east at the San Andreas and Calaveras faults or dips smoothly eastward between control points in the Santa Cruz Mountains/Gabilan Range (24- to 26-km depth) and the Diablo Range (29- to 30-km depth). McEvelly and Clymer (1975) conducted a seismic-reflection survey across the San Andreas fault south of its junction with the Calaveras and found a crustal thickness of 24 km with no change in thickness across the fault. Peake and Healy (1977), however, indicated a change in crustal thickness at the fault in this area.

DIABLO RANGE

The Diablo Range, the east-central Coast Ranges between the Calaveras fault and the Great Valley, is underlain chiefly by Franciscan assemblage. These rocks constitute at least three thrust sheets or nappes that are folded into an antiform (fig. 8.4; Blake, 1981; Saleeby, 1986). The youngest thrust sheet, the Burnt Hills terrane (Blake and others, 1982; Saleeby, 1986), consists of mid-Cretaceous blueschist-facies graywacke, arkose, conglomerate, argillite, and chert, approximately equivalent in age and provenance to mid-Cretaceous forearc sedimentary rocks of the Great Valley sequence. The Burnt Hills terrane is exposed in the core of the antiform. The oldest thrust sheets are the Upper Jurassic (informal) Garzas tectonic melange (Cowan, 1974) and the Yolla Bolly terrane (Blake and others, 1982). The Garzas tectonic melange consists of mafic blueschist-amphibolite, greenstone, serpentinized peridotite, and metagraywacke; it contains fragments of Upper Jurassic rocks (Coleman and Lanphere, 1971; Suppe and Armstrong, 1972) similar to those accreted in the Sierran foothills during the Nevadan orogeny (see below). The Yolla Bolly terrane lithologically resembles the Burnt Hills terrane, although there are some important differences. Both the Garzas tectonic melange and Yolla Bolly terrane crop out on the flanks of the antiform. The Coast Range ophiolite and Great Valley sequence lie above the Franciscan rocks on the low-angle Coast Range fault, which is complexly offset by the steeply dipping Cenozoic Tesla-Ortigalita fault on the northeast flank of the Diablo Range (fig. 8.4). (We follow Jayko and others, 1987, in referring to the

“Coast Range thrust fault” as simply the “Coast Range fault”—see below.)

The velocity structure of the Diablo Range derived by Walter and Mooney (1982) from seismic-refraction data collected by Stewart (1968) includes, beneath a 3.5- to 5.3-km/s near-surface layer, a 5.7- to 5.9-km/s layer beginning at 3-km depth, a 6.7- to 7.1-km/s layer beginning at 15-km depth, and the Moho at 29-km depth (fig. 8.4A). Importantly, a strong reflection is observed from the layer boundary at 15 km, indicating a strong velocity contrast between upper and lower crust. Blümling and Prodehl (1983) reanalyzed the same data and derived a similar velocity structure, except that they interpreted more phases in the data and added a lower-crustal low-velocity layer (5.3? km/s), with its base at about 26-km depth.

Seismic-reflection data have been collected in the eastern Diablo Range (Zoback and Wentworth, 1986) and compiled with other seismic data (Wentworth and others, 1987). These reflection data include a band of strong reflectors in the upper crust that dips shallowly east (reflectors a, fig. 8.4A), a weak reflector in the middle crust that dips shallowly west (reflector b), and a weak reflector at about 30-km depth (reflector c). The shallowly west-dipping reflector b, appears to link the top of the Great Valley basement with the top of the 6.7- to 7.1-km/s layer (Wentworth and Zoback, 1989).

Between 3- and 15-km depth, seismic velocities in the Diablo Range are well bracketed by velocity-depth curves predicted for end-member rocks of the Franciscan assemblage (fig. 8.5B; Steward and Peselnick, 1977; Lin and Wang, 1980). Within this depth range, the observed velocities also are slightly lower than those predicted for most granitic rocks (see fig. 8.5A). Between 15- and 20-km depth, the observed velocities agree well with those predicted for gabbro (fig. 8.5B; Lin and Wang, 1980) or, possibly, high-grade metamorphic rocks (Birch, 1960; Christensen and Fountain, 1975).

The 6.7- to 7.1-km/s layer in the Diablo Range may represent the middle and lower crust of an island arc or several imbricated island arcs. If so, this layer might include mixed intermediate and mafic plutonic rocks, including compositions from granodiorite to gabbro, as well as metamorphic rocks (see description of the Coast Range ophiolite by Evarts, 1977). Its relatively high velocity indicates that rocks of mafic composition must dominate or that the rocks are of amphibolite to granulite facies. This “island arc” interpretation is consistent with linking this layer to rocks beneath the Great Valley and thence to rocks of the Sierran foothills, which represent the middle and upper crust of island arc(s) (Saleeby, 1986). The 6.7- to 7.1-km/s layer, however, may also represent middle and lower oceanic crust, or diabase and gabbro, similar to the lowest layer of oceanic crust at the

west end of transect C2 (fig. 8.4A). The 6.7- to 7.1-km/s layer is too thick, however, to represent a single layer of oceanic crust. It consists of either several slices of tectonically underplated oceanic crust or of oceanic crust that has been augmented by mafic intrusions after underplating. If the low-velocity zone of Blümling and Prodehl (1983) is present, the 6.7- to 7.1-km/s layer may include oceanic sedimentary rocks tectonically underplated along with the oceanic crust.

We show a fault contact between the Franciscan assemblage and the 6.7- to 7.1- km/s layer in the Diablo Range to reflect the eastward transport of a wedge of Franciscan rocks (fig. 8.4B), similar to that discussed by Wentworth and others (1984). This interpretation departs from that of Saleeby (1986), who linked the shallowly east-dipping reflectors in the eastern Diablo Range (a, fig. 8.4A) with a hypothetical subduction zone or thrust fault beneath the Great Valley and Sierran foothills (see section below entitled “Discussion—Tectonic Wedging”).

GREAT VALLEY AND SIERRAN FOOTHILLS

Rocks of the Great Valley are known from exposures in an upturned section on the east side of the Diablo Range and from wells. The upturned section rests structurally above the Franciscan assemblage on the low-angle Coast Range fault, although in many places this relation is obscured by younger high-angle faults. This upturned section includes, from oldest to youngest, Middle and Late Jurassic Coast Range ophiolite and a related tuffaceous unit; Upper Jurassic and Cretaceous Great Valley sequence, which is chiefly forearc flysch; lower Cenozoic postarc marine and terrestrial sedimentary rocks; and upper Cenozoic continental-arc sedimentary rocks (Mad-dock, 1964; Evarts, 1977; Bartow and others, 1985).

At the latitude of transect C2, the Coast Range ophiolite is interpreted to be a (rifted) island-arc assemblage because it contains abundant silicic volcanic and intrusive rocks (Bailey and Blake, 1974; Evarts, 1977; Hopson and others, 1981; McLaughlin and others, 1988b). Its contact with the overlying sedimentary rocks, though faulted in most places, is believed to be fundamentally depositional (Bailey and others, 1970); on transect C2 it is demonstrably depositional (Evarts, 1977).

The Great Valley sequence and younger rocks exposed in the upturned section in the eastern Diablo Range appear to be nearly twice as thick as the section of sedimentary rocks penetrated in wells farther east in the Great Valley (fig. 8.4). Some of this apparent westward thickening results from the stratigraphic addition of older rocks to the basal part of the section in the west; some may be caused by imbrication along thrust faults (Wentworth and others, 1984). Similar apparent thickening

west of the synclinal axis of the Great Valley has been documented in other localities as well. In the southern Great Valley, Wentworth and others (1984) indicated an apparent doubling of thickness west of the axis, and in the northern Great Valley, an apparent trebling of thickness.

Most of the basement rocks that have been penetrated by wells in the Great Valley have been identified as granitic rocks (Saleeby, 1986). Rocks exposed in the Sierran foothills, east of the Great Valley, may be related to basement rocks beneath the Great Valley, but they are not so dense or magnetic (see below; fig. 8.4A).

Deep structure along transect C2 in the Great Valley has been elaborated in some detail by Colburn and Mooney (1986), Holbrook and Mooney (1987), and Dean Whitman and others (unpub. data, 1985) from seismic-refraction data, and by Wentworth and others (1987) primarily from seismic-reflection data. Seismic velocities in the sedimentary section range from 1.6 to 4.1 km/s where these velocities can be clearly ascribed to sedimentary rocks, such as near well No. 1 (fig. 8.4A). In the eastern Diablo Range, velocities as high as 4.7 km/s may also be due to sedimentary rocks (fig. 8.4A). East of the synclinal axis in the Great Valley, reflections within the sedimentary section are subparallel to the top of basement, which is marked by the disappearance of reflections (f, fig. 8.4A). West of the synclinal axis, these reflections (d, fig. 8.4A) diverge slightly from the inferred top of basement (e, fig. 8.4A).

Beneath the sedimentary rocks of the Great Valley are several layers of increasing seismic velocity: a 5.5- to 5.7-km/s layer, 1.5 to 2 km thick (layer 1), a 6.0- to 6.3-km/s layer, 2.5 to 6 km thick (layer 2); a 6.6- to 6.75-km/s layer, 4 to 7 km thick (layer 3); and a 6.9- to 7.2-km/s layer, about 7 km thick (layer 4) (fig. 8.4A). In addition, there is a thin, laterally discontinuous 7.0-km/s layer embedded in the top of layer 3. Well No. 1 indicates that layer 1 is granitic rocks. Farther west, however, this layer may be interpretable either as granitic rocks or as Franciscan assemblage, which have similar velocities at this depth (fig. 8.5). In the original data of Colburn and Mooney (1986) and Holbrook and Mooney (1987), there is no perceptible reflection from an interface between layers 1 and 2 (as there is, for example, between layer 1 and the overlying sedimentary rocks), and so these two layers may, in fact, grade into one another. Layer 2 could then also be granitic rocks, and layers 1 and 2 together would constitute a velocity-depth section similar, for example, to upper crust of the batholithic Salinian block (figs. 8.4A, 8.5). Layers 3 and 4 (6.6-7.2 km/s), which are analogous to the lower-crustal layer in the Diablo Range (6.7-7.1 km/s), may represent the middle and lower crust of accreted island arc(s) and (or) oceanic crust. The Moho is well documented at about 27-km depth. Deep reflection

data beneath the Great Valley (Wentworth and others, 1987) indicate a conspicuous east-dipping band of reflections (g, fig. 8.4A) and less conspicuous subhorizontal and west-dipping reflectors.

Rocks of the Sierran foothills consist of Lower to Upper Jurassic mafic to felsic volcanic and plutonic rocks and related sedimentary rocks (argillite, chert, and flysch) that were accumulated or emplaced in an island-arc setting (Clark, 1964; Schweickert and Cowan, 1975; Saleeby, 1982; Schweickert and Bogen, 1983). The basement and metamorphic wallrocks for the intrusive rocks are tectonically disrupted and polymetamorphosed Paleozoic ophiolitic rocks (approx 300 Ma; Saleeby, 1982).

The island arc(s) in which the Jurassic rocks of the Sierran foothills were formed collapsed against the margin of the North American Continent during the Late Jurassic Nevadan orogeny (Jones and others, 1976). How this collapse occurred is problematic. Steeply east-dipping faults and upright antiforms are seen in the Sierran foothills, but a study by Moores and Day (1984) of surface relations 300 km north of transect C2 indicates obduction of the arc(s) on west-dipping thrust faults. These rocks were intruded during the Early Cretaceous by mafic to intermediate plutons belonging to the western phase of Sierra Nevada plutonism (Evernden and Kistler, 1970).

The deep structure of the Sierran foothills is known from the reconnaissance seismic-refraction experiment of Spieth and others (1981), the reflection profiling of Zoback and Wentworth (1986), and the compilation of reflection, refraction, and potential-field results by Wentworth and others (1987). The refraction data can be modeled with a 6.2-km/s basement from near the surface to about 30-km depth, a 6.6-km/s lower crust, and a Moho at 39-km depth. Other models are possible, however, and the Moho may be as shallow as 30 km (Spieth and others, 1981). We have projected the seismic-reflection results and gravity/magnetic boundary of Wentworth and others (1987) from 45 to 60 km southward onto transect C2. Two conspicuous west-dipping sets of reflections are visible, as well as a few subhorizontal reflectors. The gravity/magnetic boundary, however, has a moderate eastward dip.

Our projection of the results of Wentworth and others (1987) is uncertain not only because of the distances involved but also because their profile terminates on the east in an area that is anomalous both geologically and geophysically. In this area, batholithic rocks (trondhjemite) engulf most accreted rocks of the Sierran foothills (Jennings, 1977) and are associated with a gravity low (Oliver and others, 1980). Our projection, however, may be defensible as follows. (1) The batholithic rocks responsible for the gravity low probably do not extend below 10-km depth (R.C. Jachens, oral commun., 1988); most of the reflectors that we have projected are largely below

that depth. (2) The modeled gravity/magnetic boundary is approximately similar in shape throughout the length of the Great Valley (Andrew Griscorn, oral commun., 1988); in our projection, we have attempted to correct for the difference in azimuth between transect C2 and the profile of Wentworth and others (1987) by assuming a strike parallel to the Great Valley.

Given the geologic and seismic constraints discussed above, we have interpreted the cross section through the Great Valley and Sierran foothills (fig. 8.4B), using some of the ideas of Wentworth and others (1984, 1987) for the configuration of an inferred tectonic wedge of Franciscan rocks, and some of the ideas of Saleeby (1986) for structure within crystalline rocks. The uppermost part of our cross section (to approx 2-km depth) on the east flank of the Diablo Range (fig. 8.4A) was supplied by R.C. Evarts (written commun., 1989). Below this area, we have added a hypothetical west-dipping thrust fault to bring the Great Valley sequence beneath the easternmost block of the Coast Range ophiolite and to grossly satisfy the velocity constraints of Dean Whitman and others (unpub. data, 1985; fig. 8.4A). East of the Coast Range ophiolite, we postulate thrust faults that largely follow bedding planes in the upturned section of the Great Valley sequence, similar to those postulated by Wentworth and others (1984) for the northern Great Valley. These "backthrust" faults are required for emplacement of the wedge and help explain the thickening of the Great Valley sequence in the western limb of the syncline (see section below entitled "Discussion—Tectonic Wedging"). From the easternmost backthrust fault in the Great Valley to the San Andreas fault, we have modeled the discontinuity between variably reflective rocks of lower velocity (Franciscan assemblage, Coast Range ophiolite, and Great Valley sequence; 1.7–5.8 km/s) and poorly reflective rocks of higher velocity (mafic rocks of the Diablo Range and crystalline basement of the Great Valley; 5.5–6.8 km/s) as the floor thrust fault of the wedge. Wentworth (1987) presented a similar interpretation.

The details of composition and structure in the crystalline rocks beneath the Great Valley and Sierran foothills are speculative. Saleeby (1986) interpreted these rocks to consist fundamentally of slabs or nappes of island-arc and oceanic rocks obducted along west-dipping Nevadan thrust faults intruded by chiefly Early Cretaceous Sierran granitic plutons. We have adopted this basic scheme and added some details, interpreting layers 1 and 2 in the basement beneath the Great Valley (5.5–6.3 km/s; see above) as post-Nevadan felsic plutonic rocks, although, as noted above, the western part of layer 1 (5.5 km/s) may be Franciscan assemblage. We interpret the east-dipping gravity/magnetic boundary of Wentworth and others (1987) as the average top of mafic crust

(pre-Nevadan gabbro, diabase, or basalt) in the inferred obducted sequence. Alternatively, this boundary may be the average top of mafic, magnetic intrusions in the crust (post-Nevadan gabbro) or the average base of felsic, nonmagnetic intrusions (post-Nevadan granitic rocks). At the location where this boundary was actually modeled, it may be the average base of a large trondhjemite intrusion. We associate the east-dipping reflections beneath the central Great Valley (g, fig. 8.4A) with the thin, discontinuous 7.0-km/s layer of Holbrook and Moonhey (1987), although the depth correspondence is imperfect, and we interpret this feature as a gabbroic dike. Alternatively, these east-dipping reflections may represent an east-dipping fault zone. Following Saleeby (1986), we correlate the upper and lower west-dipping bands of reflections in the eastern Great Valley and Sierran foothills (h, j, fig. 8.4A) with the Bear Mountain and Melones fault zones, which may represent Cenozoic reactivations of inferred west-dipping Nevadan thrust faults.

DISCUSSION—TECTONIC WEDGING

GEOLOGIC HISTORY

Wentworth and others (1984) interpreted the juxtaposition of Franciscan assemblage and a coeval section consisting of Coast Range ophiolite and Great Valley sequence as having occurred during landward movement of the Franciscan assemblage as a tectonic wedge. They reinterpreted the "Coast Range thrust fault" of Bailey and others (1970), a subduction megathrust between the Coast Range ophiolite and the Franciscan assemblage, as the roof thrust of the wedge. More recently, the thrust nature of the "Coast Range thrust fault" has been reevaluated. Jayko and others (1987), testing an hypothesis by Platt (1986), produced abundant evidence that the contact between Franciscan assemblage and Coast Range ophiolite is a detachment surface along which the upper plate was extended during uplift of the Franciscan assemblage. Their evidence is the consistent attenuation, as opposed to repetition, of geologic section across this discontinuity and associated faults above it. They proposed the term "Coast Range fault" for this discontinuity, which we adopt here. Evidence of attenuation is present even on transect C2, in that the two outcrops of the Coast Range ophiolite in the eastern Diablo Range (fig. 8.4A) represent an abridged section of ophiolite: The western outcrop is partially serpentized ultramafic rock of the basal part of an ophiolite, whereas the eastern outcrop is the sill complex and volcanic flows of the upper part of an ophiolite. These two parts of the ophiolite are now juxtaposed across the crooked, steeply dipping Tesla-Ortogonalita fault. Although this fault now offsets the

Coast Range fault, it may represent reactivation of a normal fault that originally soled into the Coast Range fault (compare Raymond, 1973).

The extensional nature of the Coast Range fault poses several problems for emplacement of the Franciscan assemblage as a tectonic wedge. Where is the roof thrust fault of the wedge? How did the Franciscan assemblage reach its current position with an extended overlying section of the Coast Range ophiolite and Great Valley sequence? Was the Franciscan assemblage uplifted from beneath the western Great Valley? The apparent continuity between the Great Valley basement and the 6.7- to 7.1-km/s layer in the Diablo Range indicates a negative answer to the last question.

These problems can be solved if the extensional event was separated in time and space from the compressional event, or tectonic wedging. Jayko and others (1987) reviewed the published evidence regarding the geologic history of extensional faulting. In one place, the Coast Range fault and associated faults are overlapped by sedimentary rocks of Oligocene and younger age, and in another place by sedimentary rocks of Paleocene and younger age. The occurrence of detritus derived from the Franciscan assemblage in Paleocene and Eocene strata of the Coast Ranges (Dickinson, 1966; Berkland, 1973) indicates that the lower plate was exposed by the early Tertiary. Jayko and others (1987) inferred that uplift of the Franciscan assemblage and associated extensional faulting in the upper plate occurred during the Late Cretaceous and (or) early Tertiary.

The history of compressional tectonics in the Coast Ranges is sparse and varies from place to place. In the northern Coast Ranges, thrust faulting and folding began during the early Tertiary (Blake and others, 1987; M. C. Blake, Jr., oral commun., 1989), and compressional deformation is continuing today in rocks of the northern Great Valley (Harwood and Helley, 1987). In the southern Coast Ranges, at least four Cenozoic deformations or uplifts, indicated by unconformities or eastward-migrating depocenters, have ages of late Paleocene, late Eocene to early Miocene, late Miocene, and late Pliocene (Namson and Davis, 1988; Namson and others, 1990; Rentschler and Bloch, 1988). Modern thrust faulting and folding still is occurring, as indicated by the 1983 Coalina earthquake (see chap. 5; Eaton, 1990).

Landward movement of the Franciscan assemblage as a wedge may have even begun in the Mesozoic. In the northern Coast Ranges, several northwest-striking faults (Paskenta, Elder Creek, and Cold Fork faults) offset rocks structurally above the Franciscan assemblage (but not the Franciscan assemblage itself) and represent major discontinuities in the depositional environment of the Great Valley sequence (Jones and Irwin, 1971). These faults, which have displacements of tens of

kilometers to as much as 100 km, are interpreted to have moved primarily during the Cretaceous (Jones and Irwin, 1971), although the latest limit on the time of movement is about 3.4 Ma (Hardwood and Helley, 1987; M. C. Blake, Jr., oral commun., 1989). Wentworth and others (1984) and Jayko and others (1987) interpreted these faults as tear faults in the plate structurally above a wedge of Franciscan assemblage.

In light of the above data and interpretations, we postulate (1) that uplift of the Franciscan assemblage and extension of the upper plate, consisting of Coast Range ophiolite and Great Valley sequence, occurred during the Cretaceous (or, at the latest, during the early Tertiary, if Cretaceous movement on the Paskenta-Cold Fork fault system is not linked to landward wedge transport) well west of the present Diablo Range; and (2) that a tectonic wedge of Franciscan assemblage was subsequently driven landward, with the extended upper plate riding passively atop it. This wedge is interpreted to have moved along a floor thrust fault aligned with the contact between the Great Valley sequence and its crystalline basement. To the west of the present Diablo Range, where movement initiated, the basement was an outboard part of the Coast Range ophiolite. Beneath the Great Valley, where the movement is presently occurring, the basement is similar to the Coast Range ophiolite but contains numerous younger plutons. A roof thrust fault apparently developed only near the east tip of the wedge (fig. 8.4B); presumably, erosion kept pace with uplift near the tip. Differential vertical or horizontal movements of the wedge may have produced tear faults, such as the Paskenta, Elder Creek, and Cold Fork faults, and may have reactivated extensional faults to produce complex faults, such as the Tesla-Ortogonalita fault.

PAST AND PRESENT TECTONIC REGIMES

The Mendocino triple junction has moved northward through offshore central California during approximately the past 20 Ma, and subduction of the Farallon plate (or its derivative) was replaced by transform motion of the Pacific plate past North America (see chap. 3; Atwater, 1970, 1989). If tectonic wedging occurred during the late Mesozoic and Cenozoic, in association with all of the episodes of tear faulting or compression outlined above, then clearly it was driven during both subduction and transform regimes. At present, it is being driven by a transform regime. At least two additional arguments can be made that wedge motion—indeed, probably a major fraction of wedge motion—occurred during the subduction regime. The first argument is simply based on geometry: The east boundary of the Coast Ranges, inferred to coincide approximately with the buried tip of the wedge, largely parallels Mesozoic structures in the

Sierran foothills and the Great Valley rather than the late Cenozoic San Andreas fault (Wentworth and Zoback, 1989; C.M. Wentworth, oral commun., 1990). The second argument, developed below, is based on the total apparent displacement of the wedge.

If the inferred tectonic wedge of Franciscan assemblage extends to the San Andreas fault, as we have shown (fig. 8.4B), then a minimum shortening of about 70 km has occurred along faults at the top and bottom of the wedge in the Diablo Range. Likewise, in the northern Coast Ranges, the inferred tear faults in the plate above the wedge have a total displacement—and, thus, shortening—of many tens of kilometers (Wentworth and others, 1984), possibly as much as 100 km (Jones and Irwin, 1971).

Although a transform regime has replaced a subduction regime in central California over approximately the past 20 Ma, plate-margin compression, necessary to drive the wedge, has persisted for only approximately the past 5 Ma (Page and Engebretson, 1984). At about 5.5–4.5 Ma, transform motion was also transferred from offshore faults to the modern San Andreas fault system (see chap. 3; Atwater, 1989; Humphreys and Weldon, in press). Present plate-margin compression is understandable from (1) the slight misalignment of the direction of relative plate motion (N. 35° W.; Minster and Jordan, 1978) and the strike of the San Andreas fault (N. 40° W.), and (2) the opening of the Basin and Range province. Crouch and others (1984) calculated from these two effects a rate of shortening across the Coast Ranges that, integrated over the past 5.5 Ma, predicted a total shortening of 28 to 72 km. Most of this shortening could be accounted for in small fault displacements and folds distributed throughout the Coast Ranges (Crouch and others, 1984). Thus, the minimum shortening of 70 to 100 km represented by the tectonic wedge, as discussed above, would appear to equal or exceed the maximum shortening calculated for the transform regime, a result suggesting that some, if not most, of the wedge motion occurred during the subduction regime.

Shear coupling between the subducting plate and overlying accretionary prism (Franciscan assemblage) could conceivably drive the wedge during the subduction regime. Such a mechanism has been postulated for southern Alaska by Fuis and Plafker (in press). To drive the wedge during a transform regime appears to require a less obvious mechanism, such as plate-margin compression combined with differing deformation in the upper and lower crust. Such a mechanism is developed below.

Sibson (1982) pointed out, on the basis of strength considerations, that ductile flow could be expected in the middle crust, below the maximum depth of earthquake hypocenters. Several workers (Crouch and others, 1984; Namson and Davis, 1988; Eaton and Rymer, in press)

have postulated a decollement near the base of the seismicity in the Coast Ranges (avg 15-km depth; see chap. 5; Wesson and others, 1973) into which thrust and oblique-slip faults on both sides of the Coast Ranges sole. They envision differential movement between upper and lower crust caused by differing alignment of the transform faults in these two layers, or by shortening of the lower crust by ductile thickening.

We have incorporated the idea of a Coast Range-wide detachment in our cross section (fig. 8.4B). In the Diablo Range, we show a young thrust fault at the base of the inferred tectonic wedge soling into the brittle-ductile transition zone, which in this area is, coincidentally, near the interface between Franciscan rocks and mafic crust. Although we also indicate soling of the San Gregorio-Hosgri fault into such a zone and underthrusting of the Salinian block by the early Tertiary accretionary prism, focal mechanisms in this region indicate pure strike slip on the San Gregorio-Hosgri fault (see chap. 5) and argue against this interpretation. Such an interpretation of a Coast Ranges-wide midcrustal detachment requires that the deformational style and (or) location of the San Andreas fault system change from the upper to the lower crust.

If we have correctly inferred the geologic history of wedge movement, it is remarkable that such movement has apparently occurred in two quite different tectonic regimes, a subduction regime and a transform regime.

SOUTHERN CALIFORNIA

The crustal structure of southern California is complicated by the Big Bend in the San Andreas fault, situated between the Coast Ranges and Transverse Ranges, and by onshore spreading centers of the East Pacific Rise, situated in the Salton Trough (figs. 8.2, 8.3). The Big Bend is thought to result from westward movement of the Sierra Nevada relative to the Mojave Desert, along the Garlock fault (Hill and Dibblee, 1953). The San Andreas fault crosses the Transverse Ranges, between the Big Bend and Salton Trough, at an angle oblique to relative plate motion, while somehow remaining a largely vertical, strike-slip fault.

The onshore spreading centers in the Salton Trough are situated at echelon offsets between the San Andreas, Imperial, and Cerro Prieto faults (see fig. 3.8; Lomnitz and others, 1970). These three faults are interpreted as transform faults; the San Andreas links the northernmost spreading center in the Salton Trough with the Mendocino triple junction. A progressive decrease in spreading rate northward along the East Pacific Rise is inferred to give rise to movement on the San Jacinto, Elsinore, San Miguel/Newport-Inglewood, and other faults in southern

California and Mexico (Lomnitz and others, 1970; Elders and others, 1972).

First, we discuss a transect across southern California, Centennial Continental-Ocean Transect C3 (Howell and others, 1985). Second, because of the three-dimensionality of the geology and tectonics in southern California, we include a discussion of block motions, largely from Weldon and Humphreys (1986).

TRANSECT C3

We modify and reinterpret the section of Centennial Continent-Ocean Transect C3 (Howell and others, 1985) that extends from Santa Catalina Island to the Colorado Desert (fig. 8.2). This section of the transect crosses four blocks or provinces, the California Continental Borderland (hereafter referred to simply as the "borderland"), Peninsular Ranges, Salton Trough, and Chocolate Mountains (fig. 8.6). The transect crosses the Newport-Inglewood, Elsinore, San Jacinto, and Imperial strike-slip faults. Constraints for the transect include surface geology, isotopic studies, seismic-refraction profiling (which is sparse, except in the Salton Trough), tomographic studies, and potential-field studies.

BORDERLAND

The borderland is broken up by right-slip faults into several northwest-trending blocks. Our cross section (fig. 8.6) begins on the easternmost block, the "Catalina terrane" (Howell and others, 1985), bounded on the east by the Newport-Inglewood fault. The Catalina terrane is underlain, beneath patches of Tertiary volcanic rocks, by Franciscan assemblage, on the basis of outcrops on Santa Catalina Island (Platt, 1975, 1976; Jones and others, 1976) and submarine dredge and core samples (Vedder and others, 1974). The block west of the Catalina terrane, the "San Nicholas terrane" (Howell and others, 1985), is inferred to be underlain, beneath Cenozoic marine sedimentary rocks, by rocks similar to the Great Valley sequence and Coast Range ophiolite of central California, possibly in fault contact with Franciscan assemblage at depth (Vedder and others, 1974).

A reversed seismic-refraction profile just west of Santa Catalina Island indicates *P*-wave velocities of 5.8 km/s to 6-km depth and of 6.7 km/s to the Moho at about 24-km depth (fig. 8.6A, Shor and Raitt, 1958). This velocity-depth section is similar to that for the Diablo Range of central California (see above), where Franciscan rocks are equated with the 5.8-km/s interval, and middle and lower crust of island arc(s) and (or) oceanic crust are equated with the 6.7-km/s interval. In this region, there is no clear evidence of landward movement of the Franciscan assemblage as a tectonic wedge, although

such evidence may surface during future investigations. As in the Diablo Range, the lower crust must have been brought to its present 18-km thickness by (1) imbrication of slices of island-arc crust, (2) tectonic underplating of several thicknesses of oceanic crust, and (or) (3) magmatic underplating. Subduction continued beneath the borderland until sometime between 30 and 20 Ma (see Atwater, 1970), depending on the latitude to which the borderland is palinspastically restored.

PENINSULAR RANGES

The Peninsular Ranges are underlain in the west by supracrustal rocks, including, from top to bottom, Cenozoic marine sedimentary rocks, Cretaceous forearc sedimentary rocks, Lower(?) Cretaceous and Upper Jurassic andesite (Santiago Peak Volcanics), and Middle Jurassic flysch (Bedford Canyon Formation) that was disrupted and overturned before the Late Jurassic (Larsen, 1948; Jennings, 1977; Criscione and others, 1978). These rocks are intruded by Early Cretaceous plutons of the Peninsular Ranges batholith that include chiefly tonalite and gabbro and show no special age trends (static magmatic arc; Silver and others, 1979). About 80 km east of the coastline, both prebatholithic and batholithic rocks change (fig. 8.6A): To the east, the prebatholithic rocks are dominantly metamorphosed clastic rocks of amphibolite grade, and the batholithic rocks are chiefly tonalite and granodiorite whose ages decrease progressively eastward (from 105 to 80–90 Ma; migrating magmatic arc; Silver and others, 1979). Major-element chemistry and oxygen isotopes indicate that deep crustal rocks in the west half of the batholith are dominantly primitive and tholeiitic but, in the east, more aluminous and oxidized (fig. 8.6A). Older crust that was once at the Earth's surface is inferred at depth in the east (Silver and others, 1979).

Seismic constraints for the deep structure of the Peninsular Ranges are sparse. Using blasts at the Corona Quarry in the northernmost Peninsular Ranges, Gutenberg (1951) and Shor (1954) obtained an unreversed refraction profile, extending southward to the United States-Mexican border, along with a reflection record at the blast site. Interpretation of these data by Shor and Raitt (1958) indicated velocities of 5.9 km/s to 8-km depth, 6.8 km/s to 26-km depth (with a possible low-velocity zone in this interval), and 7.0 km/s to the Moho at 30- to 32-km depth (fig. 8.6A). In contrast, a study by Nava and Brune (1982) using a blast at the same quarry, reversed by an earthquake in Baja, Mexico, indicated a Moho depth of 42 km. Hearn and Clayton (1986a, b) used as many as 600,000 arrivals from local earthquakes in southern California to map the velocity of the crust and upper mantle, using tomography. Their map indicates

that the west half of the Peninsular Ranges has a higher average upper-crustal velocity and a lower average mantle velocity in comparison with the east half. Their map of P_n delays for the Peninsular Ranges suggests no crustal root and an average crustal thickness of nearly 30

km. Gravity modeling of the Peninsular Ranges (Fuis and others, 1984) and isostatic calculations also indicate a maximum crustal thickness of 30 to 33 km. In our cross section (fig. 8.6B), we adopt a maximum crustal thickness of 33 km.

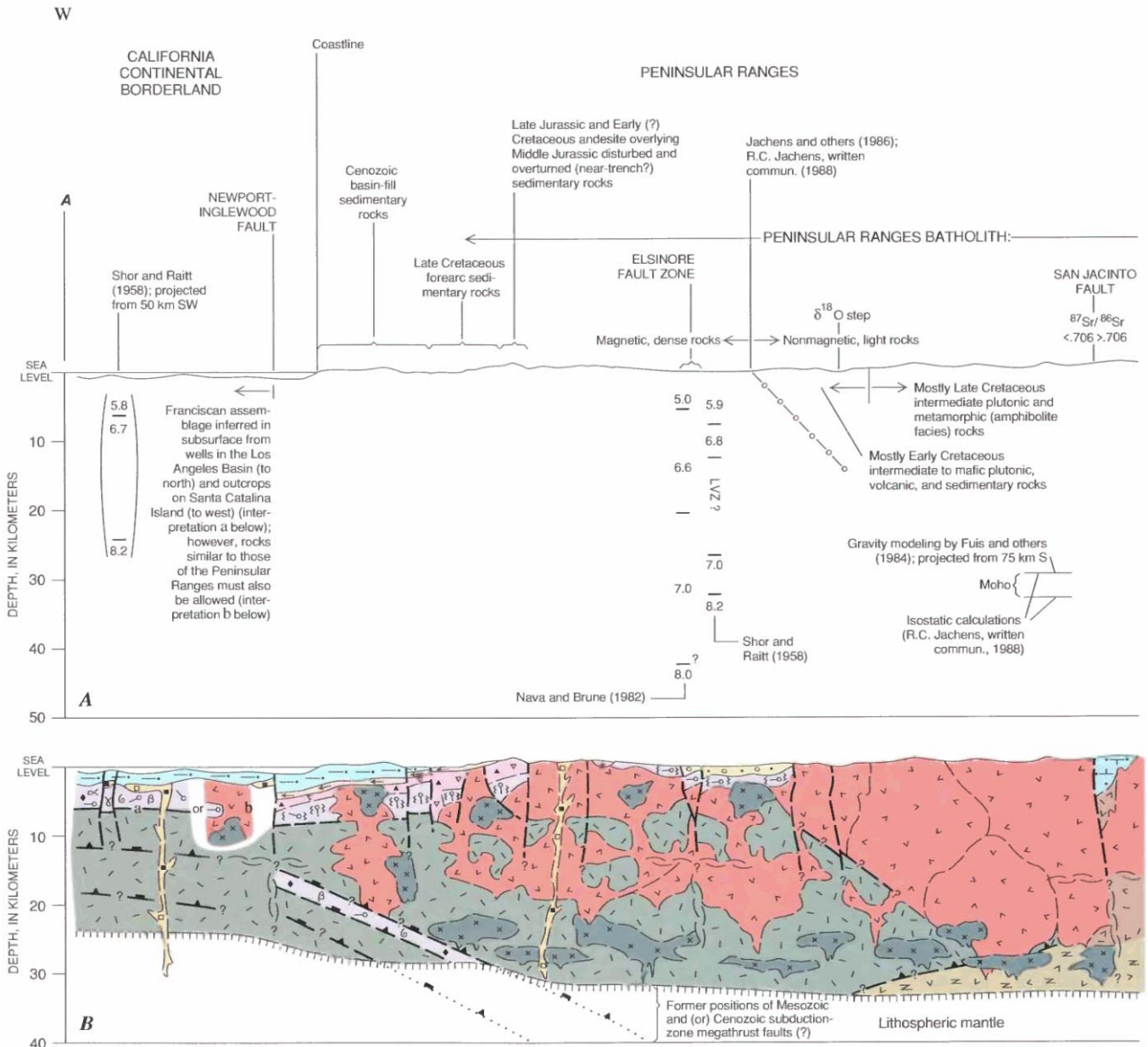
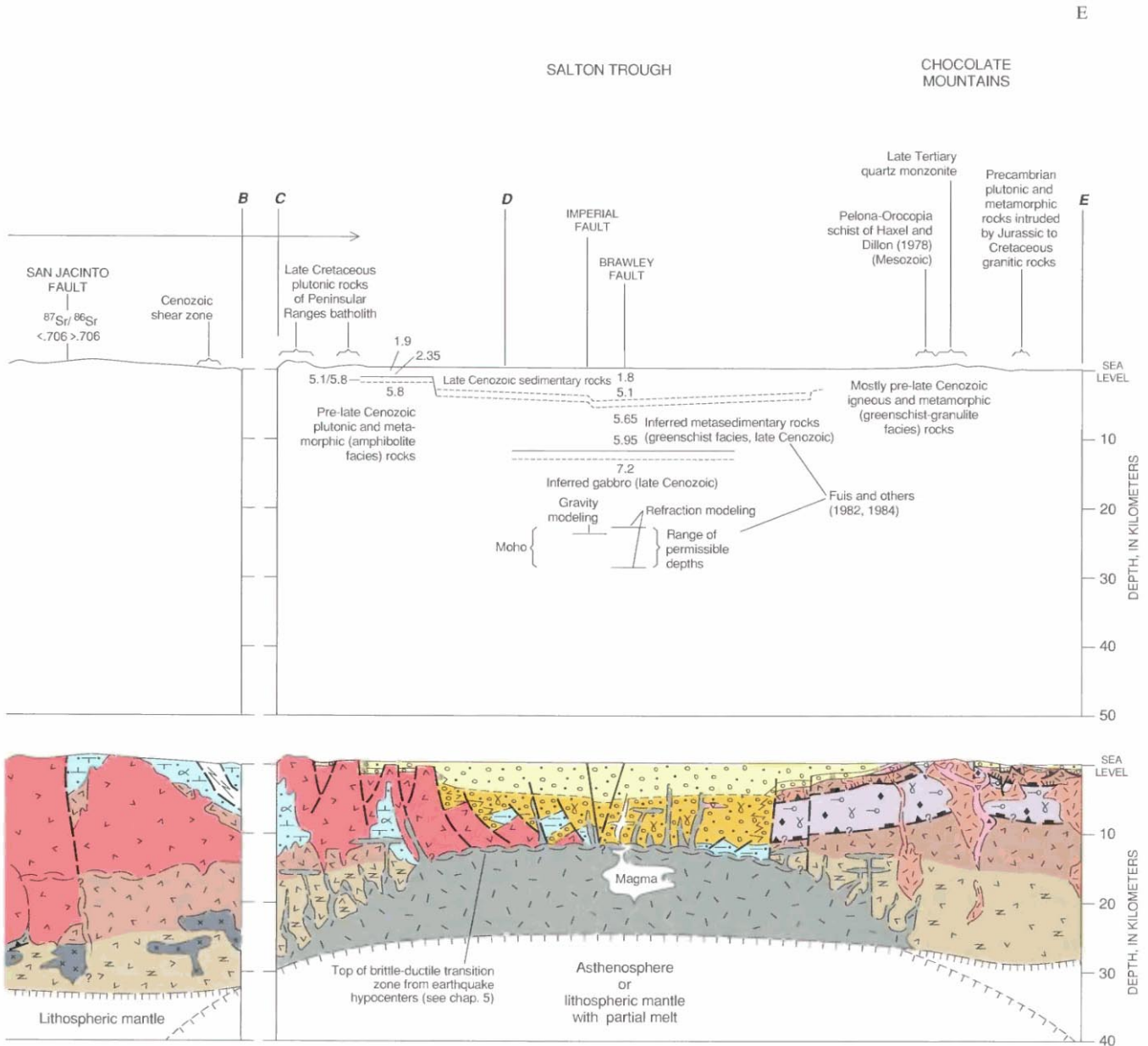


FIGURE 8.6.—Crustal structure of southern California. A, Surface geology, isotope data, and models of seismic-refraction, gravity, and magnetic data for part of Centennial Continent-Ocean Transect C3 (see Howell and others, 1985). B, Reinterpretation of Transect C3. Major features in figure 8.6B include, from west to east, (1) Franciscan assemblage overlying mafic crust in the borderland; (2) Peninsular Ranges batholithic block, consisting of

west half inferred to be underlain at depth by mafic (island arc or oceanic) crust and east half inferred to be underlain at depth by intermediate continental Precambrian(?) rocks; (3) late Cenozoic rift, the Salton Trough, whose central part is inferred to be underlain by entirely new crust that includes, from top to bottom, sedimentary rocks, thermally metamorphosed sedimentary rocks, and gabbro generated at onshore

An additional constraint on crustal structure is the modeling by Jachens and others (1986; R.C. Jachens, written commun., 1988) of strong magnetic and gravity steps (500 nT and 40 mGal, respectively) in the central Peninsular Ranges: A moderately east dipping boundary

is modeled between more magnetic, dense rocks on the west and less magnetic, lighter rocks on the east. This boundary is poorly defined at the latitude of our transect; it correlates approximately (within 15 km or so) with the boundary between the east and west halves of the



spreading center; and (4) Pelona-Orocopia schist of Haxel and Dillon (1978) (similar to the Franciscan assemblage), interpreted to compose tectonic wedge. Tectonic wedge in feature 4 is postulated to have been obducted onto continental crust (see text); its tip would lie well east of east end of cross section. This reinterpretation differs from Howell and others' (1985)

primarily in interpreting mafic crust at shallower depths beneath the borderland and western Peninsular Ranges (5–8 km versus 11–15 km) to better match seismic and potential-field results. See figures 8.2 and 8.3 for location of Transect C3; see figure 8.4 for explanation. No vertical exaggeration.

Peninsular Ranges batholith, as discussed above (fig. 8.6A). In the cross section (fig. 8.6B), we interpret an eastward deepening of mafic rocks, including prebatholithic and (or) batholithic mafic rocks (gabbro, diabase, and metamorphic rocks), along this magnetic/gravity boundary. R.C. Jachens (oral commun., 1989) indicated that, in some places, this boundary is so planar as to be interpretable as a fault. As beneath the borderland, the mafic rocks beneath the Peninsular Ranges may have reached their current thickness by thrust imbrication, tectonic underplating, or magmatic underplating. We speculatively show some tectonic underplating on the west side.

SALTON TROUGH

The Salton Trough is the landward extension of a ridge/transform-fault system, the East Pacific Rise, of the Gulf of California (see fig. 3.13). This system became well established during the late Cenozoic (approx 5 Ma) as the plate boundary jumped inland from offshore Baja California (Atwater, 1970, 1989; Humphreys and Weldon, in press).

The Salton Trough is underlain by upper Cenozoic sedimentary rocks and minor amounts of volcanic rocks, which are exposed chiefly around its edge and are penetrated in wells. Onset of rifting and major subsidence in the Salton Trough was followed by marine incursion during the latest Miocene to late(?) Pliocene, as indicated by the Imperial Formation (Dibblee, 1954; Powell, 1984). The thick Cenozoic sedimentary section is offset by Quaternary faults, both exposed and buried, and is intruded by Quaternary volcanic rocks, both silicic rocks that form volcanoes at the two inferred onshore spreading centers (fig. 8.7) and mafic rocks that are penetrated in geothermal wells (Elders and others, 1972; Robinson and others, 1976). Faulting in the Salton Trough occurs primarily on conjugate northwest- and northeast-striking faults and is largely strike slip (Johnson and Hadley, 1976; Johnson, 1979; Fuis and others, 1982). North-south-striking faults, however, such as the north end of the Imperial fault, the Brawley fault, and north-south-striking seismicity lineaments (that outline inferred spreading centers; figs. 8.1, 8.7), have normal components and lead to the subsidence that ultimately created the Salton Trough. Earthquake hypocentral depths indicate that brittle fault motion extends to about 12-km depth in the Imperial Valley but deeper in the adjacent Peninsular Ranges along the San Jacinto fault (Doser and Kanamori, 1986).

Detachment faulting on the east flank of the Salton Trough, in the Chocolate Mountains and other ranges, preceded the Pliocene and later basin-forming tectonics in the Salton Trough (Dillon, 1975; Berg and others, 1982;

Frost and others, 1982). Similar faulting on the west flank of the Salton Trough, however, may have both preceded and overlapped in time the tectonics in the Salton Trough (Wallace and English, 1982; Schultejaahn, 1984; Isaac and others, 1986).

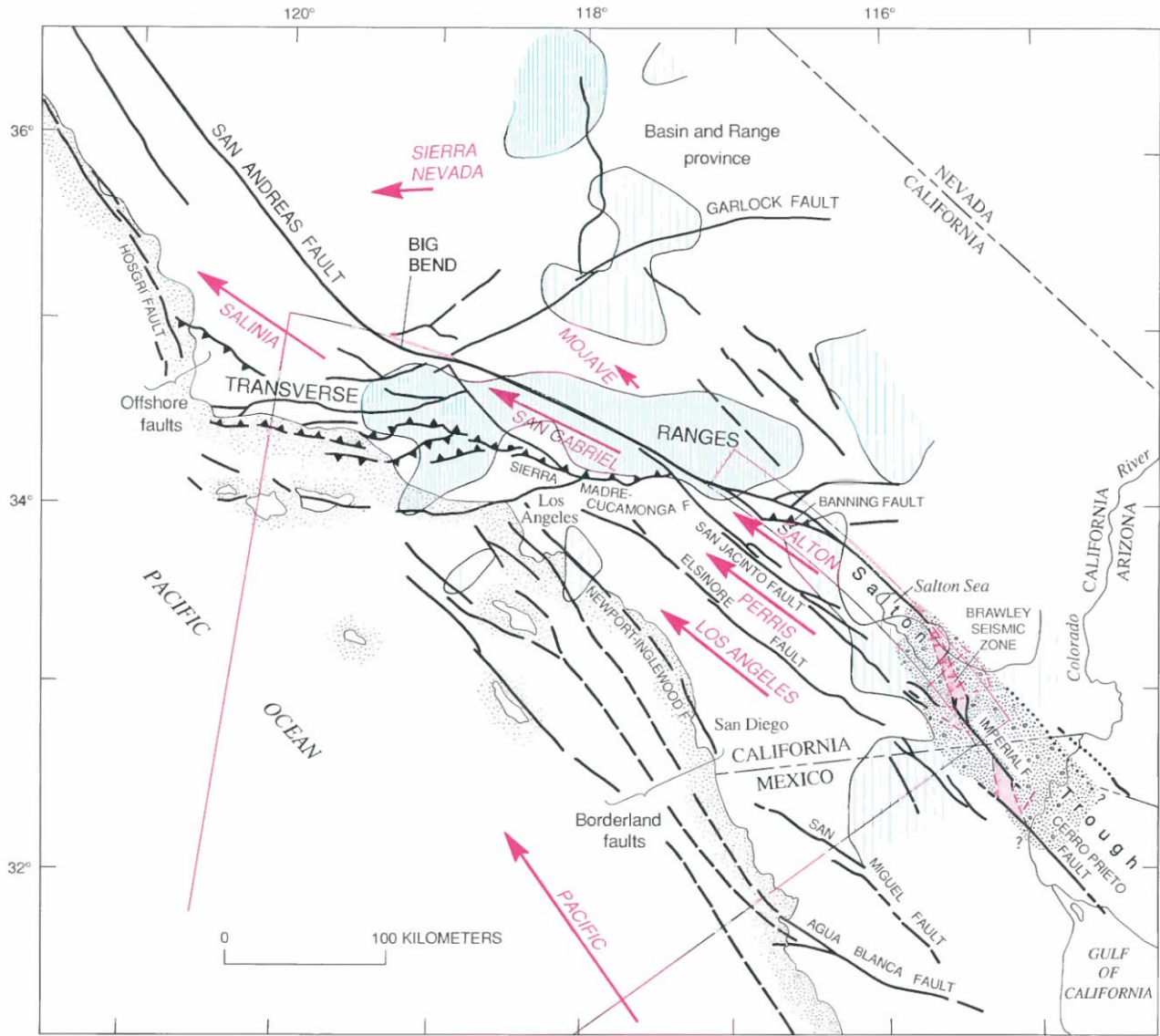
Biehler and others (1964) and Fuis and others (1982, 1984) demonstrated from seismic surveys that the sedimentary rocks (1.8–5.5 km/s) in the central Salton Trough are as much as 5 km thick (fig. 8.6A). Below 5-km depth, a low-velocity (5.6 km/s) “basement,” which is not separated from the overlying sedimentary rocks by a velocity discontinuity, is inferred to be metamorphosed (greenschist facies) sedimentary rocks (Fuis and others, 1982, 1984); this “basement” layer extends to 12-km depth. High heat flow in the Salton Trough (see Lachenbruch and others, 1985) is inferred to cause the metamorphism of the sedimentary rocks. Thus, the entire section of inferred upper Cenozoic sedimentary rocks, metamorphosed and unmetamorphosed, is as much as 12 km thick.

Below 12- to 14-km depth in the Salton Trough, a high-velocity (7.1–7.2 km/s) “subbasement” that is indicated by seismic-refraction data (fig. 8.6A) is inferred to be gabbro generated at one of the nearby spreading centers (Fuis and others, 1982, 1984). Modeling of seismic-refraction and gravity data indicate that the Moho in the central Salton Trough is 23 to 28 km deep (Fuis and others, 1982, 1984). The central Salton Trough is interpreted to be underlain entirely by late Cenozoic crust (fig. 8.6B).

Buried scarps separating old crust (plutonic and metamorphic rocks; 5.9–6.0 km/s) from new crust (sedimentary and basaltic rocks; 1.8–7.2 km/s) are visible by seismic methods on both sides of the Salton Trough (Fuis and others, 1982; Fuis and Kohler, 1984). On the west side of the rift, where the new-crust/old-crust boundary is ragged in outline (fig. 8.7), we interpret normal faults

FIGURE 8.7.—Tectonic block motion in southern California (modified from Weldon and Humphreys, 1986, and Humphreys and Weldon, in press). Various blocks (italicized names near motion vectors) move through region where the San Andreas fault trends obliquely to plate motion, between the Big Bend and the Salton Trough, without major convergence with each other. Through this region they move counterclockwise, following nearly concentric arcs (arcs and radii, thin red lines). New crust, which is forming in wake of the Salton and Perris blocks in the Salton Trough, is created by sedimentary-basin fill and gabbroic intrusions at onshore spreading centers, outlined by seismicity lineaments. High-velocity mantle beneath the Transverse Ranges is interpreted as cold, sinking lithospheric mantle, and low-velocity mantle beneath the Salton Trough as hot upwelling asthenosphere or lithospheric mantle containing partial melt (Humphreys and others, 1984; Humphreys and Clayton, in press). Motion vectors for the Mojave Desert and Sierra Nevada modified to incorporate results of Sauber and others (1986).

(fig. 8.6B); on the east side, where this boundary is linear, we interpret a strike-slip fault. In our cross section, faults on the west side of the Salton Trough are inferred to have originated by pullaway from the Cerro Prieto spreading center to the southeast; the fault on the east side is inferred to be a largely passive suture (figs.



EXPLANATION

- Motion vector of tectonic block—
Relative to North America
Vector scale 20 mm/yr
- New crust (late Cenozoic)
- Onshore spreading center
- High-velocity mantle
- Low-velocity mantle
- Seismicity lineament
- Fault—Dashed where approximately located; dotted where buried
- Thrust fault—Dashed where approximately located. Sawteeth on upper plate

8.6B, 8.7; Fuis and others, 1982). A similar rift configuration is seen, for example, in the Gulf of Elat (Gulf of Aqaba, Red Sea; Ben-Avraham, 1985).

CHOCOLATE MOUNTAINS

Rocks on the east flank of the Salton Trough are igneous and metamorphic rocks that compose two or more fault-bounded packages, or tectonostratigraphic terranes (see Howell and others, 1985). A complex of metasedimentary and mafic metaigneous rocks described by Dillon (1975) may include two Precambrian terranes, the Joshua Tree and San Gabriel terranes, described farther north by Powell (1981). This complex is intruded by intermediate to felsic Mesozoic plutons and rests on the low-angle Chocolate Mountains thrust fault above the (informal) Pelona-Orocopia schist of Haxel and Dillon (1978; see also Haxel, 1977). The Pelona-Orocopia schist consists chiefly of metagraywacke and lesser metapelite, metabasite, metachert, marble, and serpentinite (albite-epidote-amphibolite facies) of uncertain but probable late Mesozoic or early Tertiary age (Conrad and Davis, 1977; Miller and Morton 1977, 1980). It resembled the Franciscan assemblage but lacks melange.

Many workers have speculated on the depositional environment and origin of the Pelona-Orocopia schist. Haxel and Dillon (1978) postulated formation in an ensimatic rift basin with continent on both sides—not unlike the current Salton Trough. Powell (1981) favored an origin as a parautochthonous continental-marginal deposit. In any case, from its quartz content, the Pelona-Orocopia schist clearly originated near a continent and incorporated continental detritus. It was thrust beneath the continental metasedimentary-metigneous complex some time after Mesozoic plutonism (80 Ma; Powell, 1981) and before Oligocene volcanism (35 Ma; Crowe 1978; Crowe and others, 1979). The thrust fault may have been reactivated one or more times as a low-angle normal, or detachment, fault (Frost and others, 1982).

Evidence from refraction profiling in the western Mojave Desert across the Rand schist, which has been correlated with the Pelona-Orocopia schist (Ehlig, 1968), indicates relatively low-velocity crust beneath this body (max 6.4 km/s; Fuis and others, 1986) that we infer to be continental crust. We speculate that the Pelona-Orocopia schist also rests on continental crust and that the Rand and Pelona-Orocopia schists were emplaced as a tectonic wedge into continental crust in a manner similar to the Franciscan assemblage of central and northern California. We hypothesize that the metasedimentary-metigneous complex structurally above the schist is analogous to either (1) rocks of the Coast Range ophiolite/Great Valley sequence which rode passively atop the wedge in

central and northern California after being extended during uplift of the Franciscan assemblage, or (2) rocks of the Great Valley sequence which were peeled up along backthrust faults during landward movement of the wedge. In southern California, tectonic wedging clearly occurred before the present transform regime, presumably during subduction of the Farallon plate (or its derivative). The geologic data discussed above indicate that the Salton Trough has undergone extension, rather than compression, for approximately the past 5 Ma (probably even longer; see Humphreys and Weldon, in press).

Crustal thickness is unknown in the Chocolate Mountains; however, the Colorado Desert, to the east and north, has a generally thin (26–28 km) crust (fig. 8.3) and a local root (32 km deep) under the Whipple Mountains metamorphic-core complex (Fuis, 1981; Jill McCarthy, written commun., 1988).

TECTONICS—THE THREE-DIMENSIONAL PICTURE

The geology and, presumably, the deep structure of southern California illustrated along transect C3 (fig. 8.6) is grossly two dimensional as far north as the Transverse Ranges. In the Transverse Ranges, the rocks on the southwest side of the San Andreas fault are similar to those in the Chocolate Mountains. These rocks are bounded on the south and west by older, deformed strands of the San Andreas fault system (fig. 8.7; Powell, 1981). The tectonics also changes in the Transverse Ranges: Crustal-block motion swings to the west to follow the trend of the San Andreas fault, as discussed below.

Using Quaternary geologic and geodetic evidence, Weldon and Humphreys (1986) documented complex motion of crustal blocks in southern California that is not simply predictable from the motion vectors of the Pacific and North American plates. These motion vectors predict a large component of convergence across the San Andreas fault in the Transverse Ranges between the Big Bend and the Salton Trough (fig. 8.7). For a total offset on the San Andreas fault system of about 300 km (Hill and Dibblee, 1953; Crowell, 1962, 1981; Powell, 1981), a maximum of 45 km of uplift in the Transverse Ranges would be expected (Weldon and Humphreys, 1986). However, the preservation in the Transverse Ranges of upper Cenozoic sedimentary rocks and of offset bedrock features on either side of the San Andreas fault argues against such major uplift and associated consumption of crust, as does the relatively minor crustal root in the Transverse Ranges (fig. 8.3). Weldon and Humphreys (1986) constructed a kinematic model in which crustal blocks between the San Andreas fault and a system of borderland and other offshore faults rotate counterclock-

wise, parallel to the San Andreas fault, between the Salton Trough and the Big Bend (fig. 8.7). Approximately two-thirds of the relative northwestward motion of the Pacific plate past the North American plate is taken up by the San Andreas fault system, including the San Jacinto fault; approximately one-third of it is taken up by the Elsinore fault, a system of borderland faults, and offshore faults in central California, including the San Gregorio-Hosgri fault (fig. 8.7); and only a minor fraction of it is taken up within the blocks (see Humphreys and Weldon, in press).

A marked advance in the *P*-wave traveltimes of teleseismic arrivals in southern California is associated with the Transverse Ranges and extends across the San Andreas fault (Hadley and Kanamori, 1977; Raikes, 1980). Tomographic analysis of this anomaly indicates that it results from a vertical slablike region of relatively high velocity in the mantle which extends downward as far as 250 km (Humphreys and others, 1984; Humphreys, 1985; Humphreys and Clayton, in press). The amount of velocity increase, a maximum of 3 percent, is most reasonably explained by a thermal difference in the mantle. This velocity increase, coupled with a velocity decrease in the upper 90 km or so of mantle beneath the Salton Trough, led Humphreys and Hager (1984 and in press) to infer small-scale mantle convection between the Salton Trough and the Transverse Ranges. This convection involves passive rising of asthenosphere beneath the Salton Trough and cooling and sinking of lithosphere beneath the Transverse Ranges. The vertical extent of the inferred lithospheric slab beneath the Transverse Ranges, 250 km, is similar to the 300-km estimate of total offset along the San Andreas fault system. However, because the cooled mantle slab extends across the San Andreas fault, most of the mantle seems to be moving independently of the crust (fig. 8.8; Hadley and Kanamori, 1977; Humphreys and others, 1984; Humphreys, 1985; Humphreys and Hager, in press). The horizon of decoupling is apparently at or below the Moho because crustal material is not entrained in the slablike feature. Additional decoupling may be occurring in the crust, similar to that postulated for central California (Yeats, 1981; Webb and Kanamori, 1985). Decoupling at the Moho requires that the deformational style and (or) location of the San Andreas fault system change from the crust to the mantle (fig. 8.8). We note that mantle drag on the crust is required to maintain the Big Bend in the San Andreas fault because plate-edge forces alone would tend to "short-circuit" the San Andreas fault south of the Big Bend and cause most plate motion to be taken up on the San Jacinto, Elsinore, or more westerly faults (Kosloff, 1978; Humphreys, 1985).

To summarize, block motions in the region between the Big Bend and the Salton Trough result in only minor

interblock convergence in the crust. In contrast, major convergence in the lithospheric mantle is indicated by the presence of an inferred, sinking lithospheric slab.

STRUCTURE OF THE UPPER MANTLE

In addition to the Transverse Ranges and Salton Trough, other regions in California show mantle velocity anomalies that imply structure within the lithospheric mantle and even the asthenosphere. The seismic networks in California (see chap. 5) provide an abundant source of regional earthquake and teleseismic arrivals that have been used to determine this upper-mantle structure.

A detailed study of the compressional-wave velocity of the uppermost mantle in central California reveals a normal velocity of about 8.0 km/s and no evidence for

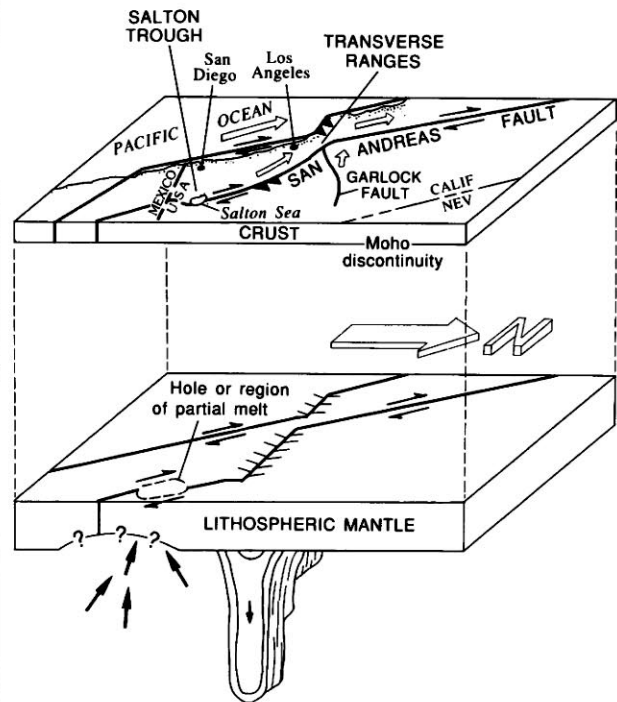


FIGURE 8.8.—Motion of crustal blocks in southern California (open arrows; see fig. 8.7) and somewhat different motion of lithospheric mantle below (solid arrows) (modified from Humphreys, 1985, and Humphreys and Hager, in press). Mantle convection cell is envisioned between the Salton Trough and the Transverse Ranges. Crust and lithospheric mantle appear to be moving independently of one another, as the San Andreas fault trends obliquely across region of inferred, sinking lithospheric mantle beneath the Transverse Ranges (see fig. 8.7). Small arrows, relative fault motion; sawteeth, upper plates of crustal thrust faults; crosslines, subduction zones in lithospheric mantle.

velocity anisotropy (Oppenheimer and Eaton, 1984). A similar study in southern California finds nearly the same average velocity, 7.95 km/s, with evidence for 2-percent velocity anisotropy (Vetter and Minster, 1981; Hearn, 1984). The fast direction is N. 75° W., approximately parallel to the San Andreas fault in southern California. Seismic-velocity anisotropy in the upper mantle has been reported elsewhere, notably in oceanic crust, and is commonly attributed to alignment of olivine in the mantle along a shear-stress direction (Bamford and others, 1979). In southern California, this shear would presumably be that associated with the motion of crustal blocks above the lithospheric mantle.

Lithospheric thickness along the San Andreas fault has been investigated by using delay times of teleseismic arrivals and thermal models (Zandt and Furlong, 1982). These studies indicate a lithospheric thickness of only 30 to 60 km for much of western California, and as little as 20 km for northern California just south of Cape Mendocino. These lithospheric thicknesses contrast with averages of 60 to 80 km for the Western United States and 120 to 170 km for the Central and Eastern United States (Iyer and Hitchcock, 1989). The thinness of the lithosphere in northern California south of Cape Mendocino is due to the creation of the San Andreas fault system itself: The transform fault is lengthening as the Mendocino triple junction migrates northward. As this junction migrates northward, the west edge of North America is sliding off the edge of the northward-moving, subducting Gorda plate, thereby creating a "window" where no subducting lithospheric slab is present (Dickinson and Synder, 1979). In this slabless window, the North American crust is initially in direct contact with the asthenosphere that has welled upward to fill the hole left by the Gorda plate (Zandt and Furlong, 1982). This geometry produces the thinnest lithosphere in California and, probably, in North America. In contrast, the lithosphere is abnormally thick (250 km) in the Transverse Ranges, where "subduction" of lithospheric mantle is occurring, as discussed above.

Velocity anomalies appear to extend even into the asthenosphere beneath western California. Aki (1982) summarized the results of Cockerham and Ellsworth (1979) and Raikes (1980) in a combined velocity-anomaly model for a depth range of about 100–225 km in the mantle (fig. 8.9). Aki suggested that the low-velocity region in central California is hot, mobile material associated with the slabless window. Such an association appears likely for the northwest-trending prong of this anomaly, as refined by the recent work of Benz and others (1990); however, the center of the anomaly, located near Long Valley caldera (figs. 8.2, 8.9), apparently has a different origin. Low-velocity regions are also associated with the Salton Trough, where asthenospheric

upwelling is inferred, and the eastern Mojave Desert, where crustal extension has occurred. The high-velocity region that crosses the San Andreas fault in southern California is similar to the one discussed above (fig. 8.7).

SUMMARY

The crust along the San Andreas fault system thickens from about 16 km at Cape Mendocino, in northern California, to about 30 km in southern California and thus is significantly thinner than the average thickness (36 km) for the conterminous United States. Lithospheric thickness (20–60 km) is also substantially less along most of the San Andreas fault system than is typical for continental areas (60–170 km). The lithosphere is thinnest at both ends of the fault system, at the Mendocino triple junction on the north, where the North American plate is sliding off the edge of the Gorda plate as it moves northward, and in the Salton Trough on the south, where

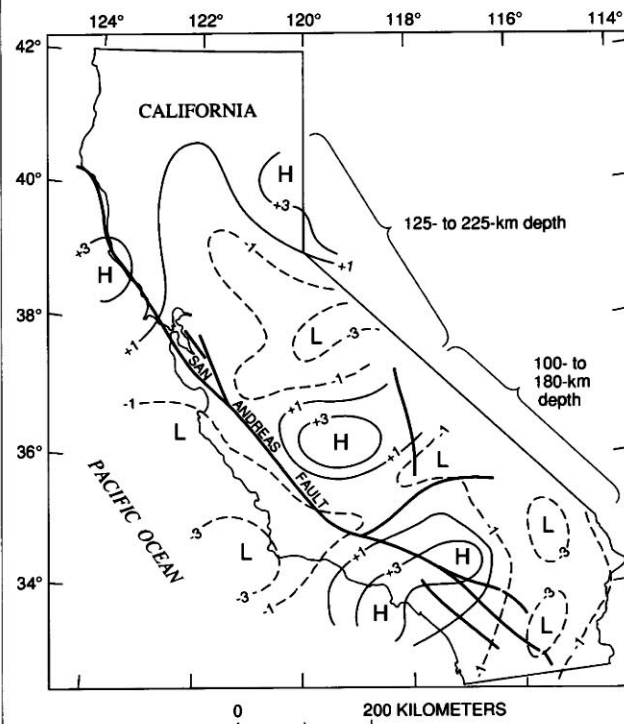


FIGURE 8.9.—Seismic-velocity anomalies in upper mantle (chiefly asthenosphere), derived from teleseismic delay-time data (Aki, 1982), for depth ranges 125–225 km (central California; Cockerham and Ellsworth, 1979) and 100–180 km (southern California; Raikes, 1980). H, high velocities (contours solid); L, low velocities (contours dashed). Contour interval, 2 percent. High seismic velocities that cross the San Andreas fault in southern California are similar in pattern to those shown in figure 8.7. Heavy lines, major faults.

onshore spreading centers of the East Pacific Rise are generating new crust in a rift between the North American and Pacific plates. In contrast, the lithosphere is abnormally thick (250 km) in the Transverse Ranges, where "subduction" of lithospheric mantle is occurring.

The crust of central California was formed at an Andean-type continental margin and has been modified by large offsets along strike-slip faults of the San Andreas fault system. East of the San Andreas fault, the Andean-marginal sequence includes a subduction complex (Franciscan rocks), a forearc basin (Great Valley sequence), and a magmatic arc (plutons of the Sierra Nevada). The subduction complex appears to have been emplaced as a tectonic wedge beneath sedimentary rocks of the forearc basin. West of the fault, displaced blocks constitute an Andean-marginal sequence that has been shortened by strike-slip faulting.

The tectonic wedge of Franciscan rocks east of the fault is reinterpreted to extend from its tip beneath the Great Valley all the way to the San Andreas fault. This interpretation is motivated by the apparent continuity between crystalline basement rocks beneath the Great Valley and mafic rocks at midcrustal depths in the Diablo Range, beneath the Franciscan rocks. The presence of extended crust atop the tectonic wedge (outliers of Coast Range ophiolite and Great Valley sequence) has led us to propose the following tectonic evolution for the wedge. (1) Franciscan rocks were uplifted and upper-plate rocks (those above the subduction zone) were extended during the Cretaceous (or, possibly, early Tertiary) well west of their current position in the Coast Ranges. (2) The Franciscan rocks and overlying extended crust were subsequently forced landward during one or more episodes in the form of a wedge that largely followed the contact between Great Valley basement and the Great Valley sequence. (3) Wedge movement began during the subduction of the Farallon plate (or its derivative) beneath central California; however, it apparently is also occurring at present, in the San Andreas transform regime. Present movement is interpreted to result from compression across the San Andreas fault system coupled with differential motion between the upper and lower crust; this differential motion is interpreted to occur on thrust fault(s) at the base of the wedge that sole into the brittle-ductile transition zone.

The crustal structure in southern California shares several features in common with central California, including, west of the fault, an Andean-marginal sequence that has been shortened or, at least, shuffled by strike-slip faulting, and, east of the fault, subduction-complex rocks that are inferred to have moved landward as a tectonic wedge into the continental rocks. However, major differences are apparent in southern California. First, east of the San Andreas fault, the Andean-

marginal sequence is incomplete: A forearc basin is absent, and the magmatic arc is diffuse. Second, new continental crust has formed in the Salton Trough, an active crustal pullapart basin, by a combination of rapid sedimentation, metamorphism, and magmatic intrusion at the onshore spreading centers. In addition, the motions of the crust and lithospheric mantle differ in southern California: The crust is moving as a collage of blocks, with only minor interblock convergence, whereas the lithospheric mantle is converging and "subducting" beneath the Transverse Ranges.

The interpretations of (1) a midcrustal detachment in the brittle-ductile transition zone in central California and (2) a crust-mantle detachment in the Transverse Ranges of southern California would appear to require that the deformational style and (or) location of the San Andreas fault system change with depth in these regions.

The properties of the lithosphere along the San Andreas fault are not at all typical of continental areas, and further characterization of these properties presents a significant scientific challenge.

ACKNOWLEDGMENTS

Stimulating discussions with C.M. Wentworth and M.C. Blake, Jr., led to some of our ideas concerning the configuration and emplacement history of the inferred wedge of Franciscan rocks in central and northern California. A. Griscom and R.C. Jachens provided insightful discussions regarding interpretation of potential-field models, and R.C. Evarts assisted us in drawing a cross section through the uppermost crust in the northeastern Diablo Range. We are also indebted to E.D. Humphreys for providing preprints of manuscripts on lithospheric motion in southern California.

REFERENCES CITED

- Aki, Keiiti, 1982, Three-dimensional seismic inhomogeneities in the lithosphere and asthenosphere: Evidence for decoupling in the lithosphere and flow in the asthenosphere: *Reviews of Geophysics and Space Physics*, v. 20, p. 161-170.
- Aki, Keiiti, Christofferson, Anders, and Husebye, E.S., 1977, Determination of the three-dimensional seismic structure of the lithosphere: *Journal of Geophysical Research*, v. 82, no. 2, p. 277-296.
- Atwater, Tanya, 1970, Implications of plate tectonics for the Cenozoic tectonic evolution of western North America: *Geological Society of America Bulletin*, v. 81, no. 12, p. 3513-3535.
- 1989, Plate tectonic history of the northeast Pacific and western North America, chap. 4 of Winterer, E.L., Hussong, D.M., and Decker, R.W., eds., *The eastern Pacific Ocean and Hawaii*, v. N of *The geology of North America*: Boulder, Colo., Geological Society of America, p. 21-72.
- Atwater, Tanya, and Menard, H.W., 1970, Magnetic lineations in the northeast Pacific: *Earth and Planetary Science Letters*, v. 7, no. 5, p. 445-450.

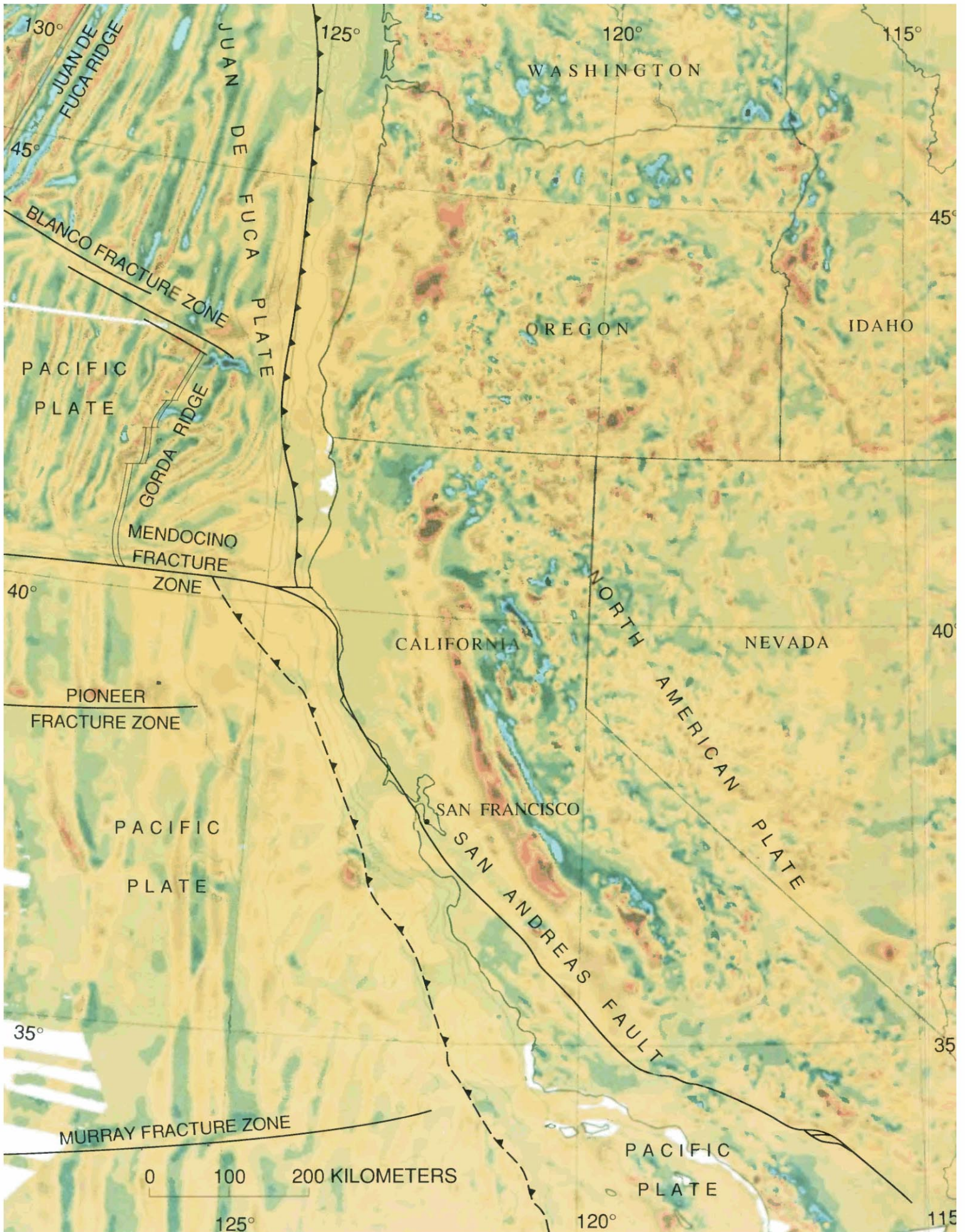
- Bailey, E.H., and Blake, M.C., Jr., 1974, Major chemical characteristics of Mesozoic Coast Range ophiolite in California: U.S. Geological Survey Journal of Research, v. 2, no. 6, p. 637-656.
- Bailey, E.H., Blake, M.C., Jr., and Jones, D.L., 1970, On-land Mesozoic oceanic crust in California Coast Ranges, in Geological Survey research, 1970: U.S. Geological Survey Professional Paper 700-C, p. C70-C81.
- Bamford, David, Jentsch, Martin, and Prodehl, Claus, 1979, *P_n anisotropy studies in northern Britain and the eastern and western United States*: Royal Astronomical Society Geophysical Journal, v. 57, no. 2, p. 397-429.
- Bartow, J.A., Lettis, W.R., Sonneman, H.S., and Switzer, J.R., Jr., 1985, Geologic map of the east flank of the Diablo Range from Hospital Creek to Poverty Flat, San Joaquin, Stanislaus, and Merced Counties, California: U.S. Geological Survey Miscellaneous Investigations Series Map I-1656, scale 1:62,500.
- Ben-Avraham, Zvi, 1985, Structural framework of the Gulf of Elat (Aqaba), northern Red Sea: Journal of Geophysical Research, v. 90, no. B1, p. 703-726.
- Benz, H.M., Zandt, George, and Oppenheimer, D.H., 1990, Seismic imaging of the subducting plate and the slabless window beneath northern California [abs.]: Seismological Research Letters, v. 61, no. 1, p. 32.
- Berg, L., Leveille, G., and Geis, P., 1982, Mid-Tertiary detachment faulting and manganese mineralization in the Midway Mountains, Imperial County, California, in *Mesozoic-Cenozoic tectonic evolution of the Colorado River region, California, Arizona, and Nevada*: San Diego, Calif., Cordilleran Publishers, p. 298-312.
- Berkland, J.O., 1973, Rice Valley outlier—new sequence of Cretaceous-Paleocene strata in northern Coast Ranges, California: Geological Society of America Bulletin, v. 84, no. 7, p. 2389-2405.
- Biehler, Shawn, Kovach, R.L., and Allen, C.R., 1964, Geophysical framework of the northern gulf province, in van Andel, T.H., and Shor, G.G., Jr., eds., *Marine geology of the Gulf of California*: American Association of Petroleum Geologists Memoir 3, p. 126-143.
- Birch, A.F., 1960, The velocity of compressional waves in rocks to 10 kilobars, part 1: Journal of Geophysical Research, v. 65, no. 4, p. 1083-1102.
- Blake, M.C., Jr., 1981, *Geologic transect of the northern Diablo Range, California*, in Frizzell, V.A., Jr., ed., *Upper Mesozoic Franciscan rocks and Great Valley sequence, central Coast Ranges, California*: Pacific Section, Society of Economic Paleontologists and Mineralogists, Pacific Section field trip guidebook, p. 35-43.
- Blake, M.C., Jr., Howell, D.G., and Jones, D.L., 1982, Preliminary tectonostratigraphic terrane map of California: U.S. Geological Survey Open-File Report 82-593, 10 p., scales 1:750,000, 3 sheets.
- Blake, M.C., Jr., Jayko, A.S., and Murchey, B.L., 1987, Structure, age, and tectonic significance of the Coast Range ophiolite and related rocks near Paskenta, California [abs.]: Geological Society of America Abstracts with Programs, v. 19, no. 7, p. 590.
- Blümling, Peter, Mooney, W.D., and Lee, W.H.K., 1985, Crustal structure the southern Calaveras fault zone, central California, from seismic refraction investigations: Seismological Society of America Bulletin, v. 75, no. 1, p. 193-209.
- Blümling, Peter, and Prodehl, Claus, 1983, Crustal structure beneath the eastern part of the Coast Ranges (Diablo Range) of central California from explosion seismic and near earthquake data: *Physics of the Earth and Planetary Interiors*, v. 31, no. 4, p. 313-326.
- Braille, L.W., Hinze, W.J., von Frese, R.R.B., and Keller, G.R., 1989, Seismic properties of the crust and uppermost mantle of the continuous United States and adjacent Canada, chap. 28 of Pakiser, L.C., and Mooney, W.D., eds., *Geophysical framework of the continental United States*: Geological Society of America Memoir 172, p. 655-680.
- Byerly, Perry, 1946, *The seismic waves from the Port Chicago [California] explosion*: Seismological Society of America Bulletin, v. 36, no. 4, p. 331-348.
- Byerly, Perry, and Wilson, J.T., 1935, The Richmond quarry blast of August 16, 1934: Seismological Society of America Bulletin, v. 25, p. 259-268.
- Champion, D.E., Howell, D.G., and Grommé, C.S., 1984, Paleomagnetic and geologic data indicating 2500 km of northward displacement for the Salinian and related terranes: Journal of Geophysical Research, v. 89, no. B9, p. 7736-7752.
- Christensen, N.I., and Fountain, D.M., 1975, Constitution of the lower continental crust based on experimental studies of seismic velocities in granulite: Geological Society of America Bulletin, v. 86, no. 2, p. 229-236.
- Clark, L. D., 1964, Stratigraphy and structure of part of the western Sierra Nevada metamorphic belt, California: U.S. Geological Survey Professional Paper 410, 70 p.
- Cockerham, R.S., and Ellsworth, W.L., 1979, Three-dimensional large-scale mantle structure in central California [abs.]: *Eos (American Geophysical Union Transactions)*, v. 60, no. 45, p. 875.
- Colburn, R.H., and Mooney, W.D., 1986, Two-dimensional velocity structure along the synclinal axis of the Great Valley, California: Seismological Society of America Bulletin, v. 76, no. 5, p. 1305-1322.
- Coleman, R.G., and Lanphere, M.A., 1971, Distribution and age of high-grade blueschists, associated eclogites, and amphibolites from Oregon and California: Geological Society of America Bulletin, v. 82, no. 9, p. 2397-2412.
- Conrad, R.L., and Davis, T.E., 1977, Rb/Sr geochronology of cataclastic rocks of the Vincent thrust, San Gabriel Mountains, southern California [abs.]: Geological Society of America Abstracts with Programs, v. 9, no. 4, p. 403-404.
- Cowan, D.S., 1974, Deformation and metamorphism of the Franciscan subduction zone complex northwest of Pacheco Pass, California: Geological Society of America Bulletin, v. 85, no. 10, p. 1623-1634.
- Criscione, J.J., Davis, T.E., and Ehlig, P.L., 1978, The age and sedimentation/diagenesis for the Bedford Canyon and the Santa Monica Formation in southern California—a Rb/Sr evaluation, in Howell, D.G., and McDougall, K.A., eds., *Mesozoic paleogeography of the Western United States: Pacific Coast Paleogeography Symposium 2: Los Angeles, Society of Economic Paleontologists and Mineralogists, Pacific Section*, p. 385-396.
- Crosson, R.S., 1976, Crustal structure modeling of earthquake data 1. Simultaneous least squares estimation of hypocenter and velocity parameters: Journal of Geophysical Research, v. 81, no. 17, p. 3036-3046.
- Crouch, J.K., Bachman, S.B., and Shay, J.T., 1984, Post-Miocene compressional tectonics along the central California margin, in Crouch, J.K., and Bachman, S.B., eds., *Tectonics and sedimentation along the California margin (volume 38): Society of Economic Paleontologists and Mineralogists, Pacific Section Annual Meeting, San Diego, Calif., 1984, Papers*, p. 37-54.
- Crowe, B.M., 1978, Cenozoic volcanic geology and probable age of inception of basin-range faulting in the southeasternmost Chocolate Mountains, California: Geological Society of America Bulletin, v. 89, no. 2, p. 251-264.
- Crowe, B.M., Crowell, J.C., and Krummenacher, Daniel, 1979, Regional stratigraphy, K-Ar ages, and tectonic implications of Cenozoic volcanic rocks, southeastern California: *American Journal of Science*, v. 279, no. 2, p. 186-216.
- Crowell, J.C., 1962, Displacement along the San Andreas fault, California: Geological Society of America Special Paper 71, 61 p.

- 1981, An outline of the tectonic history of southeastern California, in Ernst, W.G., ed., *The geotectonic development of California* (Rubey volume 1) Englewood Cliffs, N.J., Prentice-Hall, p. 583-600.
- Dibblee, T.W., Jr., 1954, Geology of the Imperial Valley region, California, in *Geology of the natural provinces*, chap. 2 of Jahns, R.H., ed., *Geology of southern California*: California Division of Mines Bulletin, 170, v. 1, p. 21-28.
- Dickinson, W.R., 1966, Table Mountain serpentinite extrusion in California Coast Ranges: *Geological Society of America Bulletin*, v. 77, no. 5, p. 451-471.
- Dickinson, W.R., and Snyder, W.S., 1979, Geometry of subducted slabs related to San Andreas transform: *Journal of Geology*, v. 87, no. 6, p. 609-627.
- Dillon, J.T., 1975, *Geology of the Chocolate and Cargo Muchacho Mountains, southeasternmost California*: Santa Barbara, University of California, Ph.D. thesis, 405 p.
- Doser, D.I., and Kanamori, Hiroo, 1986, Depth of seismicity in the Imperial Valley region (1977-1983) and its relationship to heat flow, crustal structure, and the October 15, 1979, earthquake: *Journal of Geophysical Research*, v. 91, no. B1, p. 675-688.
- Eaton, J.P., 1963, Crustal structure from San Francisco, California, to Eureka, Nevada, from seismic-refraction measurements: *Journal of Geophysical Research*, v. 68, no. 20, p. 5789-5806.
- 1990, The earthquake and its aftershocks from May 2 through September 30, 1983, chap. 8 of Rymer, M.J., and Ellsworth, W.L., eds., *The Coalinga, California, earthquake of May 2, 1983*: U.S. Geological Survey Professional Paper 1487, p. 113-170.
- Eaton, J.P., O'Neill, M.E., and Murdock, J.N., 1970, Aftershocks of the 1966 Parkfield-Cholame, California, earthquake: A detailed study: *Seismological Society of America Bulletin*, v. 60, no. 4, p. 1151-1197.
- Eaton, J.P., and Rymer, M.J., 1990, Regional seismotectonic model for the southern Coast Ranges, chap. 7 of Rymer, M.J., and Ellsworth, W.L., eds., *The Coalinga, California, earthquake of May 2, 1983*: U.S. Geological Survey Professional Paper 1487, p. 97-111.
- Eberhart-Phillips, Donna, and Oppenheimer, D.H., 1984, Induced seismicity in the Geysers geothermal area, California: *Journal of Geophysical Research*, v. 89, no. B2, p. 1191-1207.
- Ehlig, P.L., 1968, Causes of distribution of Pelona, Rand, and Orocochia schists along the San Andreas and Garlock fault, in Dickinson, W.R., and Grantz, Arthur, eds., *Proceedings of conference on geologic problems of San Andreas fault system*: Stanford, Calif., Stanford University Publications on Geological Sciences, v. 11, p. 294-305.
- Elders, W.A., Rex, R.W., Meidav, Tsvi, Robinson, P.T., and Biehler, Shawn, 1972, Crustal spreading in southern California: The Imperial Valley and the Gulf of California formed by the rifting apart of a continental plate: *Science*, v. 178, no. 4056, p. 15-24.
- Evarts, R.C., 1977, The geology and petrology of Del Puerto ophiolite, Diablo Range, central California Coast Ranges, in Coleman, R.G., and Irwin, W.P., eds., *North American ophiolites*: Oregon Department of Geology and Mineral Industries Bulletin 95, p. 121-139.
- Evernden, J.F., and Kistler, R.W., 1970, Chronology of emplacement of Mesozoic batholithic complexes in California and western Nevada: U.S. Geological Survey Professional Paper 623, 67 p.
- Frost, E.G., Martin, D.L., and Krummenacher, Daniel, 1982, Mid-Tertiary detachment faulting in southwestern Arizona and southeastern California and its overprint on the Vincent-Orocochia thrust system [abs.]: *Geological Society of America Abstracts with Programs*, v. 14, no. 4, p. 164.
- Fuis, G.S., 1981, Crustal structure of the Mojave Desert, California, in Howard, K.A., Carr, M.D., and Miller, D.M., eds., *Tectonic framework of the Mojave and Sonoran Deserts, California and Arizona*: U.S. Geological Survey Open-File Report 81-503, p. 36-38.
- Fuis, G.S., and Kohler, W.M., 1984, Crustal structure and tectonics of the Imperial Valley region, California, in Rigsby, C.A., ed., *The Imperial Basin—tectonics, sedimentation, and thermal aspects* (volume 40): *Society of Economic Paleontologists and Mineralogists, Pacific Section Annual Convention, San Diego, Calif., 1984, Papers*, p. 1-13.
- Fuis, G.S., Mooney, W.D., Healy, J. H., McMechan, G.A., and Lutter, W.J., 1982, Crustal structure of the Imperial Valley region, in *The Imperial Valley, California, earthquake of October 15, 1979*: U.S. Geological Survey Professional Paper 1254, p. 25-49.
- 1984, A seismic refraction survey of the Imperial Valley region, California: *Journal of Geophysical Research*, v. 89, no. B2, p. 1165-1189.
- Fuis, G.S., and Plafker, George, in press, Evolution of deep structure along the Trans-Alaska Crustal Transect, Chugach Mountains and Copper River basin, southern Alaska: *Journal of Geophysical Research*.
- Fuis, G.S., Walter, A.W., Mooney, W.D., and McCarthy, Jill, 1986, Crustal velocity structure of the Salton Trough, western Mojave Desert, and Colorado Desert, from seismic refraction [abs.]: *Geological Society of America Abstracts with Programs*, v. 18, no. 2, p. 107.
- Gutenberg, Beno, 1943, Earthquakes and structure in southern California: *Geological Society of America Bulletin*, v. 54, no. 4, p. 499-526.
- 1951, Travel times from blasts in southern California: *Seismological Society of America Bulletin*, v. 41, no. 1, p. 5-12.
- Hadley, D.M., and Kanamori, Hiroo, 1977, Seismic structure of the Transverse Ranges, California: *Geological Society of America Bulletin*, v. 88, no. 10, p. 1469-1478.
- Hamilton, Warren, 1969, Mesozoic California and the underflow of Pacific mantle: *Geological Society of America Bulletin*, v. 80, no. 12, p. 2409-2429.
- Harwood, D.S., and Helley, E.J., 1987, Late Cenozoic tectonism of the Sacramento Valley, California: U.S. Geological Survey Professional Paper 1359, 46 p.
- Haxel, G.B., 1977, The Orocochia schist and the Chocolate Mountain Thrust, Picacho-Peter Kane Mountains area, southeasternmost California: Santa Barbara, University of California, Ph.D. thesis, 277 p.
- Haxel, G.B., and Dillon, J.T., 1978, The Pelona-Orocochia schist and Vincent-Chocolate Mountain thrust system, southern California, in Howell, D.G., and McDougall, K.A., eds., *Mesozoic paleogeography of the Western United States: Pacific Coast Paleogeography Symposium 2*: Los Angeles, Society of Economic Paleontologists and Mineralogists, Pacific Section, p. 453-469.
- Healy, J.H., 1963, Crustal structure along the coast of California from seismic refraction measurements: *Journal of Geophysical Research*, v. 68, no. 20, p. 5777-5787.
- Hearn, T.M., 1984, P_n travel times in southern California: *Journal of Geophysical Research*, v. 89, no. B3, p. 1843-1855.
- Hearn, T.M., and Clayton, R.W., 1986a, Lateral velocity variations in southern California: 1. Results for the upper crust from P_g -waves: *Seismological Society of America Bulletin*, v. 76, no. 2, p. 495-509.
- 1986b, Lateral velocity variations in southern California: 2. Results for the lower crust from P_n -waves: *Seismological Society of America Bulletin*, v. 76, no. 2, p. 511-520.
- Hill, D.P., 1978, Seismic evidence for the structure and Cenozoic tectonics of the Pacific Coast states, in Smith, R.B., and Eaton, G.P., eds., *Cenozoic tectonics and regional geophysics of the*

- western Cordillera: Geological Society of America Memoir 152, p. 145-174.
- Hill, M.L., and Dibblee, T.W., Jr., 1953, San Andreas, Garlock, and Big Pine faults, California—a study of the character, history, and tectonic significance of their displacement: Geological Society of America Bulletin, v. 64, no. 4, p. 443-458.
- Holbrook, W.S., and Mooney, W.D., 1987, The crustal structure of the axis of the Great Valley, California, from seismic refraction measurements: Tectonophysics, v. 140, no. 1, p. 49-63.
- Hopson, C.A., Mattinson, J.M., and Pessagno, E.A., 1981, Coast Range ophiolite, western California, in Ernst, W.G., ed., Geotectonic development of California (Rubey volume 1): Englewood Cliffs, N.J., Prentice-Hall, p. 418-510.
- Howell, D.G., Gibson, J.D., Fuis, G.S., Knapp, J.H., Haxel, G.B., Keller, B.R., Silver, L.T., and Vedder, J.G., 1985, C-3: Pacific abyssal plain to the Rio Grande rift: Boulder, Colo., Geological Society of America, Centennial Continent/Ocean Transect 5, 23 p., scale 1:500,000, 3 sheets.
- Humphreys, E.D., 1985, Studies of the crust-mantle system beneath southern California: Pasadena, California Institute of Technology, Ph.D. thesis, 189 p.
- Humphreys, E.D., and Clayton, R.W., in press, Tomographic image of the southern California mantle: Journal of Geophysical Research.
- Humphreys, E.D., Clayton, R.W., and Hager, B.H., 1984, A tomographic image of mantle structure beneath southern California: Geophysical Research Letters, v. 11, no. 7, p. 625-627.
- Humphreys, E.D., and Hager, B.H., 1984, Small-scale convection beneath the Transverse Ranges, southern California [abs.]: Eos (American Geophysical Union Transactions), v. 65, no. 16, p. 195.
- in press, A kinematic model for the recent development of southern California crust and upper mantle: Journal of Geophysical Research.
- Humphreys, E.D., and Weldon, R.J., II, in press, Kinematic constraints on the rifting of Baja California, in Daupin, J.P., and Simoneit, B.R.T., eds., The Gulf and Peninsular provinces of the Californias: American Association of Petroleum Geologists Memoir 47.
- Isaac, Sharon, Rockwell, T.K., and Gastil, Gordon, 1986, Plio-Pleistocene detachment faulting, Yuha Desert region, western Salton Trough, northern Baja California [abs.]: Geological Society of America Abstracts with Programs, v. 18, no. 2, p. 120.
- Iyer, H.M., and Hitchcock, Tim, 1989, Upper-mantle velocity structure in continental U.S. and Canada, chap. 29 of Pakiser, L.C., and Mooney, W.D., eds., Geophysical framework of the continental United States: Geological Society of America Memoir. 172, p. 681-710.
- Jachens, R.C., and Griscom, Andrew, 1983, Three-dimensional geometry of the Gorda plate beneath northern California: Journal of Geophysical Research, v. 88, no. B11, p. 9375-9392.
- Jachens, R.C., Simpson, R.W., Griscom, Andrew, and Mariano, John, 1986, Plutonic belts in southern California defined by gravity and magnetic anomalies [abs.]: Geological Society of America Abstracts with Programs, v. 18, no. 2, p. 120.
- Jayko, A.S., Blake, M.C., Jr., and Harms, T.A., 1987, Attenuation of the Coast Range Ophiolite by extensional faulting, and nature of the Coast Range "thrust," California: Tectonics, v. 6, no. 4, p. 475-488.
- Jennings, C.W., compiler, 1977, Geologic map of California: California Division of Mines and Geology Geologic Data Map 2, scale 1:750,000.
- Jennings, C.W., and Strand, R.G., compilers, 1958, Santa Cruz sheet of Geologic map of California: Sacramento, California Division of Mines, scale 1:250,000.
- Johnson, C.E., 1979, CEDAR—an approach to the computer automation of short-period local seismic networks; seismotectonics of the Imperial Valley of southern California: Pasadena, California Institute of Technology, Ph.D. thesis, 343 p.
- Johnson, C.E., and Hadley, D.M., 1976, Tectonic implications of the Brawley earthquake swarm, Imperial Valley, California, January 1975: Seismological Society of America Bulletin, v. 66, no. 4, p. 1133-1144.
- Jones, D.L., Blake, M.C., Jr., and Rangin, C., 1976, The four Jurassic belts of northern California and their significance to the geology of the southern California borderland, in Howell, D.G., ed., Aspects of the geologic history of the California Continental Borderland: American Association of Petroleum Geologists, Pacific Section Miscellaneous Publication 24, p. 343-362.
- Jones, D.L., and Irwin, W.P., 1971, Structural implications of an offset Early Cretaceous shoreline in northern California: Geological Society of America Bulletin, v. 82, no. 4, p. 815-822.
- Kosloff, D.D., 1978, Numerical models of crustal deformation: Pasadena, California Institute of Technology, Ph.D. thesis, 187 p.
- Lachenbruch, A.H., Sass, J.H., and Galanis, S.P., Jr., 1985, Heat flow in southernmost California and the origin of the Salton Trough: Journal of Geophysical Research, v. 90, no. B8, p. 6709-6736.
- Larson, E.S., Jr., 1948, Batholith and associated rocks of Corona, Elsinore, and San Luis Rey quadrangles, southern California: Geological Society of America Memoir 29, 182 p.
- Lin, Wunan, and Wang, C.-Y., 1980, P-wave velocity in rocks at high pressure and temperature and the constitution of the central California crust: Royal Astronomical Society Geophysical Journal, v. 61, no. 2, p. 379-400.
- Lomnitz, Cinna, Mosser, Federico, Allen, C.R., Brune, J.N., and Thatcher, Wayne, 1970, Seismicity and tectonics of the northern Gulf of California region, Mexico. Preliminary results: Geofisica Internacional, v. 10, no. 2, p. 27-48.
- Maddock, M.E., 1964, Geology of the Mt. Boarman Quadrangle, Stanislaus County, California: California Division of Mines and Geology Map Sheet 3, scale 1:62,500.
- Mattinson, J.M., 1982, Granitic rocks of the Gabilan Range, California: U-Pb isotopic systematics and implications for age and origin [abs.]: Geological Society of America Abstracts with Programs, v. 14, no. 4, p. 184.
- Mayer-Rosa, Dieter, 1973, Travel-time anomalies and distribution of earthquakes along the Calaveras fault zone, California: Seismological Society of America Bulletin, v. 63, no. 2, p. 713-729.
- McEvilly, T.V., and Clymer, R.W., 1975, A deep crustal reflection survey on the San Andreas fault [abs.]: Eos (American Geophysical Union Transactions), v. 56, no. 12, p. 1021.
- McLaughlin, R.J., Clark, J.C., and Brabb, E.E., 1988a, Geologic map and structure sections of the Loma Prieta 7½' quadrangle, Santa Clara and Santa Cruz Counties, California: U.S. Geological Survey Open-File Report 88-752, 31 p., scale 1:24,000, 2 sheets.
- McLaughlin, R.J., Blake, M.C., Jr., Griscom, Andrew, Blome, C.D., and Murchey, B.L., 1988b, Tectonics of formation, translation, and dispersal of the Coast Range ophiolite of California: Tectonics, v. 7, no. 5, p. 1033-1056.
- Miller, F.K., and Morton, D.M., 1977, Comparison of granitic intrusions in the Pelona and Orocopia Schists, southern California: U.S. Geological Survey Journal of Research, v. 5, no. 5, p. 643-649.
- Miller, F.K., and Morton, D.M., 1980, K-Ar geochronology of the eastern Transverse Ranges and southern Mojave Desert, southern California: U.S. Survey Professional Paper 1152, 30 p.
- Minster, J.B., and Jordan, T.H., 1978, Present-day plate motions: Journal of Geophysical Research, v. 83, no. B11, p. 5331-5354.
- Mooney, W.D., and Colburn, R.H., 1985, A seismic-refraction profile across the San Andreas, Sargent, and Calaveras faults, west-central California: Seismological Society of America Bulletin, v. 75, no. 1, p. 175-191.
- Mooney, W.D., and Weaver, C.S., 1989, Regional crustal structure and

- tectonics of the Pacific Coastal States: California, Oregon, and Washington, chap. 9 of Pakiser, L.C., and Mooney, W.D., eds., Geophysical framework of the continental United States: Geological Society of America Memoir 172, p. 129-161.
- Moore, E.M., and Day, H.W., 1984, Overthrust model for the Sierra Nevada: *Geology*, v. 12, no. 7, p. 416-419.
- Namson, J.S., and Davis, T.L., 1988, Seismically active fold and thrust belt in the San Joaquin Valley, central California: *Geological Society of America of Bulletin*, v. 100, no. 2, p. 257-273.
- Namson, J.S., Davis, T.L., and Lagoe, M.B., 1990, Tectonic history and thrust-fold deformation style of seismically active structures near Coalinga, chap. 6 of Rymer, M.J., and Ellsworth, W.L., eds., *The Coalinga, California, earthquake of May 2, 1983*: U.S. Geological Survey Professional Paper 1487, p. 79-96.
- Nava, F.A., and Brune, J.N., 1982, An earthquake-explosion reversed refraction line in the Peninsular Ranges of southern California and Baja California Norte: *Seismological Society of America Bulletin*, v. 72, no. 4, p. 1195-1206.
- Oliver, H.W., Chapman, R.H., Biehler, Shawn, Robbins, S.L., Hanna, W.F., Griscom, Andrew, Beyer, L.A., and Silver, E.A., 1980, Gravity map of California and its continental margin: California Division of Mines and Geology Geologic Data Map 3, scale 1:750,000, 2 sheets.
- Olsen, J.A., 1986, Seismicity of the San Andreas fault zone in the San Francisco Peninsula area, California: *Royal Society of New Zealand Bulletin* 24, p. 87-97.
- Olsen, J.A., and Lindh, A.G., 1985, Seismicity of the San Andreas Fault from Cienega Winery to the Golden Gate, in Shearer, C.F., Minutes of the National Earthquake Prediction Evaluation Council, July 26-27, 1985, Menlo Park, California: U.S. Geological Survey Open-File Report 85-754, p. 316-324.
- Oppenheimer, D.H., and Eaton, J.P., 1984, Moho orientation beneath central California from regional earthquake traveltimes: *Journal of Geophysical Research*, v. 89, no. 12, p. 10267-10282.
- Oppenheimer, D.H., Reasenber, P.A., and Simpson, R.W., 1988, Fault-plane solutions for the 1984 Morgan Hill, California, earthquake sequence: Evidence for the state of stress on the Calaveras fault: *Journal of Geophysical Research*, v. 93, no. B8, p. 9007-9026.
- Page, B.M., and Engebretson, D.C., 1984, Correlation between the geologic record and computed plate motions for central California: *Tectonics*, v. 3, no. 2, p. 133-155.
- Peake, L.G., and Healy, J.H., 1977, A method for determination of the lower crustal structure along the San Andreas fault system in central California: *Seismological Society of America Bulletin*, v. 67, no. 3, p. 793-807.
- Plafker, George, and Galloway, J.P., eds., 1989, Lessons learned from the Loma Prieta, California, earthquake of October 17, 1989: U.S. Geological Survey Circular 1045, 48 p.
- Platt, J.P., 1975, Metamorphic and deformational processes in the Franciscan Complex, California: Some insights from the Catalina Schist terrane: *Geological Society of America Bulletin*, v. 86, no. 10, p. 1337-1347.
- 1976, The significance of the Catalina schist and the history of the southern California Borderland, in Howell, D.G., ed., *Aspects of the geologic history of the California Continental Borderland*: American Association Petroleum Geologists, Pacific Section Miscellaneous Publication 24, p. 47-52.
- 1986, Dynamics of orogenic wedges and the uplift of high-pressure metamorphic rocks: *Geological Society of America Bulletin*, v. 97, no. 9, p. 1037-1053.
- Powell, C.L., II, 1984, Bivalve molluscan paleoecology of the marine Neogene Imperial Formation in Riverside County, California [abs.]: *Western Society of Malacologists Annual Report* 17, p. 29-32.
- Powell, R.E., 1981, Geology of the crystalline basement complex, eastern Transverse Ranges, southern California; constraints on regional tectonic interpretation: Pasadena, California Institute of Technology, Ph.D. thesis, 441 p.
- Raikes, S.A., 1980, Regional variations in upper mantle structure beneath southern California: *Royal Astronomical Society Geophysical Journal*, v. 63, no. 1, p. 187-216.
- Raymond, L.A., 1973, Tesla-Ortogonalita fault, Coast Range thrust fault, and Franciscan metamorphism, northeastern Diablo Range, California: *Geological Society of America Bulletin*, v. 84, no. 11, p. 3547-3562.
- Reasenber, P.A., and Ellsworth, W.L., 1982, Aftershocks of the Coyote Lake, California, earthquake of August 6, 1979: A detailed study: *Journal of Geophysical Research*, v. 87, no. B13, p. 10637-10655.
- Rentschler, M.S., and Bloch, R.B., 1988, Flexural subsidence modeling of the San Joaquin basin, California, in Graham, S.A., and Olson, H.C., eds., *Studies of the geology of the San Joaquin basin (volume 60): Society of Economic Paleontologists and Mineralogists, Pacific Section Field Trip Guidebook*, p. 29-57.
- Robinson, P.T., Elders, W.A., and Muffler, L.J.P., 1976, Quaternary volcanism in the Salton Sea geothermal field, Imperial Valley, California: *Geological Society of America Bulletin*, v. 87, no. 3, p. 347-360.
- Roller, J.C., and Healy, J.H., 1963, Seismic-refraction measurements of crustal structure between Santa Monica Bay and Lake Mead: *Journal of Geophysical Research*, v. 68, no. 20, p. 5837-5849.
- Ross, D.C., 1972, Petrographic and chemical reconnaissance study of some granitic and gneissic rocks near the San Andreas fault from Bodega Head to Cajon Pass, California: U.S. Geological Survey Professional Paper 698, 92 p.
- 1978, The Salinian block: A Mesozoic granitic orphan in the California Coast Ranges, in Howell, D.G., and McDougall, K.A., eds., *Mesozoic paleogeography of the Western United States: Pacific Coast Paleogeography Symposium 2: Los Angeles, Society of Economic Paleontologists and Mineralogists, Pacific Section*, p. 509-522.
- Ross, D.C., and McCulloch, D.S., 1979, Cross section of the southern Coast Ranges and San Joaquin Valley from offshore Point Sur to Madera, California: *Geological Society of America Map and Chart Series*, no. MC-28H, scale 1:250,000.
- Saleeby, J.B., 1982, Polygenetic ophiolite belt of the California Sierra Nevada: Geochronological and tectonostratigraphic development: *Journal of Geophysical Research*, v. 87, no. 3, p. 1803-1824.
- 1986, C-2: Central California offshore to Colorado Plateau: *Geological Society of America, Centennial Continent/Ocean Transect 10*, 63 p., scale 1:500,000, 2 sheets.
- Sauber, Jeanne, Thatcher, Wayne, and Solomon, S.C., 1986, Geodetic measurement of deformation in the central Mojave Desert, California: *Journal of Geophysical Research*, v. 91, no. B12, p. 12633-12693.
- Schultejahn, P.A., 1984, The Yaqui Ridge antiform and detachment fault: Mid-Cenozoic extensional terrane west of the San Andreas fault: *Tectonics*, v. 3, no. 6, p. 677-691.
- Schweickert, R.A., and Bogen, N.L., 1983, Tectonic transect of Sierran Paleozoic through Jurassic accreted belts: *Society of Economic Paleontologists and Mineralogists, Pacific Section Field Trip Guidebook*, 22 p.
- Schweickert, R.A., and Cowan, D.S., 1975, Early Mesozoic tectonic evolution of the western Sierra Nevada, California: *Geological Society of America Bulletin*, v. 86, no. 10, p. 1329-1336.
- Shor, G.G., Jr., 1954, Crustal structure and reflections from the Mohorovicic discontinuity: Pasadena, California Institute of Technology, Ph.D. thesis, 158 p.
- Shor, G.G., Jr., Menard, H.W., and Raitt, R.W., 1971, Structure of the Pacific basin, in Maxwell, A.E., ed., *The sea: Ideas and observa-*

- tions on progress in the study of the seas: New York, John Wiley & Sons, v. 4, pt. 2, p. 3-27.
- Shor, G.G., Jr., and Raitt, R.W., 1958, Seismic studies in the southern California Continental Borderland, in *International Geological Congress, 20th, Mexico City, 1956, Proceedings, sec. 9, v. 2, p. 243-259.*
- Sibson, R.H., 1982, Fault zone models, heat flow, and the depth distribution of earthquakes in the continental crust of the United States: *Seismological Society of America Bulletin*, v. 72, no. 1, p. 151-163.
- Silver, L.T., Taylor, H.P., and Chappell, B., 1979, Some petrological, geochemical, and geochronological observations of the Peninsular Ranges batholith near the international border of the U.S.A. and Mexico, in Abbott, P.L., and Todd, V.R., eds., *Mesozoic crystalline rocks: Peninsular Ranges batholith and pegmatites, Point Sal Ophiolite: San Diego, Calif., San Diego State University, Department of Geological Sciences, p. 83-110.*
- Spieth, M.A., Hill, D.P., and Geller, R.J., 1981, Crustal structure in the northwestern foothills of the Sierra Nevada from seismic refraction experiments: *Seismological Society of America Bulletin*, v. 71, no. 4, p. 1073-1085.
- Stewart, R.M., and Peselnick, Louis, 1977, Velocity of compressional waves in dry Franciscan rocks to 8 kbar and 300° C: *Journal of Geophysical Research*, v. 82, no. 14, p. 2027-2039.
- Stewart, S.W., 1968, Preliminary comparison of seismic traveltimes and inferred crustal structure adjacent to the San Andreas fault in the Diablo and Gabilan Ranges of central Calif., in Dickinson, W.R., and Grantz, Arthur, eds., *Proceeding of the conference on geologic problems of the San Andreas fault system: Stanford, Calif., Stanford University Publications in the Geological Sciences, v. 11, p. 218-230.*
- Suppe, John, and Armstrong, R.L., 1972, Potassium-argon dating of Franciscan metamorphic rocks: *American Journal of Science*, v. 272, no. 3, p. 217-233.
- Thurber, C.H., and Aki, Keiiti, 1987, Three-dimensional seismic imaging: *Annual Reviews of Earth and Planetary Sciences*, v. 15, p. 115-139.
- Vedder, J.G., Beyer, L.A., Junger, Arne, Moore, G.W., Roberts, A.E., Taylor, J.C., and Wagner, H.C., 1974, Preliminary report on the geology of the continental borderland of southern California: U. S. Geological Survey Miscellaneous Field Studies Map MF-624, 34 p., scales 1:500,000, 1:1,000,000, 9 sheets.
- Vetter, Ute, and Minster, J.-B., 1981, P_n velocity anisotropy in southern California: *Seismological Society of America Bulletin*, v. 71, no. 5, p. 1511-1530.
- Wallace, R.D., and English, D.J., 1982, Evaluation of possible detachment faulting west of the San Andreas, southern Santa Rosa Mountains, California, in Frost, E.G., and Martin, D.L., eds., *Mesozoic-Cenozoic tectonic evolution of the Colorado River region, California, Arizona, and Nevada: San Diego, Calif., Cordilleran Publishers, p. 502-510.*
- Walter, A.W., and Mooney, W.D., 1982, Crustal structure of the Diablo and Gabilan Ranges, central California: A reinterpretation of existing data: *Seismological Society of America Bulletin*, v. 72, no. 5, p. 1567-1590.
- Webb, T.H., and Kanamori, Hiroo, 1985, Earthquake focal mechanisms in the eastern Transverse Ranges and San Emigdio Mountains, southern California and evidence for a regional decollement: *Seismological Society of America Bulletin*, v. 75, no. 3, p. 737-757.
- Weldon, R.J., and Humphreys, E.D., 1986, A kinematic model of southern California: *Tectonics*, v. 5, no. 1, p. 33-48.
- Wentworth, C.M., 1987, Implications for crustal structure in the western Coast Ranges, California, from studies along their eastern margin [abs.]: *Eos (American Geophysical Union Transactions)*, v. 68, no. 44, p. 1366.
- Wentworth, C.M., Blake, M.C., Jr., Jones, D.L., and Walter, A.W., 1984, Tectonic wedging associated with emplacement of the Franciscan assemblage, California Coast Ranges, in Blake, M.C., Jr., ed., *Franciscan geology of northern California (volume 43): Society of Economic Paleontologists and Mineralogists, Pacific Section Field Trip Guidebook, p. 163-173.*
- Wentworth, C.M., and Zoback, M.D., 1989, The style of late Cenozoic deformation at the eastern front of the California Coast Ranges: *Tectonics*, v. 8, no. 2, p. 237-246.
- Wentworth, C.M., Zoback, M.D., Griscom, Andrew, Jachens, R.C., and Mooney, W.D., 1987, A transect across the Mesozoic accretionary margin of central California: *Royal Astronomical Society Geophysical Journal*, v. 89, no. 1, p. 105-110.
- Wesson, R.L., Burford, R.O., and Ellsworth, W.L., 1973, Relationship between seismicity, fault creep, and crustal loading along the central San Andreas fault, in Kovach, R.L., and Nur, Amos, eds., *Proceedings of the conference on tectonic problems of the San Andreas fault system: Stanford, Calif., Stanford University Publications in the Geological Sciences, v. 13, p. 303-321.*
- Yeats, R.S., 1981, Quaternary flake tectonics of the California Transverse Ranges: *Geology*, v. 9, no. 1, p. 16-20.
- Zandt, George, and Furlong, K.P., 1982, Evolution and thickness of the lithosphere beneath coastal California: *Geology*, v. 10, no. 7, p. 376-381.
- Zoback, M.D., and Wentworth, C.M., 1986, Crustal studies in central California using an 800-channel seismic reflection recording system, in Barazangi, Muawia, and Brown, Larry, eds., *Reflection seismology: A global perspective (Geodynamics Series, v. 13): Washington, American Geophysical Union, p. 183-196.*



Studies on the gravity and magnetic fields of the San Andreas fault system span more than 30 years, but only recently have the fundamental data sets become adequate to provide a general view of the entire system. Modeling these new data defines the three-dimensional geometries of the faults and helps unravel the tectonic history of the system by "seeing through" the relatively thin cover of young sedimentary deposits and water to the older rocks below.

9. CRUSTAL AND LITHOSPHERIC STRUCTURE FROM GRAVITY AND MAGNETIC STUDIES

By ANDREW GRISCOM and ROBERT C. JACHENS

CONTENTS

	Page
Introduction-----	239
Isostatic residual gravity map-----	240
Magnetic anomaly map-----	241
Sources of gravity and magnetic anomalies-----	241
Geometry of faults in the San Andreas System-----	243
Plan view-----	243
Attitude-----	247
Fault-zone characteristics-----	249
Offsets of anomalies-----	249
Implications for plate tectonics-----	252
Mendocino triple junction-----	252
Salton Buttes spreading center-----	255
References cited-----	256

INTRODUCTION

Studies of the San Andreas fault system using the Earth's gravity and magnetic fields began before 1960 but received their main impetus during the 1970's, when work on the possibility of predicting earthquakes on this system began in earnest. Early investigations focused

mainly on short segments of the faults because only limited data were available. More extensive potential-field data sets that have been published in recent years now permit the gravity and magnetic expression of the entire fault system to be viewed in a regional context (fig. 9.1).

Gravity and magnetic data reflect, respectively, the density and magnetization of the rocks beneath the surface; and, in many situations, these properties can be closely correlated with the rock types seen in outcrop. Anomalies in the Earth's gravity and magnetic fields—for example, local deviations of the measured fields from those predicted on the basis of simplified Earth models—primarily reflect lateral variations in density and magnetization that generally are not included in such simple models. These anomalies can be interpreted qualitatively to infer the general spatial distribution of rock types in the subsurface, and quantitatively, through the use of efficient computer-based modeling techniques (Saltus and Blakely, 1983; Chuchel, 1985; Blakely and Simpson, 1986), to determine the geometries and specific locations of concealed rock bodies. Although all such interpretations are nonunique, both because many different distributions of density and magnetization can give rise to identical anomalies and because density and magnetiza-

◀ FIGURE 9.1.—Magnetic map of the Western United States and eastern Pacific Ocean, showing locations of major plate boundaries: solid line, present boundary; dashed line, former boundary; double line, spreading ridge; single line, transform fault; toothed line, subduction-zone fault or transpressional fault (sawteeth on upper plate). From

Geological Society of America (1987); used with permission. Plate boundaries from King (1969), McCulloch (1987), and Wilson (1989). Each color band represents 100 nanoteslas; values range from low (blue) to high (red); white area, no data. Bathymetric contours in meters.

tion do not uniquely define a specific rock type, the combined use of gravity and magnetic data with geologic, geochemical, and other geophysical data can be especially effective in limiting the number of acceptable interpretations.

In the sections below, we first present regional gravity and magnetic maps covering the San Andreas fault system and briefly discuss the sources, compilation methods, and limitations of the data from which they were produced and, in general terms, the sources of the anomalies shown on them. We then summarize the results of individual studies of sections of the major faults in the system and attempt to synthesize these results in terms of the geometries of the faults, the structures and rock types in the surrounding areas that are related to the faults, and the properties of the fault zones. Next, we focus on studies that relate to movement on the faults, including constraints on total displacements. Finally, we discuss the plate-tectonic implications of potential-field investigations of the fault system.

ISOSTATIC RESIDUAL GRAVITY MAP

An isostatic residual gravity map of the region surrounding the San Andreas fault system is shown in figure 9.2. We have chosen to present the gravity data in this form rather than in terms of the more common Bouguer or free-air gravity because of the generally closer correlation between isostatic residual gravity and mapped geology (Jachens and Griscom, 1985; Simpson and others, 1986). Most long-wavelength anomalies (longer than approx 250 km) on a Bouguer gravity map are caused by deep-seated density distributions that buoyantly support the topography in a manner consistent with the principle of isostasy (Simpson and others, 1986). Bouguer gravity anomalies related to isostasy are prevalent in California because of the extreme topographic relief in the State (Oliver, 1980; Jachens and Griscom, 1985), and they are particularly strong near the coast, where an eastward to northeastward decrease in gravity reflects the transition from thin oceanic crust to thicker continental crust. In such areas as California, the Bouguer gravity anomalies associated with isostatic support of topography are so strong that they tend to distort or even mask the lower-amplitude anomalies caused by density distributions in the middle to upper crust, those anomalies most easily correlatable with rocks exposed at the surface (Jachens and Griscom, 1985). Our isostatic residual gravity map has these long-wavelength isostatic effects removed, at least to first order. We emphasize that the anomalies remaining on our map are predominantly caused by lateral density variations in the middle

to upper crust and, as such, do not represent areas that are out of isostatic balance (Jachens and Griscom, 1985).

Our isostatic residual gravity map (fig. 9.2) is based on the new isostatic residual gravity map of the conterminous United States by Simpson and others (1986), who presented a detailed discussion of the data sets and procedures used to generate this map. The basic gravity-data set was compiled for the "Gravity Anomaly Map of the United States" (Society of Exploration Geophysicists, 1982) and includes 1 million on shore and 0.8 million offshore gravity observations. These data were sampled on a rectangular grid with a grid spacing of 4 km, containing Bouguer gravity values onshore and free-air gravity values at sea (Godson, 1985). To produce our isostatic residual gravity map, the offshore free-air gravity values were converted to Bouguer gravity values. The gravitational effects of the deep density distributions that support the topography within 166.7 km of each grid intersection were computed according to the Airy-Heiskanen model of isostasy (Heiskanen and Moritz, 1967) using a 5- by 5-minute topographic-bathymetric data grid and model parameters as follows: topographic density, 2.67 g/cm³; crustal thickness at sea level, 30 km; and density contrast across the base of the model crust, 0.35 g/cm³. Combined isostatic and topographic effects for the region from 166.7 km to the antipode of each grid intersection were obtained from the maps by Karki and others (1961). This model gravity field was subtracted from each Bouguer gravity grid value to yield a grid of isostatic residual gravity values; the resulting grid was contoured by computer and displayed in color-band intervals of 10 mGal to produce figure 9.2.

Limitations on the use of this map stem both from uncertainties in the point data from which the grid was constructed and from characteristics generated by the gridding process. For onshore data, uncertainties in the point data values resulting from errors in observed gravity, elevation, terrain corrections, and isostatic reductions are estimated to be less than 2 to 3 mGal for most stations, possibly larger in areas of extreme topographic relief (Simpson and others, 1986). In offshore areas, the greatest uncertainty results from conversion of the original free-air gravity data to Bouguer gravity values, using the 5- by 5-minute average bathymetry. Where the sea-bottom topography is relatively gentle, this conversion probably results in uncertainties of about 5 mGal, but in such areas as parts of the California Continental Borderland (south of lat 34° N.) and over the edge of the Continental Shelf, where water depths change rapidly, errors of several tens of milligals are possible. These conversion errors generally appear as high-amplitude, nearly circular anomalies with diameters of as much as 40 km.

Although gravity coverage along most of the San Andreas fault system is quite dense when viewed at the scale of figure 9.2, sampling of these data on a 4-km grid means that anomalies with characteristic dimensions less than several times the grid spacing are not faithfully portrayed. Our isostatic residual gravity map (fig. 9.2) is sufficient for qualitative and quantitative interpretation at the scale shown, but for more detailed interpretations, especially quantitative modeling, the reader is referred to the original data sources, such as Oliver and others (1980), Roberts and others (1981), Snyder and others (1982), and the other reports cited throughout this chapter.

MAGNETIC ANOMALY MAP

A magnetic anomaly map of the region surrounding the San Andreas fault system is shown in figure 9.3. This map is based on the magnetic anomaly map of the Western United States by Bond and Zietz (1987), which was compiled from hundreds of magnetic surveys with widely differing flight heights, flightline spacings, and sensor types.

In contrast to the lengthy series of reduction steps that were required to convert the gravity observations to the form shown in figure 9.2, very little was done to the observed magnetic data to prepare them for compilation. Although the original data were collected at many different heights, no analytic procedures were used to continue them to a common elevation. Instead, the various surveys were referenced to the International Geomagnetic Reference Field (IGRF) adjusted for the date of the survey and an arbitrary zero datum, and then combined manually by inspection. Long profiles of magnetic data collected under the National Uranium Resource Evaluation (NURE) program of the U.S. Department of Energy and by the U.S. Naval Oceanographic Office (NOO) served as guides for determining the zero datum for the various surveys. The resulting data are presented at a color contour interval of 100 nT (gammas) in figure 9.3.

Our magnetic anomaly map (fig. 9.3) is the most complete compilation available for the San Andreas fault system and is useful for qualitatively determining the location, shape, and regional setting of large magnetic bodies. However, because of the compilation methods used to construct this map and because the contour interval is relatively coarse (100 nT), it will not, in general, be adequate for detailed qualitative or quantitative examination of individual anomalies. Where detailed information is required, the reader is referred to the original sources from which our map was compiled; a comprehensive listing of these sources is given by Bond and Zietz (1987).

A particularly valuable source of aeromagnetic data over the San Andreas fault system is the profile data collected under the NURE program. In general, these data were collected along long profiles oriented east-west at a nominal height of 120 m above terrain and spaced about 5 km apart. The wide flightline spacing and low altitude of the survey lines preclude constructing realistic contour maps from these data in most places, but the long profiles are well suited for quantitative modeling. These data are available in the form of atlas folios or digital tapes for individual 1° by 2° quadrangles from the U.S. Department of Energy, Grand Junction, Colo.

When interpreting magnetic data, the inclination of the Earth's magnetic field must be taken into account because the magnetization induced in the magnetic source rocks by this field will have a similar inclination. Along the San Andreas fault, this inclination ranges from 58° to 64° downward toward magnetic north. Contoured magnetic anomalies over inductively magnetized or normally magnetized sources at these field inclinations will commonly display a dipole response, namely, magnetic lows associated with the north sides of magnetic highs. Inspection of our magnetic-anomaly map (fig. 9.3) indeed identifies numerous such magnetic lows on the north or northeast sides of major magnetic highs. In general, each magnetic low is located directly beyond the north or northeast contact of the causative magnetic mass.

SOURCES OF GRAVITY AND MAGNETIC ANOMALIES

Conspicuous features of the gravity field over the San Andreas fault system are linear highs and lows that trend subparallel to the major faults in the system. Highs (≥ 10 mGal) generally occur over exposed crystalline rocks of the Salinian block southwest of the San Andreas fault, over mafic granitic and metamorphic rocks of the Sierra Nevada and the Mojave Desert, and over Mesozoic and Tertiary layered rocks of the Franciscan assemblage, particularly in areas containing large amounts of mafic volcanic rocks (generally part of an ophiolite belt) or high-pressure metamorphic-mineral facies. Most of the deepest lows are caused by thick accumulations of low-density Cenozoic sedimentary rocks that fill tectonic basins adjacent to the faults and in the surrounding areas. Shallower lows occur over certain large serpentine bodies within the Franciscan assemblage, over felsic plutons in the granitic terranes of California, and over a young concealed granitic pluton associated with the Geysers geothermal area at lat 39° N., long 122°45' W. (Chapman, 1975; Isherwood, 1976).

Magnetic anomalies in the vicinity of the San Andreas fault system typically are caused by any one of three

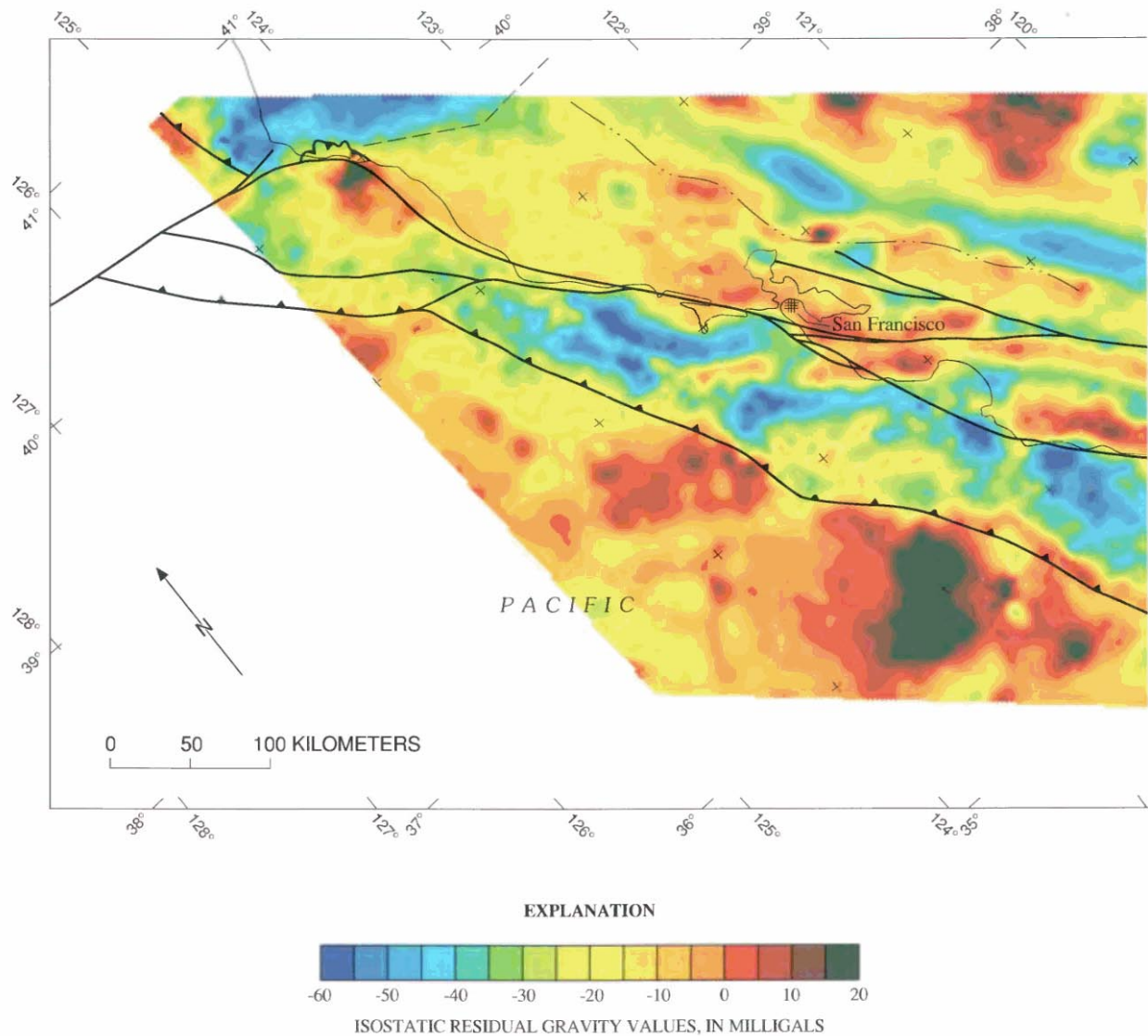


FIGURE 9.2.—Isostatic residual gravity map of the San Andreas fault system. Contour interval, 5 mGal. Faults simplified from Jennings and others (1977), McCulloch (1987), and Vedder (1987). Fault names and explanation in figure 9.4.

different rock types. The strongest anomalies generally reflect tabular bodies of serpentinite associated with the Franciscan assemblage and may also reflect the ophiolitic rocks, especially serpentinite, that locally lie above it. Mafic plutonic rocks, such as those exposed in the western Peninsular Ranges and along the west edge of the southern Sierra Nevada, can produce moderate to strong magnetic anomalies. Plutonic sources, not necessarily mafic only, probably account for most of the anomalies in the Salinian block, southwest of the San Andreas fault. Although younger volcanic rocks, in particular the mafic varieties, commonly are highly

magnetic, such rocks do not cause significant magnetic features near the San Andreas fault as shown on our magnetic anomaly map (fig. 9.3) because magnetic volcanic rocks are volumetrically unimportant at the scale of this map.

In most areas, sedimentary rocks are considered nonmagnetic because they fail to cause aeromagnetic anomalies. Along the San Andreas fault system, however, several sedimentary-rock units cause magnetic anomalies as large as 150 nT. These units include rocks of Mesozoic and Tertiary age; other units composed primarily of detrital serpentinite also produce anomalies of this

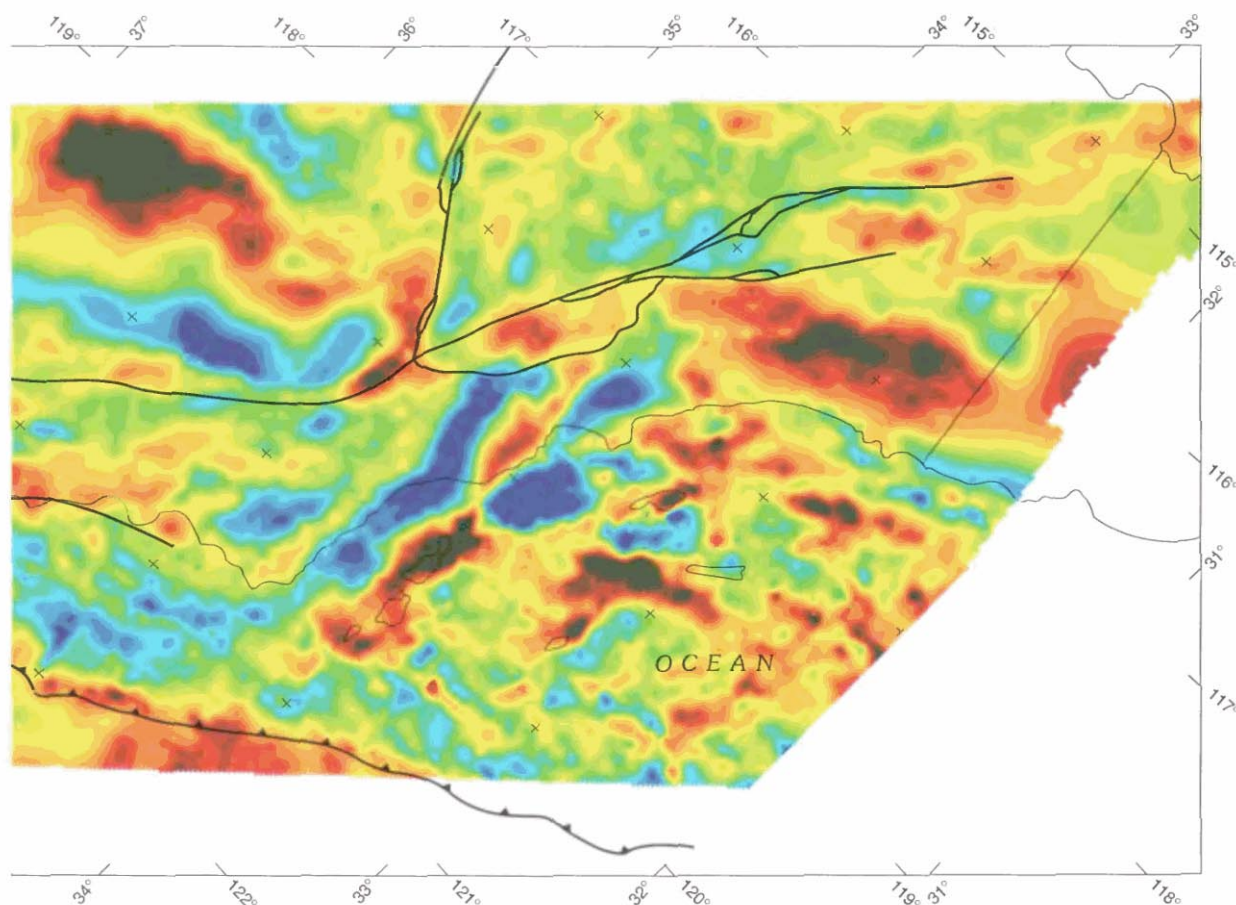


FIGURE 9.2.—Continued.

magnitude. None of these sedimentary units are areally large enough to produce magnetic anomalies visible at the scale of our magnetic anomaly map (fig. 9.3).

Near the north end of the San Andreas fault, several magnetic anomalies project landward from the linear pattern of anomalies that characterizes the oceanic crust. These anomalies reflect remanent magnetization in the oceanic crust; the source rocks are primarily basaltic volcanic rocks.

GEOMETRY OF FAULTS IN THE SAN ANDREAS SYSTEM

PLAN VIEW

The usefulness of potential-field data along the San Andreas fault system is maximized where rock masses with differing physical properties are juxtaposed. Under these conditions, geophysical anomalies arise from which the location and attitude of the fault may be calculated

(Blakely and Simpson, 1986). In general, the fault is expected to be situated at or near the steepest gradient of the anomaly. These sites are particularly helpful in areas where the fault trace or zone is concealed by young sedimentary deposits or by the Pacific Ocean. In addition, we have found that some of these data are useful in identifying the main strand of the fault zone where the presently active fault trace may not, in fact, be the original plate boundary. Some areas where the potential-field data define the locations of faults are shown on figure 9.4 and are discussed below.

Although the location of the San Andreas fault between Point Arena and Cape Mendocino is concealed by the Pacific Ocean, the aeromagnetic data show a linear magnetic anomaly, striking northwest within the Pacific plate, that is inferred to be obliquely cut off by the fault about 20 km northwest of Point Arena. Farther north, the fault trace just south of Cape Mendocino has proved particularly difficult to locate because it may be too close to shore to be resolved by marine geophysical surveys. A